The nucleohistone compartment in relation to sperm HALO formation, DNA damage and DNA sequence analysis

By

Adel Mohammed Binduraihem

Submitted in accordance with the requirements for the degree of
Doctor of Philosophy

The University of Leeds
School of Medicine

January 2017

Acknowledgement

I would like to express my appreciations and thanks for all people who have supported me during my PhD study and to develop my scientific skills as a PhD student. I would like to thank;

Dr. David Miller, my primary supervisor, for his scientific guidance and support in all stages of my study as well as writing my thesis. I am grateful to have been one of Dr. Miller's PhD students and carried out my project under his supervision.

Dr. John Huntriss, my co-supervisor, for his advice and help during my study.

Dr. David Iles, for introducing me to bioinformatics analysis, and for his guidance during my lab work, and especially for his great work in NGS data analysis.

Forough Torabi for her technical support in many experiments of my project, also Panagiotis Ntostis, for helping me during all stages of sequencing experiment as well as in the bioinformatics analysis.

And all members of Reproduction and Early Development (RED) division for their help and support during my study.

My parent for their encouragement words and prayers during my study.

My wife, Yasmin and my children, Dana and Mohammed, for their personal support at all times.

King Faisal Specialist Hospital and Research Centre (KFSH&RC) for providing me with the scholarship and the necessary financial support for this research.

St. James Hospital, sequencing facility and FISH lab teams, for their help during the DNA library productions, sequencing runs and FISH experiment.

Seacroft hospital, particularly the andrology lab, for providing us with semen samples.

Abstract

The presence of DNA damage in mature sperm may be associated with poor chromatin structure due to abnormal protamination. Interestingly, however, approximately 5-15% of the DNA in the human sperm nucleus remains bound to histones. In this study, oxidative stress was used to induce DNA damage in mature sperm aimed at investigating the integrity of sperm chromatin structure. The extent of the damage was assessed by acridine orange, alkaline comet and halo assay (Halosperm™). Experiments were designed to probe the relationship between sperm DNA fragmentation as revealed by halo dynamics and the DNA sequences that constitute the nuclear halo structure, and so provide a more robust link between the halo assay as a discriminator of high-quality sperm and paternal genes that may be disrupted in damaged sperm.

Differential Density Gradient Centrifugation (DDGC) was used to resolve human spermatozoa into 90% percoll solution (high density) and 45% percoll solution (low-density) fractions. DNA damage was induced by exposure to H_2O_2 at two different concentrations (100 and 300 μM) for fixed times. Acridine orange, alkaline comet and halo assay were used conventionally to measure the extent of DNA fragmentation in peroxide-treated cells. In a variant of the halo assay aimed at investigating the differences between protamine and histone-bound DNA, human sperm nuclei were treated with either low or high ionic strength salt solutions to generate nuclear halos. Halos produced from control (undamaged) sperm by Halosperm™ or by salt extraction were treated in suspension with restriction

enzymes to release halo-DNA, which was analysed by Next Generation Sequencing (NGS).

Results of acridine orange, alkaline comet and halo assay revealed that pellets of DDGC processed sperm were far more resistant to H_2O_2 treatment compared with interface sperm. The efficacy of halo formation as an indicator of DNA damage was shown by the high percentage of strong halos generated by Halosperm™ and salt extraction methods from sperm isolated from the pelleted sperm compared with interface sperm. Analysis of NGS data of halos generated by Halosperm™ and by low or high salt extraction of nuclear proteins suggests that approximately 2000 genes, many of developmental significance are significantly 'over-represented' in nuclear halos compared with residual (nucleoid) DNA. Moreover, the data suggests that halo-DNA was originally associated with the histone compartment of sperm chromatin.

The nuclear halo can indicate the level of DNA fragmentation in sperm, and the sequence composition of halos suggest that such fragmentation could compromise important paternally-derived DNA sequences that the oocyte may be unable to repair.

Table of Contents

List of tables

Table of Figures

List of abbreviations

AO	Acridine Orange
BC	Bovine Catalase
BSA	Bovine Serum Albumin
CTAB	hexadecyltrimethylammonium bromide
CTCF	CCCTC binding factor
ChIP	Chromatin immunoprecipitation Sequencing
DAPI	4',6-diamidino-2-phenylindole
DDB	Double DNA Break
DDGC	Differential Density gradient centrifugation
DPBS	Dulbecco's Phosphate Buffered Saline
DNA	Deoxyribonucleic acid
DTT	Dithiothreitol
DPX	Distyrene plasticizer xylene
dsDNA	Double stranded DNA
FISH	Fluorecence In Situ Hybridization
FMC	Flowcytometery
H_2O_2	Hydrogen peroxide
H1	Histone 1
H2A	Histone 2 A
H2B	Histone 2 B
H3	Histone 3
H4	Histone 4
IVF	In-Vitro Fertilisation
LMPA	Low Melting Point Agarose
LTR	Long Terminal Repeat
NMPA	Normal Melting Point Agarose
NGS	Next Generation sequencing
MARs	Matrix Attachment Regions
MNase	Micrococcal nuclease
PBS	Phosphate Buffer Saline

PRM1	Protamine 1
PRM2	Protamine 2
PVDF	Polyvinylidene fluoride
ROS	Reactive Oxygen Species
SCD	Sperm Chromatin Dispersion
SCSA	Sperm Chromatin Structure Assay
Sp-TALP	Sperm Tyrode's Albumin-Lactate-Pyruvate
ssDNA	single stranded DNA
TH1	Testis Histone 1
TH2B	Testis Specific Histone 2B
TP1	Transition protein 1
TP2	Transition protein 2
TUNEL	The terminal deoxynucleotidyl transferase
8-OHdG	8-Hydroxyguanosine

Symbols

ºC	Degree Celsius
%	Percentage
µm3	Cubic micrometer per micron
µL	Microlitre
mg/mL	Milligram per millilitre
mL	Millilitre
M	Molar
mM	Milimolar
µM	Micromolar
nm	Nanometre
U/mL	Units per millilitre

Chapter 1: Introduction

1.1 Background

The molecular quality of maternal and paternal gametes is an essential prerequisite to achieving successful fertilisation and normal embryo development. The embryo's early development is governed in the main by molecules originating in the oocyte, including proteins and RNAs (Trounson and Gosden, 2003). However, the importance of the paternal genome to early embryo development is also now becoming more apparent (Barroso et al., 2009). Initially, spermatozoa were described as essentially passive cells whose sole role was the delivery of the paternal genome to the egg (Hecht et al., 2011; Miller et al., 2005). Nowadays, however, it is recognised that spermatozoa deliver more than the paternal genome to the egg and that these specialized cells may play a significant role after the fertilisation process by introducing paternal RNAs, which may be crucial for early embryo development (Boerke et al., 2007; Barroso et al., 2009). Many studies, for example, have suggested that sperm RNAs are probably involved in fertilisation and early embryo developmental processes (Ostermeier et al., 2005; Hosken and Hodgson, 2014; Miller, 2014).

In mammals, the chromatin of the sperm nucleus consists of highly basic proteins (mostly histones and protamines) and DNA (Grudzinskas and Yovich, 1995). These proteins are involved in the molecular remodelling and packaging of the paternal genome in the sperm nucleus. Unlike somatic cell DNA, sperm DNA is hypercondensed into a crystalline-like state virtually devoid of water (Dadoune et al., 2004).

Although sperm DNA has a unique nucleoprotein (histone to protamine) replacement strategy, which occurs in later stage of spermatogenesis, some histones remain bound to the DNA in the mature sperm (Miller et al., 2010). Recent studies have indicated that these retained histones have a non-random distribution in sperm chromatin and the sperm nucleus (Arpanahi et al., 2009; Hammoud et al., 2009). Interestingly, mammalian spermatozoa vary in their chromatin condensation pattern and histone-protamine ratio. For example, approximately 5-15% of the DNA in the human sperm nucleus remains bound to modified histones, while the majority (85%) is associated with protamines (Zalensky et al., 2002). In contrast, in other mammalian species, for example, bovine sperm chromatin contains a lower proportion of retained histones (<5%) compared with human sperm (Ioannou et al., 2016). Also, more than 98% of the murine spermatozoon genome is packaged in protamine (Li et al., 2008).

Male infertility contributes approximately 40 to 50% of infertility problems overall (Kumar and Singh, 2015). Traditional methods of sperm selection for assisted reproduction are based on various parameters, such as sperm count, motility, and morphology, which are not sufficiently effective to guarantee normal DNA integrity (Lo Monte et al., 2013). Although several techniques have been introduced to treat male infertility, including Intra-Cytoplasmic Sperm Injection (ICSI), the clinical pregnancy success rates still fall between 26.6% and 30.1% depending on maternal age (Andersen et al., 2008). Despite the introduction of many new methods and techniques to achieve higher assisted reproduction outcomes, scientists have argued that there is a need for sperm evaluation at the molecular level. Several studies show clear evidence that sperm infertility or dysfunction may be caused by abnormal chromatin structure (Miller et al., 2010;

Spano et al., 2000; Wiland et al., 2016) and it has been reported that altered chromatin structure causes detrimental effects to the post-fertilisation process and early embryo development (Fraga et al., 1996; Miller et al., 2010; Borini et al., 2006; Morris et al., 2002).

In this introduction, spermatogenesis, mature sperm chromatin organisation by histone-protamine replacement, the function of sperm nucleoproteins, sperm DNA damage and their possible effects on fertility and embryo development are considered.

1.2 Spermatogenesis

1.2.1 Spermatogenesis in mammals

Spermatogenesis in mammals is considered as the process of paternal germ cell development, which produces mature haploid gametes (23 chromosomes in humans) that are capable of fertilising the mature female gamete. These fundamental processes of cell proliferation and differentiation are similar in various animals, and the genes responsible for spermatogenesis are highly conserved (White-Cooper and Bausek, 2010). Spermatogenesis occurs within seminiferous tubules in the testes, which contain a mixture of Sertoli cells and germ cells surrounding by a wall of peritubular cells. Sertoli cells play a vital role in germ cells and support crucial events of spermatogenesis and in the operation of a functional testis (Griswold, 1998; Sharpe et al., 2003). Also, the seminiferous epithelium is divided by Sertoli cells into two compartments: an adluminal compartment where cells are isolated behind a physical blood-testis barrier and a basal compartment where cells are in close proximitly to the basal lamina, which is surrounded by myoid cells (Figure 1).

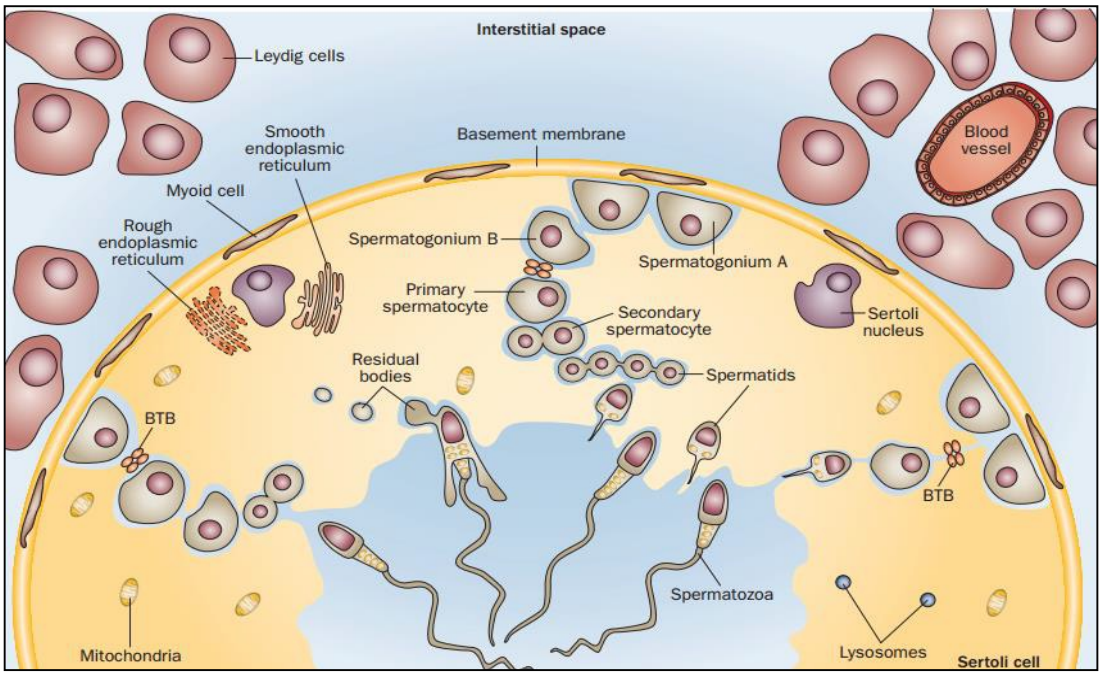

Figure 1: A model for spermatogenesis in mammals, which is the cellular transformation that generates paternal haploid germ cells from diploid spermatogonia type A. Spermatogonium type A divides into spermatogoium type B that undergoes meiotic stage and proliferates into primary spermatocyte that enters meiosis I and form haploid secondary spermatocytes. Then, spermatocyte produces four spermatids through meiosis II. These spermatids migrate to the lumen, where mature spermatozoa, including removal of cytoplasm and tail formation, are formed and released. Adapted from: (Rato et al., 2012)

The development of spermatogenic cells occurs in highly organised overlapping waves at different stages of mitotic, meiotic and post-meiotic phases of cellular proliferation and division (Rathke et al., 2014). In general, the more mature male germ cells lie closer to the lumen, while the less mature germ cells are located close to the basement membrane. It follows that the development of male germ cells is split mainly into three stages: spermatocytogenesis, spermatocyte meiosis and spermoigenesis (Sharpe, 1994). Spermatogenesis initiates with a mitotic proliferation of stem cells called spermatogonia located in the basal region of seminiferous tubules of the testis. Moreover, three types of spermatogonia have been identified: undifferentiated type A spermatogonia (dark and pale) and differentiated type B spermatogonia. Type A-dark cells serve to maintain the reserve of spermatogonia stem cells, while, type A-pale cells undergo mitotic

proliferation to produce identical spermatogonial stem cells destined for spermatogenesis. Type B stem cells divided mitotically to form pre-leptotene primary spermatocytes, which undergo meiosis I, followed by meiosis II to give more specialised haploid secondary spermatocytes (Dym, 1994). Interestingly, this post meiotic stage involves dynamics of gene expression including recombination of homologous chromosomes to form haploid genome. Thus, each of these completed meiotic diploid spermatocytes has the potential to generate four round haploid spermatids, however, these spermatids are still transcriptionally active (Oliva and Castillo, 2011). Although spermatids are genetically haploid, they are phenotypically diploid because they remain connected to one another by cytoplasmic bridges (Figure 2).

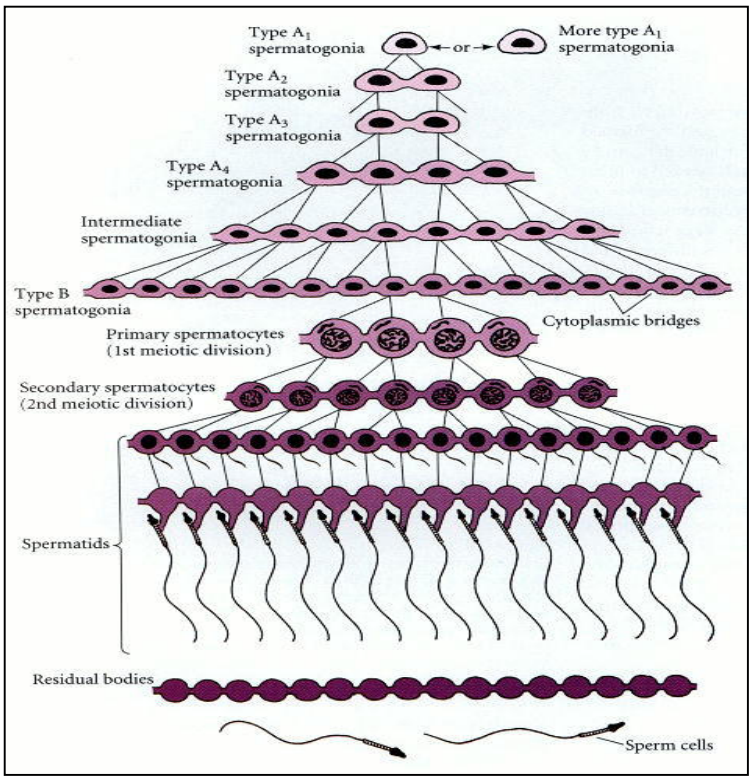

Figure 2: A diagram showed the development of spermatogenic cells (including spermatogonia, spermatocyte, spermatid and mature sperm), which occurs in highly organised overlapping waves at different stages of mitotic, meiotic and post-meiotic phases of cellular proliferation and division (which involves dynamics of gene expression including recombination of homologous chromosomes to form haploid genome). Adapted from (Gilbert, 2000)

Spermatids undergo dramatic morphological changes throughout spermiogenesis, including nuclear condensation, reduction of cytoplasmic volume, forming an acrosome and flagellum, as they transform into mature spermatozoa (De Kretser et al., 1998). Mature sperm display a wide diversity of sizes and shapes among species. In mammals, mature spermatozoa consist of head, neck, middle piece, principal piece and end piece (Toshimori, 2009). The sperm cell's head contains a nucleus and an acrosome over the tip (Figure 3). The sperm's mid-piece consists of a ring of five mitochondria, which provide the energy (ATP production) to power tail movement. Meanwhile, the flagellum of the sperm contains the axoneme, which drives the spermatozoon forward (Figure 3). The paternal gamete nucleus contains three main structural elements: compacted chromatin, RNA, and the nuclear matrix, which consists of DNA loops (Johnson et al., 2011), as well as nucleoproteins (protamines and histones), while, the acrosome contains functional lysosomal enzymes, such as hyaluronidase for penetrating the egg (Lin et al., 1994).

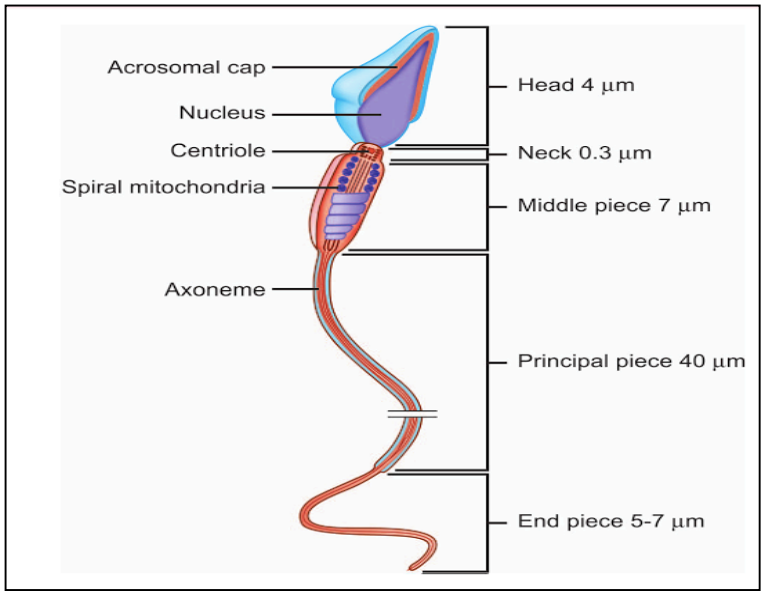

Figure 3: A model for human mature spermatozoon showed the main tree morphological parts of a mature sperm (head, mid-piece and tail). Also, it indicated a cap that located over the anterior part of the head known as an acrosome, as well as a haploid nucleus, which covers most of the head area. Adapted from (Talwar and Sindhu, 2012)

It has been suggested that there are fundamental differences between human and other species throughout spermatogenesis. For instance, the represented estimates of the duration of spermatogenesis are varied between species, for example, in humans 64 days compared with bulls 49 days (Guraya, 2012). Additionally, according to World Health Organisation (WHO) report (2010), only low percentage of produced sperm (4%) can be classified as normal in young normozoospermic men, which is lower than in bulls for example, in which >90% of produced sperm can be categorised as normal (Cooper et al., 2010). Unlike in humans, the morphological structure of the mature bovine spermatozoa contains a second compact cap known as “galea capities”, which lies over the head of the sperm and covers the acrosome region (Hancock, 1952).

1.2.2 Sperm histones and nucleosomes

During spermatid elongation, the DNA is repackaged and reorganised into a far tighter and more compact form than is typical in somatic cells (spermiogenesis), and which unlike somatic cells is transcriptionally inactive (Roca and Mezquita, 1989). In mammals, sperm chromatin structure can be divided into two structural domains. The majority (85-98%) of sperm DNA is packaged by protamines, and the remainder is packaged by histone-containing nucleosomes (Ioannou et al., 2016).

In mammals, there are five groups of histones present in the nucleus of somatic cells: histone 1 (H1) (the linker histone), histone 2A (H2A), histone 2B (H2B), histone 3 (H3) and histone 4 (H4). Histones are highly charged basic nucleoproteins present in the eukaryotic nucleus, and consist of 100-300 amino acids (Stein and Stein, 1989). Despite the size of the human genome, which is

2.91 billion base pair (bp) (Lander et al., 2001), histones can package the genome in 10^5-fold by looping DNA in 1.65 turns of a left-handed coiled pattern around the canonical histones of core nucleosomes (Luger et al., 1997). However, this DNA wrapping is inadequate for the sperm nucleus, which can compact the paternal genome in ~10^6-fold (Razin et al., 2007). In chromatin, the basic unit of packaging is nucleosome, which consists of two groups of the four core DNA-binding core histones: H2A, H2B, H3 and H4 with molecular weight 10,000-16,000 Daltons (Miller et al., 2010; Poccia, 1986). The height of the nucleosome disk is about 5.7 nm and its diameter is about 11 nm, however, each nucleosome is composed of ~ 146-147 bp of DNA wrapped around a set of eight core histones known as the histone octamer (H2A/H2B and H3/H4) and connected by 20-80 bp of linker DNA (Luger, 2003; Lusser, 2002) (Figure 4). The interactions between the core histones and DNA is substantially electrostatic, which makes it possible to extract histones from DNA using salt containing buffers (Stein and Page, 1980).

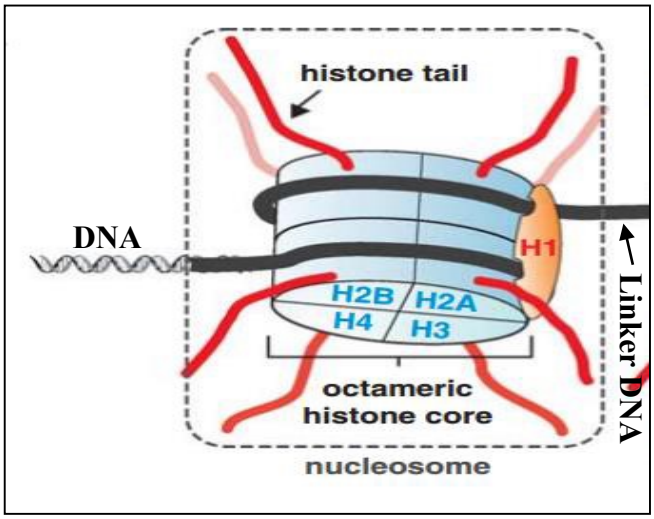

Figure 4: A modal for nucleosome structure in somatic cell showed the basic unit of packaging (nucleosome), which consists of two groups of the four core DNA-binding core histones: H2A, H2B, H3 and H4 (octameric histone core). In addition, linker histone (H1) is positioned on the side of the nucleosome core particle to stabilise the chromatin structure. Adapted from: (Füllgrabe et al., 2011)

1.2.3 Protamines

Protamines are small, highly basic sperm-specific DNA binding proteins synthesised in the final phases of spermatogenesis of many species, in which compacting the spermatid genome into an inactive transcriptional status (Balhorn, 2007). It has been suggested that protamines have originally evolved from a somatic-like histone protein precursor, through a protamine-like intermediate, via a mechanism of vertical evolution (likely mechanism of a frame-shift mutation). This evolutionary hypothesis allows protamine to acquire positively charged amino acids to form a compact structure with the negatively charged genomic DNA (Lewis et al., 2004). Protamines are only found in male gametes and consist of polypeptides of between 50-110 amino acids (molecular mass 4,000–12,000 Dalton). They are rich in arginine (up to 70%), which is responsible for the high protamine-DNA binding affinity (Kimmins and Sassone-Corsi, 2005). Protamines form a very complex structure with DNA.

In most species, the sperm nucleus contains two protamines, namely: protamine 1 (PRM1) and the family of protamine 2 (PRM2) (Biegeleisen, 2006). PRM1 has been reported in all analysed mammalian spermatozoa, whereas, PRM2 is formed by different components of the protamine 2 family (PRM2, PRM3, and PRM4) (Andrabi, 2007). Protamines are derived from four different genes on chromosome 16, however, not all of them are expressed in the same species (Oliva et al., 2006) (Figure 5).

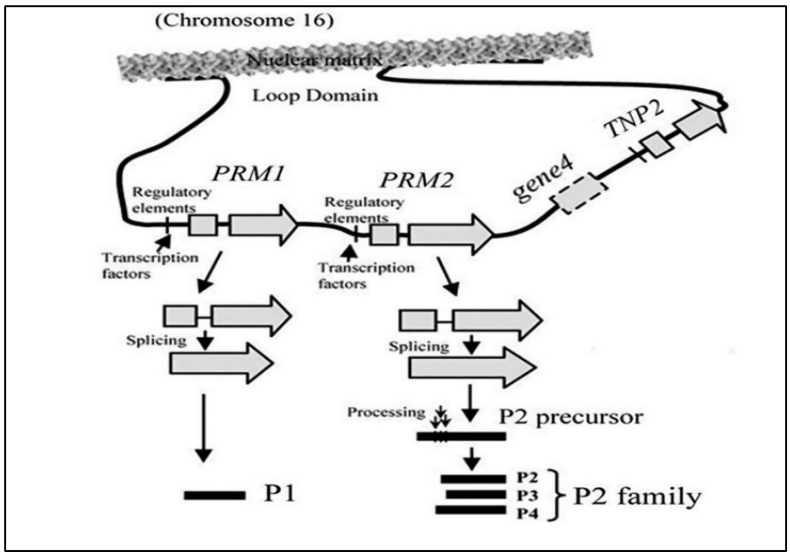

Figure 5: A genomic structure of protamine genes (protamine 1 and 2) in chromosome 16, which organised in a form of loop domain. The genomic sequences of the loop domain include transition protein 2 gene, a sequence of gene 4 and protamine 2 family (PRM 2 consists of protamine 2, 3 and 4 components). Adapted from (Francis et al., 2014)

PRM2, for example, is only present in few mammals, and it is slightly larger than PRM1 with 63 amino acids in mice for example (Chauviere et al., 1992). However, most mammals, such as bovine sperm nucleus express only PRM1, which is highly cross-linked by disulphide bridges (Balhorn, 1982), whereas humans and mice express both PRM1 and PRM2 (Kimmins and Sassone-Corsi, 2005). Protamines form disulphide bonds as post-translational modifications during epididymal transit in late spermatogenesis to achieve maximally condensed sperm chromatin (Villani et al., 2010). In sperm, it has been reported that several species have differences in the number of disulphide bonds based on the type of protamine present in the nucleus.

Previous studies of human sperm have determined that alterations in PRM1/PRM2 ratio can lead to nuclear immaturity (Colleu et al., 1996) and that reduced integrity of sperm DNA is correlated with altered ratios of protamines (Aoki et al., 2005). For example, according to Balhorn et al. (1988), the PRM1/PRM2 ratio in normal sperm samples was 0.98 ± 0.12 compared to 1.58

± 0.24 in infertile patients. In addition, a reduction in PRM2 has been reported in some infertile men that may be related to subsequent abnormal embryo development (Oliva, 2006; Torregrosa et al., 2006). Therefore, it seems that protamines have various functions, and as a result, studying the origin of the protamine contribution among different species, might help to understand the impact of protamine deficiency on sperm DNA integrity and fertilisation. Both histones and protamines, are thought to be essential for DNA packaging and repackaging during spermatogenesis and formation of the paternal pronucleus (Miller et al., 2010). In mammalian sperm, in late stages of spermatogenesis (spermatid stage), most canonical histones and the testis-specific histone variants are removed and replaced with transition protein (TP1 and TP2), which are then replaced by protamines (Meistrich, 1978; Johnson et al., 2011).

1.2.4 Sperm chromatin reorganisation by histone-protamine replacement

In mammals, sperm nuclear status is determined by two remarkable events that occur during spermatogenesis, namely nuclear maturation and replacing the somatic-histones with protamines (Agarwal and Said, 2003). During the formation of spermatozoa, the chromatin condensation mechanism is primarily based on histone replacement. Although the histone removal mechanism is incompletely understood, experimental evidence suggests that it occurs in three phases (Gaucher et al., 2010). These phases are nucleosome instability, histone hyperacetylation, and histone replacement (first by transition proteins and then by protamines) (Gaucher et al., 2010). Sperm DNA is packaged in this particular manner to keep the chromatin in a volume that can be accommodated within the unusually small sperm nucleus (Dadoune et al., 2004). In the somatic cell nucleus, 160-200 base pairs of DNA is wrapped twice around a histone octamer

(nucleosome) (Figure 4) (Gilbert et al., 2004), and then further wound to form solenoid domains (Figure 5). This type of histone-based DNA packaging, typical of somatic cells, leads to a lower condensation state compared to sperm cells. Nucleosome size and their packaging into solenoids is a limiting factor in the efficiency of DNA condensation. In the mammalian sperm nucleus, however, protamines replace histones as the dominant DNA binding protein, and the DNA-protamine complex is coiled into a doughnut (toroid) shape configuration, which ensures packaging into the smallest possible space (Figure 6). The length of DNA that can be packaged into the protamine-based toroidal structures is approximately 50 kb, which provides greater compaction than that available in a typical somatic cell nucleus (Miller et al., 2010). Typically, the chromatin of mammalian spermatozoa is ten times more condensed than in the interphase nuclei of somatic cells (Figure 6) (Pogany et al., 1981; Wiland et al., 2016).

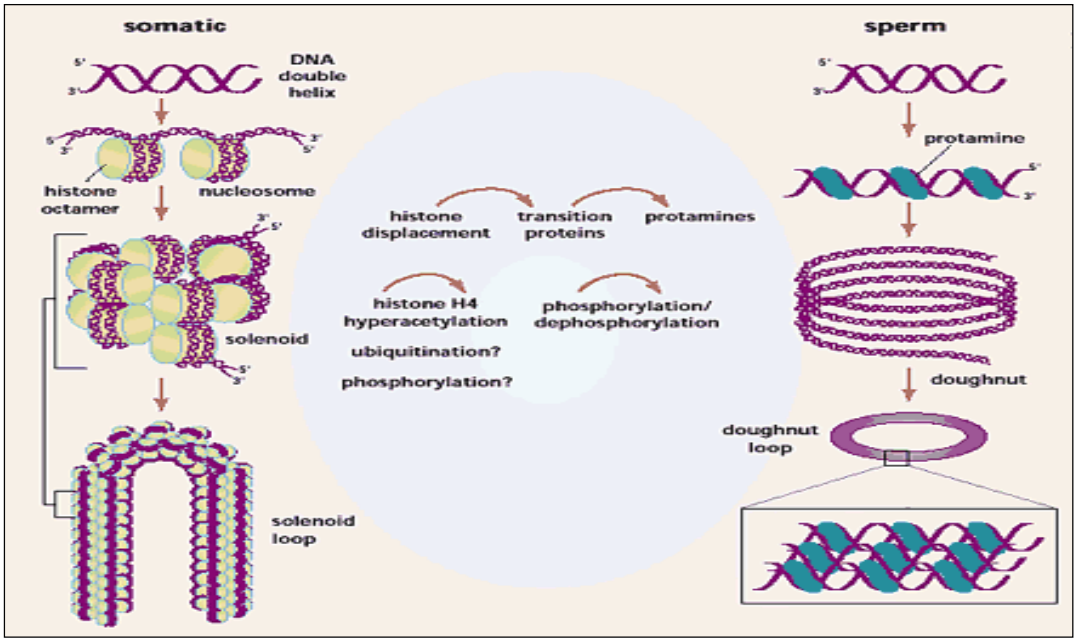

Figure 6: A model of DNA packaging in somatic cell and mammalian sperm (right). In somatic nucleus, nucleosome is formed by wrapping the DNA twice around histone octamers, which are then accumulated in a coiled pattern to form solenoid loop. Whereas, in sperm nucleus, histones are replaced by protamines, which are then bind to the DNA and then coiled into a doughnut domain. The protamine-DNA complex show a tight compacting of chromatin. Histone replacement is supported by modifications of histones such as histone H4 acetylation, phosphorylation and ubiquitination. Adapted from: (Braun, 2001)

To achieve this level of condensation, protamine first binds to the minor groove of the DNA strand and later, the DNA-protamine complexes fits into the major groove of adjacent DNA-protamine complex to package the DNA into toroidal stacks within the sperm nucleus (Balhorn, 1982) (Figure 7). Therefore, packaging DNA by protamine makes the DNA highly stable. Moreover, this more highly condensed chromatin may help to optimise sperm head shape and so help achieve optimal motility. Furthermore, higher compaction could serve to protect the DNA from extraneous damage (Schulte et al., 2010). Sperm quality may therefore depend on the unique structural and organisational aspects of its DNA packaging. In humans and probably other mammals, the condensation of sperm chromatin commences at the posterior end of the nucleus and proceeds apically towards the anterior end (Dadoune, 1995). How is this repackaging achieved? Previous studies observed a wave of histone acetylation during spermatogenesis, which can be considered one of the first signals for the DNA repackaging process (Grimes and Henderson, 1983; Palmer et al., 1990; Tanphaichitr et al., 1978) (Figure 7). According to Govin et al., (2004), an acetylation signal for histone hyperacetylation was detected during condensation of many metazoan spermatids. Another study showed that histone acetylation may cause alterations in nucleosome-DNA stability that leads to their destabilisation (Benson et al., 2006). Furthermore, the direction of DNA packaging seems to be occurred in parallel with the direction of histone acetylation (from the posterior to the anterior end) (Hazzouri et al., 2000a), which indicates that histone hyperacetylation mechanism is an initiation point of histone-protamine replacement as well as chromatin remodeling (Govin et al., 2004).

DNA is organised into loop domains attached to a nuclear matrix (Klaus AV et al., 2001) and the reorganisation in spermatozoal chromatin may occur at four levels. Firstly, sperm DNA attaches to the nuclear annulus (chromosomal anchoring). Then, the DNA binds to the nuclear matrix at matrix attachment sites (MARs) and forms DNA loop domains with an average size of ~27 kb within the sperm nucleus (Kramer and Krawetz, 1996). As a result of replacing histones by protamines, DNA is reorganised into the compact toroidal units described earlier (Barratt et al., 2010) (Figure 7). The final step is a rearrangement, whereby chromosomes are positioned in a non-random pattern (Agarwal and Said, 2003) within the nucleus (including the sperm nucleus). Zalensky and Zalenskaya (2007) demonstrated that chromosomes are not randomly distributed in the sperm nucleus and that centromeres are located at the centre of the nucleus, with telomeres paired around the periphery of the sperm cell.

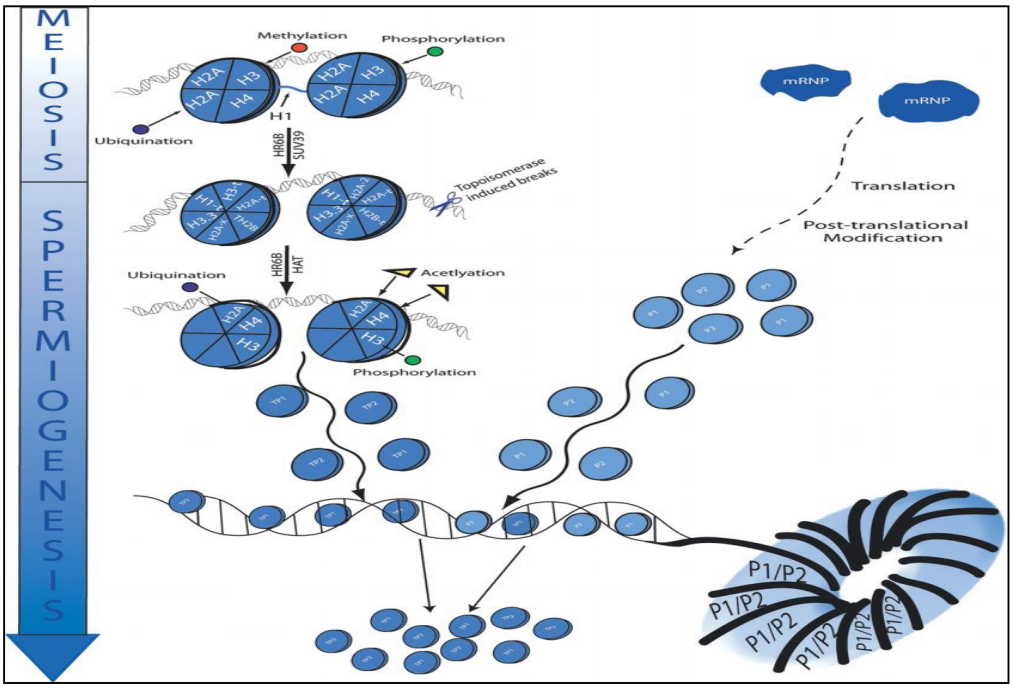

Figure 7: A model highlighted the key factors throughout histone-protamine exchange. During spermatogenesis, testis-specific histones are replaced by the transition proteins, following the action of hyperacetylation of H4, which is the key factor in DNA repackaging process. In sperm maturation stage, protamine 1 and 2 undergo binding to DNA and replace the transition proteins. Adapted from: (Carrell et al., 2007)

1.2.5 Post-testicular sperm nuclear maturation

The mature spermatozoa are released from the Sertoli cell compartment into the lumen of the seminiferous tubules, before sperm transport to and through the epididymis where they undergo post-testicular maturational changes essential for supporting fertilization. This process is called sperm maturation, where sperm undergo many structural modifications, including lipids and proteins, and develop the forward motility (Clermont, 1972). In this final stage, disulphide bonds between protamine molecules are established to stabilise sperm chromatin condensation (Katz, 1983).

1.3 Importance of histones retention in the mature sperm nucleus

Despite the general histone replacement process in spermatogenesis, some nucleosomes remain in mature sperm as all canonical histones can be detected (Gusse et al., 1986; Zalensky et al., 2002; Hammoud et al., 2009; Arpanahi et al., 2009). There are two hypotheses for the incomplete histone-protamine replacement in the mature sperm nucleus. Nucleosome retention occurs naturally and nucleosomes are randomly distributed in the nucleus with no functional status (Mao et al., 2010). Alternatively, nucleosomes are non-randomly distributed because they either were functionally important during spermatogenesis or will become functionally important following fertilisation (Van der Heijden et al., 2006; Vavouri and Lehner, 2011).

Experimental evidence has shown that sperm chromosomes are not randomly distributed in the sperm nucleus. A previous study, for example showed that sperm chromosomes are arranged in the same location from cell to cell (Hazzouri et al. 2000). Other studies using Chromatin Immunoprecipitation with DNA sequencing (CHIP-seq), or microarraying (CHIP-chip) (Hammoud et al., 2009)

reported that histone retention is associated with chromatin domains containing important developmental gene promoters or regulators and imprinted loci, indicating that these gene sequences are also likely to be non-randomly distributed. As sperm nucleosomes (including those with modified histones (Miller et al., 2010)) must be transferred to the oocyte (Teperek and Miyamoto, 2013), many studies suggest by retaining histones and protamines, DNA packaging of the sperm chromatin transfers an important epigenetic signal to the zygote (Hammoud et al., 2009). Therefore, chromatin repackaging itself and its epigenetic characteristics may be a significant hereditary component of the male gamete.

Differential nuclease sensitivity of sperm chromatin also suggests a conserved potentially functional aspect of DNA packaging in these cells. A number of studies have reported that certain domains of sperm chromatin are more sensitive to digestion with endonucleases because these domains contain the retained sperm nucleohistones (Arpanahi et al., 2009). Analysis of the DNA released by micrococcal nuclease (MNase) digestion of sperm chromatin, for example suggests that endonuclease sensitive compartments are highly enriched in regulatory sequences important in development. These regulatory sequences include CCCTC binding factor (CTCF) and gene promoter sequences (Arpanahi et al., 2009). In human sperm, for example, major regulators of embryonic development, such as *HOX* genes, that normally regulate important developmental processes in the embryo are associated with nucleosomes (Govin et al., 2010). Moreover, several investigations have shown that some sperm nucleohistones carry methyl or acetyl modification patterns with a specific distribution, which might also have influences on the expression of paternal DNA

in the zygote and early embryonic development (Pittoggi et al., 1999; Li et al., 2008; Hammoud et al., 2009). Methylation of DNA, which is commonly located on the 5 carbon of cytosine residues (5-mC), is considered to be important for epigenetic regulation in various types of cell (Figure 8). Similarly, it has been suggested that retention of modified histones in sperm may be because they play a role in epigenetic phenomena in the early zygote after fertilisation (Miller et al., 2010).

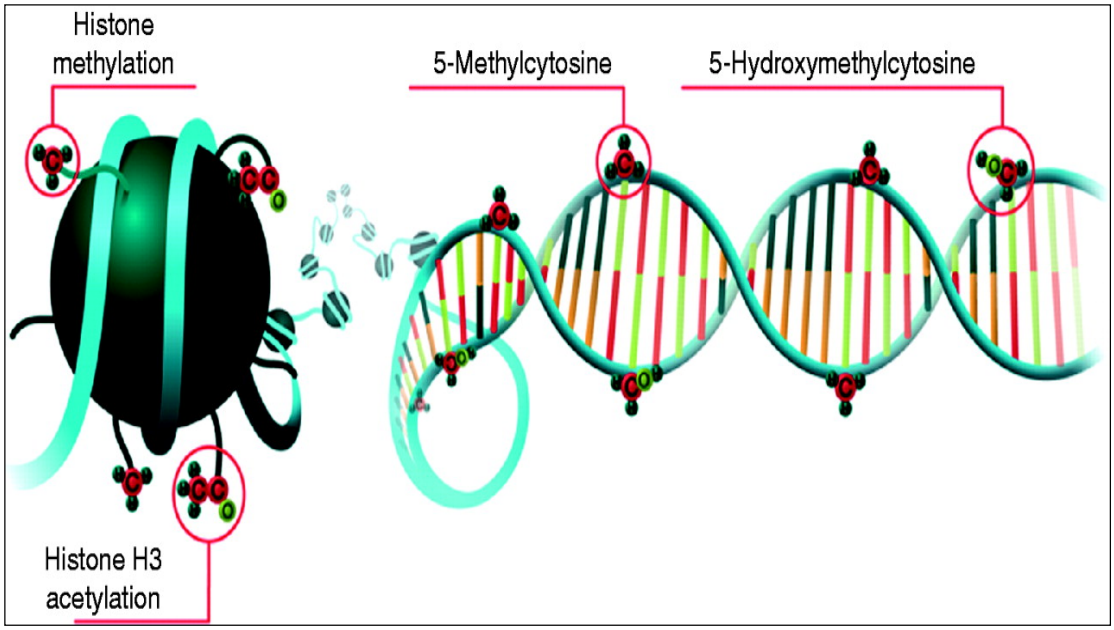

Figure 8: A model for DNA methylation and histone modifications regularly found in the sperm nucleus, showed the histone tail methylation and acetylation, in addition, 5-methylcytosine (5-mC), histone H3 acetylation and 5-hydroxymethylcytosine, which are believed to play a crucial role in gene expression and support gene activation. Adapted from: (Jenkins and Carrell, 2012).

While modified sperm nucleosomes may play a crucial role in normal embryo development, Kono (Kono et al., 2004) produced viable mouse offspring from two haploid sets of maternal genomes. These viable parthenogenetic embryos were developed from reassembled zygotes by introducing fully grown oocytes into non-growing eggs (MII stage). The second eggs were knocked out for *H19* and *Igf2* genes before being injected into the wild-type oocytes. Both genes were expressed in parthenogenetic embryos and moreover, normal pups were born.

These findings showed that viable parthenotes (gynogenetic clones) can be generated without requiring the paternal genome, which indicated that paternal chromatin seems not to be essential at fertilisation (Miller, 2015).

1.4 The sperm nuclear matrix

Previous observations have suggested that the internal organisation of the eukaryotic cell nucleus is structurally supported by the nuclear matrix, a construct described originally in somatic cell nuclei by Berezney and Coffey in 1974 (Berezney and Coffey, 1974; Miller et al., 2010; Razin et al., 2014a). In addition, it was proposed that the nuclear matrix is protein-based, because it was not lost following treatment with DNAse (Wilson and Coverley, 2013). As in somatic cells, several studies have suggested that chromatin of the sperm nucleus is anchored to the nuclear matrix via loop domains (Ward and Coffey, 1990; Kramer and Krawetz, 1996). In the somatic nucleus, these nuclear matrix attachment regions have been found to be associated with actively transcribed genes (Ciejek et al., 1983). Sperm chromatin are thought to be ‘fixed’ to the nuclear matrix through site-specific sequences identified as Matrix Attachment Regions (MARs) (Figure 9) (Johnson et al., 2011). Despite the researchers’ finding that MARs are involved in the DNA-nuclear matrix attachment, however, there is no clear evidence for such molecular contributing (Razin et al., 2014a).

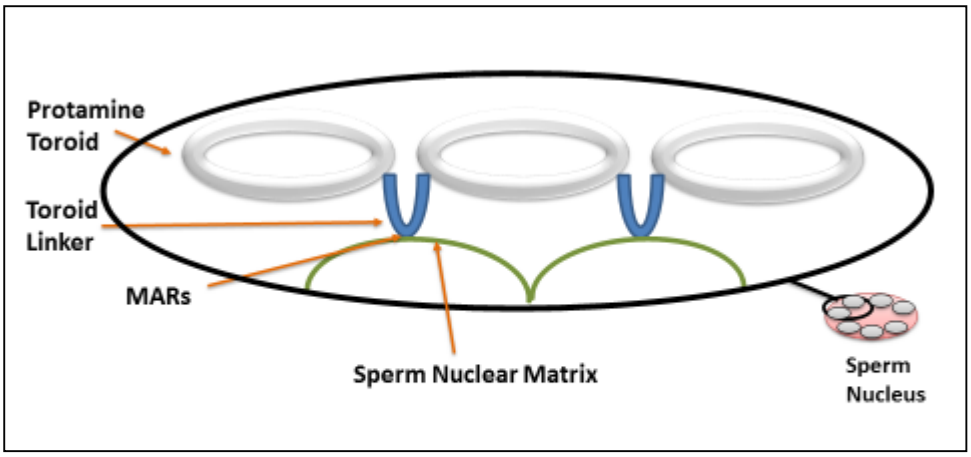

Figure 9: A model for protamine-DNA toroids, which are organised into loop domains (donut-shape) to form the sperm chromatin structure. These loop domains are attached to the nuclear matrix by toroid linkers (nucleosomal linker), which are suggested to be DNase-sensitive regions and located within MARs.

As indicated earlier, DNA loop domains are probably attached at their bases to the sperm nuclear matrix by MARs and MARs may play a crucial role in DNA replication by facilitating the transition from closed chromatin loops (condensed form most likely comprising the dispersion halo) to functional loop domains (accessible form, more closely associated with the matrix) (Ostermeier et al., 2003) (Figure 10). The differential sensitivity of the transcriptionally active genes to digestion by exogenous nucleases and the likely association of sites of transcription (and DNA replication) with the nuclear matrix also supports the notion of a more dynamic nuclear organisation at play in active cell nuclei (Cook and Brazell, 1980; Jackson, 2005). According to a study on human and mouse data (genome-wide nucleosome-positioning) that was investigating the chromatin structure, RNA polymerase II seems to play a role linking chromatin organisation and exon-intron structure (Schwartz et al., 2009).

Several studies have shown that these organisations also apply to sperm chromatin based on DNA sequence (Sotolongo and Ward, 2000; Nadel et al., 1995). Other findings have shown that the organisation of DNA loop domains in

sperm chromatin are necessary for initiating early embryonic development (Ward et al., 1999a; Sotolongo et al., 2005). Therefore, sperm chromatin organisation is likely to be a fundamental aspect of the paternal genome's ability to support the formation of a viable developmentally competent embryo.

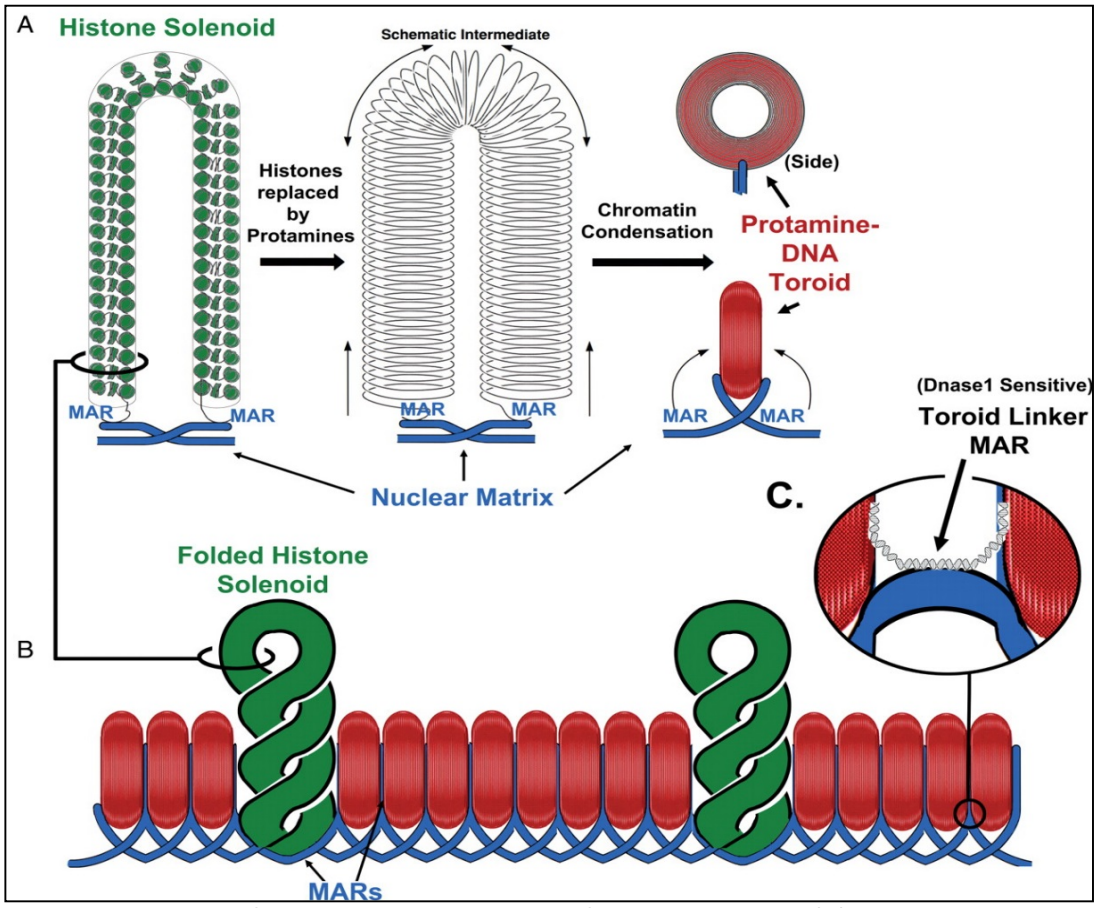

Figure 10: A model for the three major domins of sperm chromatin. (A) histone-protamine replacement during spermatogenesis, which package the DNA into tightly compacted toroids. (B) A suggested organisation of protaimine toroids that stack side by side and may be included some DNA retained histones (green solenoid). (C) The DNA strand that may be linked the protamine toroids and bound to histone as well as matrix attachment regions (MARs). Adapted from: (Ward, 2010).

Supporting the importance of the matrix, Ward and his team (Ward et al., 1999a) discovered that a sperm nuclear halo which contained a stable and intact nuclear matrix with its associated DNA was all that was required to support the ability of sperm to fertilise oocytes (by ICSI) and contribute successfully to the development of around 30% of viable embryos to live offspring. Additionally,

sperm nuclear matrices with intact MARs support the initiation of DNA replication, even when the bulk of the DNA has been removed. In contrast, ICSI of sperm with an unstable, detergent treated nuclear matrix failed to support the development of live offspring. Similarly, Shaman and his team (Shaman et al., 2007b) were able to generate paternal pronuclei by injecting restriction digested sperm nuclear halos (matrix attached) into oocytes, whereas, naked sperm DNA injected into oocytes, could not form pronuclei or support DNA synthesis. An earlier study (Mohar et al., 2002) used mouse sperm nuclei treated with an ionic detergent and 2 M salt to extract the nuclear matrix-unbound DNA. Such treated sperm nuclei supported 73% embryo development with normal mitotic chromosomal formation following injection into the oocyte. This embryo developmental rate was reduced to 32% after injection of the egg with sperm treated with an ionic detergent, 2 M of salt and dithiothreitol (DTT). Stewart and his team (Mounkes and Stewart, 2004) also have achieved live pups from a knockout mouse for Lamin B1 and B2 genes that have a role in chromatin organisation, however, these born alive mice suffered from heart defects, which lead to death at 10 weeks. Therefore, sperm DNA and an intact sperm nuclear matrix are needed to support normal development and the assumption that sperm DNA by itself is the only component that is required for embryo development remains controversial (Mohar et al., 2002).

Nevertheless, the whole concept of a nuclear matrix is still controversial as other observations of chromatin dynamics do not support the concept of the nuclear architecture (Jackson, 2005; Razin et al., 2014a). For example, chromatin dynamics in yeast nuclei contradict the concept of a fixed nuclear architecture in highly active eukaryotic cells (Jackson, 2005; Jackson, 2003). The existence of

an ‘independent’ dynamic DNA scaffolding structure has been challenged by others suggesting that the nuclear matrix is actually a ‘construct’ formed by DNA itself as it condenses and decondenses in response to transcriptional activity but does not exist as a functional structure in its own right (Razin et al., 2013). It is possible, however, to detect stable sites of DNA attachment to the nuclear matrix in inactive sperm nuclei (Kalandadze et al., 1990) and chicken erythrocytes (Razin et al., 1985). The detection of this type of higher order DNA organisation in transcriptionally inactive sperm and bird red cell nuclei (Bernardi, 2015) supports the likelihood that it exists independently of nuclear transcription.

1.5 The nuclear halo

The DNA dispersion nuclear halos consist of chromatin from which part or all of the associating DNA binding proteins (in sperm, for example, including histones and protamines) have been removed (Fernandez et al., 2005a; Shamsi et al., 2011). However, this displacement of DNA binding proteins does not necessarily cause loss of DNA from the nucleus because the DNA remains associated with particular attachment points throughout the nuclear matrix, which resists protein extraction (Figure 10). Nuclear halo formation most likely requires intact chromatin and an intact nuclear matrix. According to Ward et al. (1989), the sperm nuclear halo is comprised of extensions of about 46 kb of naked or relaxed loops of DNA spreading out from the nuclear matrix with the loops at their bases held fast by linkage to MARs (Shaman et al., 2006) (Figure 11).

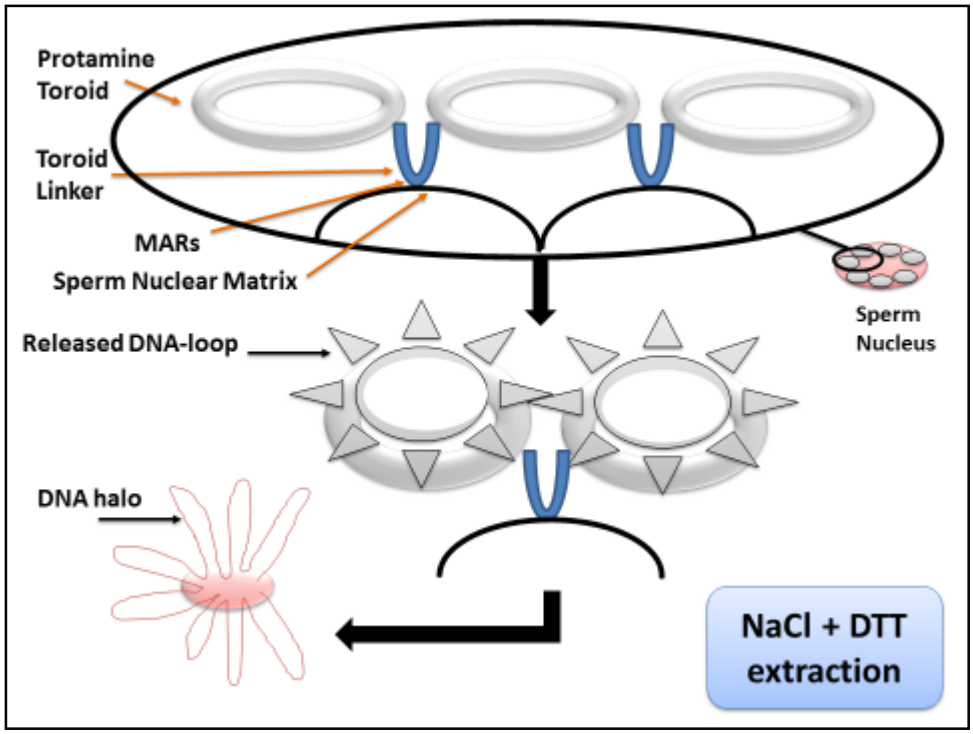

Figure 11: A model for protamine-DNA toroids, which are organised into loop domains (donut-shape) to form the sperm chromatin structure. Due to exposing sperm nucleus to NaCl and DTT treatment, these loop domains produced halo formation (after the nucleoproteins extraction), however, these loops were still attached to the nuclear matrix.

As indicated earlier, one model proposes that sperm DNA is packaged into toroidal structures with a 60-100 nm diameter by nucleoprotamines (Brewer et al., 1999). These structures seem to correspond to the loop domains forming the sperm halo after dispersion of supercoiled DNA (Aranda-Anzaldo et al., 2014; Ward et al., 1989). These toroids may be bound together by linker regions, probably packaged by nucleosomes that help to anchor the chromatin to the nuclear matrix (Shaman et al., 2007b; Ward et al., 1999a; Ward, 2010) (Figure 12). One possibility is that the final chromatin configuration in mature spermatozoa reflects where actively transcribed genes and origins of replication occurred in spermatogenesis (Kramer and Krawetz, 1996). The linker nucleosomes, however, cannot account for the amount of DNA that is not repackaged by protamines in mature sperm.

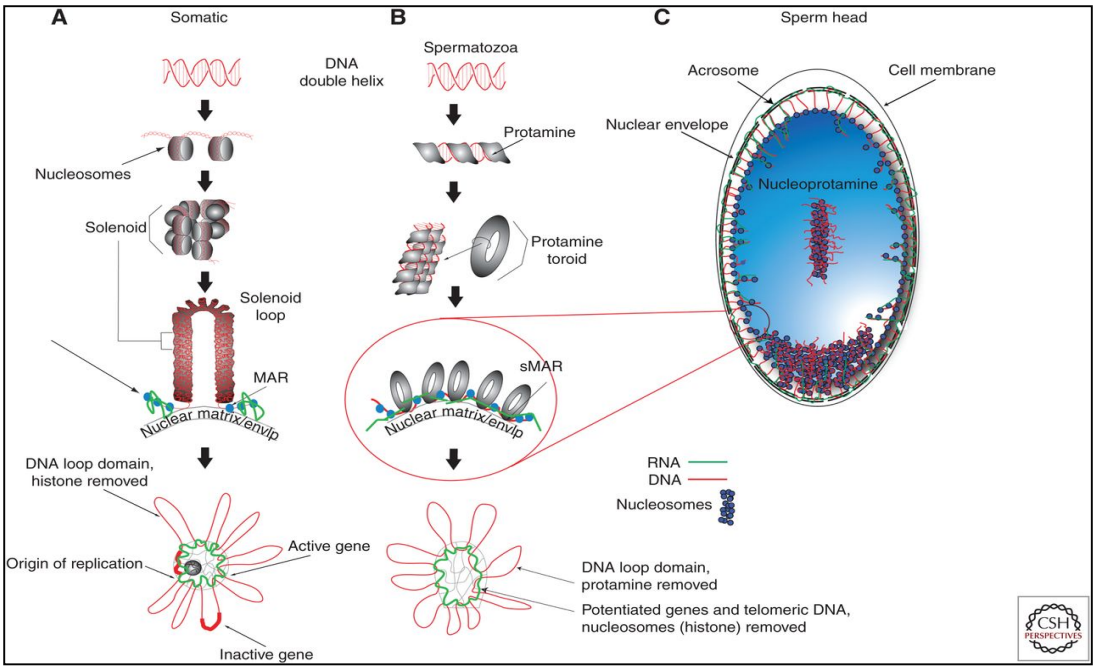

Figure 12: A model for DNA packaging in somatic cells (A), spermatozoa (B) and sperm head (C). In the nucleus of somatic cells, DNA is packed by nucleosomes into solenoid loop, which is proposed to be attached to the nuclear matrix through MARs. While, in spermatozoa, DNA is packed by protamine toroids into more complexed structure. By releasing the nucleohistones from nuclei by salt-extraction, halos are formed from DNA loops, which remain attached to the nuclear matrix. Adapted from: (Miller, 2015).

Methods for generating and visualising nuclear halos at the microscopic level are obtained by treating cell nuclei with salt solutions of varying strength, often containing detergents to extract soluble nucleoproteins (Galaz-Leiva et al., 2012b; Fernandez et al., 2003; Ward et al., 1999a). Comparable techniques have been used over the past forty years, aimed at understanding the chromatin structure and its accessibility to endonuclease digestion or salt solutions in relation to gene expression. Sanders M. (1978), for example, reported three different types of nucleosome fractions were released from somatic cells using three different concentrations of salt solutions. Following endonuclease digestion, 13% of the DNA was extracted using 0.2 M NaCl with no histone recovered and 30% of histone 1 (H1) was released by increasing the salt concentration to 0.3 M NaCl, whereas, the remaining nucleosomes were solublised by 0.6 M NaCl.

Similar salt extraction approaches have been taken to probe sperm chromatin composition (Gardiner-Garden et al., 1998; Olivares et al., 1993). These extraction techniques promote the dispersion of chromatin loops from the nucleus, which generate the matrix-attached dispersion halo of left-handed supercoiling DNA surrounding the compact, remaining nucleoid (Vogelstein et al., 1980). In the experiments reported herein (Chapter 2), high and low salt extractions were used to disturb the chromatin structure and produce dispersion halos. In addition, halos were obtained using the Halosperm^{TM} kit which is a commercially available sperm chromatin dispersion (SCD) test that provides a clinically relevant measure of DNA fragmentation (Fernandez et al., 2005a).

The extraction methods used by various investigators will generate dispersion halos in suspension equivalent to the Halosperm process. Similar processes have been used previously to characterize the nucleosomal component of sperm chromatin, reported to be enriched in critical developmental gene sequences (Hammoud et al., 2009; Arpanahi et al., 2009). No connection, however has ever been made between the halo sequences themselves and the DNA fragmentation that the dispersion halo measures. As the nucleosomal compartment represents more loosely packed sperm DNA, it is possible that compared to the protamine-bound compartment, this compartment is more susceptible to DNA damage. By digesting and sequencing DNA from the dispersion halo and its associated nucleoid, it should be possible to connect sperm DNA fragmentation (Fernandez et al., 2005b) with the paternally-derived DNA sequences that may play important roles in early embryo development.

1.6 Sperm DNA damage and its relationship with halo formation

Unrepaired DNA breaks may occur during the process of chromatin modification, and DNA damage can also be induced by external oxidative stress (Agarwal et al., 2003). The main factors that can exacerbate susceptibility to sperm DNA damage are defective chromatin packaging including protamine deficiency, endogenous endonuclease activity (Sakkas and Alvarez, 2010) and exogenous reactive oxygen species (Shafik et al., 2006). Additional external factors may also cause sperm DNA damage, such as testicular hyperthermia, cigarette smoking, and chemotherapy (Zini and Sigman, 2009) (Figure 13). Previous studies on sperm chromatin organisation have concluded that the way chromatin is packaged in the sperm nucleus could leave it susceptible to DNA fragmentation that may have substantial developmental consequences (Miller et al., 2010).

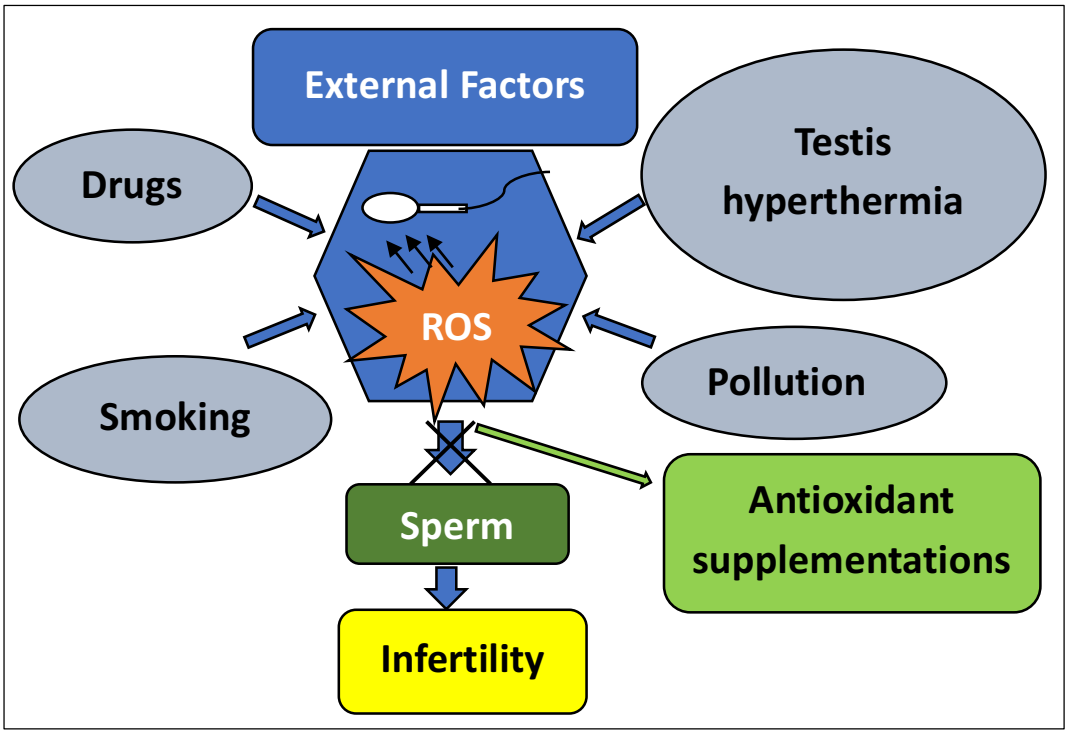

Figure 13: Major causes of sperm DNA damage as external factors, for example drugs, smoking, pollution and testis hyperthermia, which negatively affect sperm functions due to the accumulation of Reactive Oxygen Species (ROS). Also, the importance of antioxidant supplementations and their role to avoid sperm dysfunction and consequently, infertility.

The incidence of sperm DNA fragmentation may increase rapidly when samples are handled in vitro. For example, under IVF condition, an increased rate of DNA fragmentation of proven fertility samples was observed after 4 hours of incubation at 37°C, which gives an increase in DNA fragmentation of 8.3% per hour (Gosálvez et al., 2009). Sperm DNA damage is believed to be associated with male infertility and for that reason, quantifying sperm DNA damage might be a useful way to diagnose paternal infertility (Aitken and De Iuliis, 2007; Evenson et al., 2002). According to (Saleh et al., 2003), DNA fragmentation is significantly increased in men with male factor and idiopathic causes, as well as failure to initiate a pregnancy. The chances of the female partner achieving successful pregnancy is lowered when the DNA fragmentation index of her partner's sperm is 30% or higher (Shafik et al., 2006). A high rate of spontaneous pregnancy loss was observed in semen samples with >30% sperm DNA fragmentation (Zini et al., 2005). In addition, patients with abnormal sperm morphology, count and motility were found to have high levels of DNA fragmentation (Agarwal and Said, 2003; Schulte et al., 2010).

Interestingly, numerous studies have mentioned that the incorporation of histone variants in sperm chromatin leads to nucleosome instability (Bönisch and Hake, 2012; Gaucher et al., 2010). Moreover, other studies have determined that sperm from infertile patients were found to display sperm chromatin abnormalities related to protamine deficiency (Denny Sakkas, 1999). For example, PRM2 deficiency leads to sperm DNA fragmentation and early embryo death in mice (Cho et al., 2001). Consequently, these alterations in sperm chromatin remodelling may cause catastrophic DNA damage during spermatogenesis (Sakkas et al., 1999).

In recent years, the scientists have turned their intention to reactive oxygen species (ROS) that are generated naturally in the male reproductive tract and which cause oxidative stress. Although some ROS is needed during sperm maturation, excessive ROS, however, will be harmful (Agarwal and Allamaneni, 2004). Between 25% to 40% of infertile patients were reported to have high levels of ROS in their semen (Agarwal and Said, 2003; Agarwal et al., 2014). Other studies have stated that 40% to 88% of infertile men have high levels of ROS (Pasqualotto et al., 2000; Noblanc et al., 2014). Oxidative stress can be caused by an accumulation of ROS production, which resulted in an adverse effect on sperm motility, viability and acrosomal status (Agarwal et al., 2014) (Figure 14).

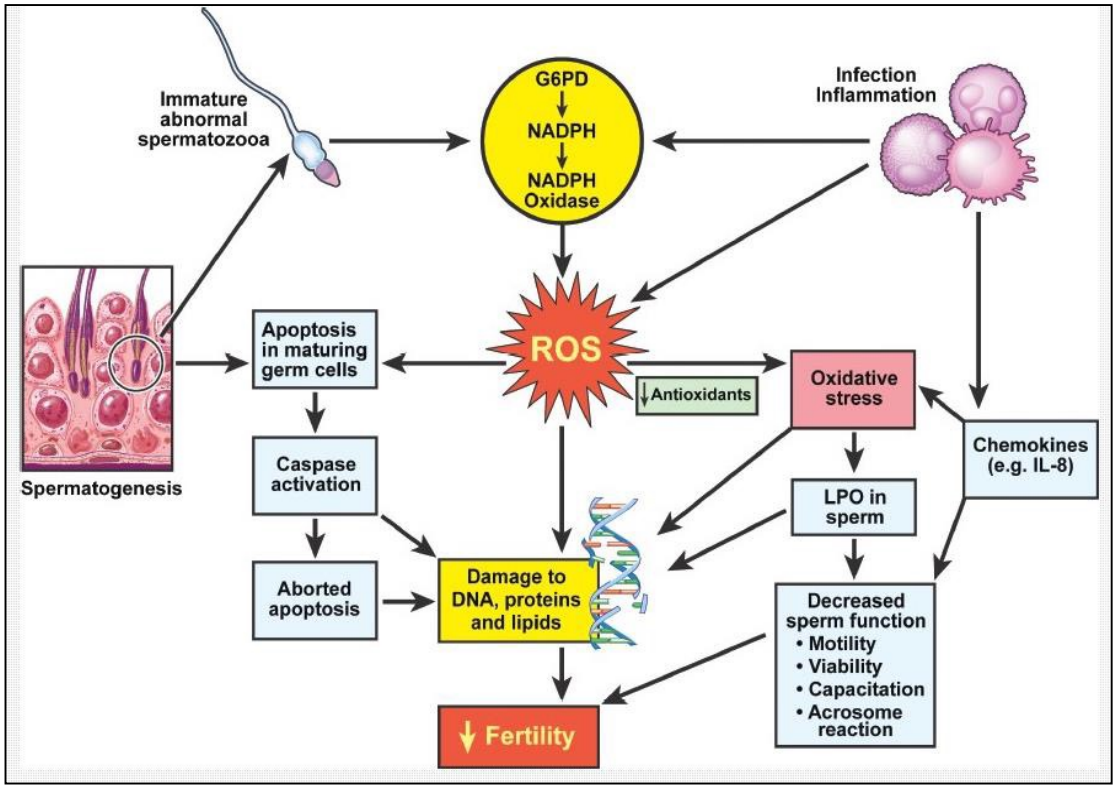

Figure 14: Various mechanisms of ROS generation in human semen, which therefore, may leads to apoptosis in maturing germ cells as well as damage the sperm DNA, proteins and lipids. Additionally, high level of ROS in the semen fluid may causes decrease in sperm function such as motility, viability, capacitation and acrosome reaction, which consequently lead to infertility. Adapted from: (Agarwal et al., 2014)

In addition, other studies have determined that oxidative stress is associated with different mechanisms of infertility in males with testicular varicocele (Enciso et al., 2006b; Cortés-Gutiérrez et al., 2016). Sperm are particularly susceptible for oxidative stress, because their membranes contain a high amount of polyunsaturated fatty acids (PUFAs) (Agarwal et al., 2014). These lipids consist of unconjugated (carbon-carbon) double bonds and methylene group. ROS attack these double bonds of lipids causing hydrogen abstraction from a carbon and oxygen insertion, which resulting to form lipid peroxyl radicals. These lipid peroxyl radicals abstract hydrogen from another lipid molecules and form lipid peroxides, which produce a large amount of aldehydes due to lipid fragmentation. This cytotoxic products can lead to loss of membrane integrity, and eventually diffuse through the cell membrane, which subsequently modifies any protein in the nucleus and cause cellular damage (Ayala et al., 2014). Some common oxidation products can be used as biomarkers of oxidative DNA damage including 8-hydroxyguanosine, protein carbonyls and nitrotyrosine (Castellani et al., 2008).

Two factors are thought to protect sperm DNA from ROS attack; compact DNA packaging and the presence of an antioxidant in seminal fluid. An imbalance between ROS production and antioxidant activities in semen may causes seminal oxidative stress (Saleh et al., 2003). Although, antioxidants are naturally found in the body, vitamin supplements including vitamin C and vitamin E may reduce oxidative damage to human sperm (McCall and Frei, 1999). Furthermore, in humans, a number of substances, such as pentoxifylline and caffeine can be added to the ejaculated semen in order to stimulate the sperm motility by protecting sperm from the impact of ROS (Henkel and Schill, 2003).

Numerous assays have been used to evaluate the relationship between the level of DNA fragmentation and the rate of fertilisation and embryo development. In recent years, various rapid molecular-based techniques have been used to measure sperm DNA damage and chromatin structure, including the TUNEL assay, Comet assay, Sperm Chromatin Structure Assay (SCSA), Sperm Chromatin Dispersion (SCD) test (Halosperm) and Acridine Orange (AO) staining (Agarwal and Said, 2004).

Like the SCD, the comet assay measures sperm DNA integrity (Hughes et al., 1999), although the latter relies on a diffusion rather than dispersion type of halo (Fernandez et al., 2005b; Cortés-Gutiérrez et al., 2016; Sestili et al., 2006). Halos of different sizes are often generated by these methods, reflecting the original DNA integrity of the extracted nuclei. With dispersion, sperm with damaged DNA (single or double-stand breaks) display small or no halos, whereas, extended halos are generated from sperm nuclei with little or no DNA fragmentation. The reverse is the case with diffusion halos. In the dispersion halo, the different halo sizes are due to the release of internal torsional stress that follows removal of the normally counterbalancing DNA binding proteins (Galaz-Leiva et al., 2012a). The torsional stresses are set up by the nuclear matrix anchoring the chromatin against the compression stress generated by compaction of the paternal genome into a relatively small space (Aranda-Anzaldo et al., 2014) (Figure 15). These halos should not be confused with those arising following DNA unwinding in alkaline solutions where (diffusion) halo sizes and hence the extent of DNA fragmentation is determined by diffusion of fragmented DNA from the nucleus (Fernandez et al., 2005a).

As indicated above, the commonly used comet assays (alkaline and neutral) depend on the generation of diffusion halos (Tomsu et al., 2002; Simon and Carrell, 2013; Simon et al., 2011b). However, unlike dispersion halos that quantify damage by measuring halo size, comet assays quantify the amount of damage by dragging the fragmented halo DNA into a tail under the influence of an electric current (Cortés-Gutiérrez et al., 2015; Fang et al., 2015) (Figure 15). These differing approaches should in theory detect fragmented DNA equally but subtle differences in sample processing may lead to different sensitivities and even to the measurement of different aspects of DNA fragmentation (Pérez-Cerezales et al., 2012).

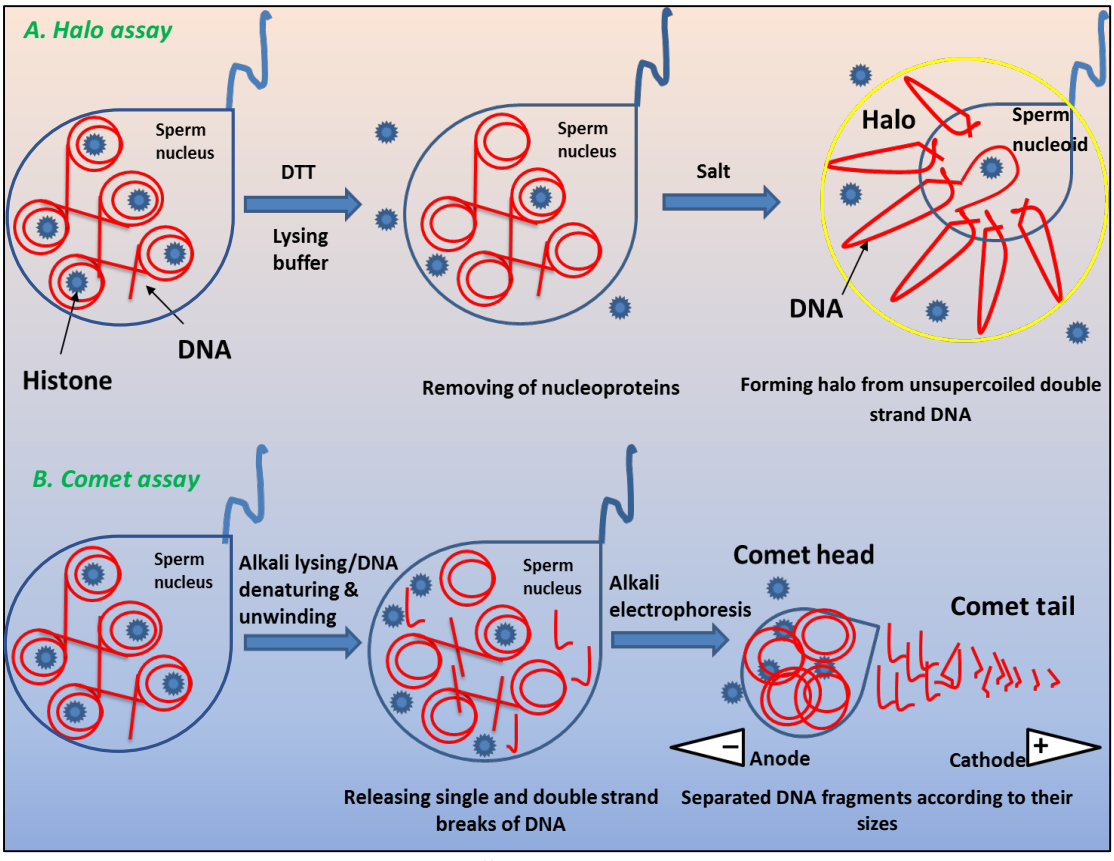

Figure 15: A diagram showed the main differences between the sperm chromatin dispersion assay used by Halosperm and the alkaline comet assay. (A) Halo formation through DTT-lysing buffer incubation and then salt extraction. (B) Comet tail formation through DTT-lysing buffer and then alkaline denaturation and unwinding of single and double strands and then releasing of the comet tail due to DNA breaks migration. The difference between the two extraction processes is minimal. Halosperm uses an acid extraction buffer, while comet uses an alkaline buffer.

1.7 Sperm chromatin remodelling after fertilisation

Paternal chromatin must be unpackaged following fertilisation to support embryonic development. The successful spermatozoon must undergo extensive molecular remodelling from highly condensed and transcriptionally inactive chromatin into a transcriptionally accessible and potentially active form. Many of the required structural changes to the paternal genome correlate with nucleoprotamine replacement by nucleohistones, which occur in the first 2-4 hours after fertilisation and is essential for pronuclear formation (Ward, 2010). Several techniques including immunocytochemistry have revealed that protamines are completely removed from the male pronucleus after anaphase II (Rodman et al., 1981). In a porcine study, it was shown that approximately 80% of the protamines were removed from the paternal chromatin within 3 hours post-fertilisation (Jenkins and Carrell, 2012) (Figure 16).

The dramatic exchange of protamines by oocyte-supplied histones is called histone-assembly activity (McLay and Clarke, 2003). Subsequently, when protamines are completely replaced, the sperm chromatin becomes hyperacetylated and therefore, more openly accessible to transcription factors as in somatic cells (Perreault et al., 1988; Rodman et al., 1981) (Figure 16). Differences in the parental chromatin demethylation dynamics after fertilisation and the moment that the demethylated chromatin of materal genome is wrapped around nucleosomes providing access to demethylating enzymes, supports the hypothesis that paternal DNA may be without packaging proteins for a brief period after protamines are removed and before replacement by histones (Spinaci et al., 2004).

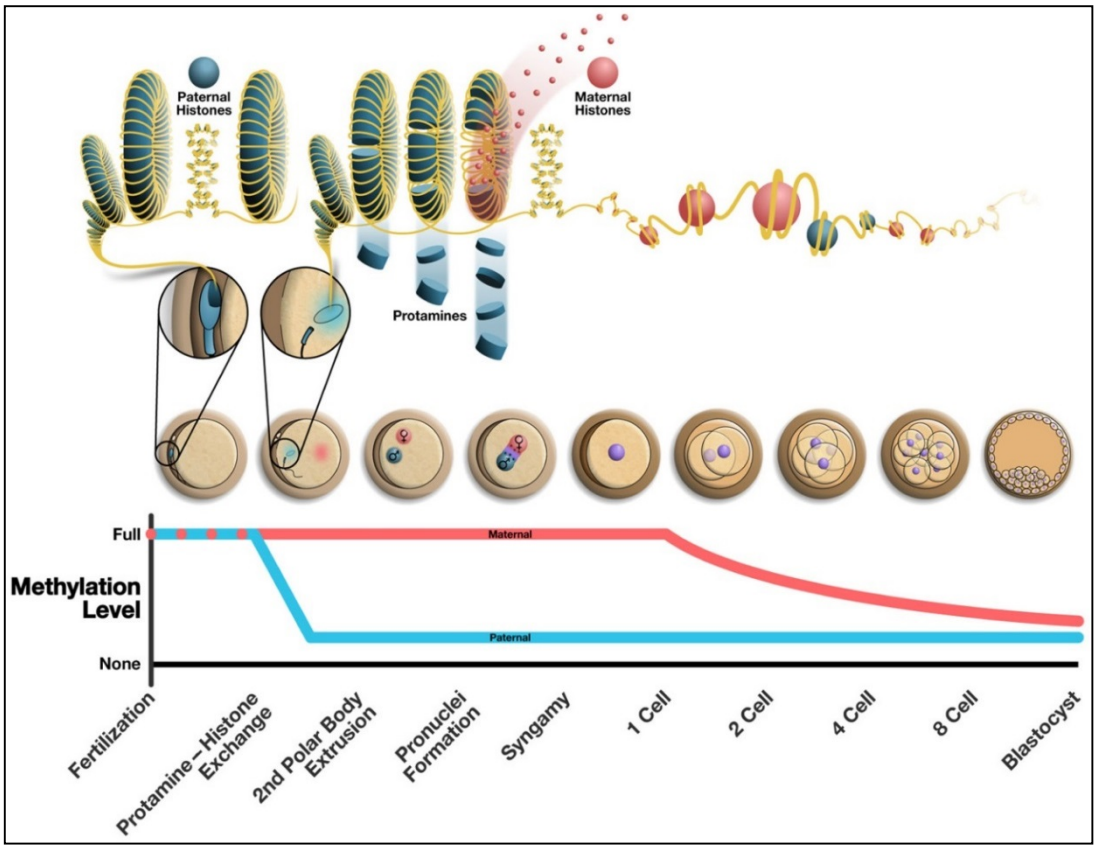

Figure 16: A model for paternal DNA decondensation and some epigenetic markers post-fertilisation. After gamete fusion, the paternal mature sperm undergo protamines replacement by maternal histones resulting in the expanding of sperm head. In addition, it demonstrates the methylation status that occurs following fertilisation in the paternal and maternal pronucleus. Adapted from: (Jenkins and Carrell, 2012)

Many studies suggest that sperm chromatin remodelling is managed by the oocyte after fertilisation (Spinaci et al., 2004). This was concluded by inhibiting protein synthesis during oocyte maturation, leading to incomplete sperm chromatin remodelling (McLay and Clarke, 2003). Moreover, in mouse embryos, sperm chromatin obtains acetylated histones from the maternal ooplasm (Wu et al., 2008) and the male genome is actively demethylated shortly after fertilisation (Li et al., 2013). However, maternal histones slow sperm histone acetylation and female DNA demethylation occurs only after the two-cell division (Santos et al., 2002; Seisenberger et al., 2013). According to Aoki et al. (1997), the replacement of protamines by oocyte histones after fertilisation provides an opportunity for transcriptional factors to gain access to paternal DNA. Therefore, replication and

transcriptional activities start earlier in the male than in the female pronucleus at least in the mouse (Adenot et al., 1997). With respect to paternal and maternal pronucleus formation, the paternal genome is likely to be primed for transcription, and the enrichment of sperm promoter regions and CTCF binding sites by active histone modifications supports this idea (Hammoud et al., 2009). For example, CpG islands seem to be located close to or even within promoter regions of housekeeping genes (Rajender et al., 2011). Castillo et al. (2014a) showed that promoters packaged in sperm nucleosome are enriched in CpG islands. In addition, histone H4 acetylation may functionally cooperate with sites of DNA methylation at CpG islands to activate transcription in early zygote development (Lusser, 2002; Van der Heijden et al., 2006).

1.8 Linking sperm chromatin packaging and DNA damage with compromised embryonic development

Spermatozoa with damaged DNA still have the potential to fertilise the egg; however previous experimental observations showed that embryo development was frequently compromised depending on the extent of DNA fragmentation (Rybar et al., 2004; Ahmadi and Ng, 1999). Sperm chromatin organisation including incomplete protamination of sperm DNA packaging may lead to abnormal chromatin repackaging that is critical for early embryo development (Loutradi et al., 2006; Cho et al., 2003), probably due to increased DNA fragmentation, which subsequently harms embryonic development (Ioannou et al., 2016). Increased levels of sperm DNA fragmentation may contribute to implantation failure (Carrell, 2003), and also higher rates of early pregnancy loss (Aoki et al., 2005; Keel, 2010). In human, the effect of sperm DNA fragmentation

is observed at each stage of embryo development and most notably following zygotic transcriptional activation (4-8 cells stage), when the embryo shifts from a maternal to an embryonic gene expression programme (Simon et al., 2014). As nucleosome retention seems to be associated with promoters of some signaling and developmental transcription factors such as *NANOG, OCT4* and *SOX2* (Carrell and Hammoud, 2010), the correct positioning of nucleosomes in sperm chromatin may be important for ensuring that nucleosome-packaged genes are poised and more accessible for activation during embryo development (Vavouri and Lehner, 2011), (Arpanahi et al., 2009; Saida et al., 2011; Hammoud et al., 2011). As developmental genes are probably packaged into nucleosomes in sperm, they might be at greater risk of exogenous DNA damage as nucleosomal regions are in a more structurally open conformation that is less protected from iatrogenic factors than protamine-bound regions (Kong et al., 2012).

According to Hammoud et al. (2011), the outcome of histone modification analysis from sperm of infertile men and couples with embryonic failure suggests that nucleosomes may be more randomly distributed in infertile men, which could also make the sperm DNA more vulnerable to damage. Excessive genotoxic damage in developmental promoter sequences may make them incompetent for early transcription processes after fertilisation (Simon et al., 2014). Correct packaging of sperm DNA may also transfer an epigenetic signal to the zygote (Stuppia et al., 2015), alterations of which might lead to abnormal embryo development (Stuppia et al., 2015; Oliva and Ballescà, 2012). Where there is an abnormal reduction in the retention of nucleosomes (with or without modified histones) at imprinted loci or on developmental promoters, embryogenesis may be compromised.

Although the relevance of correct sperm chromatin packaging and DNA integrity to embryonic development is clear, the mechanistic impact of their deregulation is still unclear. In the sperm nucleus, DNA damage can have many different causes during spermatogenesis including apoptosis, single or double strand breaks, damage incurred during chromatin reorganisation and fragmentation induced by endogenous or exogenous factors including high levels of ROS (Sakkas and Alvarez, 2010). Several assays have been developed to assess sperm DNA fragmentation, including Acridine orange, Tunel, Comet and Sperm Chromatin Dispersion (SCD) assays. The SCD has been commercially developed for clinical use as the Halosperm™ assay, where there is a relationship between halo size and the extent of DNA fragmentation in sperm nuclei (see Chapter 1, section 1.5). As the sperm halo is likely to be dependent on the relationship between DNA and its binding proteins, it is a good model for connecting regions that are most susceptible to sperm DNA damage with gene sequences that are crucial for the development of embryogenesis. Investigating the halo, including its relationship to nucleosome retention and its DNA sequence composition might help to mechanistically link the assay with developmental anomalies such as, for example, the higher rates of miscarriage in infertile couples (Robinson et al., 2012; Coughlan et al., 2015).

Thesis aims and objectives

The hypothesis of this research predicts that histones but not protamines would be released from sperm nuclei during halo formation. Moreover, halo fractions are enriched with DNA sequences for developmental genes that play important roles in early embryo development following fertilisation. These embryonic developmental genes including transcription factors are packaged by retained nucleosomes. To test this hypothesis, my research programme has the following objectives;

- Visualising and quantifying sperm DNA damage using different slide based assays including acridine orange, alkaline comet, Halosperm and immunocytochemistry.
- Investigating the localisation of and relationship between regions of chromatin susceptible to salt extraction, including the nucleohistone and nucleoprotamine compartments in intact, decondensed and halo forming sperm nuclei.
- Developing different types of dispersion halos using low and high strength salt buffers and the Halosperm buffer and investigating
    a. The composition of the halos by Next-generation DNA sequencing.
    b. The organisation and fate of histones and protamines during halo formation.

Chapter 2: Exploring the sperm nucleoproteins by Immunocytochemistry, western analysis, and HALO-Fluorescence in situ hybridisation (HALO-FISH)

2.1 Introduction

2.1.1 Detection of histones and protamines

During the latter stages of spermatogenesis, chromatin structure undergoes extensive changes. In most species, this remodelling process is fundamental for sperm functionality (Sassone-Corsi, 2002). This remarkable DNA reorganisation is achieved by histone-protamine exchange (Agarwal and Said, 2003). Early in mammalian spermatogenesis, the chromatin is packaged by somatic histones, which are exchanged by testis-specific histones and subsequently by transition proteins. In late spermatids, transition proteins are finally substituted by highly basic protamines (Oko et al., 1996). In other species like fish and birds, however, the nucleoprotein replacement may occur directly from histone to protamine associated chromatin without any intermediate packaging (Yu et al., 2000). As a result of histone removal and replacement by protamine, chromatin conformation is reformed into a more highly condensed nuclear structure (ten-fold greater than can be achieved by nucleosomes), which helps to protect the paternal DNA integrity against chemical and physical disruption (Rathke et al., 2014). However, previous evidence has suggested that the process of histone-protamine exchange in mature sperm of some species such as human and murine, is incomplete (Balhorn et al., 1977; Tanphaichitr et al., 1978).

The mature human sperm nucleus, for example, contains 5-15% of retained histones with the remainder packaged by protamines with evidence presented

for each of these nucleoprotein compartments being associated with a distinct DNA sequence composition (Ward et al., 1989; Gardiner-Garden et al., 1998; Hammoud et al., 2009). Also, methylation studies on human sperm have demonstrated that retained histones are not randomly distributed in the sperm nucleus and are associated with promoter regions of developmental genes (Erkek et al., 2013).

Previously, a study has determined the salt concertation that necessary to extract nucleohistones from sperm nucleus without disturbing the nucleoprotamine compartment (Gatewood et al., 1987). It has been found that nucleohistones were not disassociated from sperm chromatin at NaCl concentrations up to at least 0.65 M, whereas, protamines were began released at 0.9 M of NaCl (Gatewood et al., 1987). Therefore, in the current study, two concentrations of NaCl, low (0.65 M) and high (2.0 M), were used to extract histones and protamines from sperm chromatin.

2.1.2 Detection of DNA damage in spermatozoa

A number of studies have determined that the production of 8-Hydroxyguanosine (8-OHdG) is associated with sperm DNA integrity in male reproduction as high levels of 8-OHdG has been found in infertile patients (Shen et al., 1997; De Iuliis et al., 2009; Guz et al., 2013). The hydroxyl radical (OH) is one of the most critical oxidative radicals that can cause DNA damage. This oxidative-free radical mainly attacks the C8 position in the guanine, which leads to the formation of 8-hydroxy-2-deoxyguanosine. Then, with one electron transfer, 8-OHdG is generated (Valavanidis et al., 2009). The accumulation of this oxidise base adduct (8-OHdG) in spermatozoon triggers the base excision repair pathway (base adduct removal mechanism) by activating an oxoguanine glycosylase 1 (OGG1) to release the 8-

OHdG residues in the extra- cellular space (Smith et al., 2013). The result of OGG1 activation is, therefore, generated abasic sites, which can destabilise the sperm chromatin making it more susceptible to DNA fragmentation (Aitken et al., 2013). The oxidative production of 8-OHdG was first discovered by Kasai et al. (1984) and can be used as a general biomarker of oxidative damage to DNA (Kasai, 1997; Filomeni et al., 2015) (Figure 17).

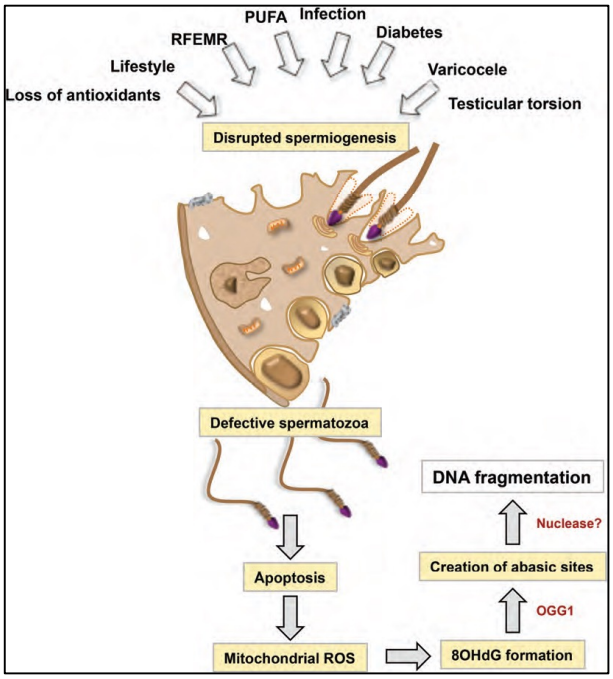

Figure 17: A diagram showed different environmental factors that can disturb the later stages of spermatogenesis and lead to generate poorly condensed chromatin. These spermatozoa with poorly compacted chromatin can be more vulnerable to ROS attack. High levels of ROS product can generate oxidised DNA base adducts (8-OHdG), which activate glycosylase 1 (OGG1) in order to remove 8-OHdG out of the chromatin by forming abasic sites. These oxidative changes can lead to DNA fragmentation. Adapted from: (Aitken et al., 2013)

2.1.3 HALO-Fluorescence in situ hybridisation (FISH)

Sperm fertility may rely on the molecular and architectural structure of the chromatin and its organisation within the sperm nucleus. Evidence showing that these sperm chromatin domains package distinctive DNA sequences, suggests that the relationship and organisation of histone and protamine packaged DNA may be important (Hammoud et al., 2009; Arpanahi et al., 2009). One feature of

all nuclei, including sperm, is that their chromatin can be made to 'spool' out from the nucleus and form distinctive halos (see chapter 1, section 1.5). Halo dimensions perhaps correlate with sperm viability making halo formation a useful tool for examining structural and architectural as well as compositional differences in sperm chromatin (Fernández et al., 2005). A previous study has shown evidence on the utility of Halo assay to detect sperm DNA fragmentation in comparison with other assays, for example, SCSA and TUNEL (Chohan, K.R. et al., 2006). Halo assay has displayed high correlation ($r > 0.90$) with SCSA (as a gold standard), which thus confirm the validity of Halo assay (Fernández et al., 2006; Muriel et al., 2006).

The mature sperm of many species have a specialised chromatin structure in which the chromatin is super-compacted as a result of protamine binding. The normal localisation of histone and protamine within the sperm genome is the most important factor in determining sperm quality. These points have been studied in human (Hammoud et al., 2011), mouse (Brykczynska et al., 2010) and in a few other animal experimental models (Dogan et al., 2015). Particularly, the position of sperm chromosomes has been analysed by using FISH technique in many studies investigating the genome distribution within the human sperm nucleus (Govin et al., 2007; Sarrate and Anton, 2009).

Additionally, the location of centromeres and telomeres is another approach that has been used to investigate chromatin organisation within the sperm nucleus. FISH techniques have indicated that telomeres are localised in the peripheral part of the nucleus, while centromeres are organised into heterochromatic regions known as the chromo-centre in the centre of the nucleus (Zalenskaya and Zalensky, 2004). Similarly to the general chromosomal investigations, the

centromeric/telomeric position tells us that the sperm genome is organised non-randomly (Foster et al., 2005). In the experiments reported herein, immnuocytochemnsitry and halo-FISH were used to visualise and confirm the localisation of sperm nuclear proteins and regions of sperm chromatin associated with both extracted halo and nucleoid DNA fractions (see chapter 1, section 1.5).

2.1.4 Experimental aims

The aim of these experiments was to investigate the relationship between the nucleoproteins in the sperm nucleus and DNA packaged by these proteins. To achieve that aim, following experiments were setup. Firstly, to establish the localisation and presence of both histones and protamines in the intact nuclei of human and bovine sperm, by immunocytochemistry using anti-histone and anti-protamine antibodies. In addition, observing the localisation of histones in the nuclear halo of human sperm following their exposure to low and high concentrations of NaCl was carried out. Secondly, the nuclear location of oxidative DNA damage was investigated in relation to the nucleohistone and protamine compartment of sperm nuclei using an anti-8-OHdG antibody. Thirdly, HALO-FISH was developed to help ensure that probes from halo and residual (nucleoid) DNA that would subsequently be sequenced were indeed derived from halo and nucleoid DNA.

2.2 Materials and Methods

2.2.1 Biological sample

Fresh human semen samples were obtained from both paid student volunteers and an andrology lab (Seacroft hospital) with 3 days abstinence from sexual activity (unproven fertility samples) (Table 1, see Appendix, page 250). According

to World Health Organisation (WHO) semen parameters, only semen samples with normal values were used in this project. The median for the given semen samples was as following;

Donors sample no.	Sperm count/mL (median)	Motility (median)	Semen volume (median)	Age
20	91.5 x 10^6	66.25%	2.75	21
Seacrfot samples no.	**Sperm count/mL**	**Motility**	**Semen volume**	**Age**
21	80 x 10^6	57.5%	1.90	34

Table 1: A table showed the information of human semen samples (median value) that obtained from donors and Seacroft hospital patients.

The human samples were processed immediately to resolve the ejaculated spermatozoa into high density 90% (nucleoid) and low-density 45% (interface) fractions.

While, bovine semen was supplied frozen from Genus, Cheshire, UK. The study was considered and nationally approved by the relevant UK Integrated Research Application System (IRAS) ethics committee (NRES 12_NE_0192) on 13th January 2013 and locally approved by the University of Leeds' School of Medicine Research Ethics Committee (SoMREC/13/017) on 28th November 2013. Numbers of straws of bovine semen from different bulls were used in this project (Table 2, see Appendix, page 250). The median for the semen samples was as following;

Bulls no.	Sperm count/mL (median)	Motility % (median)	Semen volume/straw (median)
7	72.75	57	250

Table 2: A table showed the semen samples information in the median for bovine samples that obtained from frozen straws.

2.2.2 Somatic cell removal

Round cells (non-sperm cells) were removed from samples by 60% percoll separation, sperm (approximately $5x10^6$) were washed with 100 mM NaCl, 10 mM Tris and 1 mM EDTA containing 0.1 mM phenylmethylsulfonyl fluoride (PMSF). The sperm were centrifuged at 2000 g for 5 minutes at 4°C. Washed sperm pellets were resuspended with freshly prepared 50 mM Tris-HCl, pH 8.0.

2.2.3 Sperm cell counting

After percoll gradient separation, sperm cells were counted using a haemocytometer (Vanderwall, 2008). Cells falling within the 4 large corners squares were counted and then the following formula was used to calculate the concentration of the sperm cells per mL;

Concentration (cell/mL) = counting number of sperm cells / 4 (squares) x Dilution faction x 10^3

The total number of sperm cells = concentration (cell/mL) x volume of sample (mL).

2.2.4 Sperm decondensation

Decondensation process was used to aid access for antibodies and probes for immunocytochemistry and FISH experiments as described by Ramos et al., (2008), with some modifications. Chromatin decondensing solution was used as follows: (0.5% triton X-100, 2.5 mM Dithiothreitol (DTT) and 100U/ml heparin in 1x PBS). Then, 100 µL of this solution was pipetted onto sperm and incubated in a humid container for 30 minutes for bovine sperm and 15 minutes for human sperm at room temperature. After incubation, the slides were washed once in 1x PBS for 5 minutes, and then slides were air-dried. As not all sperm nuclei in the same manner, only sperm nuclei that located in the centre of the marked spot on

slides were microscopically examined, whereas, those located at the edges were excluded.

2.2.5 Immunocytochemical localisation of histones, protamines and 8-Hydroxyguanosine (8-OHdG) in sperm nuclei

Differential Density Gradient Centrifugation (DDGC) was used to resolve fresh human ejaculated spermatozoa into high density 90% (nucleoid) and low-density 45% (interface) fractions after centrifugation of 700 g for 30 minutes (see Chapter 3, section 3.2). Sperm from both layers were washed twice with 3 mL of PBS followed by centrifugation at 800 g for 10 minutes at room temperature. Both subpopulations were resuspended in freshly prepared decondensation buffer (see chapter 2, section 2.2.4) and incubated for 15 minutes for human sperm and 30 minutes for bovine sperm at room temperature. Samples were then centrifuged at 800 g for 5 minutes at room temperature to remove the decondensation solution. Pellets were washed with 0.5 ml of PBS before centrifugation at 800 g for 5 minutes at room temperature.

The sperm concentration was adjusted to finally obtain 1 million spermatozoa by adding the appropriate volume of PBS. Ten µL of resuspended sperm was spread on a glass slide and left to dry out at room temperature. The immunocytochemistry was run according to the manufacturer's protocol (Abcam®). Slides were fixed for 10 minutes at room temperature in a fixative solution of PBS containing 2% paraformaldehyde (v/v). Then, slides were immersed in a solution of PBS and 1% Triton X-100 (v/v) for 40 minutes at room temperature to permit antibody penetration into cells. Later, slides were immersed in a blocking solution of 1 mg/ml of BSA and 100 mM of glycine in PBS for 60 minutes at 4°C to reduce non-specific interactions. After dilution (1:300) in

a blocking solution, smears were covered with 100 µL of primary antibody (see Table 3) and the slides were incubated overnight at 4°C in a humid chamber. Negative control slides were incubated with the same volume of blocking solution without the primary antibody.

The following day, slides were immersed in a washing solution of PBS and 0.1% Triton X-100 (v/v) for 10 minutes at room temperature with three repeats (a total of 30 minutes washing). A 100 µL volume of secondary antibody (see Table 3), diluted 1:500 in a blocking solution, was added on the slides which were returned to the humid box and incubated for 60 minutes at 4°C. Slides were protected from direct light to ensure maximum fluorescence activity of the secondary antibody. Then, slides were immersed in a washing solution of PBS and 0.1% Triton X-100 (v/v) for 10 minutes at room temperature. The previous washing step was repeated 3 times (a total of 30 minutes with changing the solution each time). Then, slides were left to dry completely. In the final step the samples were stained by DAPI, before covering the slides with coverslips and proceeding to imaging using an epi-Fluorescent Zeiss Axiovert microscope (Carl Zeiss Ltd, Hertfordshire, UK).

A total of 50 sperm were observed on each slide and the images were captured using the camera on the epifluorescence microscope. These images were then analysed using ImageJ software whereby the blue and red channels were split to highlight the antibody staining.

No	Antibody	Type	Company
1	Anti-core histone antibody (sheep)	Primary antibody	Abcamab7832
2	Anti-8 hydroxyguanosine antibody (mouse)	Primary antibody	Abcamab183395
3	Anti-histone H2A antibody (rabbit)	Primary antibody	Abcamab18255
4	Anti-histone H3 antibody (rabbit)	Primary antibody	Abcamab1791
5	Anti-protamine 1 antibody (goat)	Primary antibody	Santa-cruze Sc-23107
6	Anti-rabbit IgG antibody (FITC)	Secondary antibody	Abcamab6717
7	Anti-sheep IgG antibody (Alexa Fluor 647)	Secondary antibody	Abcamab150179
8	Anti-goat IgG antibody (FITC)	Secondary antibody	Santa-cruze Sc-2024
9	Anti-goat IgG antibody (HRP)	Secondary antibody	Santa-cruze Sc-2020
10	Anti-rabbit IgG antibody (HRP)	Secondary antibody	Abcamab6721
11	Anti-mouse IgG antibody (TRITC)	Secondary antibody	Abcamab6786
12	Anti-sheep IgG antibody (HRP)	Secondary antibody	Abcamab97130

Table 3: A table showed a list of primary and secondary antibodies used in immunocytochemistry and western blot experiments for both human and bovine sperm.

2.2.8 Halo formation

2.2.8.1 Halo formation using 2.0 M and 0.65 M of NaCl

Low and high salt sperm halos were generated according to the methods described by Castillo et al., (2014a) with some modifications. Briefly, sperm were resuspended in 4 ml of 50 mM Tris-HCl (pH 8.0) solution. Then, 40 µl from a 1 M DTT was added to final concentration of 10 mM and incubated for 15 minutes on ice. Next, 400 µL of 10% hexadecyltrimethylammonium bromide (CTAB) (Sigma Aldrich) was added and incubated for a further 30 minutes on ice (only samples that used in NGS experiment, sperm were treated with 10% CTAB to separate heads from tails). After the incubation, sperm were checked under the microscope to ensure that sperm tails had detached. Sperm heads were pelleted by centrifugation at 3000 g for 5 minutes at 4°C. Pellets were washed twice with 4 ml solution of 1% CTAB in 10 mM Tris-HCl (pH 8.0) and 0.05% (w/v) digitonin (Sigma Aldrich) (to minimize clumping of nuclei) at 3000g for 5 minutes. After centrifugation, pellets were washed five times with 4 ml of 1x Tris-Buffered Saline

(TBS) (50 mM Tris-Cl, pH 7.5, and 150 mM NaCl) containing 0.05% digitonin at 3000 g for 5 minutes. Pellets were then resuspended in 1 mL solution (1 mM EDTA, 10 mM Tris–HCl pH 8, 0.1 mM PMSF and 0.05% digitonin) with either low salt (0.65 M NaCl) or high salt (2.0 M NaCl) and incubated for 15-20 minutes (30 minutes for bovine sperm) on ice (Figure 16), before being centrifuged at 3000 g for 2 minutes at 4°C. Then, the nuclei were washed with 1 mL of 1x incubation Buffer (100 mM NaCl, 5 mM $MgCl_2$ and 10 mM Tris-HCl, pH 8.0), and centrifuged at 3000 g for 5 minutes at 4°C. After that, pellets were resuspended in 1 mL of 1x incubation NEBuffer 2.1 containing 0.05% digitonin, before adding restriction endonuclease enzymes.

2.2.8.2 Halo formation using Halosperm™ kit

The Halosperm™ treatment was carried out according to the manufacturer's protocol (Fernández et al., 2005) with some modification for bovine samples. The sperm washed pellets were resuspended in a 300 µL of DA solution and incubated for 7 minutes (10 minutes for bovine) at room temperature, and then centrifuged at 200 g for 5 minutes. After discarding the supernatant, the pellets were resuspended into a 300 µL of lysing solution and incubated for 25 minutes (30 minutes for bovine) at room temperature (Figure 18). After centrifugation at 200 g for 5 minutes, the pellets were washed with a 500 µL of PBS and centrifuged again at 200 g for 5 minutes. After that, pellets were resuspended in 1 ml of 1x incubation NEBuffer 2.1 containing 0.05 % digitonin, before adding restriction endonuclease enzymes.

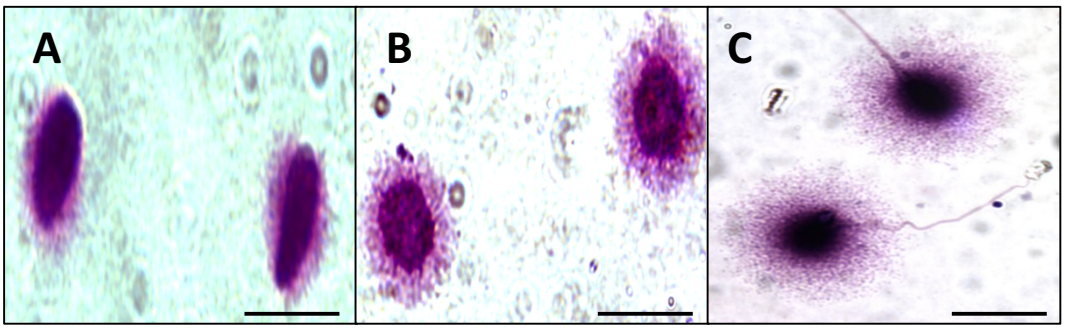

Figure 18: Microscopic images showed the difference in halo size that produced using low (0.65 M) salt **(A),** high (2.0 M) salt **(B)** and Halosperm assay **(C).** The halo size in each experiment suggested that different salt concentrations may extract different level of DNA compartment, in another word, the more salt concentration used the more loop of DNA extracted and subsequently bigger size formed around the sperm nucleus. (scale bar 20µm)

2.2.9 Recovering halo DNA using restriction digestion with (BamH 1 and EcoR1)

After halo formation, 100 U of each restriction endonuclease enzymes (BamH1 and EcoR1) (BioLabs) were added to samples in 1x NEBuffer 2.1 (BioLabs) and incubated at 37°C for 90 minutes (Wykes and Krawetz, 2003). Samples were gently agitated to allow digested DNA loops to leach out from halo formation (Figure 19). Digestion was stopped by further incubation at 65°C for 10 minutes.

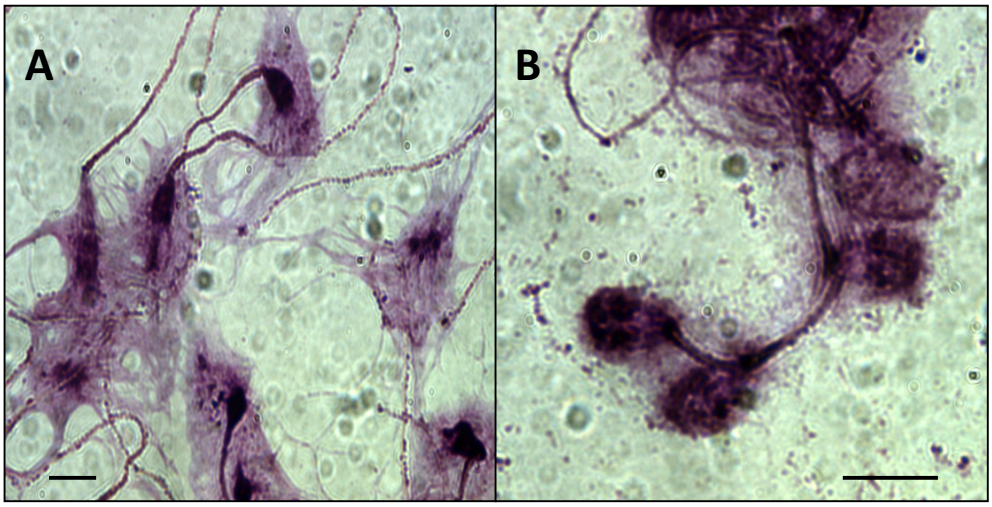

Figure 19: Microscopic images of human sperm following halo formation in suspension, which leaded to produce irregular halo-shape and sperm clumping. Two images showed the sperm halo formation before adding restriction enzymes (RE) (A) and after digesting sperm halos using RE (B). (scale bar 20µm)

2.2.10 DNA extraction using Phenol-chloroform

Following the restriction enzyme treatment, samples were centrifuged at 3,000 g for 3 minutes, then carefully digested halo-bound DNA (supernatant) was separated from nucleoid-DNA and transferred into new tubes (Figure 20). The supernatant was centrifuged at 16,000 g for 3 minutes to remove any remaining halo-bound DNA. Proteinase K (500ug/ml) (Macherey-Nagel) and 0.5% sodium dodecyl sulphate (SDS) was added to the supernatant, while, the nucleoid (protamine-bound DNA) was resuspanded with 1ml of Stop buffer (50 mM Tris-HCl, 50 mM NaCl, 0.5 ETDA and 0.5% SDS) containing proteinase K (500 µg/mL) and incubated overnight at 55°C. Both DNA fractions were then processed for DNA extraction.

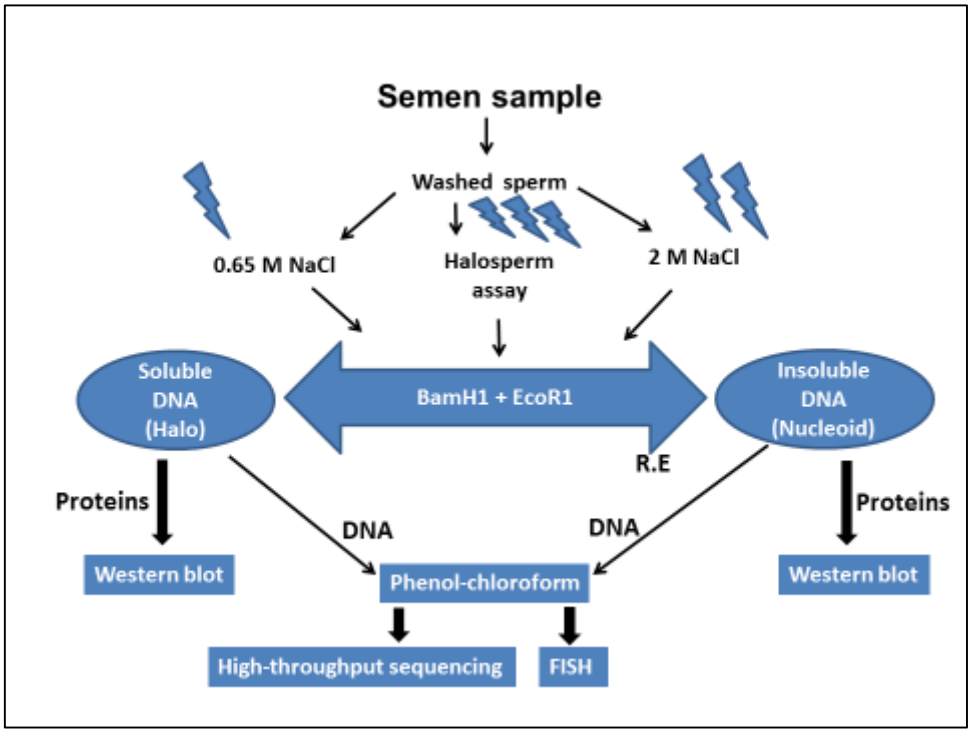

Figure 20: A diagram showed the process of different halo formations using salt solution (high and low) and Halosperm assay, followed by restriction enzyme digestion. After digestion, samples were processed either for DNA extraction, and then sequencing using High-throughput sequencer or labelled and used for FISH experiment. In addition, digested samples can be used for protein extraction.

DNA was extracted by Phenol-Chloroform in a 1:1, followed by ethanol precipitation according to the methods described by Wykes and Krawetz, (2003). Precipitated DNA was dissolved in 1 mL of Tris-EDTA (TE) buffer (1 M Tris-HCl and 0.5 M EDTA, pH 8.0) and stored at -20°C. An equal volume of phenol-chloroform solution (Sigma Aldrich) was added to the resuspended sperm pellets (protamine-bound DNA) and as well as an equal volume of phenol-chloroform solution was added to the supernatant (histone-bound DNA). Mixtures were agitated and incubated at room temperature for 30 minutes. Followed by centrifugation at 13,000 rpm for 15 minutes to separate nucleic acids from proteins and lipids. After the centrifugation, the upper aqueous phase, which contains DNA, was pipetted off and transferred to a new tube. DNA was recovered from the upper layer by precipitation using an equal volume of isopropanol (Sigma Aldrich) with (1/10) 3 M NaCl (pH 5.2) for one hour at room temperature. Followed by spinning down for 30 minutes at 13,000 rpm to pellet the DNA. Later, DNA was washed twice by adding 300 µL of 70% EtOH, before microcentrifugation and recovery of the supernatant without disturbing the pellet. Tubes were allowed to air dry for 10 to 15 minutes at room temperature. After removing the 70% EtOH completely, nucleoid-DNA was dissolved in 500 µL of 1x TE buffer and histone-bound DNA in 50 µL of 1x TE buffer. Extracted DNA was kept at 4°C overnight, before measured by Nanodrop^{TM} 1000 Spectrophotometer (Thermo Scientifics) (Figure 21).

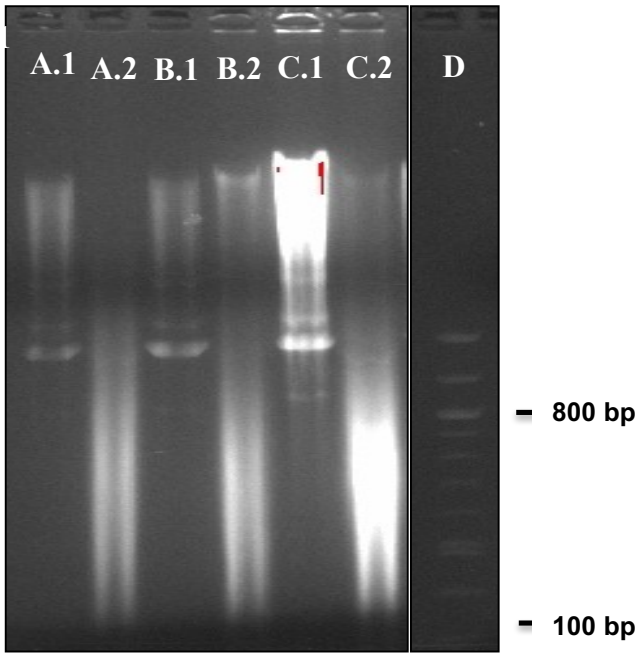

Figure 21: An image of 1% agarose gel showed smears of DNA segment with different sizes following digestion by restriction enzymes and then extracted using phenol-chloroform, (A) Halosperm assay insoluble (1) and soluble (2) digested fractions, (B) 2.0 M NaCl salt/restriction endonuclease insoluble (1) and soluble (2) digested fractions, and (C) 0.65 M NaCl salt/restriction endonuclease insoluble (1) and soluble (2) digested fractions. (D) 1kb DNA ladder.

2.2.11 Fluorescence in situ hybridisation (FISH)

Because Halosperm^{TM} assay used to assess DNA damage in the sperm nucleus as a benchmark, Halosperm kit was used in FISH experiment to confirm the digestion of the two DNA compartments (halo and nucleoid). Sperm halos were generated on hybridisation slides using Halosperm kit. Two labelled human sperm DNA probes derived from their corresponding compartments were hybridised on spread sperm on different slides, alongside an additional slide as a control for non-specific DNA binding. A commercial centromeric probe for chromosome 3 was used as a quality control for FISH reagents and hybridisation equipment.

2.2.11.1 Extracted-DNA labelling kit

To visualise halo and nucleoid compartments in sperm nuclei, a BioPrime DNA Labelling kit (CAT# 18094-011) from Invitrogen was used in this step and the procedure was run according to the manufacturer's protocol as follows:

2.2.11.2 Fluorescence probe preparation

100 ng of the extracted DNA was dissolved in 5-20 µL of diluted buffer in a 1.5 mL microcentrifuge tube. Then, a 20 µL of 2.5X random primers solution was added to the dissolved DNA on ice. After that, the DNA was denatured by heating in a boiling water bath for 5 minutes and then immediately cooled on ice. On ice, a 5 µL of 10X dNTP mixture was added to the DNA and then nuclease free water was added to a total volume of 49 µl and mixed briefly. Afterwards, a 1 µL of klenow fragment was added and mixed gently but efficiently, followed by centrifugation for 15-30 seconds. Then, this mixture was incubated in a thermocycler at 37°C for 2 hours, before the reaction was stopped by adding a 5 µL of stop buffer, which provided with the kit.

2.2.11.3 Repeated ethanol precipitation

The unincorporated nucleotides were separated from the biotinylated-DNA probe by adding 1/10 (v/v) of 3 M sodium acetate and 2 volumes of cold 95% ethanol to the mixture. Then, the mixture was mixed by inverting, before the tube was frozen at -70°C for 15 minutes. After centrifuging at 15,000 g for 10 minutes, the supernatant was carefully removed and then the pellet was left to air-dry for 5-10 minutes. After that, the complete dried pellet (probe) was resuspended in 50 µL of distilled water. Then, the probe was precipitated one more time with sodium acetate and ethanol as described previously, before the probe was resuspended

in 50 µL TE buffer and stored at -20°C.

2.2.11.4 Preparation of slides for hybridisation

FISH slides were prepared with percoll-fractionated sperm processed for the Halosperm™ test embedded in a 0.7 % dried microgel. After exposing the dried slides to DA solution and then lysing solution as the Halosperm™ test protocol (Fernández et al., 2005), the slides were fixed in 10 % of formaldehyde in 1X PBS for 12 minutes. Then, the slides were washed in cold 1X PBS for 1 minutes, before sperm cells were denatured by incubating the slides in a cold solution of NaOH 0.05/50% ethanol for 15 seconds. After that, the slides were dehydrated in 70%, 90% and 100% ethanol for 2 minutes each and allowed to air dry at room temperature. The existence of the nuclear halo formation was confirmed by staining an addition slide with Wright Giemsa stain (sigma-Aldrich).

2.2.11.5 Hybridisation procedure

A 15 µL of DNA probe–hybridisation buffer (DPHB) was prepared by adding 1.5 µL 20 x SSC, 50 % formamide (Analogo), 10 % dextran sulfate and 1 µL sheared salmon DNA to 5 µL DNA probe. The DPHB was denatured by incubation for 10 minutes in a thermocycler at 70°C and immediately cooled on ice. In next step, 15 µL of DPHB mixture was dropped on the slide (sample), and covered by a small piece of parafilm and the slides were incubated overnight at 37°C in a slide-based Leica ThermoBrite System (Fisher Scientific). After hybridisation, the slides were incubated in a post-hybridisation solution of 50 % formamide and 2X SSC for 8 minutes at room temperature, followed by an incubation in 0.2X SSC for 5 minutes at room temperature. Then, the slides were dehydrated in 70%, 90% and 100% ethanol for 2 minutes each and allowed to air dry at room

temperature. Afterward, a 100 µL of 1:1000 diluted streptavidin-FITC in PBS was dropped on the slides and covered by a small piece of parafilm, followed by incubation at 4°C for one hour. After the incubation, the slides were washed in PBS at room temperature for 5 minutes then dried in the dark. In the final step the samples were stained by DAPI, then one drop of antifade reagent was applied before covering the sample with a coverslip and proceeding to imaging using an epi-Fluorescent Zeiss Axiovert microscope (Carl Zeiss Ltd, Hertfordshire, UK).

2.2.12 Protein extraction and recovery from halo preparations

Extraction buffers used in halo formation under the differing conditions described above (low salt, high salt, and Halosperm^{TM} assay) were recovered and their nucleoproteins (representing halo fractions) were extracted and purified as described by Castillo et al., (2014a). Corresponding insoluble material (representing nucleoid fractions) were also extracted and purified.

Following the restriction enzyme digestion, samples were centrifuged at 3,000 g for 3 minutes to separate digested halo-DNA (supernatant) from remaining nucleoid-DNA (pellet) and transferred into new tubes (Castillo et al., 2014a). Pellets (nucleoid) were resuspended into RIPA buffer (150 mM NaCl, 1% NP-40, 0.5% Sodium deoxycholate, 0.1% SDS and 50 Mm Tris-HCl, pH 8.0) (Abcam) including 1x protease inhibitor cocktail (Cell Signaling Technology) and incubated for 30 minutes at 4°C. After incubation, samples were centrifuged at maximum speed for 10 minutes at 4°C. Then, supernatants were transferred to a dialysis tubing (prepared by boiling the tubing in distilled water including 5mM EDTA for 10 minutes) and dialysed for 2 hours against 1.0 L of 1X TBS, pH 7.4) Dialysis buffer was then refreshed and the solution was incubated for another two hours at 4°C, followed by a third incubation with fresh buffer overnight at 4°C. Protein

concentrations were measured using Pierce bicinchoninic acid (BCA) Protein Assay Kit (Thermo scientific). The dialysed protein was transfered to pre-cooled tubes containing Trichloroacetic acid (TCA) to a final concentration of 20% (v/v) to precipitate the protein. The sample was incubated for 20 minutes at 4°C with shaking and then centrifuged at 17,000 g for 10 minutes at 4°C to recover the precipitated protein. The solution was then washed twice in 200 µL chilled acetone and dried at room temperature for 10 minutes. Finally, the protein was resuspended in 20 µL SDS or acid-urea containing sample buffer.

2.2.13 Sperm chromatin extraction (control) for acid urea-PAGE gel

Sperm nucleoproteins were extracted as described by Oliva et al., (2006). Sperm (approximately 14 x 10^6) were separated from semen by one density layer (60%) of percoll. After washing sperm with PBS, sperm were resuspended in 200 µL of 200 mM Tris-HCl (pH 8), 0.5% Triton X-100 and 2 mM $MgCl_2$ (membrane permeabilisation). After that, sperm were centrifuged at 8,900 g for 5 minutes at 4°C and, before the supernatants were discarded. Pellets were resuspended in 200 µL H_2O containing 1 mM PMSF, and centrifuged at 8,900 g for 5 minutes at 4°C. After centrifugation, the supernatant was removed and the pellet was resuspended in 50 µL of 100 mM Tris-HCl (pH 8), 20 mM EDTA and 1 mM PMSF, and mixed by pipetting. An equal volume (50 µL) of a protein denaturation solution (6 M guanidine hydrochloride (GuHCl) and 575 mM DTT) was added and vigorously vortexed. Then, 5 times volume (1 ml) of cold absolute ethanol was added and vigorously vortexed, before incubation at -20 °C for 10 minutes (chromatin precipitation), following by centrifugation at 12,900 g for 15 minutes. After discarding the supernatants, 500 µL of 0.5 M HCl was added and incubated for 5 minutes at 37°C, before being vortexed and re-incubated at 37°C for 2

minutes. After centrifugation at 16,000 g for 10 minutes at 4°C, the supernatants were transferred into pre-chilled tubes 100% (v/v) giving a final TCA concentration of 20% and incubated at 4°C for 10 minutes. Tubes were then centrifuged at 16,000 g for 10 minutes at 4°C, before the supernatants were discarded. Pellets were then resuspended in 500 µL of 1% *β-mercaptoethanol* in acetone, then centrifuged at 16,000 g for 5 minutes at 4°C. After centrifugation, pellets were air dried for 5-10 minutes and then resuspended in 20 µL of acid-urea sample buffer (5.5 M urea, 20% *β-mercaptoethanol* and 5% acetic acid).

2.2.14 SDS-PAGE gel and silver staining

SDS-PAGE gel was carried out as described by Laemmli, (1970) with some modifications. A 12.5% Acrylamide (separation) gel was prepared by mixing 1.57 ml deionised water, 1.57 ml Tris-HCl (1.5 M) pH 8.8, 50 µL 10% SDS, 2.08 ml 30% Acrylamide, 50 µL 10% ammonium persulphate (APS) and 5 µL Tetramethylethylenediamine (TEMED) (Sigma Aldrich), then the gel was left to polymerise for 30 minutes. In the next step, the 4% stacking gel was prepared by mixing 1.36 ml deionised water, 250 µL Tris-HCl (1M) pH 8.8, 20 µL 10% SDS, 340 µL 30% Acrylamide, 20 µL 10% ammonium persulphate and 2 µL TEMED, then 2 ml was layered above the solidified separating gel (12%) and left at room temperature for 30 minutes. The samples were heated at 95°C for 10 minutes, and then chilled immediately on ice just before loading. After that, the sample was loaded into the gel and electrophoresed initially at 60 V for 8 minutes in 1x SDS running buffer (15 g/L of Tris base, 72 g/L Glycine, 3 g/L SDS) to allow samples entering the stacking gel and following by 120 V for 2 hours in the resolving stage gel.

For visualising proteins, a silver stain solution was prepared as described by Morrissey, (1981) with some modifications. Firstly, the gel was washed 3 times with deionised water for 10 minutes each with shaking. Immediately, the gel was fixed with 5% ethanol and 5% acetic acid for 30 minutes with shaking. After fixation, the gel washed 3 times with deionised water for 5 minutes each with shaking. Then, the gel was stained with silver nitrate (300 mg $AgNO_3$, 1.3 mL ammonia solution in 40 ml H_2O) until bands appeared clear. Directly, the gel was washed with deionised water for 20 seconds, and then developer was added to the gel when the bands reach the preferred intensity relatively to background.

2.2.15 Acid-urea-PAGE gel and coomassie blue staining

To evaluate the presence of protamines and histones in the extraction solutions (low salt, high salt, and Halosperm^{TM} assay), western blotting was performed on these preparations, resolved by acid-urea electrophoresis. Primary antibodies against protamines (anti-PRM1) and histones (anti-H3 and anti-H2A) were used. Acid-urea-PAGE gel was carried out as described by Castillo et al., (2011) with minor modifications. Acrylamide gel was prepared by mixing 2.5 M Urea, 0.9 M Acetic acid, 15% Acrylamide, 0.5% APS, 0.5% TEMED and 4 mL deionized water, then the gel was left to solidify for 60 minutes. After that, the polymerized gel was placed into the electrophoresis apparatus and filled with running buffer (0.9 N acetic acid) and pre-electrophoresed for 90 minutes at 150 V, before substituting the running buffer with fresh buffer. After that, the samples (a total of 10 µg) were loaded onto the gel and electrophoresed at 150 V for 40 minutes, but with inverted polarity at the power supply (protamines and histones are strongly positively charged). After electrophoresis, the gel was prepared for

western blotting by transferring the protein to a polyvinylidene fluoride (PVDF) membrane at 75 V for 60 minutes (reversing polarity).

Western blotting was carried out as described by Liu et al., (2013) with some modifications. Membranes were blocked in Tris-Buffered Saline Tween-20 (TBS/0.1% Tween) containing 5% (w/v) milk powder overnight at 4°C. Then, membranes were washed 3 times for 10 minutes each in TBS/0.1% Tween (150 mM NaCl and 50 mM Tris-HCl, pH 7.5) at room temperature. Membranes were incubated with TBS/0.1% Tween, 3% milk and 15 µL primary antibody (1:200) (Table 3) for 3 hours at room temperature, then washed 3 times for 10 minutes each in TBS/0.1% Tween at room temperature. Due to the high similarity of protein sequences between human and bovine sperm (the sequence similarity of proteins was tested through EMBOSS Matcher) (see http://www.ebi.ac.uk/Tools/psa/emboss_matcher/), the same antibodies were used for both species. Following, Membranes were incubated with TBS/0.1% Tween, 3% milk and 3 µL secondary antibody (1:1000) (Table 3) for one hour at room temperature, then washed 3 times for 10 minutes each in TBS/0.1% Tween at room temperature. To visualise the immune complexes, 1:1 ratio of ECL substrate components (Bio-Rad) was prepared (0.1 ml/cm^2 of membrane) and mixed, then the substrate solution was applied to the membrane and incubated for 5 minutes. Luminescence was digitally imaged. To confirm that proteins had been transferred successfully,, gels were stained in Coomassie brilliant blue R (Sigma) for 30 minutes at room temperature and then de-stained (50% methanol, 10% acetic acid and 40% water) for 30 minutes to 24 hours at room temperature until backgrounds were clear (Brunelle and Green, 2014).

2.3 Results

2.3.1 Histone localisation in sperm nuclei

Abcam® immunocytochemical technique was used with modifications to detect the localisation of histones in slightly decondensed mature sperm of human and bovine (see chapter 2, section 2.2.4). Decondensation is needed to provide antibodies, and maybe FISH probes, greater access to their targets in the nucleus to gain information on where those targets are located and so provide evidence for potential differential sensitivity to DNA fragmentation. Strong signals were located at the posterior end of most nuclei using the anti-core histone antibody with weaker signals in other regions of the nucleus of both human and bovine sperm also detected (Figure 22-23). In addition, strong signals were obtained at the posterior end of intact human sperm nuclei using specific anti-histone antibodies (H2A and H3) (Figure 24), while strong signals of anti-H2A and anti-H3 were detected at the equatorial segment of the bovine nucleus with weaker signals at the posterior ends (Figure 25). Different patterns of signals were detected in the nuclear halo of human sperm using anti-H2A and anti-H3 (Figure 26). Strong peripherally located signals were obtained using these antibodies on sperm treated by low salt extraction (A1-A3; arrow heads). Furthermore, strong signals at the posterior ends of most nuclei were also detected, based on the still visible tail section (A1-A3; arrows). Weaker peripheral signal patterns were obtained using these antibodies following high salt extraction of sperm nuclei (Figure 27). Posterior end signals were greatly reduced or absent altogether. These data together suggest that there are two different concentrations of histone in salt-extracted sperm nuclei. One represents the halo, the other the more internal histones found towards the posterior end of the sperm nucleus.

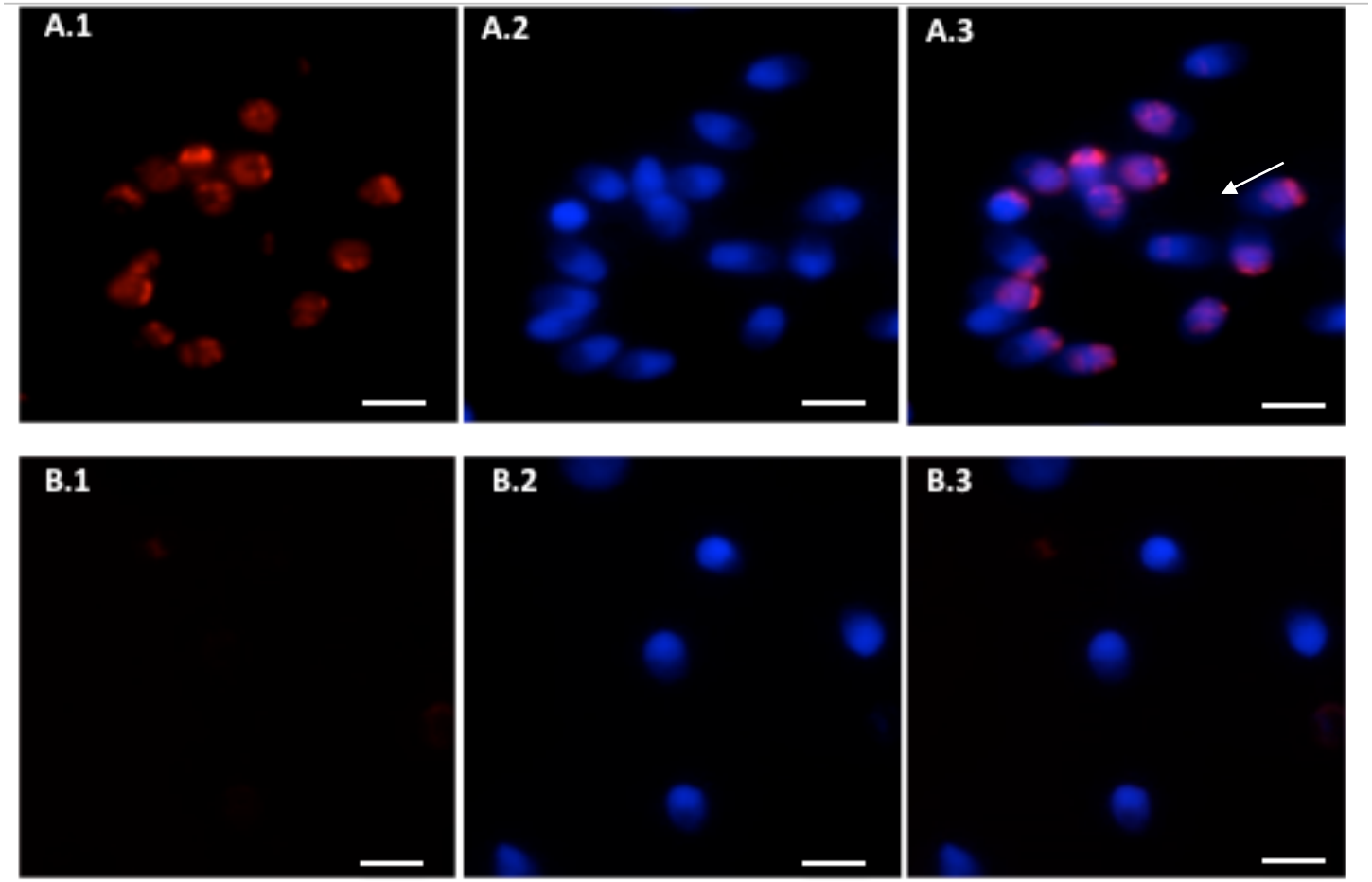

Figure 22: Histone signals in decondensed nuclei of human sperm. Strong signals were located at the posterior end of most nuclei using the anti-core histone antibody with weaker signals in other regions of the nucleus of human sperm. A: anti-core histone; A.1: histones signal (TRITC), A.2: DNA (DAPI), A.3: merged. B: control; B.1: histones signal (TRITC), B.2: DNA (DAPI), B.3: merged. The white arrow pointed in parallel to the anterior end of the sperm nucleus. (scale bar 5μm).

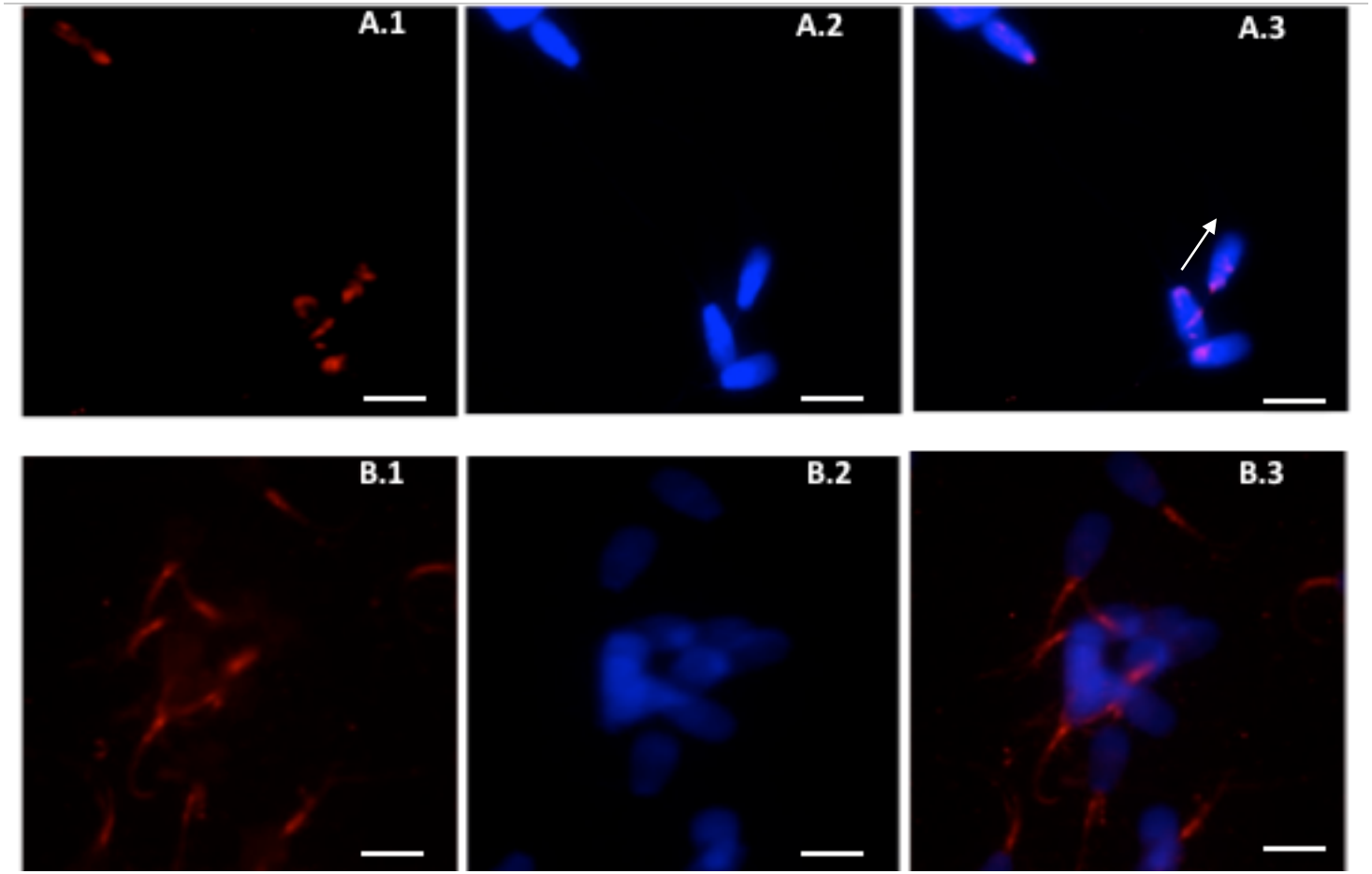

Figure 23: Histone signals in decondensed nuclei of bovine sperm. Strong signals were located at the posterior end of most nuclei using the anti-core histone antibody with weaker signals in other regions of the nucleus of bovine sperm. A: anti-core histone; A.1: histones signal (TRITC), A.2: DNA (DAPI), A.3: merged. B: control; B.1: histones signal (TRITC), B.2: DNA (DAPI), B.3: merged. The white arrow pointed in parallel to the anterior end of the sperm nucleus (scale bar 5µm)

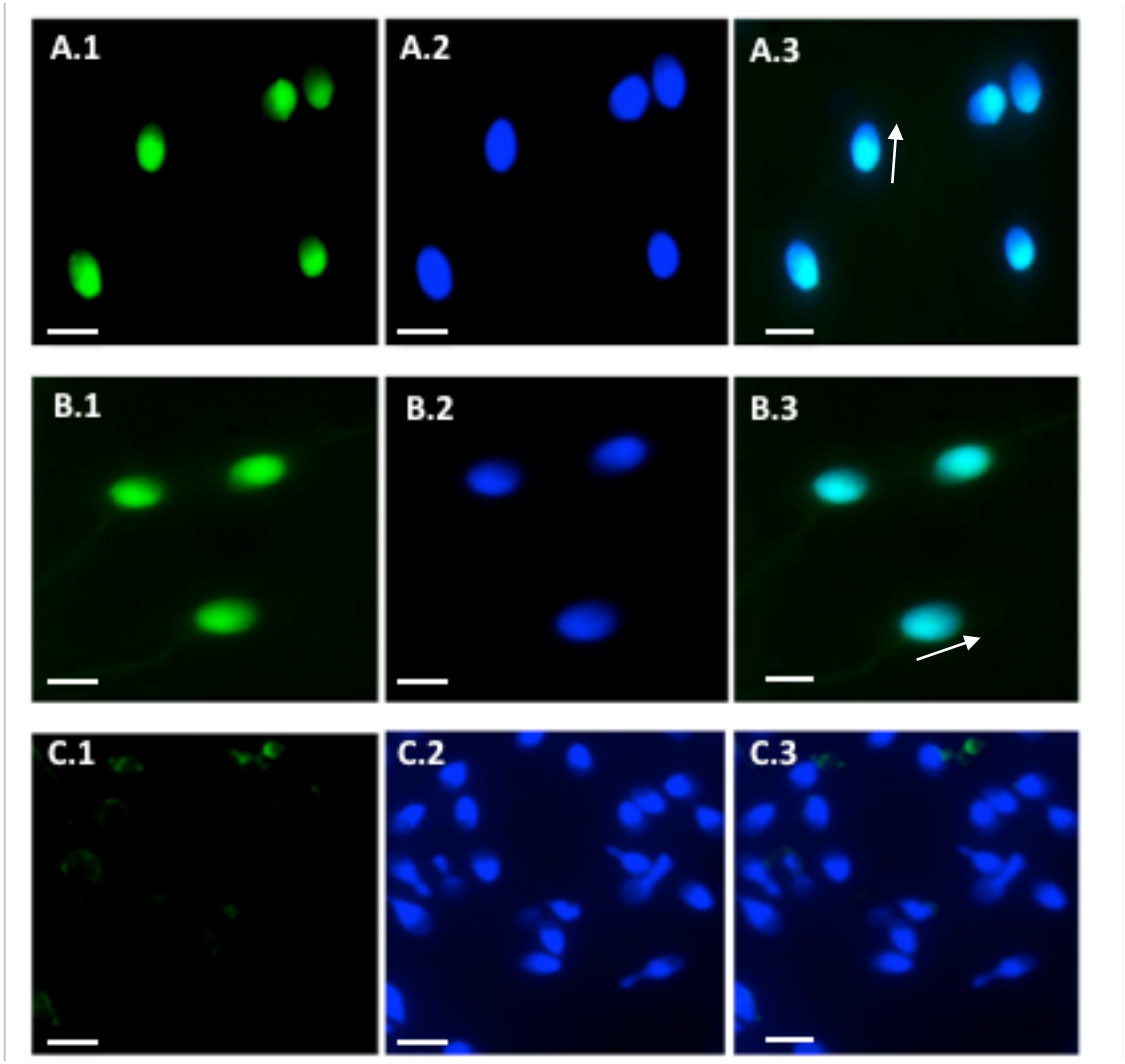

Figure 24: Histone signals in decondensed intact nuclei of human sperm using. Strong signals were obtained at the posterior end of intact human sperm nuclei using specific anti-histone antibodies (H2A and H3)
A: H2A; A.1: histones signal (FITC), A.2: DNA (DAPI), A.3: merged. B: H3; B.1: histones signal (FITC), B.2: DNA (DAPI), B.3: merged. C: control; C.1: histones signal (FITC), C.2: DNA (DAPI), C.3: merged. The white arrow pointed in parallel to the anterior end of the sperm nucleus. (scale bar 5µm).

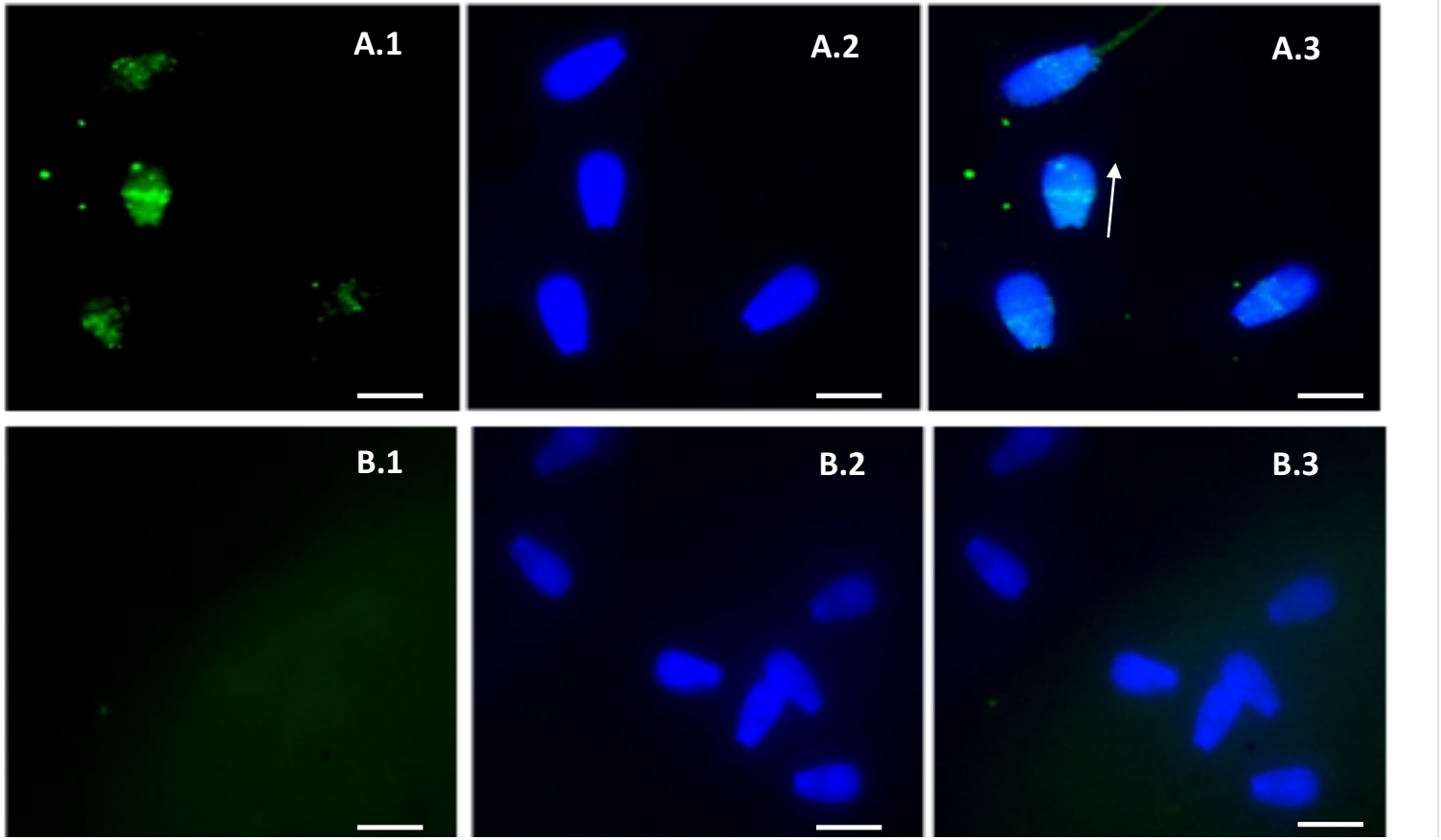

Figure 25: Histone signals in decondensed intact nuclei of bovine sperm using. Strong signals of anti-H2A and anti-H3 were detected at the equatorial segment of the bovine nucleus with weaker signals at the posterior ends. A: H2A and H3; A.1: histones signal (FITC), A.2: DNA (DAPI), A.3: merged. B: control; B.1: histones signal (FITC), B.2: DNA (DAPI), B.3: merged. The white arrow pointed in parallel to the anterior end of the sperm nucleus. (scale bar 5µm)

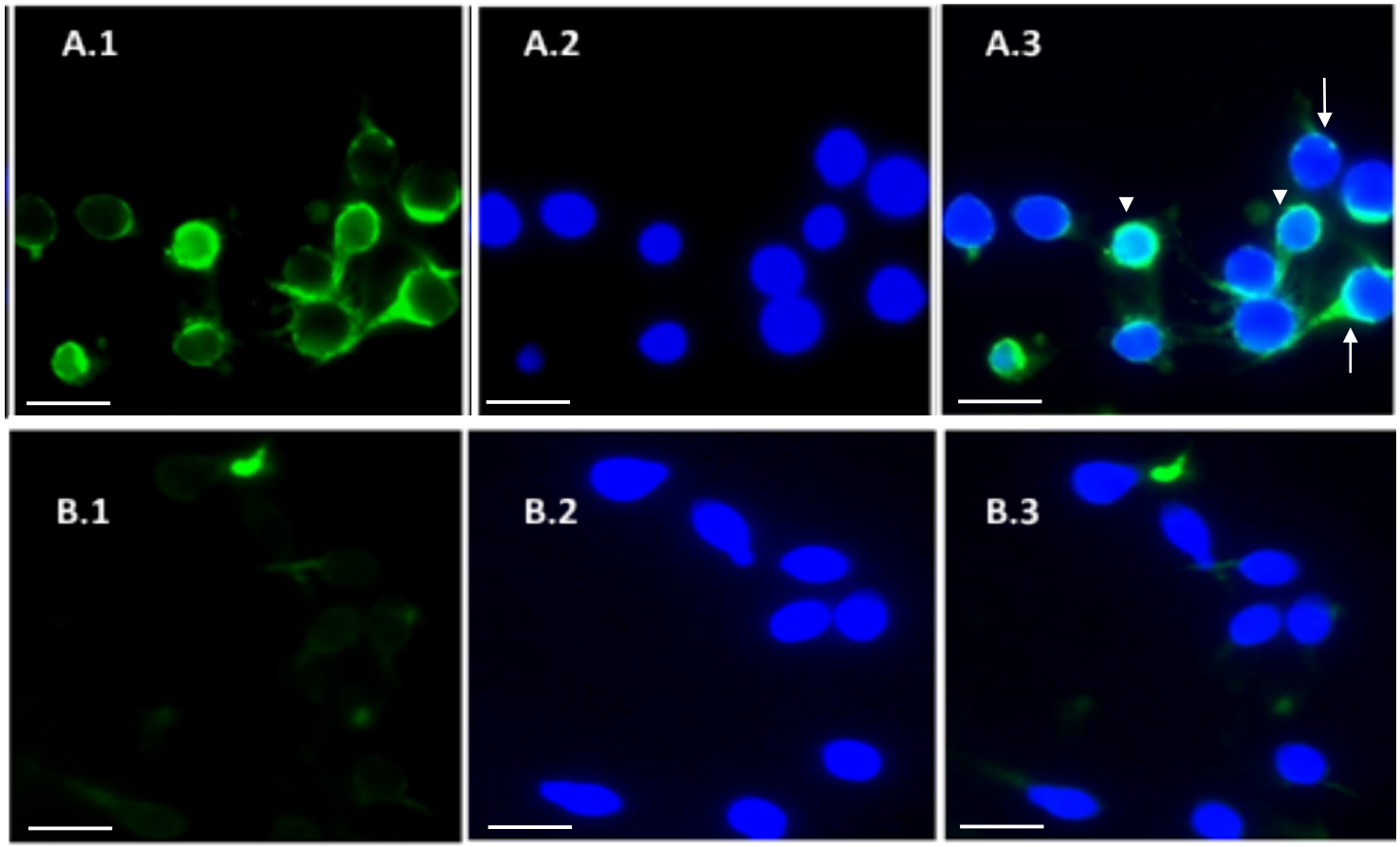

Figure 26: Histone signals in nuclear halos of human sperm using low concentration of salt. Strong peripherally located signals were obtained using histone antibodies (H2A and H3) on sperm treated by low salt extraction. Additionally, strong signals at the posterior ends of most nuclei were also detected, based on the still visible tail section. A: H2A and H3; A.1: histones signal (FITC), A.2: DNA (DAPI), A.3: merged. B: control; B.1: histones signal (FITC), B.2: DNA (DAPI), B.3: merged. (scale bar 5µm)

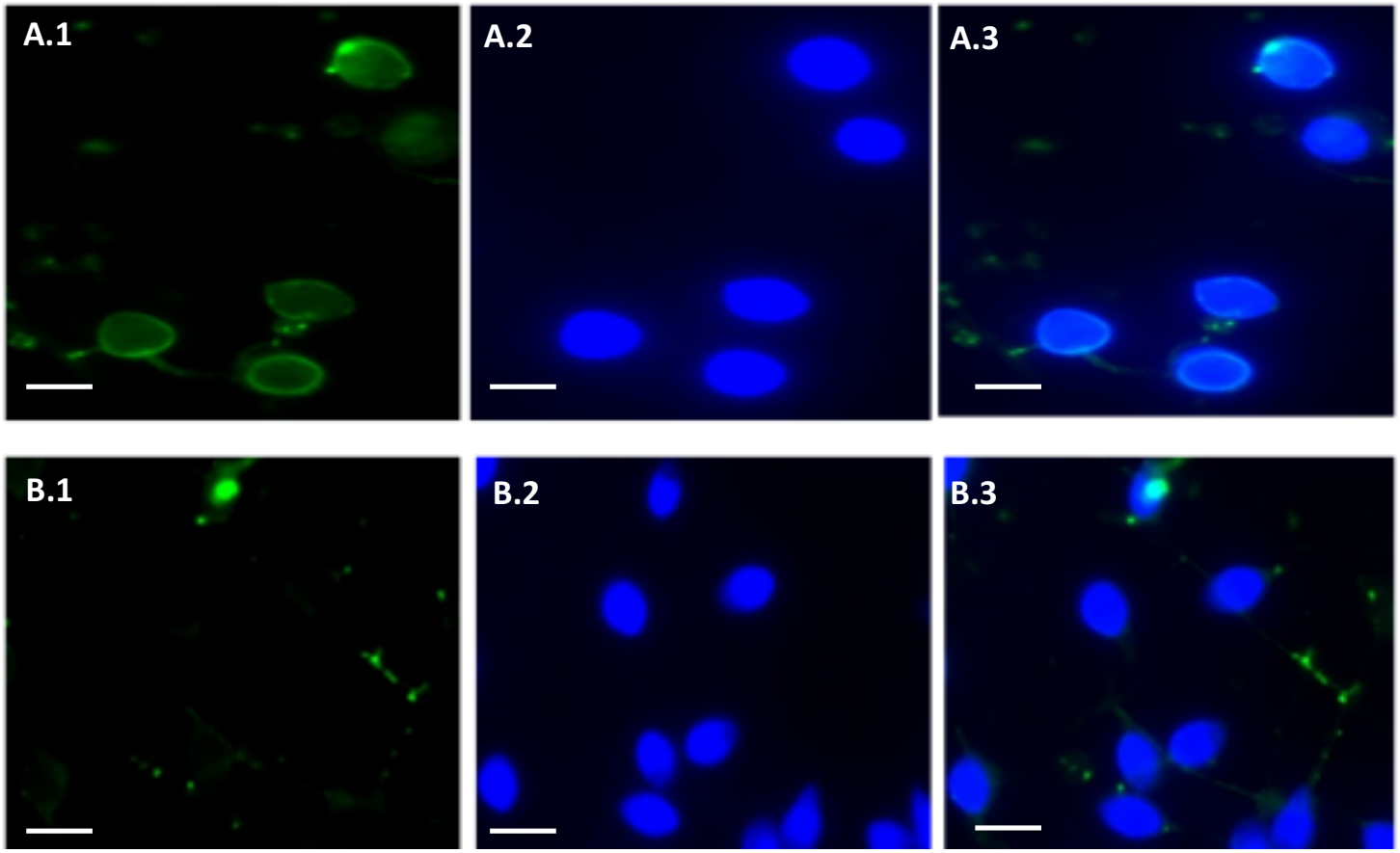

Figure 27: Histone signals in nuclear halos of human sperm using high concentration of salt. Weaker peripheral signal patterns were obtained using histone antibodies (H2A and H3) following high salt extraction of sperm nuclei (Figure 27). Posterior end signals were greatly reduced or absent altogether. A: H2A and H3; A.1: histones signal (FITC), A.2: DNA (DAPI), A.3: merged. B: control; B.1: histones signal (FITC), B.2: DNA (DAPI), B.3: merged. (scale bar 5µm)

2.3.2 Protamine localisation in sperm nuclei

Decondensation solution including heparin was needed to provide PRM1 antibody, greater access to protamine compartment in the nucleus. The localisation of protamines in the sperm chromatin of both human (Figure 28) and bovine (Figure 29) was studied using an antibody to PRM1. In human, the signal for PRM1 was distributed throughout the nucleus (24; A1-A3); however, the signal intensity was slightly increased at the posterior end of the nucleus with DTT only in the decondensing buffer. Following the addition of heparin to the decondensation solution, however, the signal became more diffuse throughout the nucleus but with some localised concentrations (24; B1-B3, arrow head). In bovine sperm nuclei (25; A1-A3), the signal for PRM1 was concentrated towards the anterior (acrosomal) end and required heparin in the decondensation solution.

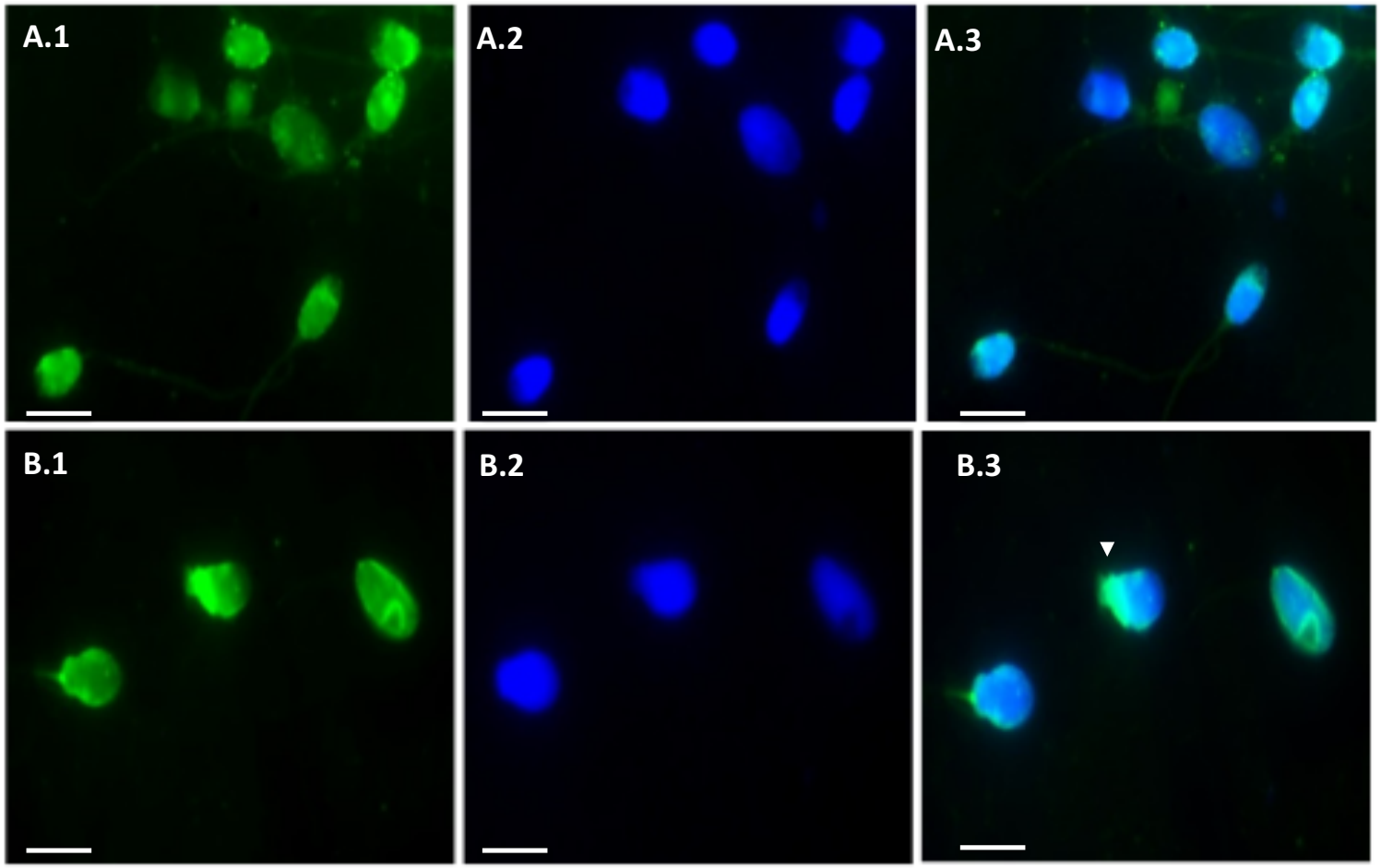

Figure 28: PRM1 signal in decondensed nuclei of human sperm. The signal for PRM1 was distributed throughout the nucleus, however, the signal intensity was slightly increased at the posterior end of the nucleus with DTT only in the decondensing buffer. Following the addition of heparin to the decondensation solution, however, the signal became more diffuse throughout the nucleus but with some localised concentrations (arrow head). A: DTT + detergent; A.1: PRM1 signal (FITC), A.2: DNA (DAPI), A.3: merged. B: DTT + 100U heparin; B.1: PRM1 signal (FITC), B.2: DNA (DAPI), B.3: merged. (scale bar 5µm)

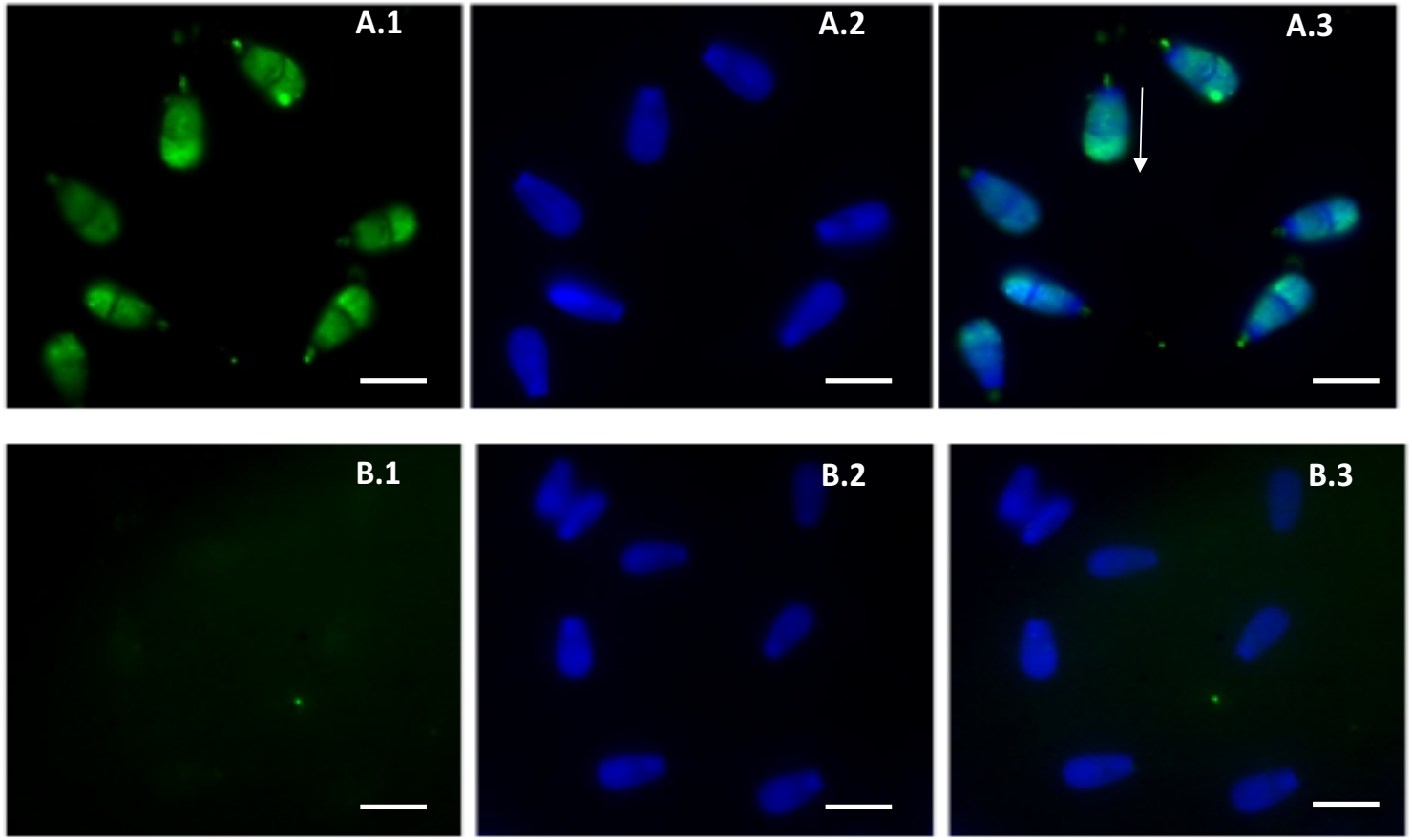

Figure 29: PRM1 signal in decondensed nuclei of bovine sperm (DTT + 100U heparin). PRM1 signal in decondensed nuclei of bovine sperm (DTT + 100U heparin). The signal for PRM1 was concentrated towards the anterior (acrosomal) end and required heparin in the decondensation solution. A: anti-PRM1; A.1: PRM1 signal (FITC), A.2: DNA (DAPI), A.3: merged. B: control; B.1: PRM1 signal (FITC), B.2: DNA (DAPI), B.3: merged. The white arrow pointed in parallel to the anterior end of the sperm nucleus. (scale bar 5µm).

2.3.3 Detection of 8-OHdG

The Abcam® immunocytochemical technique was used with modifications to detect the localisation of oxidative DNA damage in slightly decondensed mature bovine sperm (to allow antibodies to penetrate the sperm nucleus) (Figure 30). In pelleted sperm, an accumulation of 8-OHdG was detected using anti-8-OHdG antibody at the posterior part of the nucleus after incubating bovine sperm in PBS for 60 minutes (C1-C3). In addition, a strong signal was obtained at the posterior and the central regions of the nucleus after bovine sperm were exposed to 500 µM H_2O_2 for 60 minutes (A1-A3). Whereas, in interface sperm, more signal was detected in the posterior and central part of the nucleus after incubating bovine sperm in PBS for 60 minutes compared with pelleted sperm (D1-D3). Additionally, the signal of anti-OHdG antibody was more pronounced and cover most of the sperm head due to the accumulation of 8-OHdG after exposed bovine sperm to 500 µM H_2O_2 for 60 minutes (B1-B3).

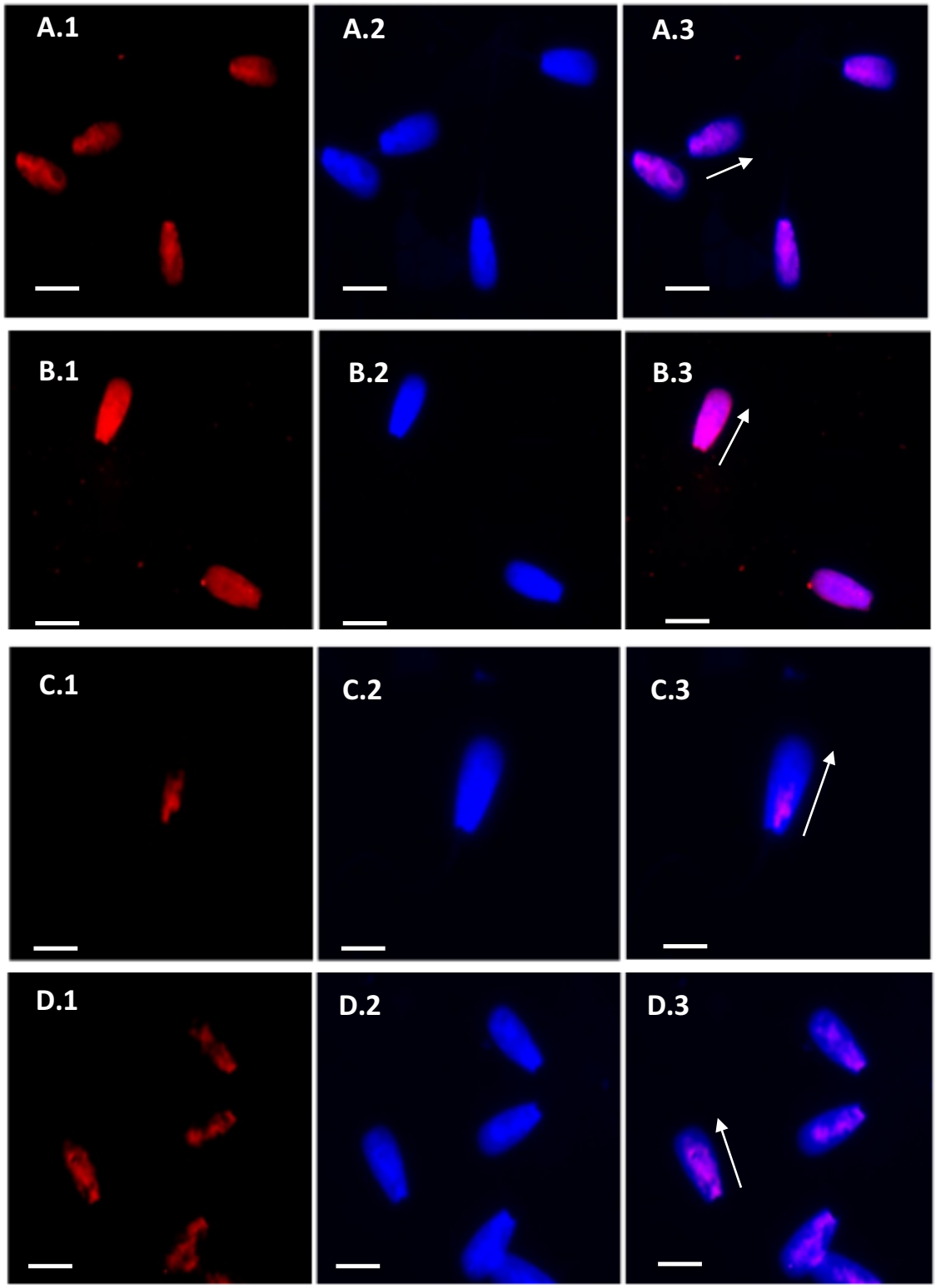

Figure 30: Anti-8-OHdG signal in intact nuclei of bovine sperm. A: pelleted-sperm incubated in 500 µM H_2O_2 for 60 minutes; A.1: Anti-8-OHdG (TRITC), A.2: DNA (DAPI), A.3: merged. B: interface sperm population incubated in H_2O_2 for 60 minutes; B.1: Anti-8-OHdG (TRITC), B.2: DNA (DAPI), B.3: merged. C: pelleted-sperm incubated in PBS for 60 minutes; C.1: Anti-8-OHdG (TRITC), C.2: DAPI, C.3: merged. D: interface sperm incubated in PBS for 60 minutes; D.1: Anti-8-OHdG (TRITC), D.2: DNA (DAPI), D.3: merged. The white arrow pointed in parallel to the anterior end of the sperm nucleus. (scale bar 5µm).

2.3.4 FISH

The commercial chromosome 3 probe showed a clear specific signal, which was detectable in each cell (Figure 31). The result of the commercial chromosome 3 probe validated the quality of FISH reagents as well as the slide hybridisation efficiency (Figure 31).

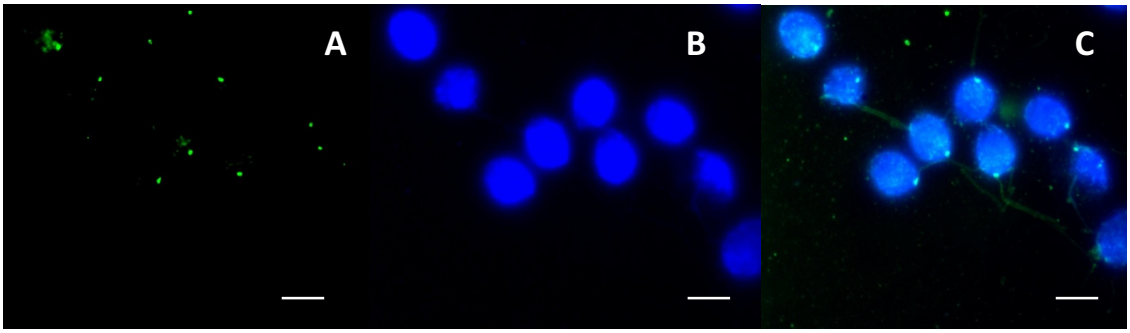

Figure 31: Slightly decondensed human sperm were hybridized with commercial centromeric probe as a control, which was labelled with FITC (appears as green). All sperm cells were stained with DAPI to visualise the cells (appears as blue). A: probe signal, B: DAPI, C: merged. (scale bar 20µm).

Labelled DNA fractions (Figure 32; A1-C2) showed clear fluorescence signals compared to the control (Figure 33; D1-F1). These strong FISH hybridization signals where the halo- and nucleoid-DNA probes correctly hybridized to their respective regions in human sperm suggested that restriction digestion and probe synthesis had worked successfully (Figure 31).

In halo-DNA, the signal was distributed strongly in the halo portion around the nucleus (A1-C1). Whereas, the signal from the nucleoid-DNA probe, was distributed throughout the sperm nucleus with weaker signals in the halo region (A2-C2). Additionally, a strong ring-shaped signal adjacent to the edge of the nucleus was observed (A2-C2). The signal of the negative salmon-DNA labelled control showed no fluorescence signal within the halo fraction (Figure 33; D1-F1). In partially decondensed sperm nuclei, halo-DNA hybridized internally with stronger localised regions of hybridisation (D2-F2).

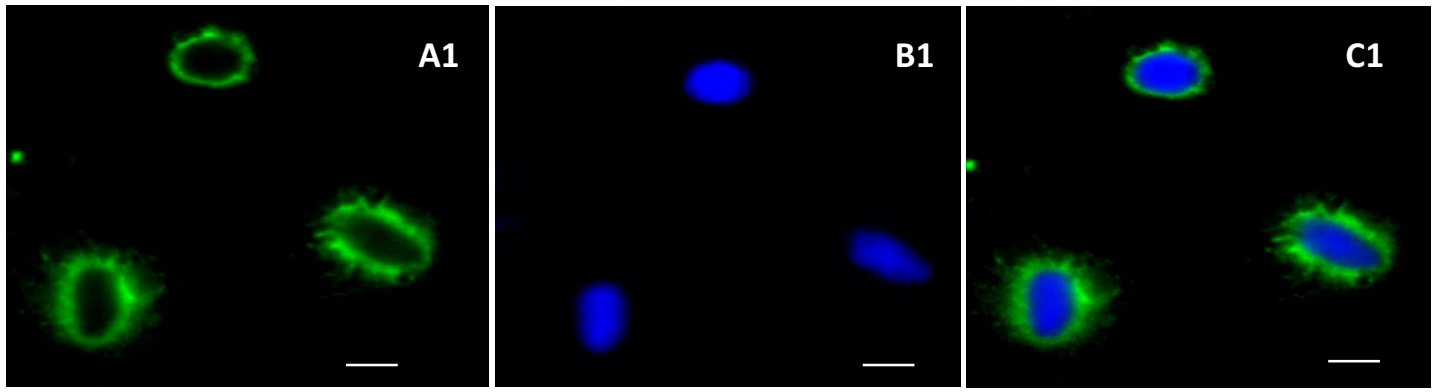

Figure 32a: Extracted halo-DNA was hybridized on human sperm, which were embedded in a micro agarose gel on a slide before formed a halo using a Halosperm kit. The DNA-probe was biotinylated and then exposed to a streptavidin-FITC, which was applied as post hybridisation (appears as green). All sperm cells were stained with DAPI to visualise the cells (appears as blue). A: probe signal, B: DNA (DAPI), C: merged. (scale bar 20µm).

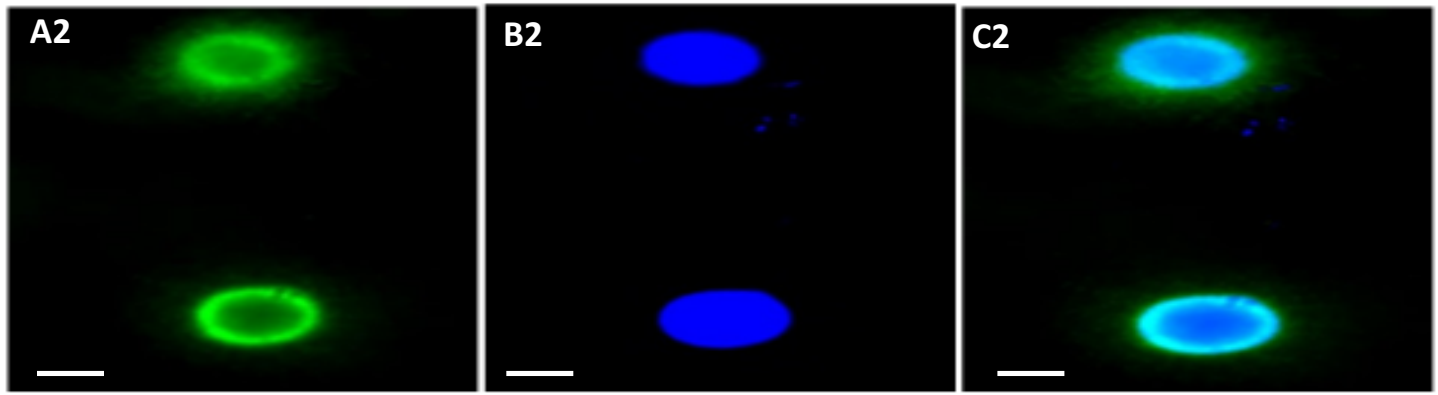

Figure 32b: Extracted nucleoid-DNA was hybridized on human sperm, which were embedded in a micro agarose gel on a slide before formed a halo using a Halosperm kit. The DNA-probe was biotinylated and then exposed to a streptavidin-FITC, which was applied as post hybridisation (appears as green). All sperm cells were stained with DAPI to visualise the cells (appears as blue). A: probe signal, B: DNA (DAPI), C: merged. (scale bar 20µm).

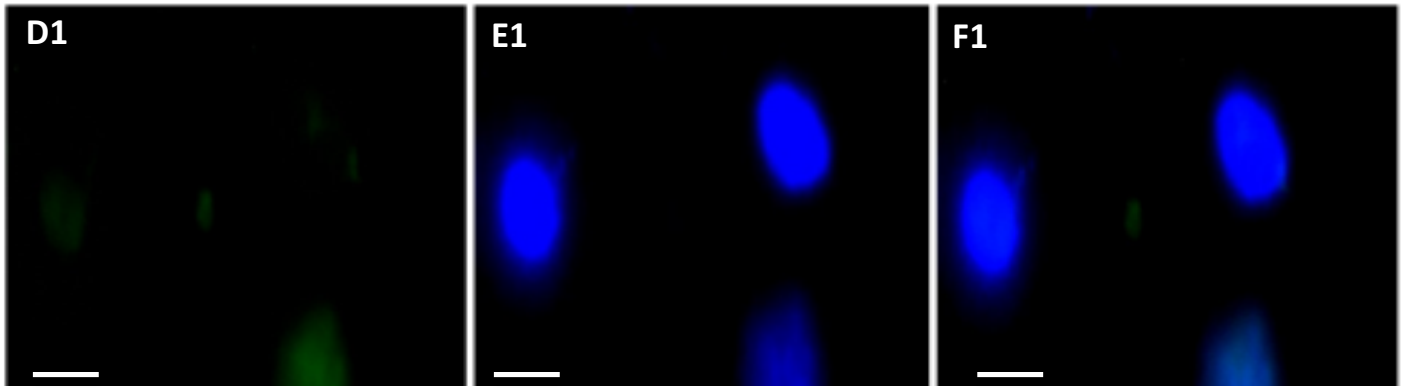

Figure 33a: Extracted salmon-DNA was hybridized on human sperm, which were embedded in a micro agarose gel on a slide before formed a halo using a Halosperm kit. The DNA-probe was biotinylated and then exposed to a streptavidin-FITC, which was applied as post hybridisation (appears as green). All sperm cells were stained with DAPI to visualise the cells (appears as blue). A: probe signal, B: DNA (DAPI), C: merged. (scale bar 5µm).

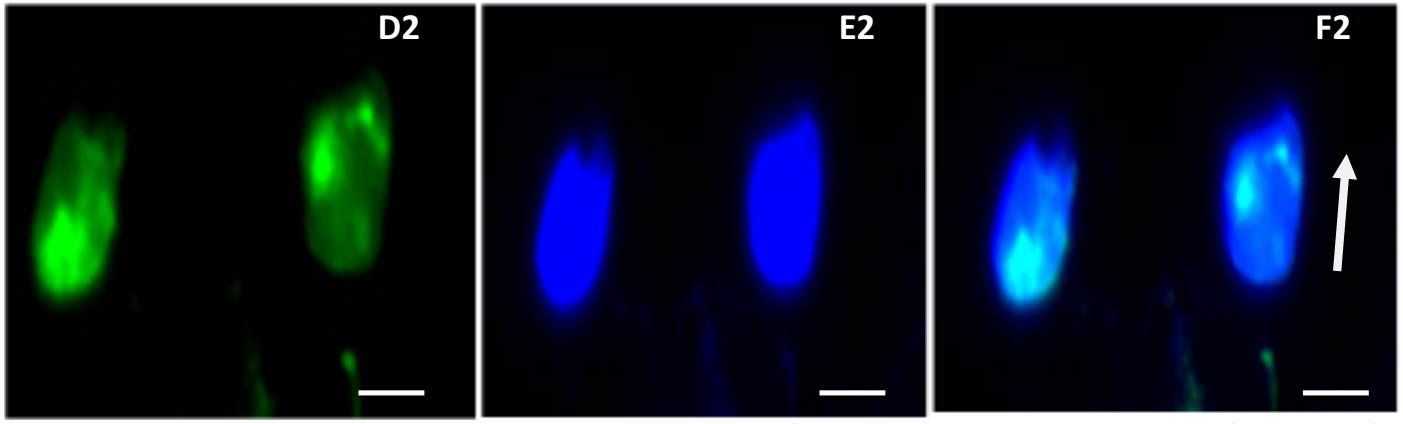

Figure 33b: Labelled halo-DNA probe was hybridized on slightly decondensed (triton X-100, 2.5 mM DTT and 100 U/ml heparin for 30 minutes) human sperm nuclei (appears as green). All sperm cells were stained with DAPI to visualise the cells (appears as blue). A: probe signal, B: DNA (DAPI), C: merged. The white arrow pointed in parallel to the anterior end of the sperm nucleus. (scale bar 20µm).

2.3.5 Western blot analysis of histones and protamines in halo preparations

The results showed that protamines were detected only in the nucleoid fractions and were absent from halo fractions (Figure 34a). Signals with different molecular masses were present in both fractions. On subsequently applying anti-histone antibodies to the same membrane, histone bands were clearly detected in both fractions (halo and nucleoid) (Figure 34b). The immunoblotting results suggest that soluble (halo) DNA fractions resulted in preferential histone extraction. Correspondingly, histone bands were observed in both fractions by applying same anti-histone antibodies to a SDS-PAGE gel (Figure 35). Similarly, in bovine, a protamine band was detected only in the nucleoid fractions (Figure 36a). In addition, histone bands were detected in both halo and nucleoid fractions after using H3 and H2A antibodies (Figure 36b). PRM1 signals were stronger in bovine sperm compared to human, which was likely because of the difference in the quantities of PRM1 in the sperm nuclei of each species. As human sperm express PRM1 and PRM2, two different bands were detected in the nucleoid fractions compared to mainly one band detected in bovine sperm (as bovine sperm express PRM1 only). Surprisingly, signals for higher molecular mass bands (weight box) were detected in both DNA-fractions of human and bovine sperm after applying anti-PRM1 (Figure 34a and 36a).

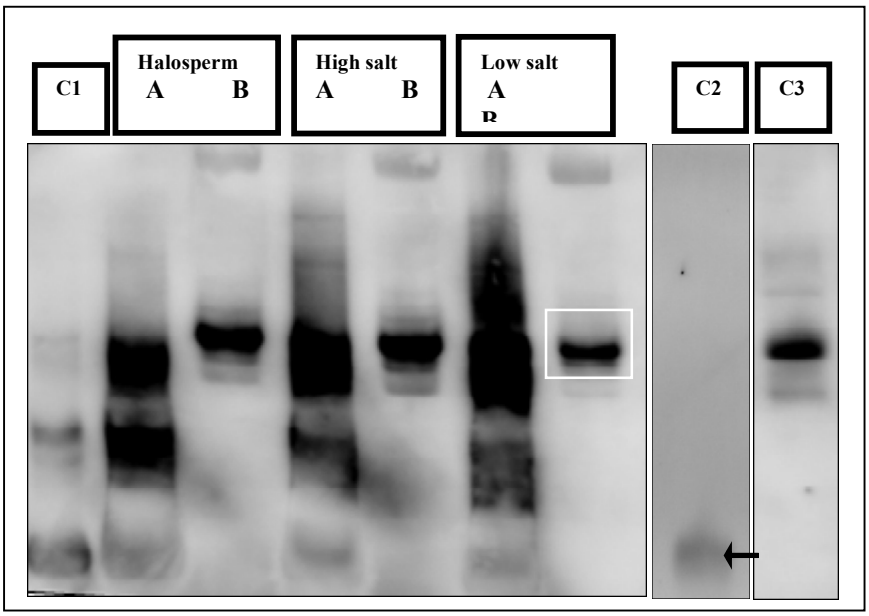

Figure 34a: A western blot of acid-urea-PAGE gel using PRM1 antibody (black arrow). Protamine bands were detected in nucleoid fractions (A), acid-extracted human sperm chromatin (C1) and purified PRM control (C2) only. Unidentified higher molecular mass signals were detected in the halo fractions (B). Controls, acid-extracted human sperm chromatin (C1), purified PRM1 (Briar patch biosciences) used as positive control for protamine 1 (C2), and purified core histones used as positive control for histones (Cayman Chemical) (C3).

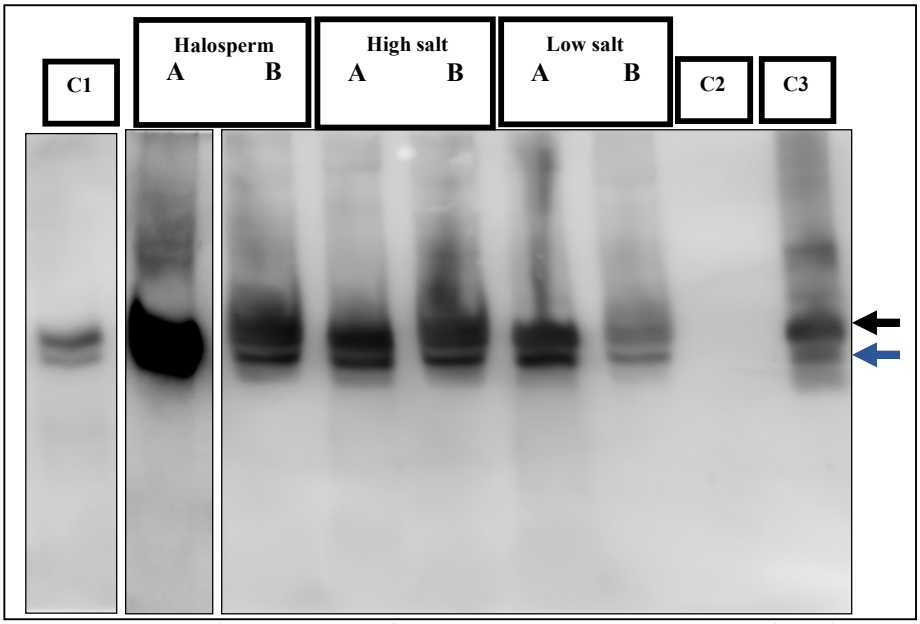

Figure 34b: A western blot of acid-urea-PAGE gel displayed the presence of H3 (black arrow) and H2A (blue arrow) bands in both fractions (halo (A) and nucleoid (B)) of each experiment using anti-H3 and anti-H2A antibodies. Controls, human chromatin (C1), purified PRM1 (Briar patch biosciences) used as positive control for protamine 1 (C2), and purified core histones used as positive control for histones (Cayman Chemical) (C3).

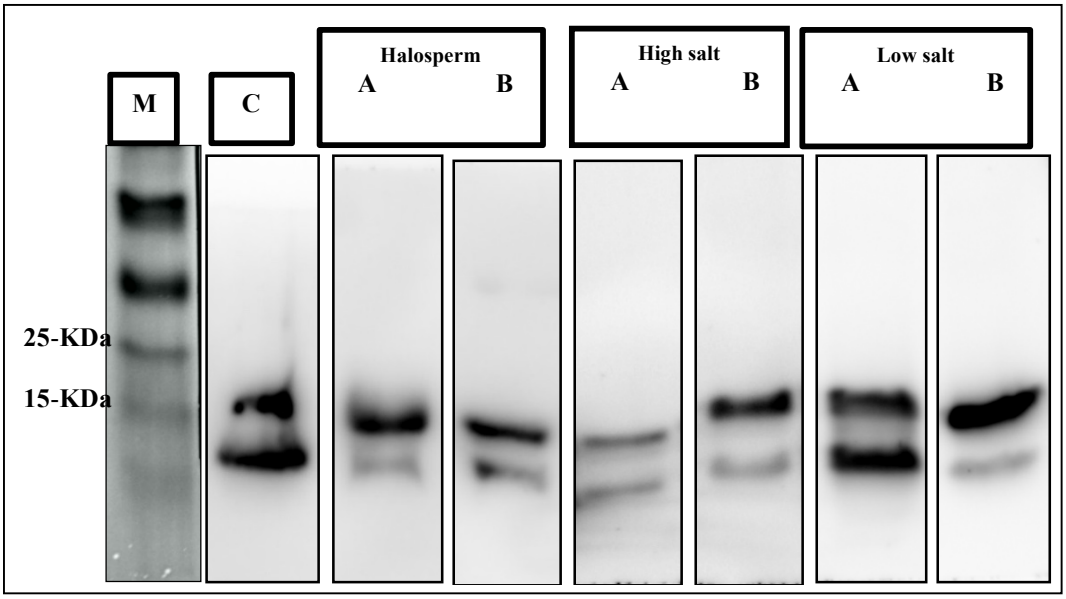

Figure 35: A western blot of SDS gel displayed the presence of histones in human sperm fractions. Anti-H2A and Anti-H3 antibodies were applied on SDS gel for both sperm fractions (halo and nucleoid), (A) halo fractions (B) nucleoid fraction (C) human chromatin used as a control (M) protein marker.

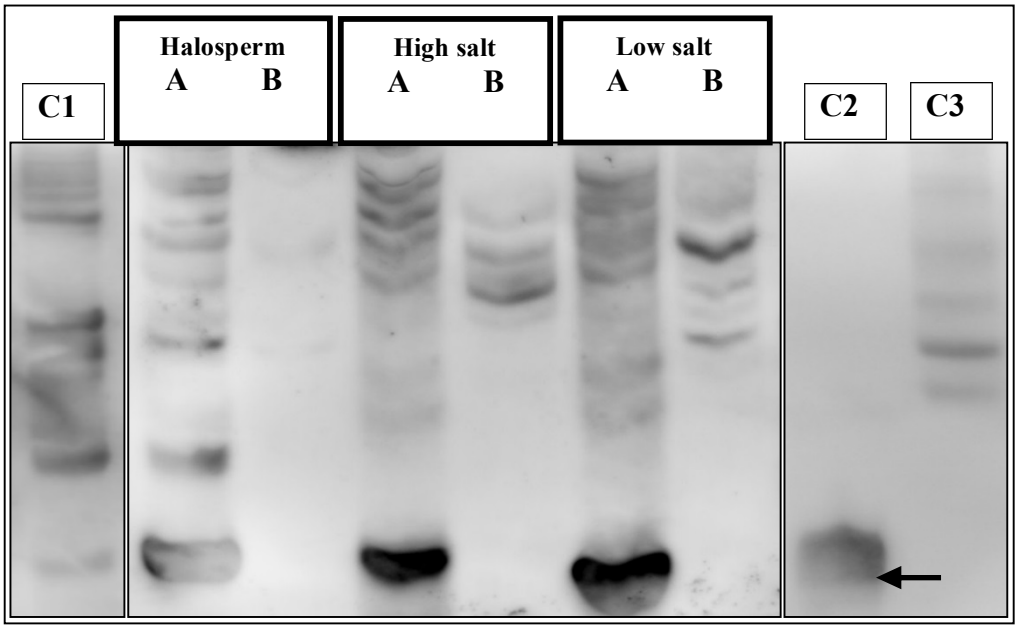

Figure 36a: A western blot of acid-urea-PAGE gel displayed the presence of PRM1 band (black arrow) in nucleoid fractions of bovine sperm that obtained by Halosperm assay. These protein bands were detected only in nucleoid fractions (A), while no such band detected in halo fractions (B). Controls; bovine chromatin (C1), purified PRM1 (Briar patch biosciences) used as positive control for protamine 1 (C2), and purified core histones used as positive control for histones (Cayman Chemical) (C3).

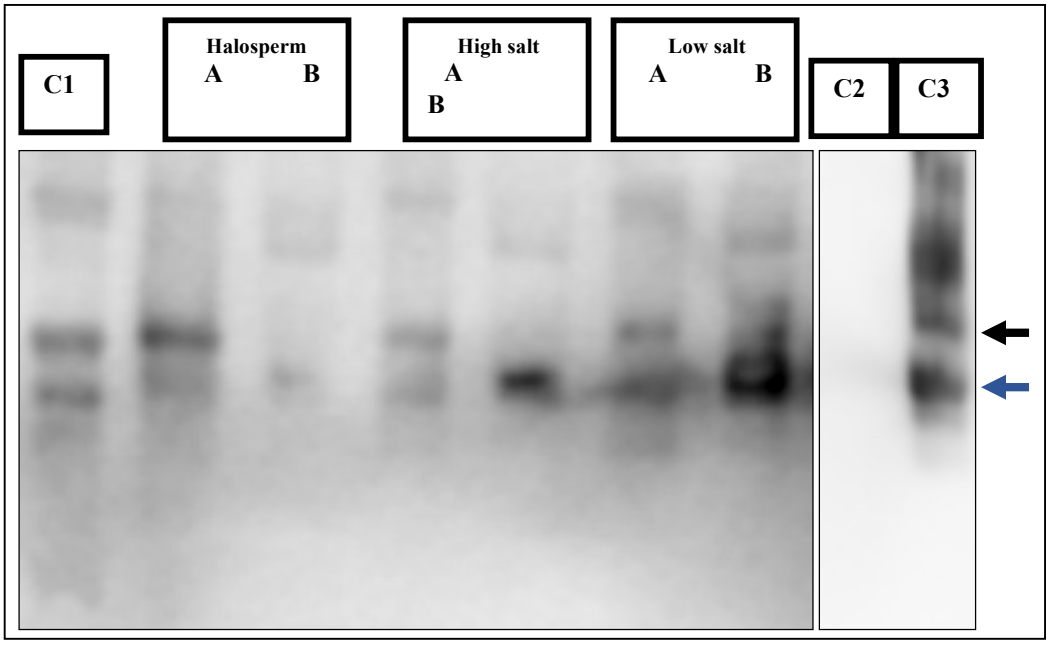

Figure 36b: A western blot of acid-urea gel displayed histones bands, H3 (black arrow) and H2A (blue arrow) in bovine sperm fractions using human anti-histone antibodies. Anti-H2A and Anti-H3 antibodies were applied on the gel for both sperm fractions (halo and nucleoid), (A) halo fractions (B) nucleoid fraction. Controls; (1) bovine chromatin, purified PRM1 (Briar patch biosciences) used as positive control for protamine 1 (C2), and purified core histones used as positive control for histones (Cayman Chemical) (C3).

2.4 Discussion

2.4.1 Localisation of histone in human and bovine sperm nucleus

Decondensation of sperm nuclei is a crucial step required to study nucleoproteins in spermatozoa using immunofluorescence with antibodies. This chromatin relaxing treatment was achieved by exposing the sperm nuclei to detergent buffers containing DTT, heparin or both reagents. In addition to DTT, heparin was occasionally added to the pre-treatment decondensation solution to allow antibodies to penetrate the nucleus more effectively (Heijden et al., 2008). Nuclear halo formation was achieved by exposing sperm nuclei to DTT with subsequent extraction of nuclear proteins by high or low salt, which dramatically affects the chromatin structure (Mohar et al., 2002; Ward, 2010).

Although the signals of the different antibodies that used in these experiments were detectable, there were signal variations from one sperm nucleus to another, which may be a result of variable antibody penetration of sperm nuclei. This heterogeneity may be due to an effect of the action of DTT as a reducing agent on disulphide bonds and heparin as a membrane destabiliser (Delgado et al., 1982). Incorrect concentration of these reducing agents might have introduced some chromatin changes into the nucleus of spermatozoa, which prevents antibodies from reaching their respective proteins (Nakai et al., 2006). Also, sperm chromosomal breakage may arise using a combination of DTT and Triton X-100 (Ward and Ward, 2004). Additionally, an incomplete decondensation process might negatively contribute to the absence of histone signal in the nucleus, which may produce a false negative result (Miller et al., 2010).

2.4.1.1 Histones in the nucleus of human sperm

Because of incomplete histone-protamine replacement, in human sperm, for example, approximately 5-15% of total nucleoproteins in sperm nuclei are retained histones (Miller et al., 2010; Zalensky et al., 2002; Ward et al., 1989; Dadoune, 1995). A previous study reported that histones are located in the posterior region of the intact nucleus of human sperm and can also be detected at the peripheral region when a limited decondensation process was employed (Li et al., 2008). In this and other studies, a corresponding distribution of core histones at the postacrosomal or posterior region of human sperm nucleus was also indicated (Van Roijen et al., 1998; Barone et al., 1994).

A high concentration of reducing agents in addition to different salt concentrations was used to generate nuclear halos with an intact nuclear matrix, and the location

of histones within this structure was explored. The results of these experiments showed that as a likely consequence of the halo structure, nucleosomal components as visualised by anti-H2A and anti-H3 antibodies are localised to the nuclear periphery. This localisation may relate to the presence of the nuclear matrix in sperm (Miller et al., 2010). Sperm treated with low salt buffer, gave an additional strong signal for histones at the posterior end of sperm nuclei, indicating that some histones remain associated with sperm DNA even after extracting nuclei with NaCl solutions (Zalensky et al., 2002). Similar patterns of histone signal were detected in the nuclei treated with low and high salt solutions, however, with high salt extraction, a lower signal intensity of histone was observed at the posterior end which may be as a result of more complete nucleoprotein extraction. According to Zalensky et al. (2002), Histones may be associated with telomeres in mature human spermatozoa and another study indicated that telomeres of human sperm chromosomes are located in the peripheral region of the nucleus (Mudrak et al., 2012), which supports the findings of this study.

2.4.1.2 Histones in the nucleus of bovine sperm

Previous studies have indicated the presence of histones in the head of bovine sperm within the perinuclear theca (H3, H2B, H3A and H4) (Tovich and Oko, 2003) and the nucleus itself (Sánchez-Vázquez et al., 2008). However, only two nuclear histones (H1 and CENPA) were previously detected in partially decondensed chromatin of bovine sperm (Douglas K. Palmer, 1990; Sánchez-Vázquez et al., 2008). In this study, although the limited decondensation process with bovine sperm nuclei may give differing results as shown by their high resistance to salt extraction (Tovich and Oko, 2003), like human sperm, the

pattern of core histone signal was located in the posterior end as well as in the central region of the nucleus, also corresponding to the pattern previously detected in human sperm (Li et al., 2008).

2.4.2 Localisation of PRM1 in human and bovine sperm nucleus

Protamine 1 has been detected in all studied mammalian spermatozoa (Balhorn, 2007; Dadoune, 1995). In this study, which is consistent with previous studies, the outcome showed that PRM1 signals were distributed throughout the nucleus of human sperm, (Yan Li, 2008). This well-distributed pattern of human PRM1 may be because protamines are the dominant DNA binding proteins in sperm and so would be expected to be found throughout the nucleus following a mild decondensation treatment (Zalensky et al., 1993).

In bovine sperm, using DTT *and* heparin in the decondensation solution is essential to obtain good signals due to the more heavily compacted chromatin of the nucleus masking epitopes (Motoishi et al., 1996). The result of this experiment showed that PRM1 was distributed throughout the nucleus, with higher signal intensities at the nuclear core. However, according to Dogan et al. (2015), morphologically normal heads of bovine spermatozoa can display a strong signal for PRM1 at the post-acrosomal region of sperm nuclei, while, the signal is strongly scattered at the sub-acrosomal and equatorial regions with weaker signals throughout the nuclei in abnormal sperm heads. Therefore, in the current study, the distribution of the fluorescent signal for PRM1 may have been affected by the decondensation conditions.

2.4.3 Western blot analysis of sperm histones and protamines

Although the similarity of the protein sequence of PRM1 is only 60% between human and bovine, PRM1 bands were detectable on the bovine blot. In this

current study, protamines could not be detected in proteins extracted from the halo fractions of human and bovine sperm (Gardiner-Garden et al., 1998; Castillo et al., 2014a; Gatewood et al., 1987), however, unidentified higher molecular mass signals in both halo and nucleoid fractions were detected. These signals may have arisen because of cross-reactivity between the anti-PRM1 antibody and histones. Unlike bovine sperm which contain PRM1 only, human sperm express both PRM1 and PRM2 (Ferraz, et al., 2010, Balhorn, 2007). As a result, additional bands were detected in the nucleoid fractions from human sperm.

As the protein sequences of H3 and H2A are highly similar (98.5% and 80%) between human and bovine, the same anti-histone antibodies were used for bovine samples. Histones were detected in extracts from both halo and nucleoid fractions of salt-extracted sperm of human and bovine nuclei (Castillo et al., 2014a). These findings support the hypothesis of higher accessibility to salt extraction of histone-rich compared with protamine-rich chromatin. However, faint higher molecular mass bands detected by the anti-histone antibodies in some halo fractions of bovine sperm may be due to the association between nucleosomal chromatin and the perinuclear theca, which could retard protein migration through the gels. Weak signals for histones in bovine sperm may arise following the mild decondensation process that reduces their presence in the sperm nucleus (Tovich and Oko, 2003). Alternatively, weaker signals may be due to the lower quantities of retained histones in bovine sperm (< 5%) compared to human (5-15%) (Ioannou et al., 2016; Palmer et al., 1990; Zlatanova and Leuba, 2004).

In this regard, the recovery of histones and absence of protamines from salt soluble fractions of human and bovine sperm chromatin suggest that halo DNA

most likely arises from nucleosome based chromatin. A previous study suggested that such an arrangement could be an efficient support for DNA replication or even transcription in the paternal pronucleus (Shaman et al., 2007b). Histones released by low salt extraction from human sperm also supports the suggestion that they are located closer to the nuclear periphery (Wykes and Krawetz, 2003) and that DNA-loops comprising the halo may originate from that region (Iarovaia et al., 2004).

2.4.4 8-OHdG

The accumulation of ROS due to H_2O_2 exposure leads to oxidative DNA damage in sperm cells (Sharma, 2016; Agarwal and Said, 2005). Many assays were used in this study to investigate the association between oxidative stress and DNA damage in sperm as a result of exposure to H_2O_2. Additionally, as a sensitive biomarker of oxidative DNA damage, 8-OHdG was used to monitor the accumulation in the intact sperm nucleus. Results from bovine sperm, in particular, showed that DNA damage first appeared in the posterior region of the nucleus and then proceeded to extend towards the anterior end of the nucleus, which correlates with the results of immunocytochemistry for the nucleohistone location in bovine sperm. Strong signals for 8-OHdG were detected throughout the nucleus of sperm after prolonged exposure of sperm to H_2O_2, indicating high levels of DNA damage. Moreover, in sperm from interface (45%) layers, signals for 8-OHdG were higher compared with sperm from the 90% population after incubation in PBS alone or PBS containing H_2O_2 incubation for 60 minutes. The results demonstrate variable levels of resistance to external oxidative stress factors between these two sperm subpopulations (90% and 45%), which is associated with corresponding variations in the highly compact structure of sperm

chromatin. Moreover, the signal of 8-OHdG showed that DNA damage is likely to occur first in the posterior end of the sperm nucleus in bovine, where the core histone signals have been reported in previous studies (Li et al., 2008). The similar albeit less extensive damage observed in 45% sperm incubated under control conditions without peroxide, may be due to higher levels of existing damage (Brahem et al., 2011) or possibly due to activation of endogenous endonuclease activity (Sakkas and Alvarez, 2010).

2.4.4 FISH

In this experiment, the results of sperm halo-FISH confirmed that both DNA fractions (halo and nucleoid) were efficiently accessed and digested by restriction enzymes (*Eco R1* and *Bam H1*) and labelled using the Bioprime system. In this regard, the halo-probe fluorescence signal was detected mainly within the halo regions, which indicated that the extracted halo-DNA was efficiently separated from the residual nucleoid-DNA. Nucleoid-probe fluorescence signals were detected strongly within the nucleus, with much weaker signals within the halo region. Hence, the probes mainly recognised their corresponding regions, adding confidence to the likelihood of our detecting regional differences in DNA sequence composition that could shed light on the impact of DNA fragmentation in relation to halo formation (see Chapter 5). Additionally, according to Ward and Coffey (1990), even after enzyme digestion, approximately 5-15% of halo-DNA remains attached to a nuclear matrix, which consequently becomes a part of the undigested nucleoid fraction.

Interestingly, the intense signals appearing as a ring-shape structure within the edge of the nucleoid may point to the hypothetical structure of sperm DNA loops that are thought to be attached at particular sites on the nuclear matrix (Ward et

al., 1999a; Miller et al., 2010). These findings corresponded with the results of histone distribution in sperm nuclei following halos generated by low and high salt extraction (see Chapter 2). Several groups have reported that an intact nuclear matrix is required for halo formation from sperm nucleus (Ward et al., 1999a; Johnson et al., 2011; Ward, 2013; Ward and Coffey, 1990). Also, the sperm nuclear matrix is preserved within the undigested nucleoid portion and not detached by enzyme endonuclease digestion (Shaman et al., 2007b).

Chapter 3: Assessing sperm DNA fragmentation in relation to chromatin condensation state using acridine orange, alkaline comet and aniline blue staining

3.1 Introduction

There are a number of assays in common use that can determine the ability of cells to survive an insult. Viability in response to a toxic insult can be assessed by treating cells with a genotoxic or cytotoxic factor such as hydrogen peroxide (H_2O_2) then measuring the effect of the toxin on cell survival and viability. Staining to distinguish between live and dead cells is one method for testing sample cell population viability following such exposure (Nandi et al., 2010). Several stains including aniline blue (AB) staining can be used to study chromatin-packaging maturity in sperm (Sellami et al., 2013) (Figure 40). In this regard, sperm DNA may be somewhat more protected from oxidative insult than somatic cell DNA by two factors; tighter packaging of sperm chromatin and antioxidants that are present in semen (Agarwal and Said, 2003). However, sperm are still susceptible to oxidative stress which can cause DNA damage due to large amounts of polyunsaturated fatty acids in the structure of their plasma membranes (Sharma and Agarwal, 1996; Sanocka and Kurpisz, 2004). Membrane damage arises through lipid peroxidation leading to lipid degradation, which can lead to DNA damage (Hosen et al., 2015).

Human sperm DNA damage has a negative effect on embryo development and has been implicated in several embryological anomalies leading to a lowering in embryo implantation rates and an increase in miscarriage rates and the frequency of developmental diseases in new-born (Valcarce et al., 2013).

This chapter focused on oxidative damage of sperm DNA, which was induced by using variable concentrations of H_2O_2. Fragmentation was detected using acridine orange (AO) and alkaline comet assay. As sperm chromatin maturity corresponds with susceptibility to DNA damage, aniline blue staining (Erenpreiss et al., 2001) of human spermatozoa isolated from 90% and 45% fractions of density gradient centrifugation was carried out.

AO emits a red fluorescence following excitation with a monochromatic 488 nm blue laser light when associated with a single-stranded DNA (ssDNA), while under the same excitation conditions, dye emits a green fluorescence when associated with double-stranded DNA (dsDNA) (Figure 37) (Evenson et al., 1986).

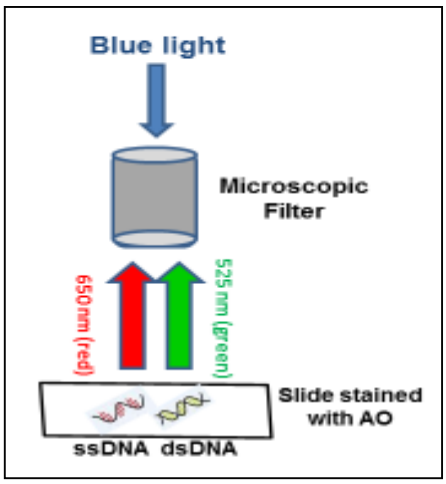

Figure 37: A diagram showed AO excitation that induced by blue light through a microscopic filter. AO emits a red fluorescence with a monochromatic 488 nm blue laser light when associated with a single-stranded DNA (ssDNA), while under the same lighting conditions; double-stranded DNA (dsDNA) emits a green fluorescence.

In this experiment, AO staining on slides was used to visualise stained sperm to locate the DNA damage in the nucleus in human and bovine spermatozoa. Whereas, the alkaline comet assay or single cell gel electrophoresis was used to measure DNA strand breaks and alkaline labile sites in individual sperm cells. The comet assay was initially applied to sperm by Singh et al. (1989). The assay

was optimised for modified alkaline conditions to detect both double and single stranded DNA breaks at a single cell level due to its sensitivity for detecting a low degree of DNA damage (Speit et al., 2009). According to Lewis and Agbaje (2008), the alkaline comet assay can detect DNA damage arising from as few as fifty single strand breaks per cell. Unlike the neutral comet assay which detects only double-stranded DNA breaks, under alkaline electrophoresis conditions, high pH causes relaxation in the DNA supercoiling which allows the DNA strand breaks to decondense and migrate from the sperm nucleus in the direction of the anode during a short electrophoresis step. Therefore, migrated DNA segments form a comet tail, which contains small DNA fragments. Whereas, a comet head contains undamaged DNA, which remains in the nucleus due to the lack of free ends. Therefore, Olive Tail Moment (OTM) DNA was used as an indication of DNA damage (Figure 38). For instance, the greater the loss of DNA supercoiled loops, the more segments of DNA migrate out from the comet head (Olive and Banath, 2006). After electrophoresis, cells stained with ethidium bromide can be visualised using a fluorescent microscope with a photometric camera. In this experiment, the capacity of the modified alkaline comet assay to detect DNA integrity was assessed only in bovine spermatozoa.

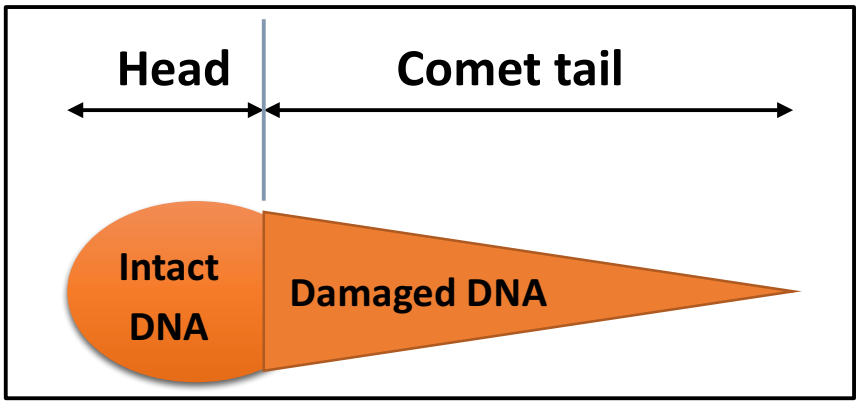

Figure 38: A model for comet assay that reveals damaged DNA (dsDNA and ssDNA), which migrate toward the anode and subsequently form a comet tail. Whereas, intact DNA (undamaged) remains in the comet head.

3.1.1 Experimental aim

The aims of this experiment were first; to show sperm isolated from percoll gradients demonstrate variable levels of resistance to external oxidative stress factors, which are associated with corresponding variations in the highly compact structure of sperm chromatin. Sperm were processed by density gradient centrifugation into high (viable) and low (non-viable) density fractions and stained by aniline blue to evaluate the chromatin maturity. These two subpopulations of sperm were then exposed to H_2O_2. Second, to visualise the origin of DNA damage in the sperm nucleus before and after exposure to H_2O_2 by using slide-based acridine orange assay. Third, applying also the alkaline comet assay to evaluate the state of sperm chromatin structure before and after exposure to H_2O_2.

According to Evenson et al. (1980), there is a similarity in the dynamics of DNA fragmentation between human and bovine spermatozoa, which led to the use of bovine sperm as an animal model in this study.

3.2 Materials and Methods

3.2.1 Sperm preparation

A percoll (Sigma Aldrich) based density gradient separation using two density layers, 45% and 90% was used to separate bovine and human semen into two subpopulations: namely a higher-quality pelleted-sperm (90% pellet) and a lower-quality interface-sperm (between 45 and 90%) (Figure 39).

Figure 39: Separated human semen into two sperm subpopulations, namely pellet (90%) and interface (45%) by using Differential Density Gradient Centrifugation (DDGC)

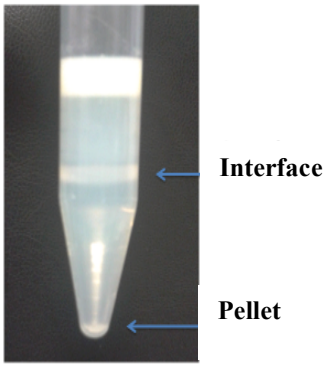

3.2.1.1 General sperm preparation

Human and bovine sperm were separated into two subpopulations by DDGC method as described by Malik et al., (2011) and Parrish et al., (1995). Frozen bovine semen (0.5 mL straws) was thawed at 39°C for 30 seconds. Human semen frozen in 0.5mL aliquots with cryoprotectant medium (sperm freezing medium, ORIGIO) was thawed at 37°C for 20 minutes. Depending on the sperm count, either semen from a single sample was used or several samples from the same bovine or human donor were pooled together. The thawed semen was layered gently above a two-layer gradient comprising 2 mL of 45% (upper) and 2 mL of 90% (lower) percoll in a 15 mL plastic tube. The 90% percoll solution was prepared as follows; 45 ml of percoll medium was mixed with 5 ml of 10X Sp-TALP buffer (31.0 mM KCl, 100.0 mM NaCl, 3.0 mM NaH_2PO_4 and 100.0 mM HEPES, (pH 7.3) to which was added 2.0 mM $CaCl_2$, 0.40 mM $MgCl_2$, 21.6 mM Lactic acid and 25.0 mM $NaHCO_3$).

The final osomolality of 90% percoll solution was adjusted to 280-300 mosmols/kg (by using 10X PBS or dH_2o) as measured by freezing point depression. A 45% percoll was prepared by mixing the 90% percoll solution 1:1 with 1x Sp-TALP (10 mM NaCl, 10 mM HEPES, 0.3 mM NaH_2PO_4, 3.1 mM KCl, 25 mM $NaHCO_3$, 21.6 mM Lactic acid, 2 mM $CaCl_2$, 0.40 mM $MgCl_2$, 1 mM

pyruvate, 1% Bovine Serum Albumin (BSA) (pH 7.3). The gradient layers and semen were centrifuged at 700 g for 30 minutes for bovine sperm and 600 g for 20 minutes for human sperm. The sperm pellet and interface layer (that positioned between the 45% and 90% percoll) were isolated in two separate tubes. Both the sperm pellet and interface layer were resuspended with Sp-TALP (for bovine sperm) or Suprasperm wash (ORIGIO) (for human sperm) and then centrifuged at 900 g for 10 minutes. The previous step was repeated once more. The concentration of the sperm pellets in both tubes was counted using hemocytometer chamber and then resuspended to a concentration of 1 x 10^6 sperm/mL with PBS.

3.2.2 Aniline blue staining

sperm chromatin integrity was evaluated by aniline blue staining (Sati and Huszar, 2013). 10 µL volumes (~1 x 10^4) of washed sperm from each subpopulation (pellet and interface) were smeared onto coated slides and left to dry at room temperature. Samples were then fixed in 3:1 methanol/acetic acid (v/v) for 30 minutes at room temperature. After air-drying, the slides were stained in 2.5% (w/v) AB (Sigma Aldrich) in 2% acetic acid solution (ready to use staining) for 5 minutes. After that, the slides were rinsed in distilled water for 5-7 minutes and followed by air-drying. Slides were scanned in a raster-like pattern and images were captured with a photometric camera using a computerised leica DMRB DIC Bright-field microscope. Sperm were assessed and counted visually by two observers independently.

The proportions of stained versus unstained sperm from both subpopulations were normally distributed; therefore, data were compared and statistically analysed with GraphPad prism using a two-way *ANOVA* and Sidak's multiple

comparisons test with at least 50 spermatozoa assessed per sample per group (pellet and interface).

3.2.3 Sperm decondensation

Described in detail in chapter 2 in section 2.2.4

3.2.4 Inducing DNA damage by exposure of sperm to H_2O_2

DNA damage was induced into sperm cells using H_2O_2 as described by Chohan et al., (2004). A 30% stock solution of H_2O_2 (Sigma Aldrich) was diluted to 100 and 300 µM and added to 50 µL of sperm suspension and incubated for 60 minutes at 4°C. A similar sample of sperm suspension was mixed with an equal volume of 1x PBS and used as a control. After H_2O_2 exposure, 500 µL of Quench solution (2.5ml 2% Bovine serum albumin (Sigma-Aldrich), 500 µL Bovine Catalase (Sigma-Aldrich), 0.5 mL 10x PBS and 2 mL ultrapure water) was added and pipetted until bubbles stopped forming indicating destruction of any remaining H_2O_2 (catalysing H_2O_2 to H_2O and O_2). Samples were centrifuged at 200 g for 5 minutes. The supernatants were discarded and then the sperm pellets were resuspended with 1 mL 1x PBS. Then, the samples were centrifuged again at 200 g for 5 minutes. After the supernatants were discarded, the sperm pellets were washed with 200 µL 1x PBS. An acid denaturation step was induced by exposing the samples to 500 µL of 0.1 M HCL and incubated for 30 seconds. After that, pH was neutralised by adding an equal volume (500 µL) of 0.1 M NaOH. Samples were centrifuged at 200 g for 5 minutes. The supernatant was removed before the sperm pellet resuspended with 100 µL of 1x PBS and twenty µL of resuspended sperm was spread on a coated slide and left to dry out at room temperature.

3.2.5 Acridine orange staining

Slides were fixed by carnoy-like solution and then stained with acridine orange as described by Yagci et al., (2010). Slides were fixed for 2 hours with carnoy-like solution (9:1 ratio of methanol and glacial acetic acid). After that, slides were stained with acridine orange solution (0.1 M citric acid and 0.25 mL of 0.3 M Na_2HPO_4, pH 2.5 and 6 µg/mL of acridine orange) for 5 minutes at room temperature, then slides were rinsed gently with distal water. Later, stained slides were analysed using a Zeiss LSM510-META upright confocal microscope (Zeiss LSM 510 ver4.0), where the colour of 50 individual sperm were assessed and counted per field by Image J software.

Results are expressed as a DNA fragmentation index (DFI) (ratio of red/(red + green) fluorescence) (Mohammed et al., 2015) following exposure to H_2O_2 (Figure 41-42). Additionally, mature human and bovine sperm were exposed to 6 M H_2O_2 for 60 minutes as a positive control for DNA fragmentation (Figure 40).

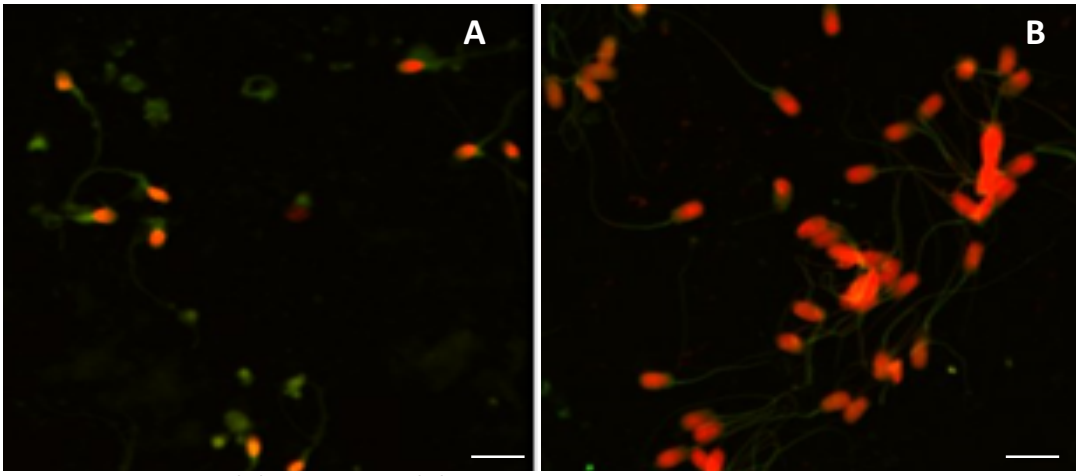

Figure 40: Human (A) and bovine (B) sperm samples, which were exposed to high concentration (6 M) of H_2O_2 and then stained with AO, and used as a positive control. Both human and bovine sperm stained with red colour due to high level of DNA damage. (scale bar 1µm)

The proportions from sperm subpopulations were normally distributed, therefore, data were compared and statistically analysed with GraphPad prism using a two-

way *ANOVA* and Sidak's multiple comparisons test to compare the ratio of DFI within and between the two groups (pellet and interface).

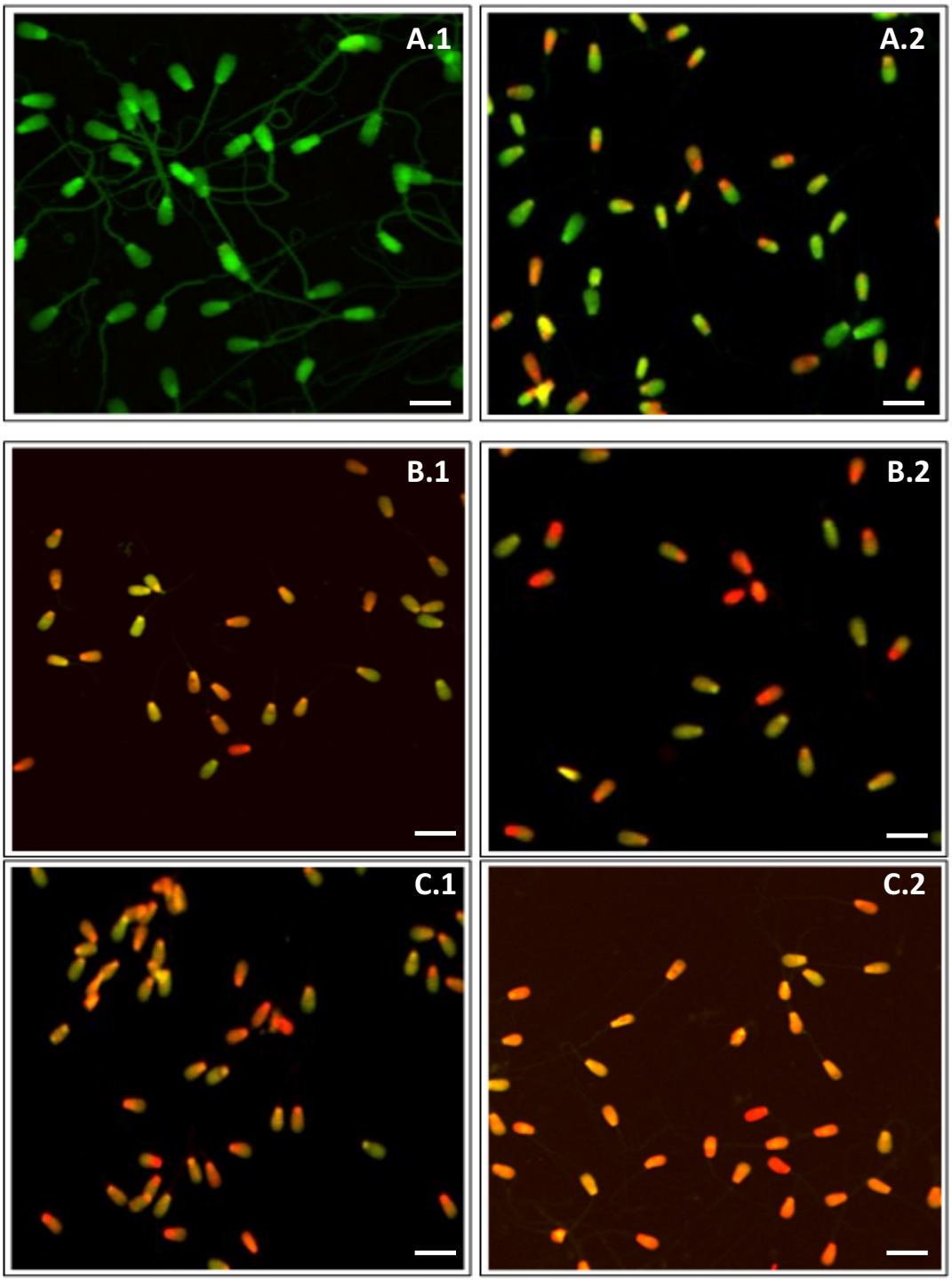

Figure 41: Microscopic images for bovine sperm exposed to different concentrations of H_2O_2, and then stained with AO. (A) Sperm incubated in PBS for an hour as a control (A.1) pelleted fraction (90%) and (A.2) interface fraction (45%), (B) Sperm incubated in 100 µM of H_2O_2 for an hour (B.1) pelleted fraction (90%) and (B.2) interface fraction (45%), (C) Sperm incubated in 300 µM of H_2O_2 for an hour (C.1) pelleted fraction (90%) and (C.2) interface fraction (45%). (Scale bar: 20 µm)

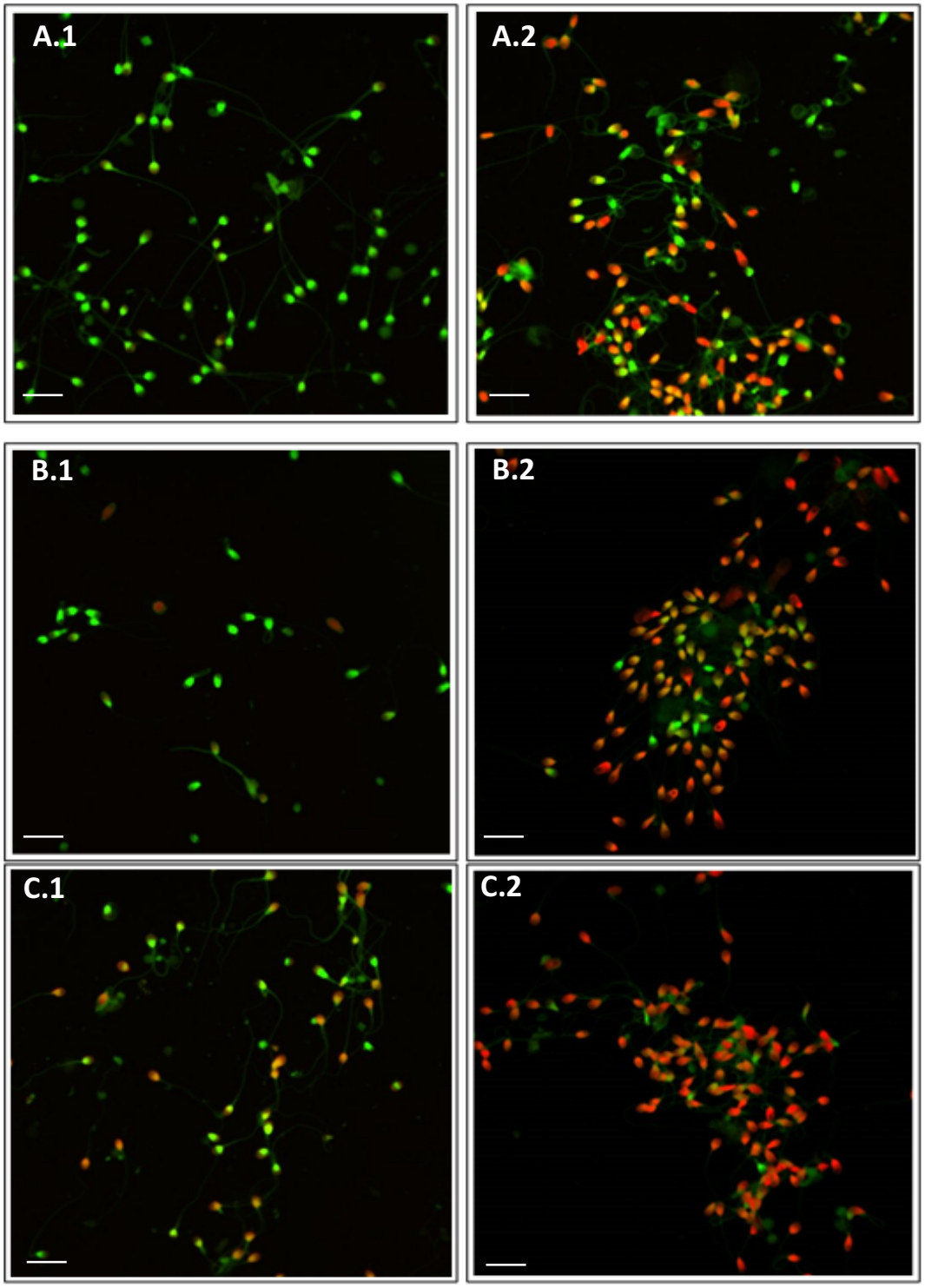

Figure 42: Microscopic images for human sperm exposed to different concentrations of H_2O_2, and then stained with AO. (A) Sperm incubated in PBS for an hour were used as a control (A.1) pelleted fraction (90%) and (A.2) interface fraction (45%), (B) Sperm incubated in 100 µM of H_2O_2 for an hour (B.1) pelleted fraction (90%) and (B.2) interface fraction (45%), (C) Sperm incubated in 300 µM of H_2O_2 for an hour (C.1) pelleted fraction (90%) and (C.2) interface fraction (45%). (Scale bar: 10 µm)

3.2.6 Alkaline comet assay

The alkaline comet assay was carried out according to Hughes et al., (1998) with some modifications. Microscopic slides were dipped up to the frosted area in a 1% solution of hot normal melting point agarose (NMPA) (Bioline) in Dulbecco's Phosphate Buffered Saline (DPBS) and gently removed. Immediately, the underside of slides was wiped to remove agarose, and then slides were kept overnight in a box on a flat surface to dry. A 10 µL of sample suspension (approximately 1 X 10^5 sperms) was added to 75 µL of 0.5% warm low melting point agarose (LMPA) (Thermo Fisher) in DPBS. The sperm (bovine) suspension was then layered onto the prepared slide and covered immediately with a cover slip to spread out agarose evenly. Immediately, the slide was placed on a cold block for a minimum 30 seconds, and then the cover slip was removed gently to avoid disruption of the agarose. Another layer of 0.5% LMPA (75 µL) was added onto the second layer and covered with a coverslip, then left at room temperature to solidify. The cover-slip was removed, and then slides were immersed in a coplin jar containing freshly prepared cold lysis buffer (2.5 M NaCl, 100 mM Na_2EDTA, 10 mM TRIS (pH 10) with 1% Triton-100 X, added immediately before use) at 4°C for a minimum 1 hour. Followed by, a further incubation at 40°C with 40 mM of dithiothretol (DTT) for 3 hours to reduce the disulfide bonds. Then, slides were incubated with 0.1 mg of proteinase K at room temperature for 90 minutes to remove proteins. After removing the proteinase K solution, slides were immersed in fixed concentrations of H_2O_2 (100 and 300 µM) in PBS for one hour at 4°C, followed by further incubation in PBS for another hour at 4°C. A horizontal electrophoresis tank was filled with freshly prepared cold running buffer (300 mM NaOH, 1 mM EDTA (pH 13.0) at 12-15°C. Slides were placed horizontally in that

gel electrophoresis tank with the frosted edge to the edge of the cathode and incubated for 20 minutes to unwind the DNA. The running buffer's level was adjusted to approximately 0.25 cm above the slide's surface and the voltage adjusted to 25 V at 300 mA (0.714/cm) by decreasing or increasing the buffer level in the electrophoresis tank. After electrophoresis, slides were immersed in a neutralisation buffer (0.4 M Tris, pH 7.5) and incubated for 5 minutes at room temperature. Slides were drained of excess buffer and stained with 25 µL of 20 µg/mL ethidium bromide in a dark room for 20 minutes. Stained slides were examined under a computerised leica DMRB DIC fluorescence microscope. Finally, fifty individual sperm were scanned in a raster-like pattern and images captured with a photometric camera. The Comets were quantified using Image J software (OpenComet).

Results are expressed as an Olive Tail Moment (OTM) DNA following exposure to H_2O_2 (Figure 43). A number of microscopic images were obtained for bovine sperm after, which exposed to H_2O_2 before staining with ethidium bromide (Figure 44). By using OpenComet (image J), the OTM DNA was measured on each image to determine the head and tail of each cell (Figure 43). Statistically, the data were normally distributed, therefore, two-way *ANOVA* used to compare the Olive Moment DNA in both pellet and interphase sperm subpopulations.

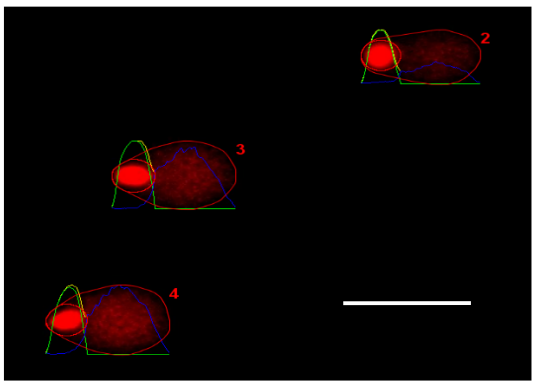

Figure 43: An image showed the assessment of the DNA damage in the tail comet using image J. software (OpenComet) in alkaline comet assay. (scale bar: 25 µm)

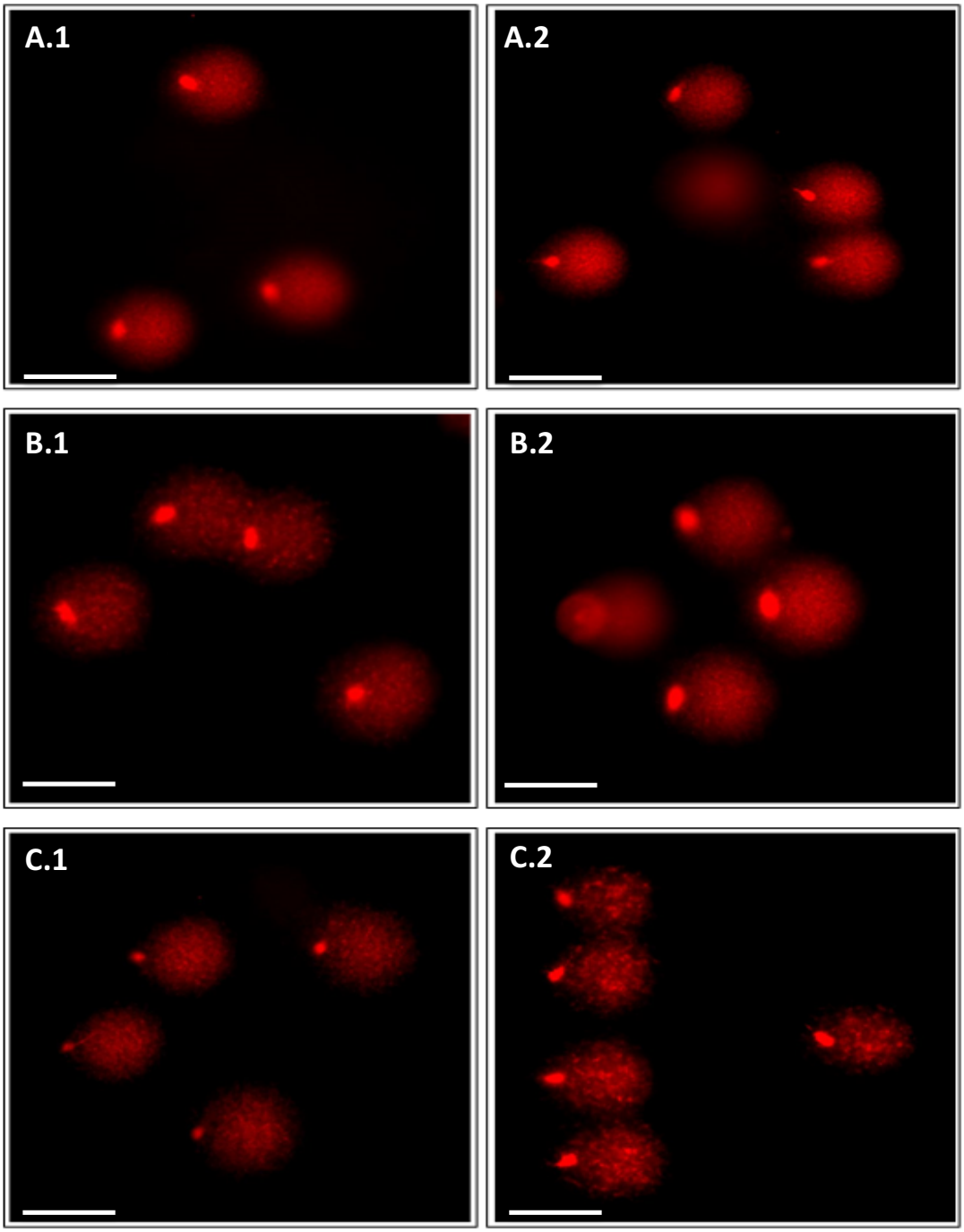

Figure 44: Microscopic images for bovine sperm exposed to different concentrations **of** H_2O_2**,** and then stained with ethidium bromide. **(A)** Sperm incubated in PBS for an hour as a **c**ontrol **(A.1)** pelleted fraction (90%) and **(A.2)** interface fraction (45%), **(B)** Sperm incubated in 100 µM of H_2O_2 for an hour **(B.1)** pelleted fraction (90%) and **(B.2)** interface fraction (45%), **(C)** Sperm incubated in 300 µM of H_2O_2 for an hour **(C.1)** pelleted fraction (90%) and **(C.2)** interface fraction (45%). (Scale bar: 20 µm)

3.3 Results

3.3.1 Aniline blue staining and quantitation

Spermatozoa were assessed for chromatin condensation and maturity by aniline blue staining. Results are expressed as the percentages of stained and partially or unstained spermatozoa in samples recovered from pellet (90%) and interface (45%) fractions. In general, sperm with no staining (-) are considered to have mature, highly condensed chromatin while sperm with partial or strong staining (+) are considered immature and with relatively decondensed chromatin containing more residual histones (Schulte et al., 2010). A number of microscopic images of aniline blue stained sperm were obtained using a bright field microscope (Figure 45).

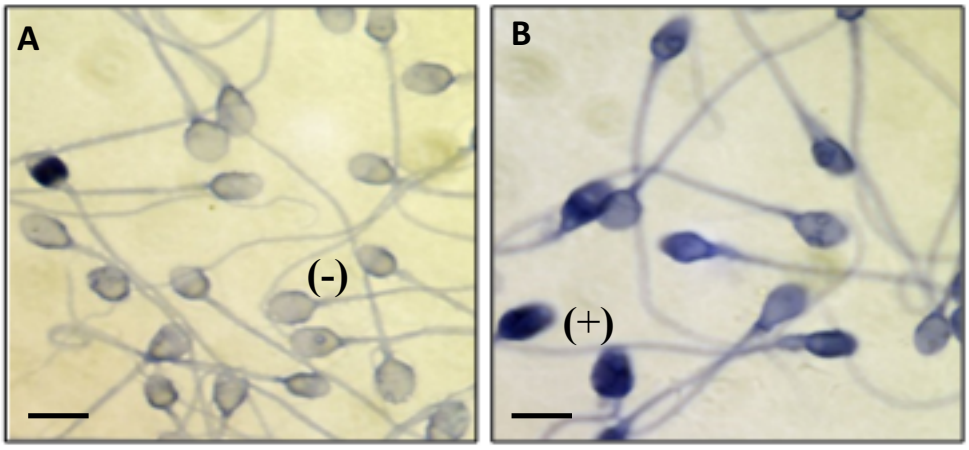

Figure 45: Microscopic images showed two populations of human sperm separated by percoll gradient fractions into (A) 90% pellet (B) 45% interface stained with aniline blue. Sperm heads with normal chromatin structure do not stain or stain weakly, and those with abnormal chromatin structure stained dark-blue. (Scale bar: 20 μm)

Comparing aniline blue staining in 45% and 90% fractions, the percentage of non-stained sperm was statistically significantly higher ($p \leq 0.0001$) in 90% fractions and conversely, the proportion of stained sperm in 45% fractions was statistically significantly higher than in 90% fractions ($p \leq 0.0001$) (Figure 46).

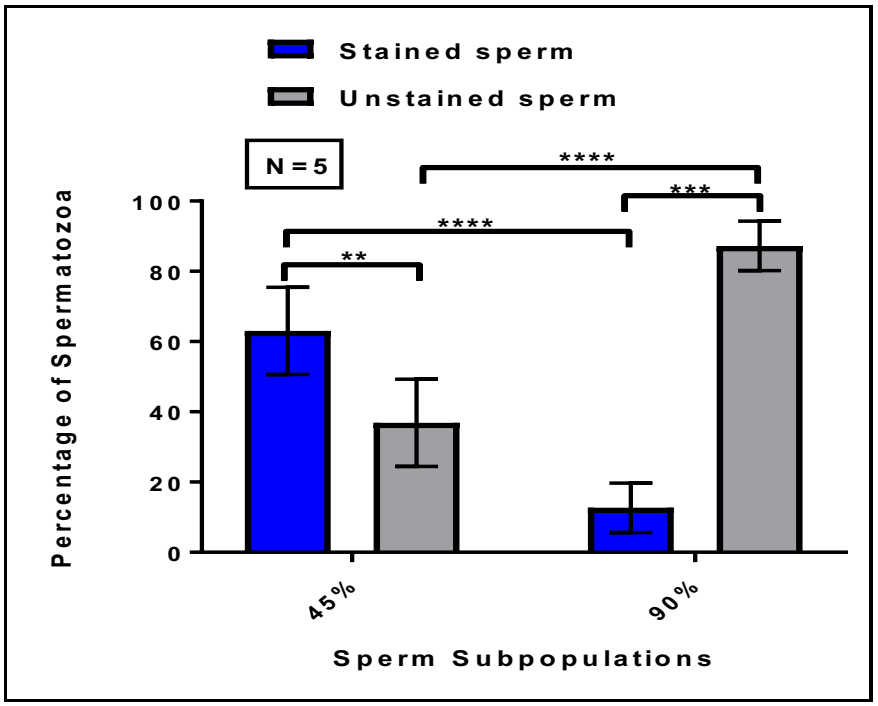

Figure 46: A bar graph shows the percentage of human sperm stained with aniline blue staining, which assessed sperm chromatin compaction in both pelleted and interface subpopulation. (Mean ± SD)

The AB staining indicated that sperm from the two DDGC fractions have differing relative levels of chromatin compaction and so it is likely that the subpopulations of sperm from these fractions will also have different sensitivities to oxidative stress. To test this hypothesis, levels of DNA damage induced by different concentrations of H_2O_2 (100 and 300 µM) in human and bovine spermatozoa from the two DDGC fractions were evaluated by fluorescence microscopy following AO staining and the comet assay.

3.3.2 DNA damage assessed by AO

As it was difficult to induce or to detect DNA fragmentation in intact bovine sperm by AO staining following exposure to 50 µM and 100 µM of H_2O_2, a short chromatin decondensation step was carried out to relax the chromatin structure sufficiently to provide greater access prior to exposure to H_2O_2 (Figure 47).

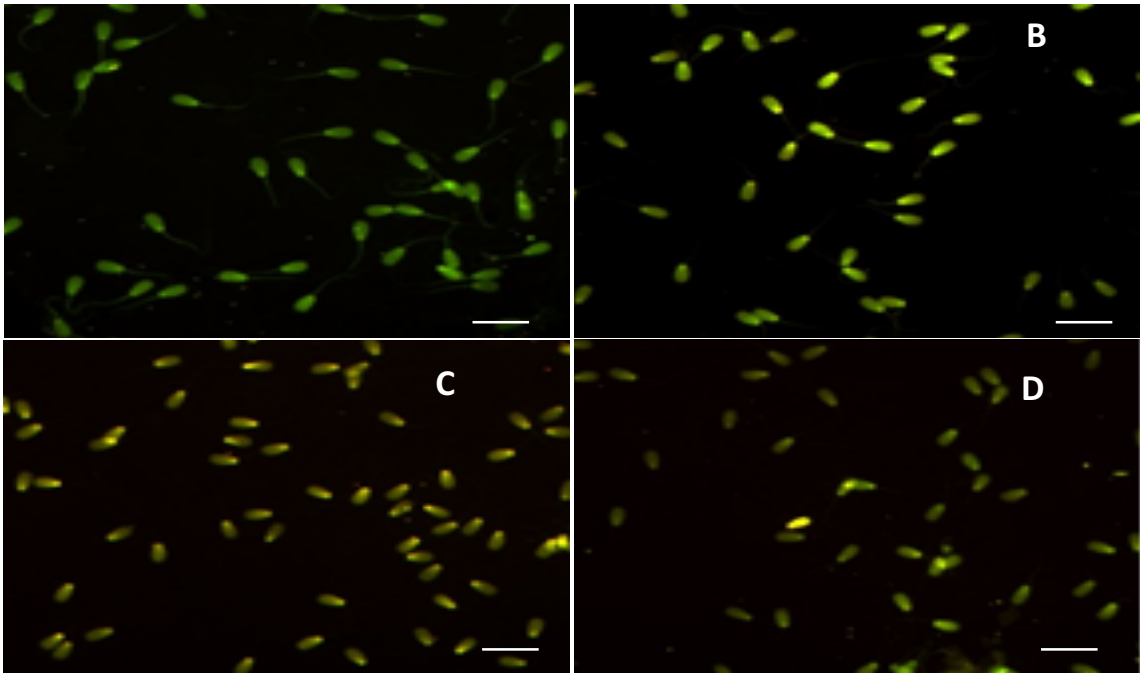

Figure 47: Microscopic images of bovine sperm after exposure to different concentrations of H_2O_2, and then stained with AO. Pelleted sperm treated with 50 µM (A) 100 µM (B) and interface layer treated with 50 µM (C) and 100 µM (D) (scale bar 5µm)

Comparing AO staining in 45% and 90% fractions, in human, the mean DFI in controls (no H_2O_2) in 45% fractions was almost double (around 0.4%, $p \leq 0.01$) than in 90% fractions. Whereas, the mean DFI at 100 µM of H_2O_2 showed no significant differences between 90% (0.35%) and 45% (0.43%) fractions (Figure 46), while, the mean DFI in 45% fractions was significantly higher ($p \leq 0.01$) compared to 90% fractions (Figure 48).

Similarly, in bovine, the mean DFI in controls (no H_2O_2) was almost double (around 0.38%, $p \leq 0.001$) than in 90% fractions (around 0.19%). Moreover, in 45% fractions, the mean DFI at 100 µM of H_2O_2 was significantly higher ($p \leq 0.01$) compared to 90% fractions, while, after increasing the concentration of H_2O_2 to 300 µM, no significant difference was obtained between 45% and 90% fractions (Figure 49).

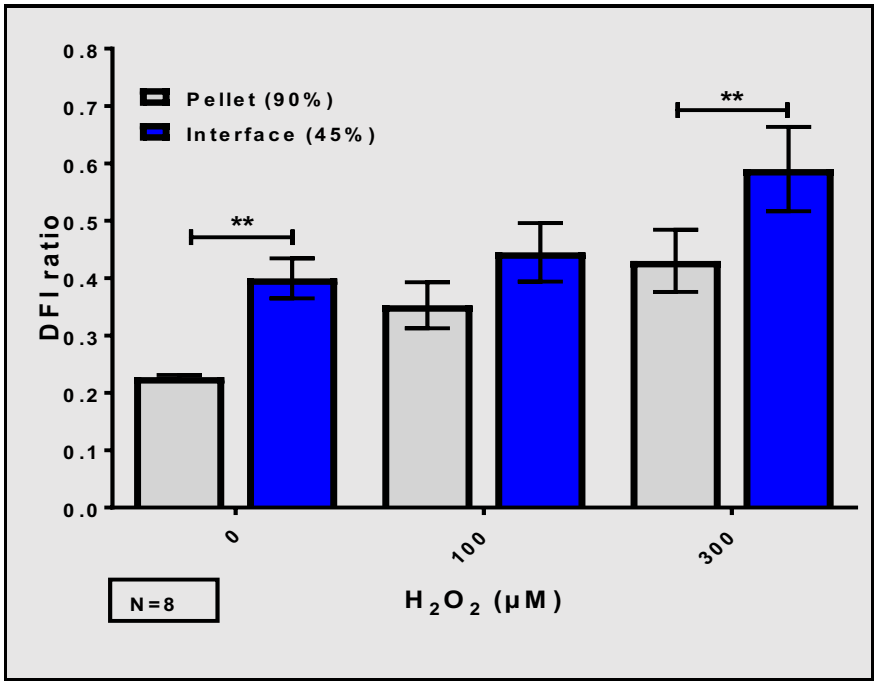

Figure 48: A bar graph shows the DFI of AO which represents the levels of DNA damage with different concentrations of H_2O_2 in both pelleted and interface human sperm. (Mean ± SEM)

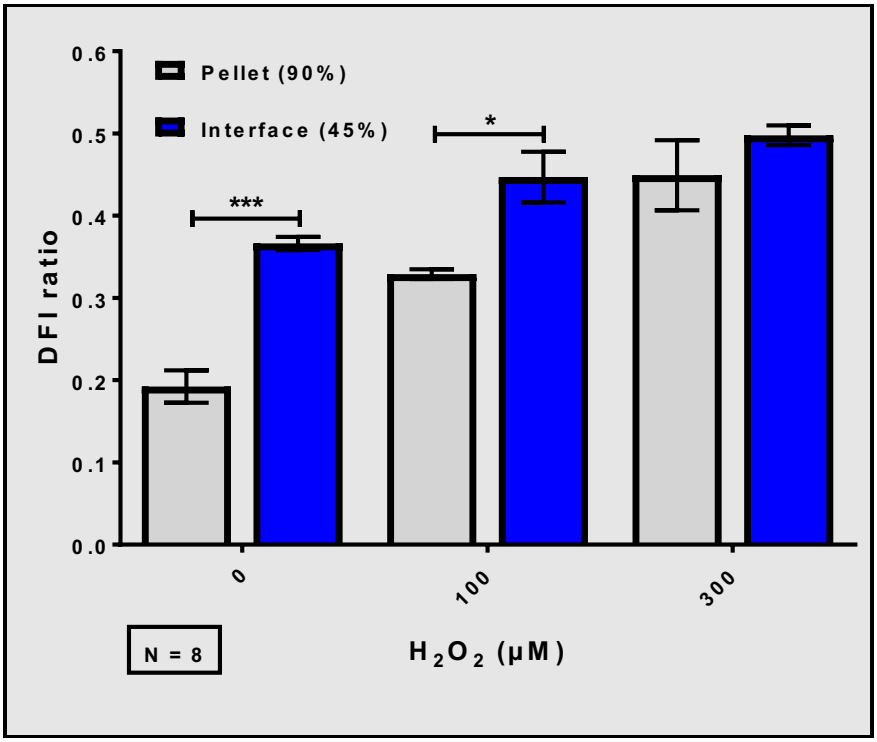

Figure 49: A bar graph shows the DFI of AO which represents the levels of DNA damage with different concentrations of H_2O_2 in both pelleted and interface bovine sperm. (Mean ± SEM)

3.3.3 DNA damage assessed by alkaline comet assay

3.3.3.1 90% versus 45% fractions

Analysis of the OTM DNA showed no statistical significant differences (p>0.05) between 90% and 45% fractions following exposure of 100 and 300 µM of H_2O_2 compared with the controls (not treated with H_2O_2) (Figure 50).

In 90% fractions, however, the OTM DNA at 100 µM of H_2O_2 was statistically significant (p<0.01) compared with the controls (no H_2O_2), and less significant (p<0.05) at 300 µM H_2O_2. Whereas, in 45% fractions, there were no significant differences (p>0.05) in the OTM DNA at 100 and 300 µM of H_2O_2 compared with the controls (Figure 50).

Figure 50: A bar graph showed a statistical comparison of the percentages of head DNA in 90% and 45% fractions of bovine sperm with different concentrations of H_2O_2. (Mean ± SD)

3.4 Discussion

3.4.1 Effects of decondensation chemical

As shown in Chapter 2 section 2.2.4, the decondensation was a required process in bovine sperm, in particular, to help acridine orange penetrating the sperm

nucleus and stain the DNA segments in the nucleus. It was difficult to induce DNA fragmentation in intact bovine sperm, even after exposure to 50 μM and 100 μM of H_2O_2. Therefore, a short chromatin decondensation step was carried out to relax the chromatin structure sufficiently to provide greater access prior to exposure to H_2O_2. However, in the comet assay, decondensation process was not required as there was decondensation step in its protocol.

3.4.2 Assessed sperm DNA damage using AO, comet and AB

The highly condensed structure of sperm chromatin helps to protect the cell from the effect of genotoxic agents (Villani et al., 2010). Alterations in spermatozoal chromatin can arise from different causes; for example, defective apoptosis and abnormal chromatin compaction during spermatogenesis or excessive generation of ROS. In addition, DNA damage can be induced by external factors such as smoking, toxins or oxidative stress (Chohan et al., 2006). In this study, the effects of exposure to H_2O_2 on the DNA chromatin integrity of human and bovine sperm was investigated using AO staining and the comet assay. AO is most often used as an indicator of DNA damage in spermatozoa (Barratt et al., 2010). Additionally, the comet assay is a popular technique that is frequently used to assess DNA damage in spermatozoa due to its sensitivity for indicating very low levels of DNA damage in individual cells (Speit et al., 2009).

As AB staining provides a measure of chromatin compaction, relating to excess retention of histones, the assay can indicate whether a sperm is more or less likely to be susceptible to DNA fragmentation (Auger et al., 1990). These assays have been used in the IVF clinic to assess DNA fragmentation and chromatin maturity in sperm of infertile patients with varicoceles, for example, as an indicator of sperm quality (Dadoune et al., 1988; Liu and Baker, 1992). Furthermore, many

studies use AO staining to assess DNA damage and examine the treated cells by a flow cytometry (FACS) (Evenson and Wixon, 2006; Golan et al., 1997; Hughes et al., 1997). In this study, AO staining was carried out on glass slides to visualise the extent and origin of DNA damage in the sperm nucleus. Although the AO test on a slide is not as sensitive as FACS for assessing DNA fragmentation, it has the advantage of allowing the visualisation of stained sperm including the location of the DNA damage in the sperm nucleus.

Several variations of the comet assay have been standardised principally depending on the type of cells that are analysed, for example, by increasing the length of incubation in lysing buffer and the concentrations of reagents (Singh et al., 1988). In addition, some technical steps in the protocol may have also been modified due to the type of cells being examined. Sperm, for example, are highly DNA condensed cells and should be exposed to DNA damage-inducing agents like H_2O_2 after lysing and proteinase K incubations (particularly in bovine) (Donnelly et al., 1999). In this study, both (90% and 45%) subpopulations were exposed to H_2O_2 at two different concentrations (100 and 300 µM) after the lysing buffer incubations and sperm not treated with peroxide were used as control. Major differences between the two post-density gradient subpopulations were observed by both AB and AO, before and after H_2O_2 exposure. In the controls, for example, results showed that the majority of spermatozoa isolated from 90% fractions generated green AO nuclear fluorescence, which indicates that this subpopulation of sperm had mostly undamaged DNA. Similarly, the majority of the sperm isolated from this subpopulation were not stained with AB, which indicates that sperm from this subpopulation had good chromatin compaction, whereas, in the sperm population isolated from 45% fraction, the mean DFI of the

(peroxide untreated) control population was approximately double that of the 90% fraction. Correspondingly, the sperm isolated from 45% fraction were mostly darkly stained with AB, which indicated that sperm isolated from 45% fraction may have more relaxed (less compact) chromatin due to defects in their chromatin structure that could leave them more susceptible to further DNA fragmentation (Brahem et al., 2011). However, unexpectedly in the comet assay, the controls demonstrated a high percentage of tail DNA (>50%). Although these peroxide untreated sperm showed a high percentage of DNA tail, there was a significant effect of H_2O_2, particularly in 90% fractions. While, there was no significant differences in 45% fractions after exposure of different concentrations of H_2O_2, which may be a consequence of existing chromatin immaturity (as AB showed) or high existing levels of DNA fragmentation (as AO showed) in such sperm subpopulation.

These findings demonstrated that differential density gradient separation segregates sperm efficiently into populations with little or no DNA fragmentation. Although there was a significant correspondence between DNA damage and higher concentrations of H_2O_2 in both species, sperm isolated from their respective 90% fraction demonstrated more resistance to the external oxidative stress factor than the 45% subpopulations, which indicates that sperm represented in 90% fractions were of higher quality. The results of AO staining highly corresponding with the results of AB in relation to chromatin compaction and DNA fragmentation. Also, in the comet assay, the results showed a significant increase in DNA damage in 90% fractions following exposure to 100 and 300 μM of H_2O_2. Nevertheless, the results of the comet assay may be considered as accurate but not precise due to the high levels of DNA damage in

the controls, which might be produced either by the protocol itself, high levels of sperm alkali-labile sites (Del Mazo, 2013) or DNA fragmentation due to endonuclease activation (Olive and Banáth, 2006). Also, as the controls showed high levels of DNA damage, exposing sperm cells to 100 μM of H_2O_2 may be sufficient to induce highest levels of DNA damage in the nucleus, therefore, increasing the concentration to 300 μM may not cause any further significant damage to the DNA. According to Olive and Banáth (2006), DNA fragmentation assessed in the comet tail is not necessarily the result of the direct effect of the oxidative stress factors, however, extensive DNA damage can be caused by membrane and internucleosomal DNA fragmentation via apoptosis (Wlodkowic et al., 2011). As a result, in order to avoid the influence of apoptotic DNA damage, 'viability check' tests, for example, nigrosin-eosin and trypan blue tests, are common tests that can be carried out on sperm before it undergoes the comet assay (Collins et al., 2008). Also, freezing and thawing process may increase fragmentation levels of DNA in the sperm nucleus (McEvoy et al., 2014). Therefore, the differences between the two sperm subpopulations (90% and 45%) can be significantly changed by using fresh semen instead of frozen samples. As the results showed, 45% fractions behaved similarly in AB, AO and the comet assays, which were different from 90% fractions. Comparable, 90% fractions also behaved similar in AB, AO and the comet assays.

In AO assay, particularly in bovine sperm, it was noticed that DNA damage was likely to first appear in the posterior end of the sperm nucleus (near the annulus). This and previous studies have shown that histones are present in the nucleus of bovine sperm, close to the annulus, which is a similar location to their location reported in human sperm (Li et al., 2008; Valcarce et al., 2013). Also, the results

of anti-8-OHdG showed that DNA damage first appeared in the posterior region of the nucleus and then proceeded to extend towards the anterior end of the nucleus, which corresponds with the results of both AO and immunocytochemistry for the nucleohistone location in bovine sperm. Consequently, further studies can be considered to investigate the relationship between the starting point of DNA breaks and sperm nuclear histones compartment using different techniques such as FISH.

Chapter 4: Assessing sperm DNA fragmentation in relation to chromatin condensation state using Halosperm™ assay

4.1 Introduction

The sperm chromatin dispersion (SCD) assay measures DNA fragmentation by the extent of halo formation following extraction of sperm proteins (Figure 51). (Fernandez et al., 2005a). The commercial application (Halosperm™), is now being used widely in the clinic. However, unlike the alkaline halo or comet assay, where sperm nuclei with high levels of DNA damage form halos of fragmented and diffused DNA while sperm with undamaged DNA produce small or no halos (Sestili, 2009). The SCD assays relies on the development of larger halos dependent on the level of unfragmented DNA, with fragmented DNA leading to the generation of small or no halos (Galaz-Leiva et al., 2012b). With SCD, halo formation is based on the removal of nuclear proteins, which frees the chromatin from restraints counteracting torsional stresses within the nucleus resulting from DNA packaging and liberates double strand DNA loops (Fernández et al., 2011). The absence or presence of DNA damage with either halo type is determined by measuring the halo size, although with reverse interpretation (Fernandez et al., 2005b). To generate and visualise halos, intact sperm are usually immobilised in an agarose matrix and treated with detergents and acid or alkaline salt buffers to lyse the cells and denature the DNA. Halos arise from the diffused or dispersed DNA loops and are visualised by microscopy with chromogenic (Giemsa, for example) or fluorogenic (ethidium bromide, for example) reagents (Enciso et al., 2006a).

The effects of oxidative damage were originally assessed on sperm DNA using the acridine orange and alkaline comet assays (Chapter 3). In this chapter, the effect of oxidative damage was assessed on dispersion halos (Halosperm). SCD was assessed because its halos rely on the presence of unfragmented DNA and it was reasoned that recovered dispersion halo DNA would be a more appropriate platform than the alkaline diffusion halo for DNA sequencing aimed at exploring the composition of this compartment. Assessing the dynamics of halo formation using the dispersion assay, however, should give complementary results to AO and alkaline comet assays and this was tested during the course of these experiments.

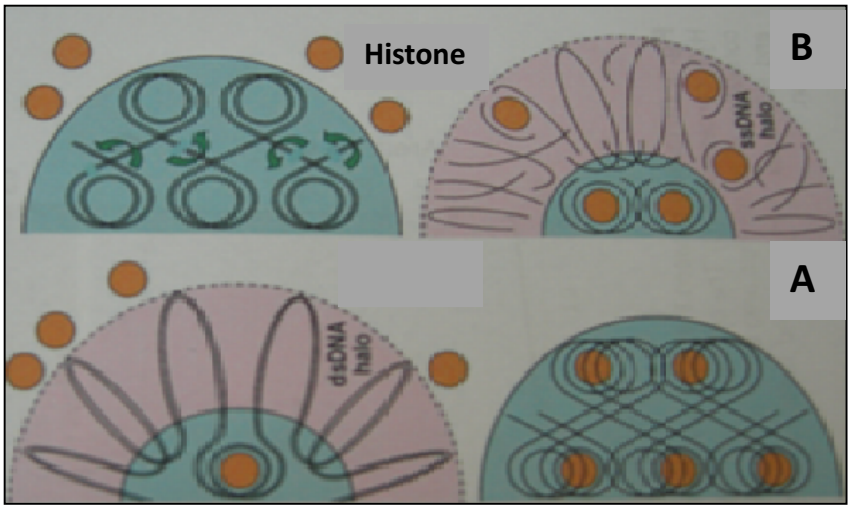

Figure 51: A diagram shows two types of halo formation, first, sperm nuclei with low levels of DNA fragmentation subjected to an acid extraction process develop halos of dsDNA, the extent of which rely on the tension released by the extraction of DNA binding proteins (Halosperm™ test) **(A)**. In contrast, sperm nuclei with high levels of DNA fragmentation subjected to an alkaline extraction process release their fragmented ssDNA forming simple halos (around the sperm head) of diffused DNA loops depending on the extent of DNA fragmentation **(B).** Adapted from: (Galaz-Leiva et al., 2012b).

4.1.1 The aims of this experiment

The aim of this experiment was to examine the dynamics of dispersion halo formation in sperm isolated following DDGC, including assessment of their resistance to external oxidative stress, associated with their sedimentation

characteristics (90% or 45% fractions) and their corresponding levels of DNA compaction. As the dynamics of DNA fragmentation in human and bovine spermatozoa are similar (Evenson et al., 1980), bovine sperm were also used in this study.

4.2 Materials and Methods

4.2.1 Sample preparation

Described in detail in chapter 3 in section 3.2.1

4.2.2 Slide preparation

slides were prepared according to the manufacturer's protocol (Fernández et al., 2005). Frosted microscopic slides were coated with 1% agarose and left to air dry. Micro-centrifuge tubes (1.5 ml) containing 0.7% (w/v) of low-melting point agarose were placed in a water bath at 90–100°C for 5 minutes until the agarose had dissolved and then held in a water bath at 37°C for 5 minutes. After 5 minutes of incubation for temperature equilibration at 37°C, 25 µL of the diluted sperm sample (approximately 2 X 10^6 sperms) was added to the Micro-centrifuge tubes and mixed with the liquefied agarose. Of the sperm–agarose mix, 25 µL were pipetted onto the gel-treated side of the slides (precoated with agarose), and covered with a 22- by 22-mm coverslip (avoiding air bubbles). The slides were placed on a cold plate in the refrigerator (4°C) for 5 minutes to allow the agarose to produce a microgel with the sperm cells embedded within.

4.2.3 H_2O_2 exposure

After the cover-slips were gently removed, the slides were immediately immersed horizontally into two different concentrations of H_2O_2 (100 and 300 µM). A similar slide of sperm-agarose mix was immersed horizontally into 1X PBS and used as a control. After H_2O_2 exposure, the slides immediately incubated horizontally in

HCl (0.1 M) for 30 seconds, followed by incubation for another 30 seconds in NaOH (0.1 M). Then, the slides were washed with PBS for 5 minutes.

4.2.4 Halosperm™ assay

The Halosperm™ assay was carried out according to the manufacturer's protocol (Fernández et al., 2005) with some modification for bovine samples. A denaturation solution (DA) was prepared by mixing 80 µL of the denaturation solution (tube labelled DA), which provided with the kit, with up to 10 mL of water and mixed for 15 seconds. After removing the cover-slip, the slides were immediately immersed horizontally into the DA solution and incubate for 10 minutes for bovine and 7 minutes for human sperm at room temperature. Then, slides were incubated horizontally into the lysing solution for 25 minutes (30 minutes for bovine) at room temperature. Afterwards, the slides were washed in distilled water for 5 minutes at room temperature. Then, the slides were dehydrated horizontally with increasing concentrations of ethanol (70, 90 and 100%) for 2 minutes each and left to air-dry. After that, the slides were stained with 1:1 diluted (v/v) solution of Wright-Giemsa stain (sigma-Aldrich).

4.2.5 Wright's Giemsa stain

For bright-field imaging of halos, sperm were stained with Giemsa solution (0.4% w/v, in a buffered methanol solution, pH 6.9) (sigma-Aldrich) and PBS (1:20) for 30–45 minutes as described in the manufacturer's protocol. Slides were briefly washed in tap water and allowed to dry. Stained halos were examined under a computerised leica DMRB DIC Bright-field microscope at 100x magnification. Finally, halos were scanned and images captured with a photometric camera. The sperm-halo size was quantified using Image J software. The variables for both subpopulations were normally distributed, therefore, all data was analysed

using two-way *ANOVA,* Sidak's multiple comparisons test using GraphPad prism to compare the halo size within and between the two groups (pellet and interface).

4.2.6 Acridine orange

Described in detail in chapter 3 in section 3.2.5

4.3 Results

DNA fragmentation was measured in 50 spermatozoa from both 90% and 45% fractions of human and bull spermatozoa following exposure to H_2O_2. Results are expressed as the mean ±SEM of the halo area size (mm^2) of sperm treated with 100 µM and 300 µM of H_2O_2 using image J software (Figure 56). The extent of DNA damage was also tested on human and bovine sperm by staining halos with AO (Figure 55). Examples from both human and bovine sperm used for measuring halo formation after exposure to H_2O_2 and staining with Wright's Giemsa solution are shown in Figure 53-54. Mature human and bovine sperm were exposed to 6 M of H_2O_2 for one hour to produce a positive control of DNA fragmentation (Figure 52).

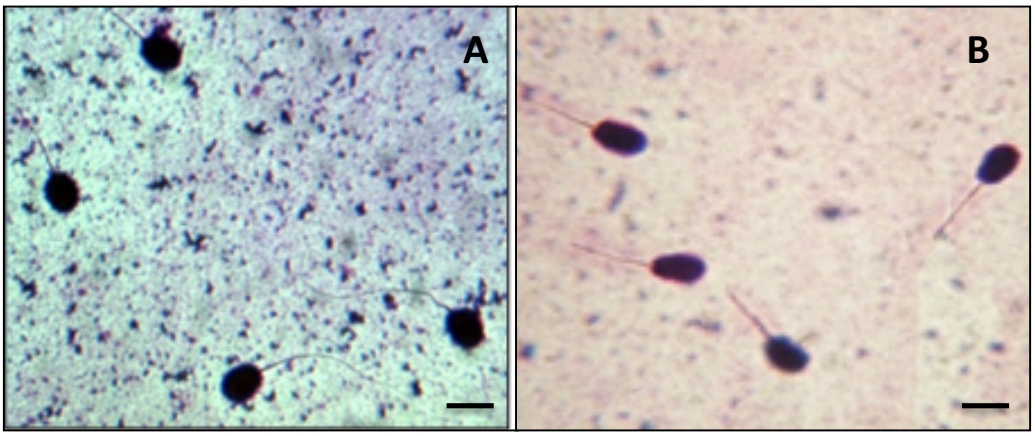

Figure 52: Human **(A)** and bovine **(B)** sperm after exposing to high concentration (6 M) of H_2O_2 and then stained with wright's Giemsa staining were used as a positive control. (scale bar 20µm)

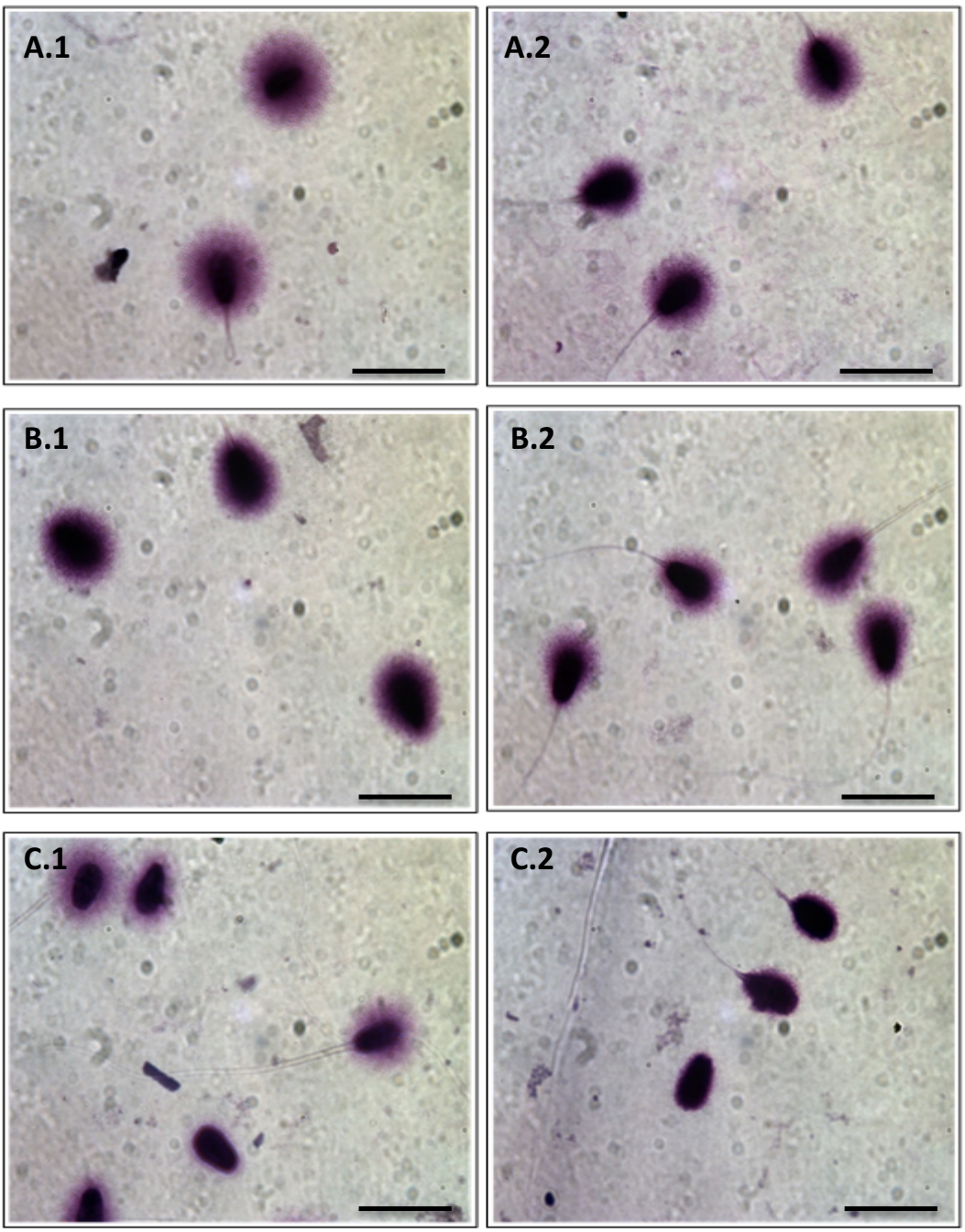

Figure 53: Microscopic images for bovine sperm exposed to different concentrations of H_2O_2, and then stained with wright's Giemsa staining. **(A)** Sperm incubated in PBS (0 µM of H_2O_2) for one hour were used as a control **(A.1)** pelleted fraction (90%) and **(A.2)** interface fraction (45%), **(B)** Sperm incubated in 100 µM of H_2O_2 for an hour **(B.1)** pelleted fraction (90%) and **(B.2)** interface fraction (45%), **(C)** Sperm incubated in 300 µM of H_2O_2 for an hour **(C.1)** pelleted fraction (90%) and **(C.2)** interface fraction **(45%).** (Scale bar: 20 µm)

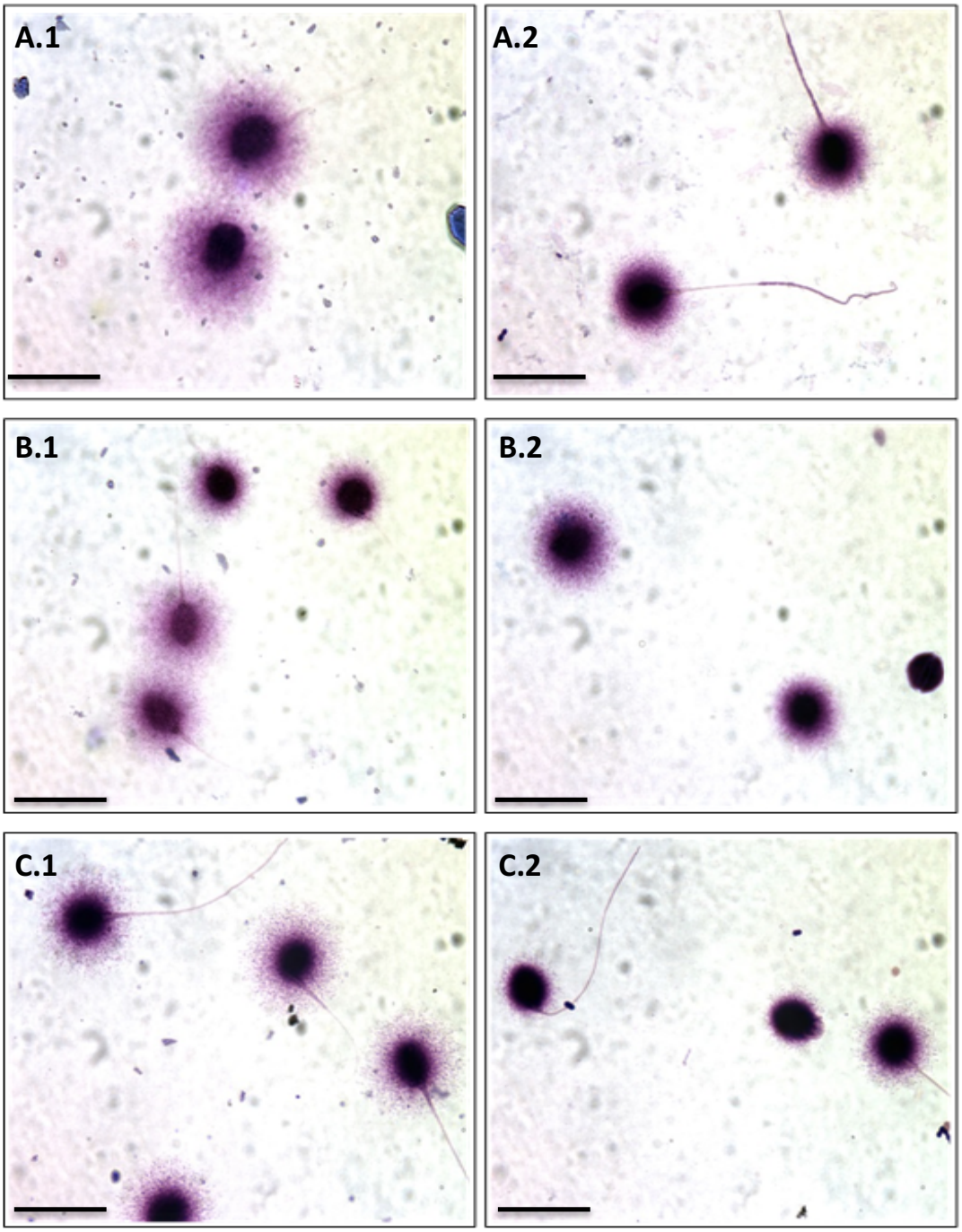

Figure 54: Microscopic images for human sperm exposed to different concentrations of H_2O_2, and then stained with wright's Giemsa staining. **(A)** Sperm incubated in PBS (0 µM of H_2O_2) for one hour were used as a control **(A.1)** pelleted fraction (90%) and **(A.2)** interface fraction (45%), **(B)** Sperm incubated in 100 µM of H_2O_2 for an hour **(B.1)** pelleted fraction (90%) and **(B.2)** interface fraction (45%), **(C)** Sperm incubated in 300 µM of H_2O_2 for an hour **(C.1)** pelleted fraction (90%) and **(C.2)** interface fraction **(45%).** (Scale bar: 20 µm)

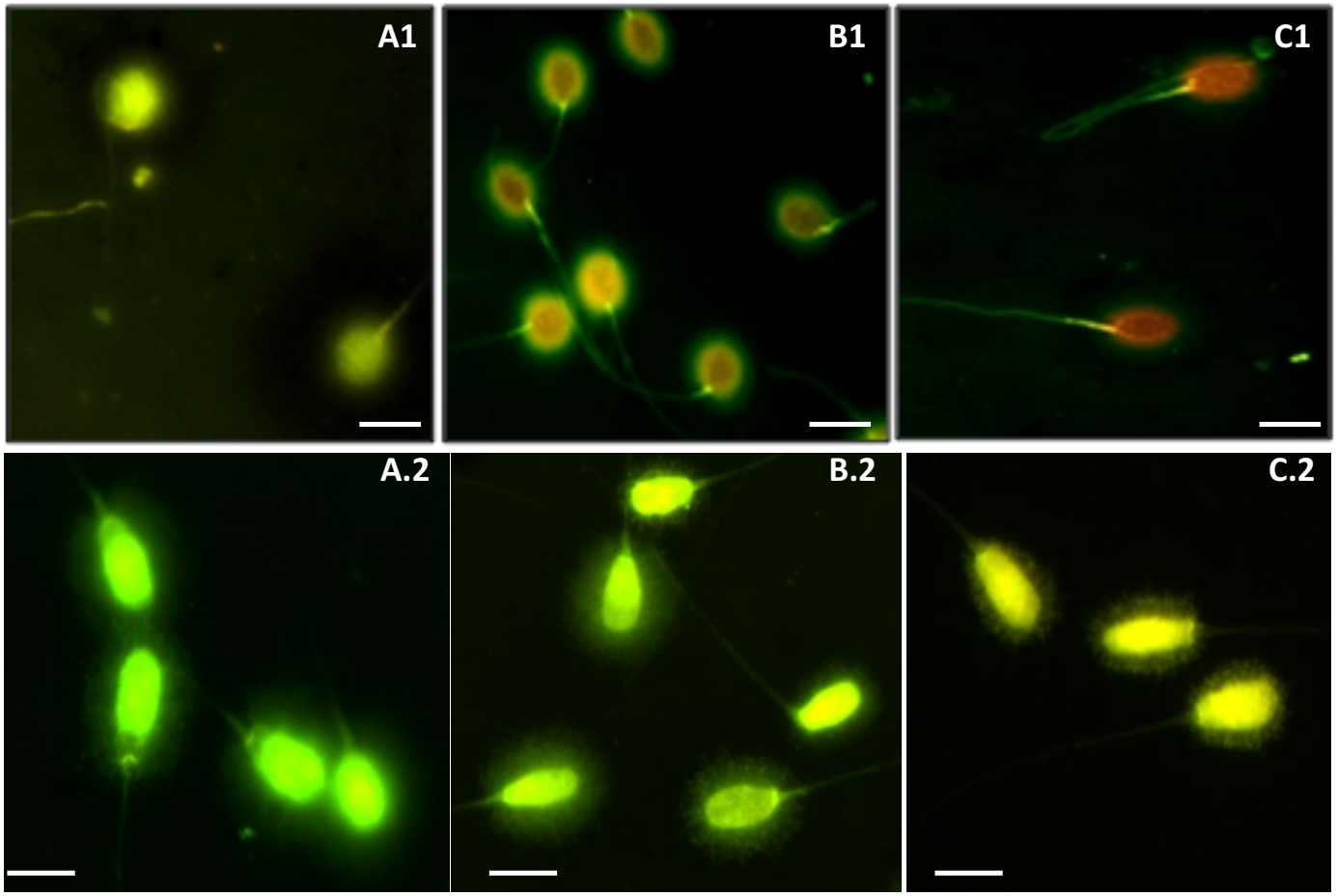

Figure 55: Sperm halo formation after exposure to different concentrations of H_2O_2, 0 µM (A), 100 µM (B) and 300 µM (C), and then stained with AO. AO results showed an increase in the levels of DNA damage, which caused a correspondingly significant decrease in the halo size. Whereas, in bovine, AO results showed lower levels of DNA damage and smaller halo size compared to human sperm, which may be due to the higher resistance of bovine chromatin to higher concentrations of H_2O_2. (1) Human sperm and (2) bovine sperm (scale bar 25µm)

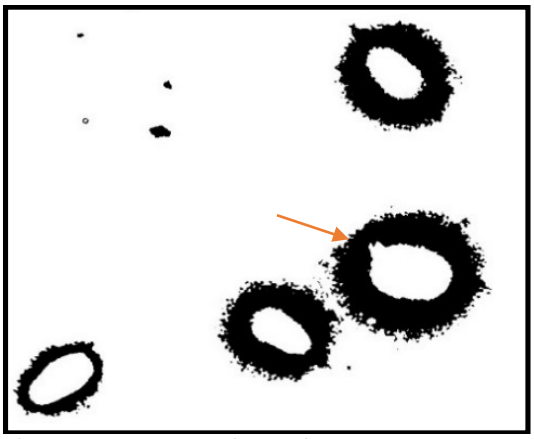

Figure 56: The size of sperm halo area (arrow) measured and captured by image J software. Halo formation appears with black colour, whereas, nucleoid appears white.

4.3.1 Effects of peroxide on DDGC separated sperm

In the human 90% fractions, sperm halo sizes (mm^2) at 100 µM and 300 µM H_2O_2 were significantly smaller ($p \leq 0.01$) compared to the controls (no H_2O_2). (Figure 57). In bovine, the halo size was significantly ($p \leq 0.05$) smaller at 100µM H_2O_2 compared to control (no H_2O_2), and smaller still ($p \leq 0.0001$) at 300 µM compared to control (Figure 57).

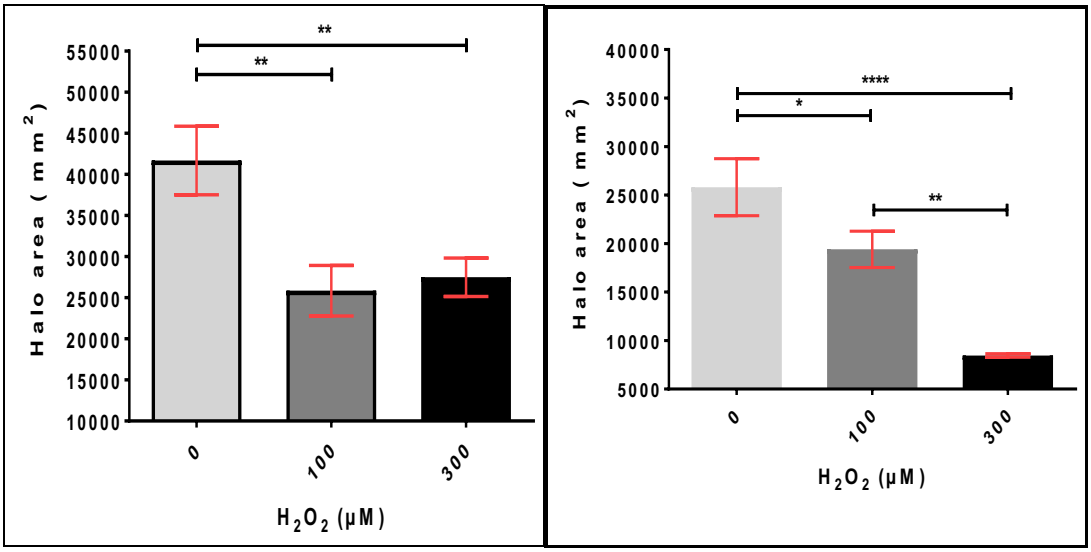

Figure 57: Bar graphs showed a statistical comparison of halo area size in pelleted (90%) bovine (right) and human sperm (left) with different concentrations of H_2O_2. (Mean ± SEM)

In the human 45% fractions, sperm halo size was only significant ($p \leq 0.01$) at 300µM H_2O_2 compared to control (no H_2O_2). However, there was no significant differences ($p > 0.05$) at 100 µM compared to control and 300 µM (Figure 58). In bovine sperm, the halo size was significant ($p \leq 0.05$) at 100µM H_2O_2 compared to control (no H_2O_2). Moreover, the halo size was significantly ($p \leq 0.01$) smaller at 300 µM compared to the untreated cells. While, there was no significant differences ($p>0.05$) in the halo size between 100 and 300 µM (Figure 58).

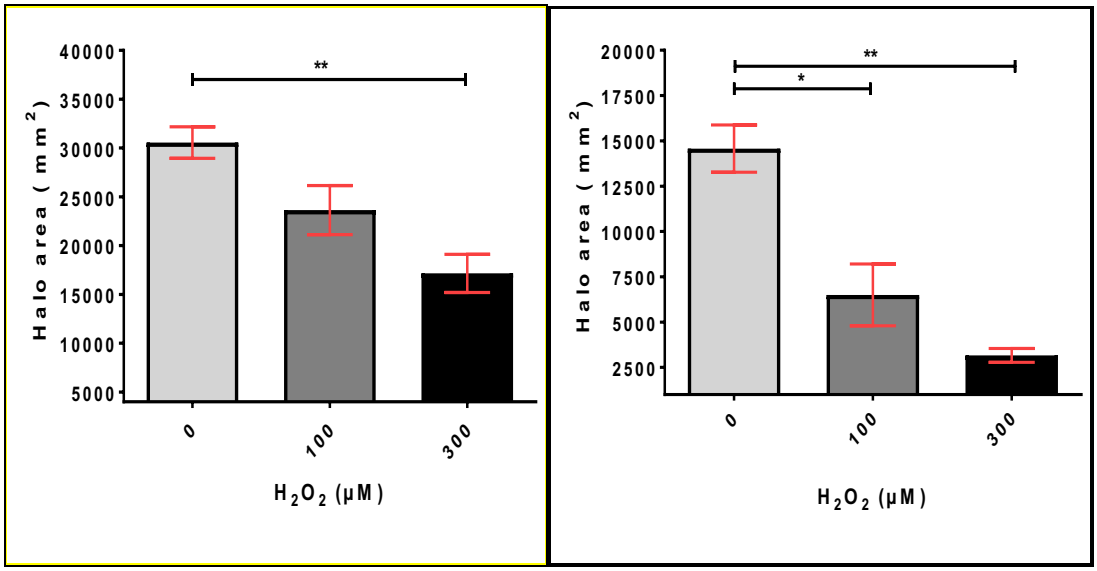

Figure 58: Bar graphs show a statistical comparison of halo area size in interface (45%) bovine (right) and human sperm (left) with different concentrations of H_2O_2. (Mean ± SEM)

In addition, the data were examined by comparing the differences in the halo size between sperm subpopulations in each concentration of H_2O_2. In human sperm with no H_2O_2 treatment, the halo size showed a significant difference ($p<0.05$) between pellet and interface sperm (Figure 59). In addition, there was significant difference ($p<0.005$) in the halo size between pellet and interface sperm after exposure to 300 µM H_2O_2 (Figure 59).

In bovine, there was significant difference ($p \leq 0.01$) between pellet and interface sperm with no H_2O_2 treatment and more pronounce ($p \leq 0.005$) at 100 µM H_2O_2 (Figure 60).

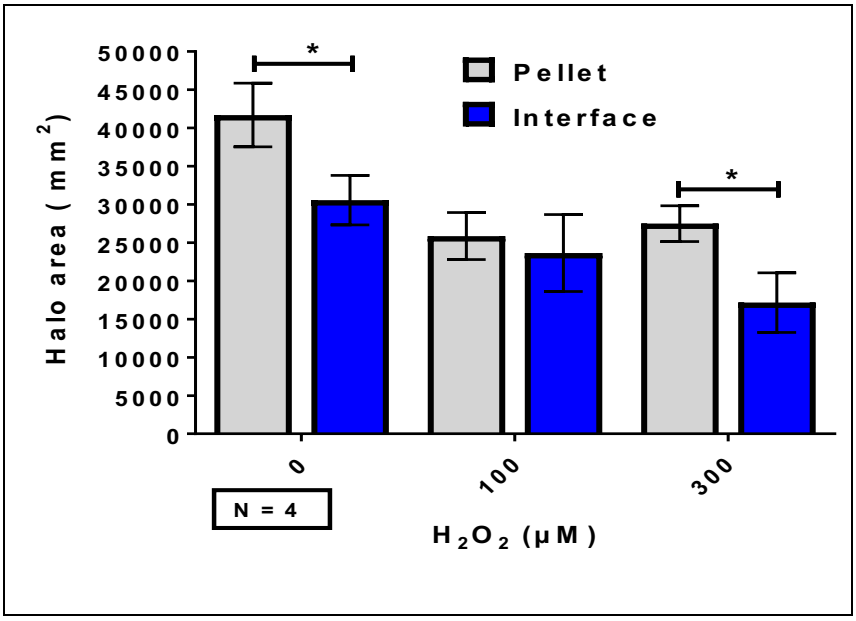

Figure 59: A bar graph showed the average size of Halo in both pellet and interface layers of human sperm at three different concentrations of H_2O_2. (Mean ± SEM)

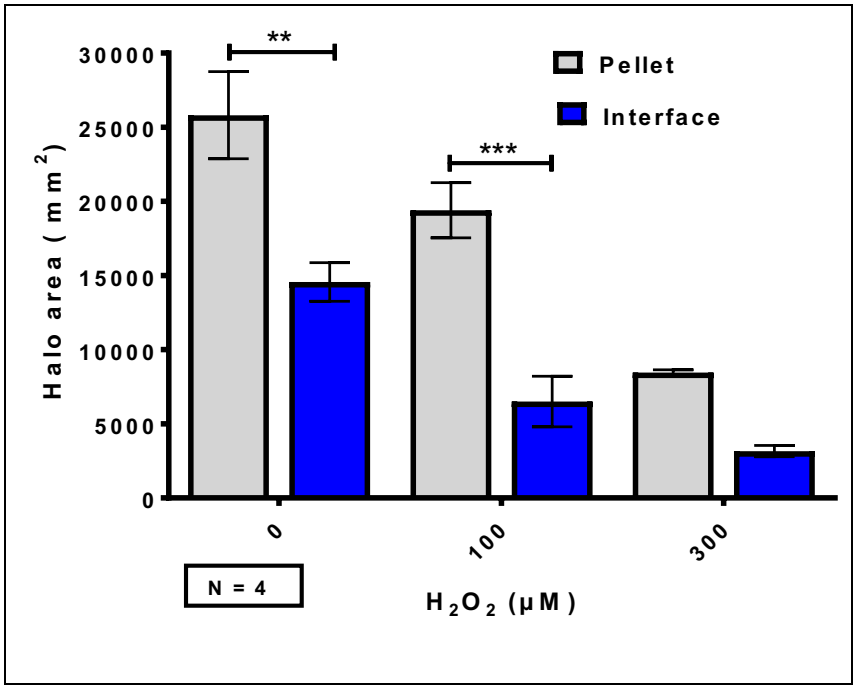

Figure 60: A bar graph showed the average size of Halo in both pellet and interface layers of bovine sperm at three different concentrations of H_2O_2. (Mean ± SEM)

4.4 Discussion

Clinically, sperm DNA fragmentation has been found to have an impact on embryo quality and subsequently on pregnancy rates (Anifandis et al., 2015). According to Avendaño et al. (2010), pregnancy rate was 3.5 times higher in IVF couples when sperm DNA fragmentation index was less than 17.6% (measured by using TUNEL assay). Various techniques have been used to evaluate sperm DNA damage in patients undergoing IVF treatments. For example, the sperm chromatin dispersion assay is being used in IVF clinics (Lewis, 2013) and like other DNA fragmentation assays, SCD estimates the levels of DNA damage by measuring the degree of DNA fragmentation in sperm nuclei (Fernandez et al., 2005a). The Halosperm™ assay may be a useful diagnostic method to evaluate clinically the DNA integrity of sperm, which is required to achieve pregnancy (Bashiri et al., 2016). Additionally, Halosperm™ assay can determine a high degree of DNA damage in some infertile males, for example in patients with varicocele, which may have affected the nuclear structure of sperm chromatin (Fernandez et al., 2005b). A previous study, using the Halosperm™ assay indicated that there was a significant correlation ($r=0.69$; $p< 0.001$) between undamaged sperm DNA expressed as sperm with big halos and damaged DNA expressed as DNA fragmentation index as well as their significant impact on embryo quality and pregnancy rate (Tandara et al., 2014). However, systematic reviews and meta-analysis studies were distributed to evaluate the significance of measuring sperm DNA fragmentation using variable methods such as TUNEL, Comet, SCSA and SCD (or Halo assay). A recent meta-analysis review of 18 studies for medically assessed reproduction (IVF and ICSI) of SCD showed that the predictive accuracy for pregnancy was poor. However, there was significant

heterogeneity across the selected SCD studies with low sensitivity and specificity (0.59 and 0.39) (Cissen et al., 2016). Another meta-analysis review, which has less reliable outcomes (as it was limited by high study heterogeneity and poorly controlled clinical parameters) suggested that direct measurements of DNA damage using methods such as TUNEL and comet assays may be better predictors of IVF outcomes compared to indirect methods (measuring intact DNA) such as Halosperm^{TM} assay (Simon et al., 2017).

In this study, Halosperm™ assay was used to produce halo-DNA, which was then extracted and used as platform for DNA sequencing. By using acid denaturation and lysing buffer, dispersed DNA loops that may have a higher susceptibility to DNA damage are released and form halos around the sperm nucleus, which can then be stained and visualised. In this experiment, computerised digital images were used to analysis the average halo size for both human and bovine sperm. The results of this experiment showed a significant negative correlation between halo size of sperm and exposure to increasing concentrations of H_2O_2. The halo size of most number of spermatozoa in both species (human and bovine) decreased with increasing levels of H_2O_2. Moreover, comparisons of the subpopulations (pellet and interface) in both species demonstrated significant correlations between DNA integrity and resistance to the effect of the external peroxide stress. The observation in this experiment suggested that H_2O_2 had a direct effect on the chromatin structure of bovine and human sperm, which consequently caused DNA damage (Villani et al., 2010). Also, the DNA damage rate was found to be positively correlated with increased concentration of H_2O_2. In bovine, however, the halo size of sperm was smaller compared to those in human either before or after H_2O_2 treatment, which suggests that there were

structural variations between bovine and human spermatozoa in terms of chromatin accessibility. Although, the halo size of human sperm isolated from 90% fraction slightly increased after exposure to 300 μM H_2O_2 compared to 100 μM, the statistical difference was not significant, which may be because of sperm cells reached their highest levels of DNA damage following exposure to 100 μM of H_2O_2, therefore, increasing the concentration to 300 μM would not cause any further significant damage to the DNA itself. In human, sperm halos generated with different concentrations of H_2O_2 and then stained with AO showed an increase in the levels of DNA damage, which caused a correspondingly significant decrease in the halo size. Whereas, in bovine, AO results showed lower levels of DNA damage and smaller halo size compared to human sperm, which may be due to the higher resistance of bovine chromatin to higher concentrations of H_2O_2. Also, in both species, AO results showed that the higher the levels of DNA damage in the sperm nucleus, the smaller size of halos.

Chapter 5: Isolating halo and nucleoid DNA, following by Next-Generation DNA Sequencing (NGS) sequencing

5.1 Introduction

The histone retention phenomenon of mammalian sperm has triggered a wide interest and debate among scientists regarding its functional significance. Studies have applied Chromatin Immunoprecipitation (ChIP) based procedures to investigate the association of histone-binding DNA with regulatory regions including developmental gene promoters (Arpanahi et al., 2009; Hammoud et al., 2011).

The study reported herein aimed to investigate sperm halo composition using high-throughput DNA sequencing and relate the outcomes to what is known about the equivalent histone compartments of sperm nuclei and the likely sensitivity of these compartments to DNA damage. As sperm from two mammalian species (human and bovine) were investigated, different concentrations of salt were tested and used to generate nuclear halos and to extract proteins (including histones) from sperm nuclei in the process. In this method, halo and corresponding nucleoid DNAs were recovered and used to construct DNA libraries for a next-generation sequencing. Library construction was optimised to generate short paired-end sequence reads that were subsequently mapped to the appropriate human or bovine reference genome with paired-end alignment (Figure 61). These aligned reads can theoretically cover the entire genome (Mardis, 2008) and the investigation of their formation and DNA sequence composition is justified in the context that sperm halo dimensions may correlate with sperm viability (Chohan et al., 2006).

Genomic DNA-seq requires the assembly of sequence reads to enable the identification of genomic features including coding and non-coding regions, regions containing repetitive DNA sequences etc that are not usually considered to be tissue or cell-specific. RNA-seq, in contrast, is more often concerned with gene expression levels in particular cells or tissues.

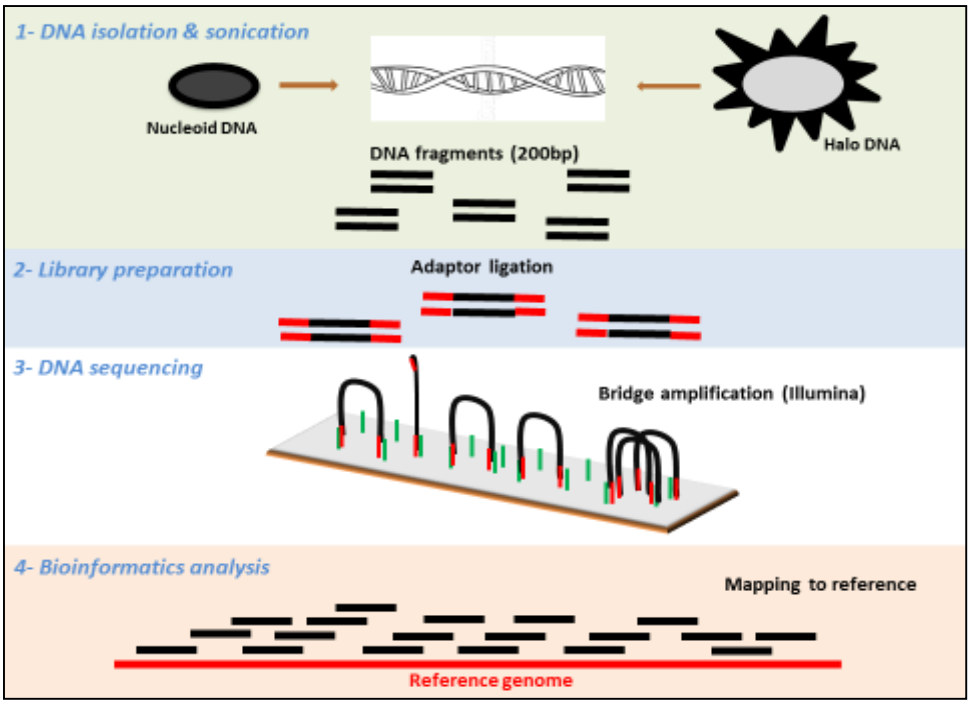

Figure 61: A diagram shows the main four steps for DNA Hi-seq. First, DNA was extracted from both sperm halo and nucleoid fractions. Second, the DNA was fragmented to a size of 200 bp for DNA library input. Third, the DNA fragments were tagged with library indexes and adaptors, before PCR amplification with specific primers. Fourth, the DNA fragments attached to the flow cell through bridge amplification method. Finally, the Hi-seq data was analysed and mapped to the reference genome.

In the characterisation of sperm halos, an intermediate context exists where the physical characteristics of potential differential DNA packaging in the cells of interest are under investigation. Depending on how the chromatin is accessed, such physical differences should lead to enrichments of particular DNA sequences that can be detected using sequence-counting algorithms. To this end, a Model-based Analysis for ChIP-Seq (MACS) algorithm (Zhang et al., 2008) was used to analyse the DNA data generated from both halo and nucleoid DNA

compartments. Moreover, in this project, MACS2 was to set to compare halo and nucleoid DNA for differential enrichment analysis and to highlight the enriched regions in HALO-DNA. Full details are provided in Materials and Methods below.

5.1.1 Experimental aims

The aims of this experiment were to investigate the DNA sequence composition of sperm halos and to relate the information provided with the dynamics of halo formation under differing experimental conditions including oxidative stress. A limited characterisation of DNA binding proteins released during and recovered on halo formation was also undertaken. Sperm halos were generated by salt extraction and also by the commercially available Halosperm^{TM} assay kit (Fernández et al., 2005). Once formed, halos were digested with restriction enzymes to solubilise their DNA and DNA from the remaining nucleoid fractions was similarly processed to generate DNA for sequencing (see Chapter 2, section 2.2.10). A deep high-throughput DNA sequencing of these two fractions (halo and nucleoid; see Appendix) was carried out to help shed light on these observations.

5.2 Materials and Methods

5.2.1 Somatic cell removal

Described in detail in chapter 2 in section 2.2.2

5.2.2 Sperm cell counting

Described in detail in chapter 2 in section 2.2.3

5.2.2 Halo formation

Described in detail in chapter 2 in section 2.2.9

5.2.3 Separation halo-DNA from nucleoid-DNA using restriction endonuclease enzymes (BamH 1 and EcoR1)

Described in detail in chapter 2 in section 2.2.9

5.2.4 DNA extraction using Phenol-Chloroform

Described in detail in chapter 2 in section 2.2.10

5.2.5 Library preparation

All steps in the protocol were carried out according to the manufacturer's protocol (NebNext Ultra DNA Library Prep Kit for Illumina #E7370S/L).

5.2.5.1 Measuring DNA concentration using NanoDrop™ 1000 and PicoGreen assay

In order to measure the amount of the input/output DNA for sequencing, a Nanodrop spectrophotometer (NanoDrop™ 1000) and Quant-iT™ PicoGreen® broad-range dsDNA kit (Invitrogen) were used for pre and post DNA-library production. Firstly, PicoGreen broad-band standards were diluted 10X by dH_2O to final concentration as follows: 0 ng/mL, 5 ng/mL, 10 ng/mL, 20 ng/mL, 40 ng/mL, 60 ng/mL, 80 ng/mL and 100 ng/mL. After equilibrated the kit components to room temperature, a master mix of the working solution was prepared by diluting the Picogreen reagent 1:200 in Qunt-iT buffer, 1 µL of Picogreen reagent and 197 µL of Qunt-iT buffer for each sample and the eight standards. Then, 198 µL of the working solution was loaded in each well of the microplate (Costar 3915 balck flat-bottomed 96-well). Two µL of each broad-band standard (from lowest to highest in wells A12-H12) was added in separate wells and mixed. Two µL of each sample was added in separate wells and mixed will (the plate was covered with a foil whilst transferring the samples). The microplate was gently mixed by moving the plate back and forth on bench and before placement in a florescence microplate reader. The standard curve was used to determine the DNA concentration. An equal concentration of the halo and nucleoid DNA samples were used for library preparation.

5.2.5.2 DNA shearing

An equal concentration of the input DNA (10 ng) per sample in a total volume of 55.5 µL was transferred to Covaris glass microtubes. Then, each DNA was sheared for 145 seconds to generated DNA fragments of an average size of 200 bp by using ultrasonicator (Covaris). After shearing, the size of the DNA fragments was confirmed using Bioanalyzer.

5.2.5.3 NEB Next End Prep reaction

Starting material of between 5 and 1000 ng of fragmented DNA was prepared in a volume of 55.5 µl. Then, a 3 µL volume of End prep Enzyme Mix and 6.5 µL of End Repair Reaction buffer (10x) were added. The solution was mixed by pipetting followed by a quick spin. The solution was then placed in a thermocycler under the following conditions;

30 minutes at 20°C
30 minutes at 65°C
Hold at 4°C

5.2.5.4 Adaptor Ligation

As the input DNA was less than 100 ng, adaptors were diluted 10-fold in 10mM Tris-HCl. A mixture of 15ul of Blunt/TA ligase buffer, 2.5 µL of diluted adaptors and 1 µL of ligation enhancer was added to the End prep reaction and mixed by pipetting. A brief centrifugation ensured that all liquid was drawn to the bottom of the tubes were then incubated at 20°C for 15 minutes in a thermocycler. After the incubation, 3 µL of enzyme (USER^{TM}) provided with the kit was added to the ligation mixture and mixed well. The mixture was incubated again at 37°C for another 15 minutes.

5.2.5.5 Size selection of Adaptor-ligated DNA

A 13.5 µL volume of distilled water was added to the ligation mixture to make the total volume 100 µL. Then, a 55 µL of resuspended AMPure XP beads was added to the 100 µL ligation mixture and mixed by pipetting followed by incubation for 5 minutes at room temperature. After a brief centrifugation, samples were placed on an appropriate magnetic stand to separate the beads from the supernatant. After 5 minutes incubation at room temperature, the supernatant (containing DNA) was transferred to a fresh tube. 25 µL aliquots of fresh beads were added to the supernatants and mixed before incubating for 5 minutes at room temperature. The mixture was then centrifuged and placed on the magnetic stand at room temperature. After incubation for 5 minutes at room temperature, the clear supernatant was removed and discarded (contains unwanted DNA). While the tube was on the stand, 200 µL of freshly prepared 80% ethanol was added to wash the beads. After incubation for 30 seconds at room temperature, supernatants were discarded and the tubes left on the magnetic stand to air dry for 10 minutes. The targeted DNA was eluted from the beads by adding 23 µL of elution buffer and gently mixed by pipetting. After a brief centrifugation, tubes were placed on the magnetic stand and incubated 5 minutes at room temperature, following which, 23 µL of supernatant was transferred to a new PCR tube containing 1 µL of index primer, 25 µL of PCR master mix and 1 µL universal PCR primer for amplification. The preparation was then placed in a thermocycler and run under the following programme;

30 seconds at 98°C
10 seconds at 98°C
30 seconds at 65°C
30 seconds at 72°C
for 13 cycles
5 minutes at 72°C, and hold at 4°C

5.2.5.6 Cleanup of PCR amplification products

50 µL aliquots of resuspended APMure XP beads were added to the PCR reaction (50 µL) and mixed by pipetting. The mixture was then incubated for 5 minutes at room temperature. After a brief centrifugation, tubes were placed on the magnetic stand and incubated for 30 seconds at room temperature. Supernatants were discarded and the tube left on the magnetic stand to air dry for 10 minutes. The targeted DNA was eluted from the beads by adding 33 µL of elution buffer and mixing, following which, tubes were placed on the magnetic stand and incubated 5 minutes at room temperature. Twenty-eight µL aliquots of the supernatant were transferred to fresh PCR tubes and the size distribution of the DNA was check on an Agilent high sensitivity chip.

5.2.5.7 Quality Control analysis using the Agilent Bioanalyzer

In order to measure the quality of the input/output DNA for sequencing, an Agilent high sensitivity DNA kit was used for pre and post DNA-library production. The pre-prepared gel-dye mix was left at room temperature for 30 minutes. Then, a new high sensitivity DNA chip was placed on the chip priming station, and 9 µL of the gel-dye mix was pipetted in the well-marked . The chip priming station was then closed and the plunger was pressed down until it was held by the clip. After 60 seconds, the clip was released and then the plunger was slowly pulled back to the 1 mL position. Nine µL of the gel-dye mix was pipetted in the other three wells marked G. Then, a 5 µL of marker was pipetted in all sample wells as well as the ladder well. After pipetting 1 µL of high sensitivity DNA ladder in the ladder well, 1 µL of each sample was pipetted in each of the 11 sample wells. Afterwards, the chip was placed horizontally in the adaptor and vortexed at 2400

rpm for 1 minutes. Within 5 minutes, the chip was run in an Agilent 2100 Bioanalyzer.

5.2.5.8 Bovine and human sperm DNA-seq bioinformatics analysis: high-salt and low-salt halos verses nucleoid fractions

5.2.5.8.1 NGS-pipeline and data analysis

With assist of OMIX bioinformatics services (University of Leeds), raw NGS (Hi-seq) DNA data, which had been sequenced on the Illumina high-throughput DNA-seq platform for all fractions from both human and bovine spermatozoa, were downloaded from an inbox on Leeds University's share-serve (xserve7). Then, the quality of the data was enhanced through a trimming process (see Appendix, page 224) to remove the adaptor bases as well as filtering out the low-quality reads (Figure 63). The output files (Fastqc) were used to align the sequence onto the respective genome references (*hg38 and bosTau8*). The generated *BAM* files were then processed through the MACS2 peak-calling algorithm (Feng et al., 2011) to test for enriched regions in each DNA fraction of all samples (Figure 62).

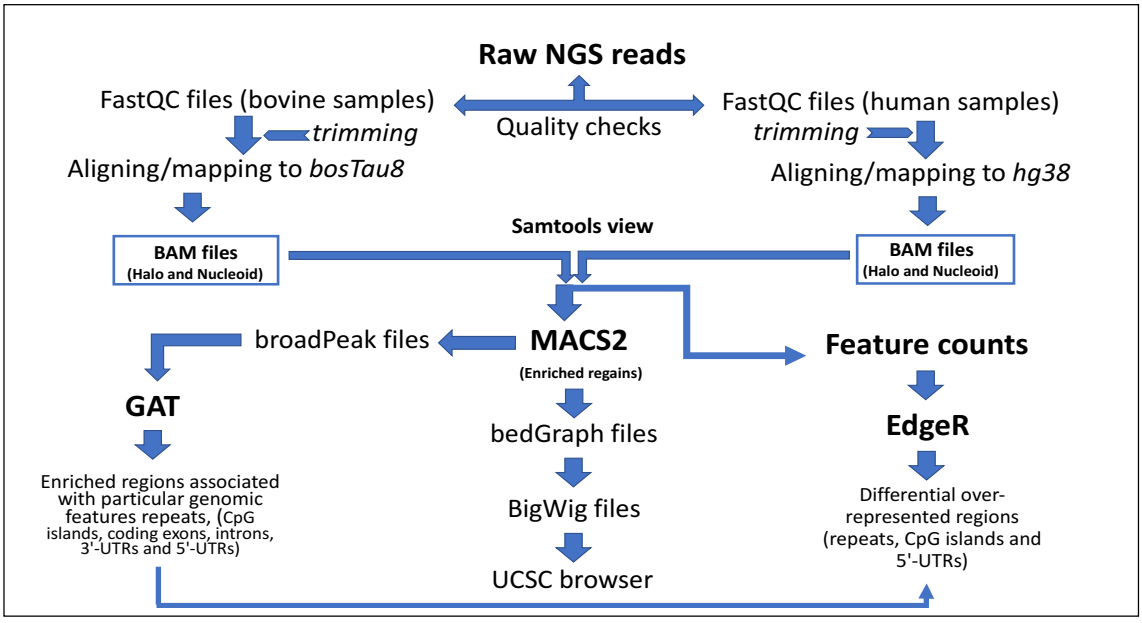

Figure 62: A flow chart showed the bioinformatics pipelines developed for the Hi-seq data analyses using bioinformatics tools.

5.2.5.8.2 QC and *Fastq* processing

Reads were inspected using *FastQC (see http://www.bioinformatics.babraham.ac.uk/projects/fastq)* run from the command line ($ fastqc *fq.gz) and processed with *trim_galore* (see http://www.bioinformatics.babraham.ac.uk/projects/trim_galore/), which by default, trims the Illumina *TruSeq* universal adapter (AGATCGGAAGAGC) and removes reads shorter than 20 bases and reads with a quality (Phred) score below 20. The trimmed forward and reverse *Fastq* files were then validated to match up read pairs. Orphan reads were discarded and *FastQC* was then re-run again on the validated reads to assess QC outcomes (Figure 63).

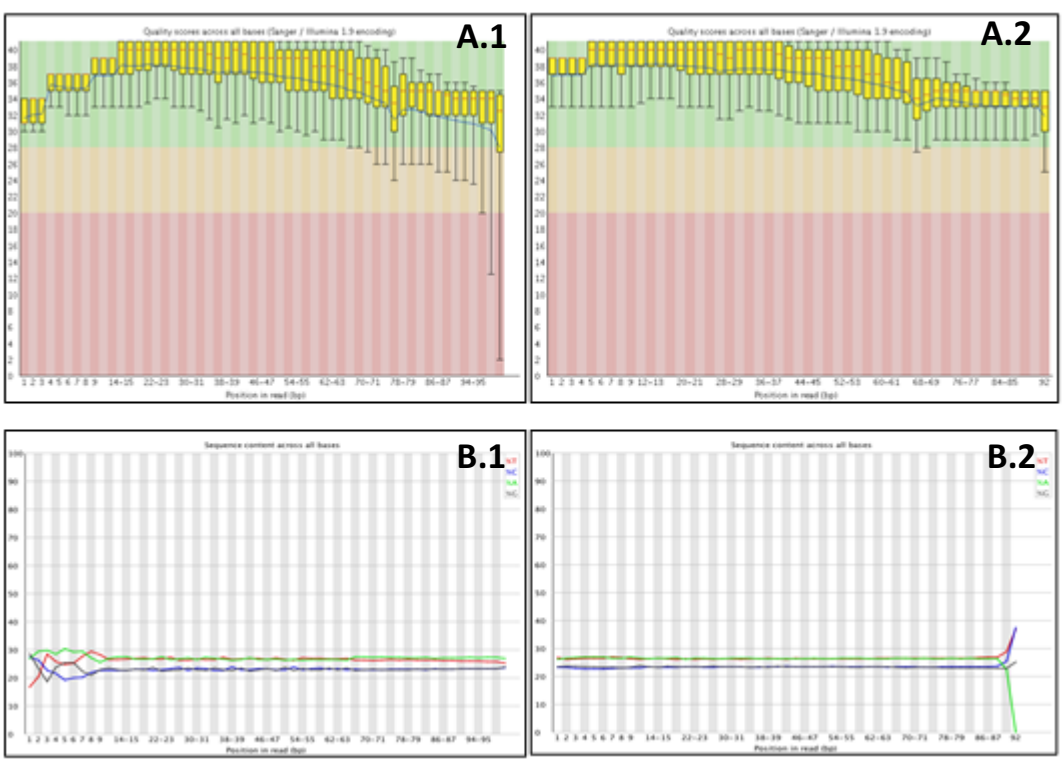

Figure 63: Fastqc images show the quality checks for the sequences across all bases before the reads filtered out (A.1) and after filtering (B.1) to remove the reads that below the green zone, also, the sequence content before trimming process for the adaptor bases (A.2) and after trimming (B.2).

5.2.5.8.3 Alignment and mapping

Genome sequences were indexed using the *subread* (buildindex) function (Shi and Liao, 2013). Then, validated human reads were aligned to the *hg38* index and bovine reads were aligned to *bosTau8* using the *subread* aligner (Liao et al., 2013) run in R (Team, 2013). Initially, two different options were used for alignments; one to report unique alignments only, and the other to report up to ten best multi-mapping alignments. The object of this step was to assess the impact of sequenced repetitive DNA on read mapping efficiency. For the final analysis, options were chosen to report both uniquely mapped reads and the one best mapping location for multi-mapping reads (ties being rejected) (see Appendix 1.1). Then, output aligned *BAM* files were generated by *subread* (output_format) function (Shi and Liao, 2013). Samtools view (see http://www.htslib.org/doc/samtools.html) was used to remove unmapped and incorrectly paired reads. Also, Picard MarkDuplicates (https://broadinstitute.github.io/picard/) was used to remove PCR & optical duplicates.

5.2.5.8.4 Feature counts

By using the aligned *BAM* files as input files, the *featureCounts* function (Liao et al., 2014) of the *subread* package was used to count reads mapping to repeats, CpG islands, coding exons, introns, 3'-UTRs and 5'-UTRs in both the halo and nucleoid fractions with differences between halo and nucleoid representation based on the Fisher's Exact test variant, EdgeR (Robinson et al., 2010).

Because of their suggested role in the structural organisation of chromatin (Shapiro and Sternberg, 2005), *RepeatMasker* (Tempel, 2012) was used to examine repetitive sequences in all NGS data. RpM analysis identified different

types of DNA repeats in the sequencing data, including microsatellite, long terminal (LTR) and Alu repeats, which were distributed throughout the genome. EdgeR (Robinson et al., 2010) was used to compare repeat presence in both halo and nucleoid fractions.

5.2.5.8.5 MACS2 analyses

Model-based Analysis of ChIP-Seq v2 (MACS2) (version 2.1.0.20140616) (see https://github.com/taoliu/MACS/) was used to compare read mapping depths in experimental (halo) against control (nucleoid) fractions obtained for bespoke high and low salt experiments as well as for Halosperm samples. The *BAM* files from the alignments were used directly as input data with analysis options, which can be found in the Appendix (page 218).

The output files from the analyses comprise, first, an *Excel* file of 'peaks' (regions of enrichment in the experimental fractions compared to the controls). Second, a *broadPeak* file of the same for upload to a genome browser. Third, *bedGraph* files summarising the depth of read mapping across the genome in the experimental fractions with the background lambda taken into account. The *bedGraph* files were converted to *bigWig* binaries using the UCSC tool *bedGraphToBigWig* with custom shell scripts (see Appendix 1.3). The *BigWig* format permits more rapid access to the data from the UCSC Genome Browser from a suitable cloud server. All outputs are accessible using the commands, which can be found in the Appendix (page 219).

5.2.5.8.6 Genome Association Testing (GAT)

The Genome Association Tester (GAT) package (Heger et al., 2013) (see http://gat.readthedocs.org/en/latest/) was used to explore the possibility that enriched regions associated with particular genomic features more frequently

than might be expected by chance based on the Monte Carlo sampling method (Lin, 2005). As a first step, the locations of human and bovine 5' and 3' -UTRs, coding exons, introns, promoters and CpG islands were downloaded from the UCSC table browser. Overlapping intervals in each dataset were merged using the *mergeBed* function from the *bedTools* suite (Quinlan and Hall, 2010). Promoter and intron intervals were trimmed using the *bedTools subtractBed* function (see http://bedtools.readthedocs.org/en/latest/). Shell scripts were then used to annotate and build merged annotation files for the analyses. Intergenic regions were identified by subtracting the annotated intervals from the whole genome using the *bedTools* function *complementBed*. All regions were then combined into a single annotation file.

The occurrence of CpGs and CpG islands is not uniform across the genome, and recent work has shown the existence of 'isochores', > 200 kb regions of homogeneous base composition, in complex genomes (Weber et al., 2005; Costantini et al., 2006; Cozzi et al., 2015). Because GC% can also affect DNA-seq efficiency, the human and bovine genomes were processed using the tool *isoSegmenter* (see https://github.com/bunop/isoSegmenter) to generate a file of isochore intervals to correct for potential sequencing bias. Finally, the genome interval files were further trimmed to remove sequence gaps. The files that were input into GAT are given in the Appendix (page 224). The same commands were used for bovine high salt and human low salt data after editing to reflect different input and output files.

5.2.5.8.7 Visualising NGS data and deriving ontological descriptions

The enriched genomic regions were mapped to human and bovine Ref-Seq features (exons, introns, promoters, CpGs, 5′ UTRs and 3′ UTRs). The UCSC

(Genome browser website) was used as a source of human (hg38) and bovine (bosTau8) genomic data (Fujita et al., 2010) and to provide visual mapping of the sequence analysis data. In addition, biological and developmental process aspects of gene ontology for enriched regions were derived and illustrated using the Panther gene (Thomas et al., 2003) and DAVID gene ontology database (Huang et al., 2007) (by using default settings).

5.2.6 Quantitative Polymerase Chain Reaction (qPCR)

A real-time PCR (Light Cycler 480 II Roche) was used as a validation tool for verifying DNA-seq result. Firstly, the primers were designed using *Primer3* and *Primer-Blast* from three particular enriched regions in halo fractions (*MOB3B, CYTH3* and *CAPS2*) and additional three enriched regions in nucleoid fractions (*SLC7A14, DHX30* and *MAP4*) from 0.65 M NaCl experiment (Table 4). The annealing temperature for the primers was optimised by applying six different temperatures (58°C, 59°C, 60°C, 61°C, 62°C and 63°C). In addition, primer efficiency was tested by using 2-fold serial dilutions (1/2, 1/4, 1/8, 1/16 and 1/32). Three biological DNA replicates from 0.65 M and 2 M NaCl experiments were used with each primer. The qPCR reaction was prepared in a total volume 20 µL as follows: 10 µL SYBR® Green qPCR master mix (Applied Biosystems), 0.6 µL of each primer, 7.8 µL water and 25 ng DNA template (equal concentration of DNA per sample was measured by Qubit® dsDNA HS Assay (Thermo Fisher)). Then, the enrichment fold change of the DNA regions was calculated in each experiment by using the values of Crossing point (Cp).

Intervals	Primer Sequence	
MOB3B	Forward	GGACCCCAGAATCTCAGCTT
	Reverse	CTTTCGAGACAGTGGAAGCG
CYTH3	Forward	TTCACCCCACTCGCGAAAA
	Reverse	AATGCTCTCCCTTTTCTGGC
CAPS2	Forward	AGAAGTACTTGCTGGCTGGA
	Reverse	TTTGGCCCTTTCCCTGCT
SLC7A14	Forward	CACCACTGTCACGTTCAACC
	Reverse	TGAAGGAGGCAAACTTGTTG
MAP4	Forward	CAAAACCCACTACAGAGCCC
	Reverse	TCTTCCCCTCCATTTCCACC
DHX30	Forward	TGGAGGCTTTGGGAATACAC
	Reverse	ACCTTGCCAAGTGGACTGAG

Table 4: A table showed the primer sequences that used in qPCR experiment.

5.2.6.1 Specificity of NGS result

In order to validate the NGS result, six enriched intervals of 0.65 M NaCl experiment were evaluated by qPCR. The fold of enrichment of each interval was calculated as;

Fold of enrichment = $2^{\wedge Cp}$

5.3 Results

Around 30 million sequencing reads were generated for each fraction following illumina sequencing. Different bioinformatics codes were used to analyse the NGS data and sorted into different output files according to the targeted genomic features.

5.3.1 Sperm DNA repeats analysis

Different DNA repeats were differentially located in halo and nucleoid fractions. As repetitive DNA sequences constitutes up to 90% of the genome (Rao et al., 2010), the enrichment of repetitive sequences was used to help localise chromosomal regions present in each DNA fraction. Different distribution patterns were detected among chromosome regions of human sperm (Figure 65). However, most analyses found that telomeric and centromeric regions were

significantly enriched in nucleoid fractions produced following 0.65 M NaCl extraction, whereas, regions lying between these features, either in the q- or p-arms, were highly significantly enriched in halo fractions (Figure 64).

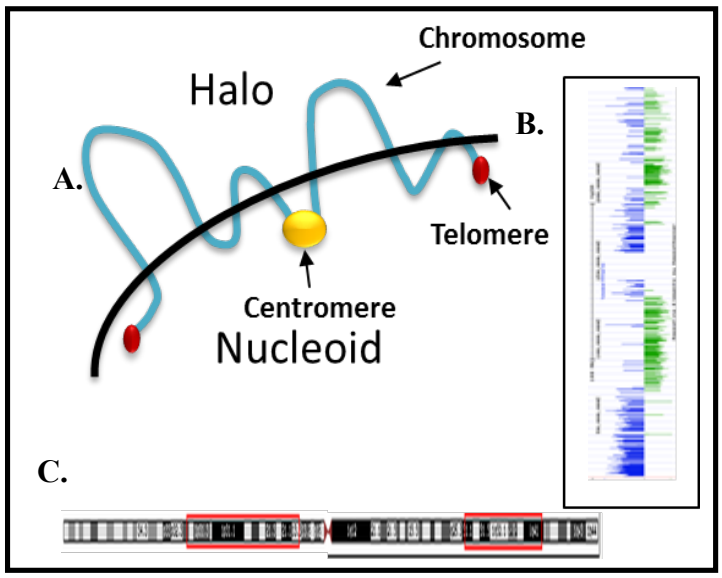

Figure 64: A. Schematic showing hypothetical relationship between chromosomal regions in human sperm after producing the low salt (0.65M NaCl) halo. **B.** an image obtained from UCSC browser showing the distribution of enrichment of repetitive sequences in Chr1 (halo (green) and nucleoid (blue)). **C.** an image of Chromosome 1 showing the enriched regions in halo fraction highlighted with red boxes.

All the repetitive sequences of Y chromosome were highly significant enriched in nucleoid fraction extracted by the low salt solution, in addition, most repetitive sequences of the X chromosome were also significantly enriched in nucleoid fraction, followed by repetitive sequences on chromosome 22, 19, 17 and 20 (Figure 65). CpG islands are associated with gene rich regions of the genome and chromosome 19, is one of the most gene rich examples in humans. Analysis of this chromosome, showed that halo fractions produced by low salt were significantly enriched in these islands (Figure 66). The halo fractions produced by using a 2.0 M NaCl solution or Halosperm assay had more repetitive and other sequences compared to 0.65 M NaCl (Figure 65), which changed the distribution of the enrichment in each chromosome (Figure 68). Also, high salt extraction resulted in a similar loss of definition to that observed with repetitive sequences

with most genomic features appearing in the halo fractions, including CpGs (Figure 69).

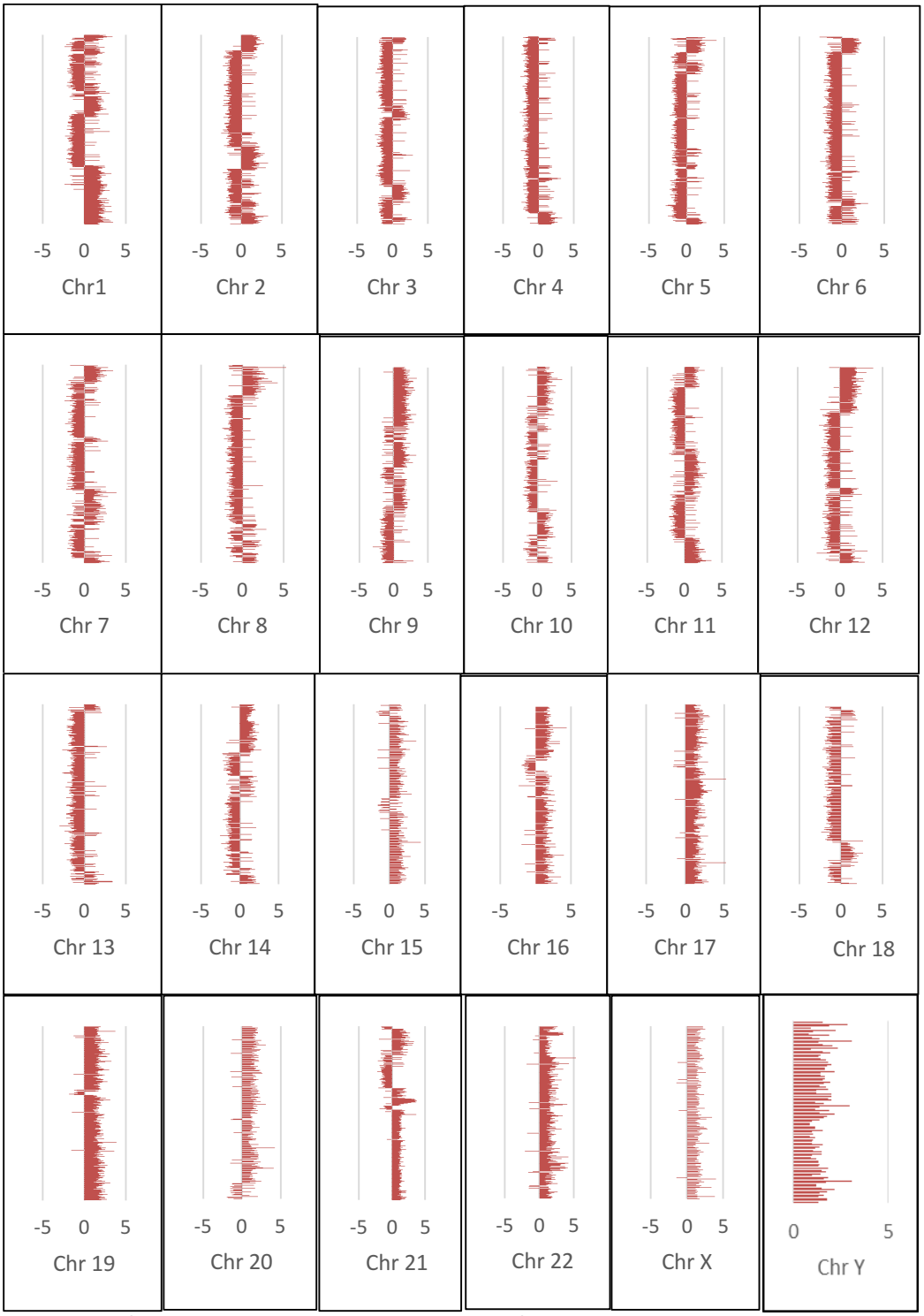

Figure 65: Clustered bars show the distribution of the DNA repeat enrichment among all chromosomes of human sperm following low salt (0.65 M NaCl) extraction. Negative logFC represents the halo fraction, while positive logFC fold represents the nucleoid fraction.

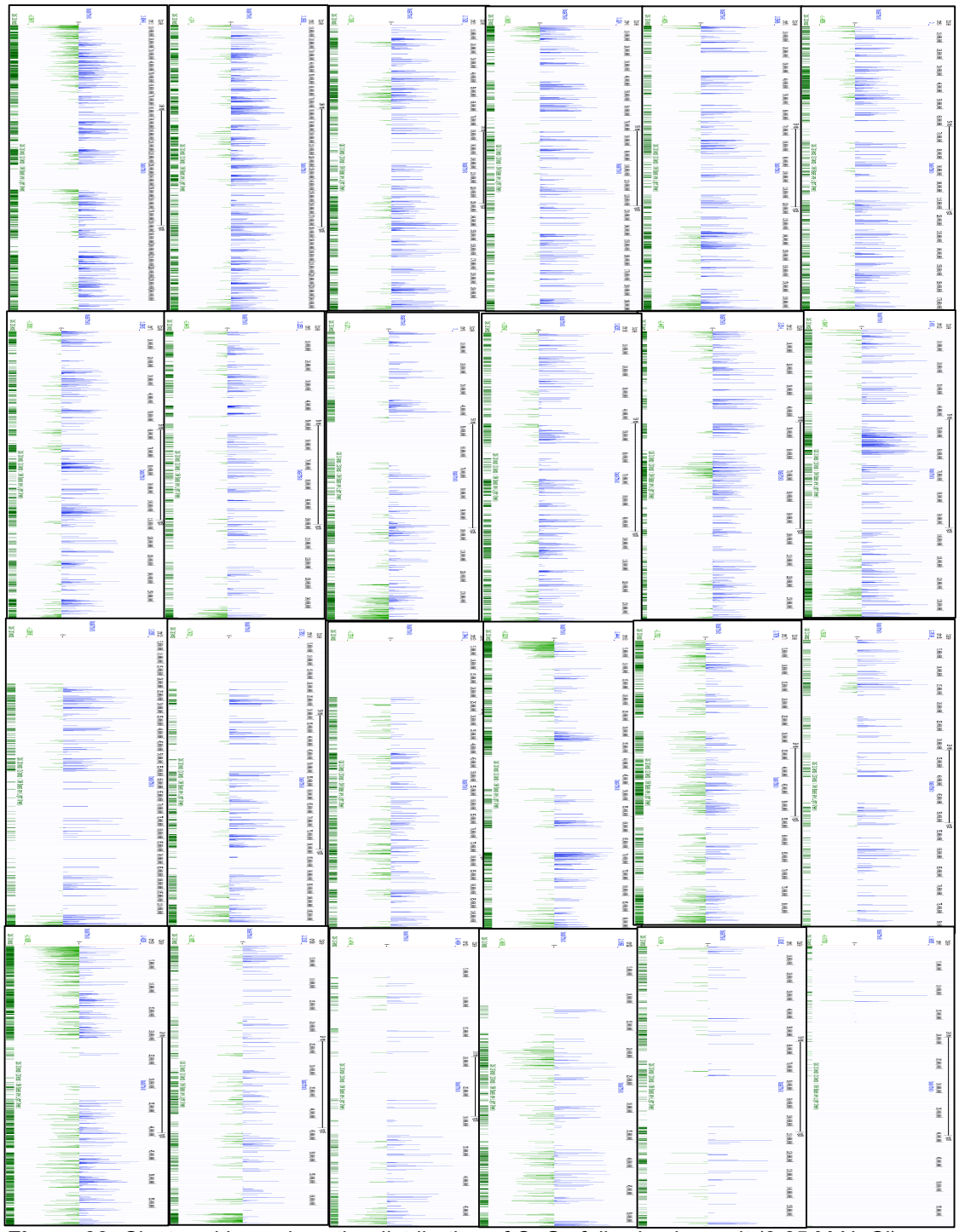

Figure 66: Clustered bars show the distribution of CpGs following low salt (0.65 M NaCl) extraction. Positive logFC represents the halo fraction (blue bars), while negative logFC represents the nucleoid fraction (green bars).

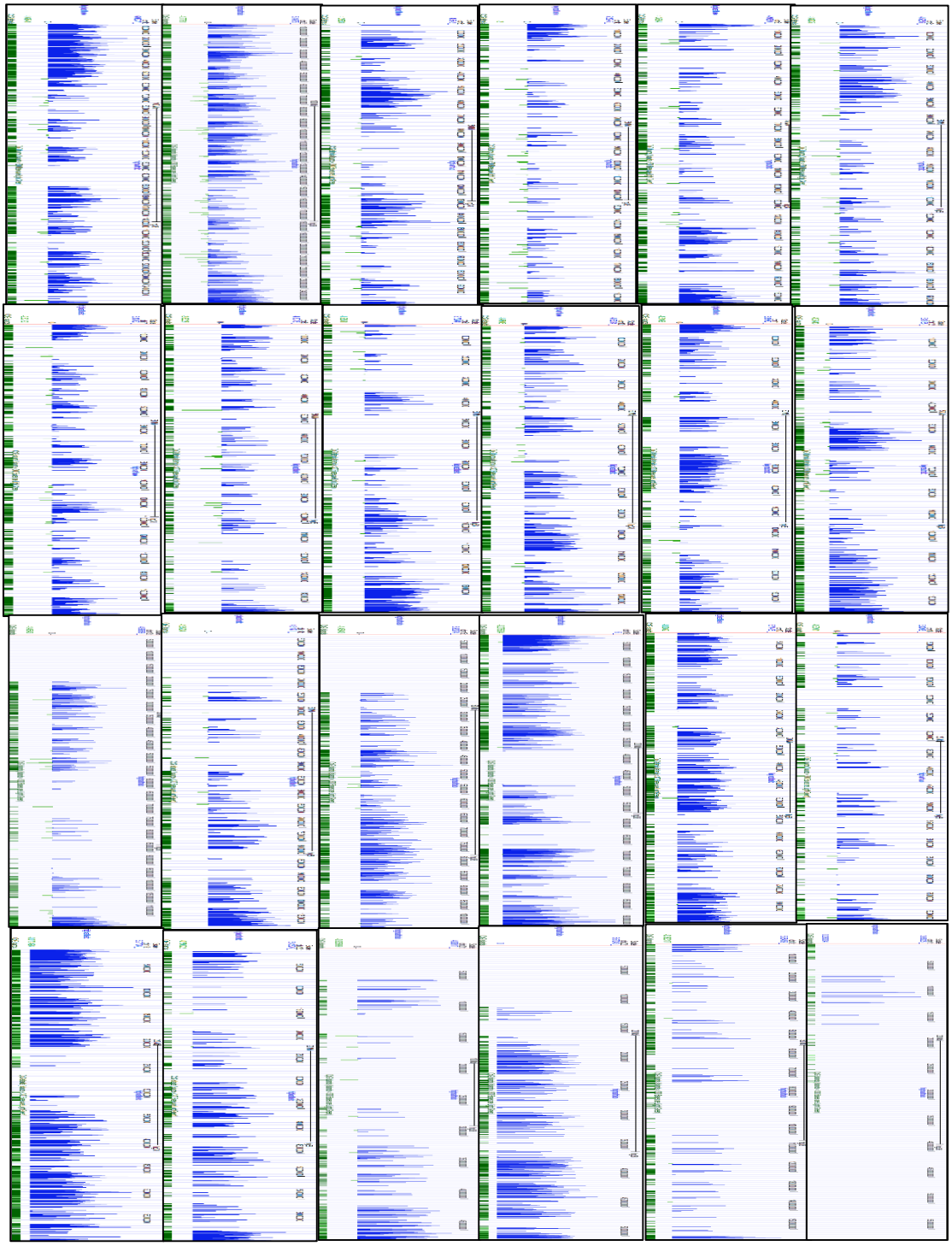

Figure 67: Clustered bars show the distribution of CpGs enrichment following high salt (2.0 M NaCl) extraction among all chromosomes of human sperm. Positive logFC represents the halo fraction (blue bars), while negative logFC represents the nucleoid fractions (green bars).

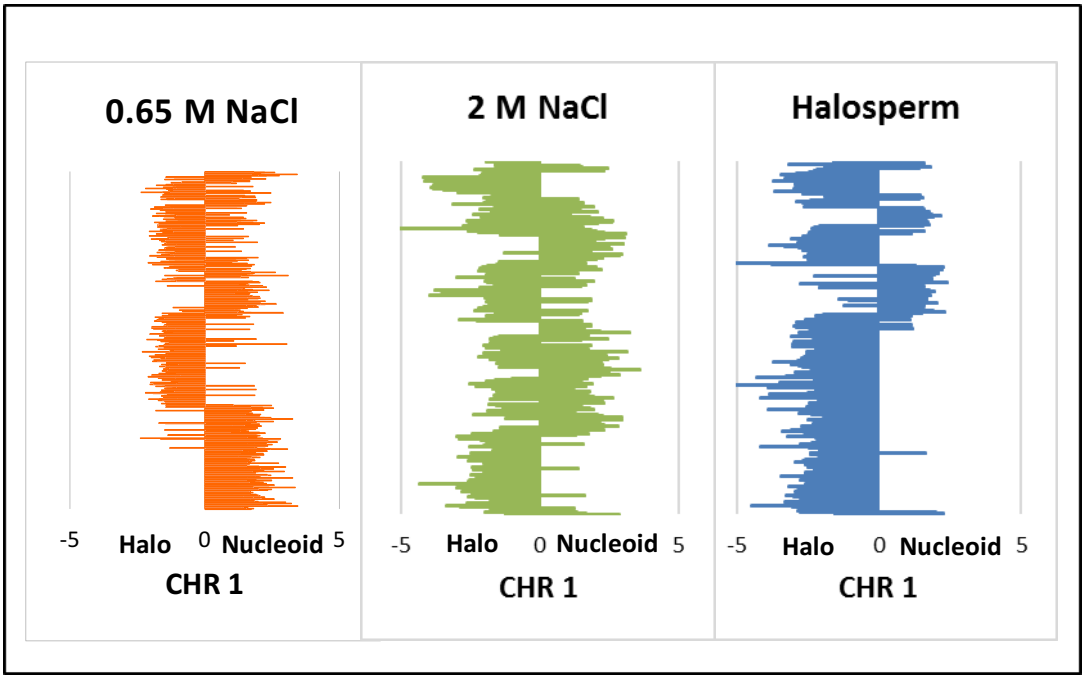

Figure 68: Three clustered bars showed different patterns of the distribution of the DNA repeat enrichment in chromosome 1 (for example) of human sperm following extraction with 0.65 M NaCl, 2.0 M NaCl and the Halosperm buffer.

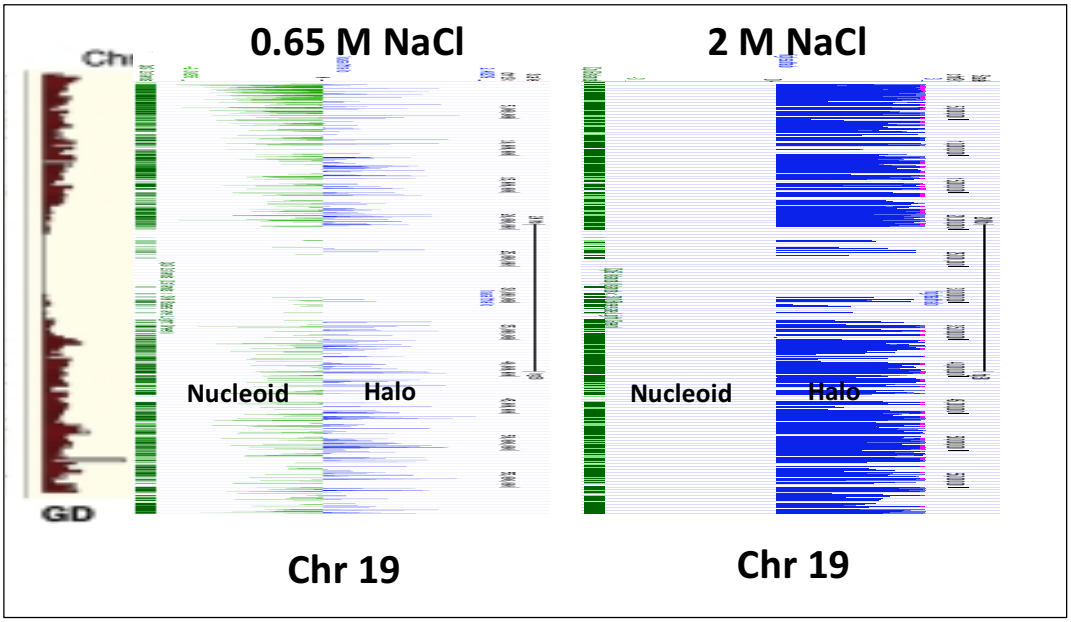

Figure 69: Two clustered bars showing different patterns for the distribution of CpG enrichment in chromosome 19 (for example) of human sperm following extraction with 0.65 M NaCl and 2.0 M NaCl. The halo (blue bars) and nucleoid (green bars) are shown. Gene density (GD) profile of chr19 was adapted from: (Arpanahi et al., 2009)

5.3.2 Association between enriched intervals and particular genomic features

In order to determine where in the genome the highly enriched sequences significantly overlapped with particular genomic features including CpGs, exons and *5*' untranslated region (5'-UTRs), a Genomic Association Test (GAT) tool was used to analyse sequence enrichments in both halo and nucleoid fractions.

In humans, the results showed significant enrichment of CpGs (x8.73 fold in 0.65 M of NaCl, x2.77 fold in 2.0 M of NaCl and x3.48 fold in Halosperm experiment), followed by 5'-UTRs and then coding exons (CDS) (Table 5a and Figure 70). Interestingly, there were no enrichments of introns in halo fractions in any of the experiments (x0.83 fold in 0.65 M NaCl, x0.96 fold in 2.0 M of NaCl and x0.96 fold in Halosperm experiments; Table 5a and Figure 70), suggesting a general exclusion of introns from halos (equally enriched in both fractions). An approximately x3 enrichment of CpGs and 5'-UTRs regions was found in halo fractions extracted by 0.65 M NaCl compared to halos extracted by 2.0 M NaCl and Halosperm assay (Table 5a and Figure 70). In addition, promoter regions were significantly ($p<0.0001$) overrepresented in halo fractions (x1.77 in 0.65 M of NaCl; x1.27 in 2.0 M NaCl and x1.36 in Halosperm assay).

In bovine, the most significant halo enriched regions were 5'-UTRs (x1.61 fold in 0.65 M NaCl and x2.36 fold in 2.0 M of NaCl), followed by CpG islands then promoters and exons regions (Table 5b and Figure 68). Unlike human sperm, an approximately x1.5 enrichment of 5'-UTRs and CpG islands regions were found in halo fractions from bovine sperm generated by 2.0 M NaCl compared to those extracted by 0.65 M NaCl (Table 5b and Figure 70). Like humans, there was no difference in the representation of intron sequences between halo and nucleoid

fractions extracted by either 0.65 M (x0.94) or 2.0 M NaCl (x1.02). Similarly, in 2.0 M NaCl, there was no association between intergenic regions (IGR) and halo enriched regions with around x1 fold in both salt experiments (Table 5b and Figure 70) (equally enriched in both fractions). Interestingly, 3'-UTRs regions were significantly ($p<0.0001$) overrepresented in halo fractions produced by 2.0 M of NaCl with x1.43 fold, whereas, in 0.65 M of NaCl, 3'-UTRs regions were enriched in nucleoid fractions (x0.88 fold).

Low salt halos		**High salt halos**		**Halosperm halos**	
genomic features	***Fold enrichment***	***genomic features***	***Fold enrichment***	***genomic features***	***Fold enrichment***
CpG	8.73	**CpG**	2.77	**CpG**	3.48
UTR5	4.33	**UTR5**	2.11	**UTR5**	2.55
CDS	2.59	**CDS**	1.93	**CDS**	2.16
lincExon	1.93	**lincExon**	1.40	**UTR3**	1.45
Promoter	1.77	**UTR3**	1.32	**lincExon**	1.43
UTR3	1.16	**Promoter**	1.27	**Promoter**	1.36
IGR	1.06	**Intron**	0.96	**Intron**	0.96
Intron	0.83	**IGR**	0.94	**IGR**	0.89

Table 5a: A table showed the most highly significant enriched regions of salt extracted halos (low and high) and Halosperm assay that overlapped with particular genomic features in human sperm.

Low salt halos		**High salt halos**	
genomic features	***Fold enrichment***	***genomic features***	***Fold enrichment***
UTR5	1.61	**UTR5**	2.36
CpG	1.50	**CpG**	2.10
Promoter	1.35	**CDS**	1.91
CDS	1.20	**Promoter**	1.59
IGR	1.00	**UTR3**	1.43
Intron	0.94	**Intron**	1.02
UTR3	0.88	**IGR**	0.94

Table 5b: A table showed the most highly significant enriched regions of salt extracted halos (low and high) that overlapped with particular genomic features in bovine sperm.

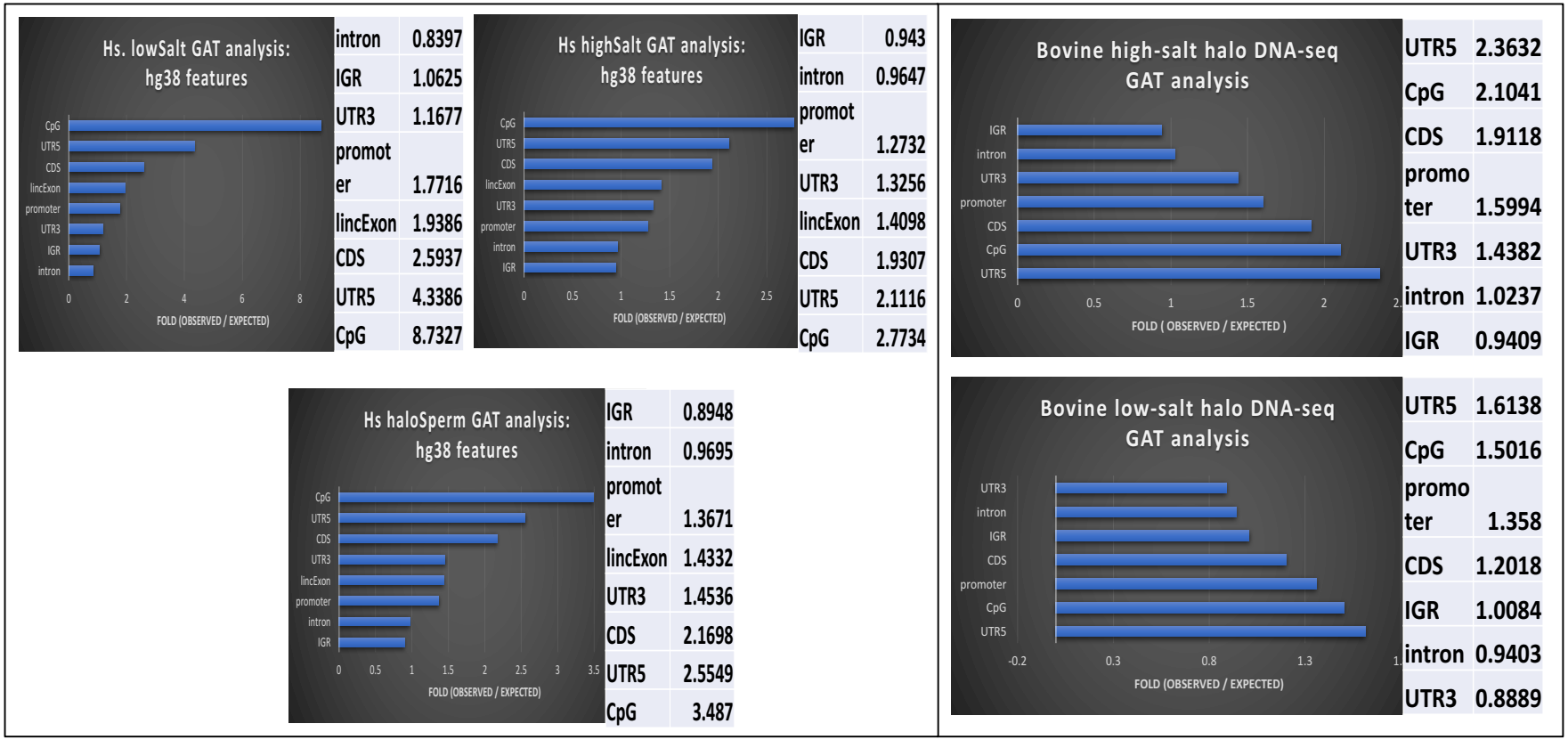

Figure 70: Images of GAT analysis showed the significant enriched regions of salt extracted halos (low and high) and Halosperm assay that associated with particular genomic regions of human (left) and bovine sperm (right).

The significantly enriched sequences in each DNA fraction were determined using MACS2 with a maximum of one duplicate read in treatment and control. GAT results showed that 5'-UTRs are highly enriched regions in the halo fractions from both human and bovine sperm. These regions are important in transcriptional regulation (Van Der Velden and Thomas, 1999). In human sperm, for example, the fold enrichment of 5'-UTR sequences in halo fractions generated following extraction of sperm nuclei by 0.65 M NaCl was lower (64% of total genes) compared to those (81% of total genes) generated following extraction by 2.0 M NaCl. The number of enriched 5'-UTR regions that remained in the nucleoid were higher (36% of total genes) in 0.65 M NaCl compared to 2.0 M NaCl (19% of total genes) (Table 6). Similar results (76% of total genes) were obtained from halo fractions extracted by Halosperm assay (Table 6 and Figure 71). This pattern of enrichment was more pronounced in bovine by comparing 0.65 M of NaCl (26% vs 74%) to 2.0 M of NaCl extraction (85% vs 15%) in both fractions (Table 6 and Figure 72).

In human, low salt halos contained more enriched gene sequences (64%) compared to those in bovine (26%), which may be due to the lower percentage of retained histones (<5%) in bovine sperm compared to human sperm (5-15%) (Ioannou et al., 2016) (Table 6).

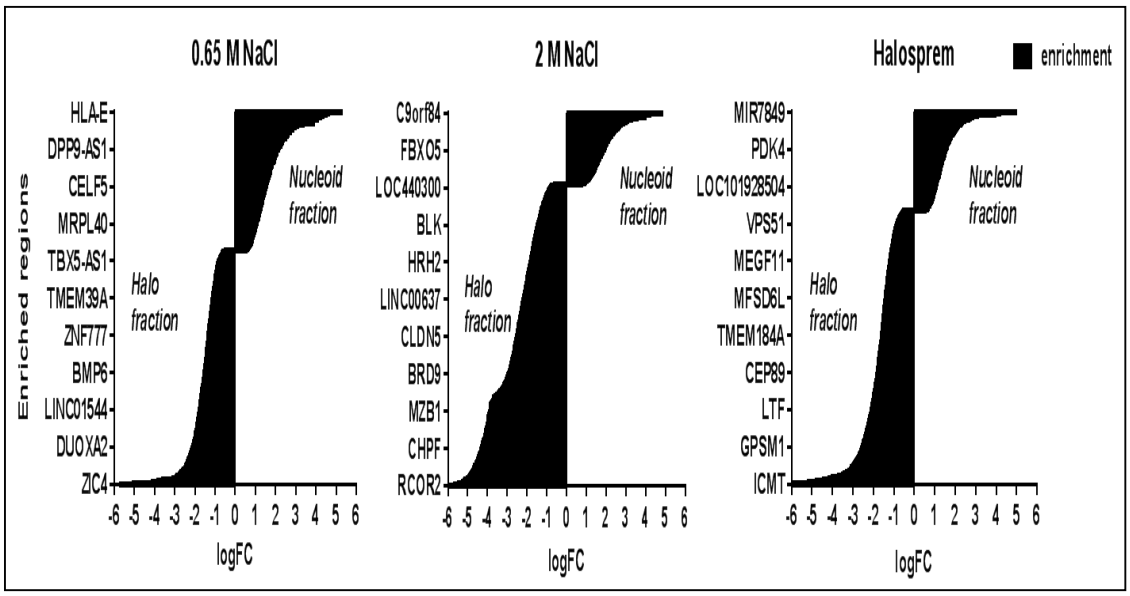

Figure 71: Clustered bars showed some of examples of the significant enrichment of 5'UTR regions in halo and nucleoid fractions generated by salt extractions and Halosperm assay on human sperm. This distribution pattern showed that different strength of salt concentration may extract different regions of sperm DNA

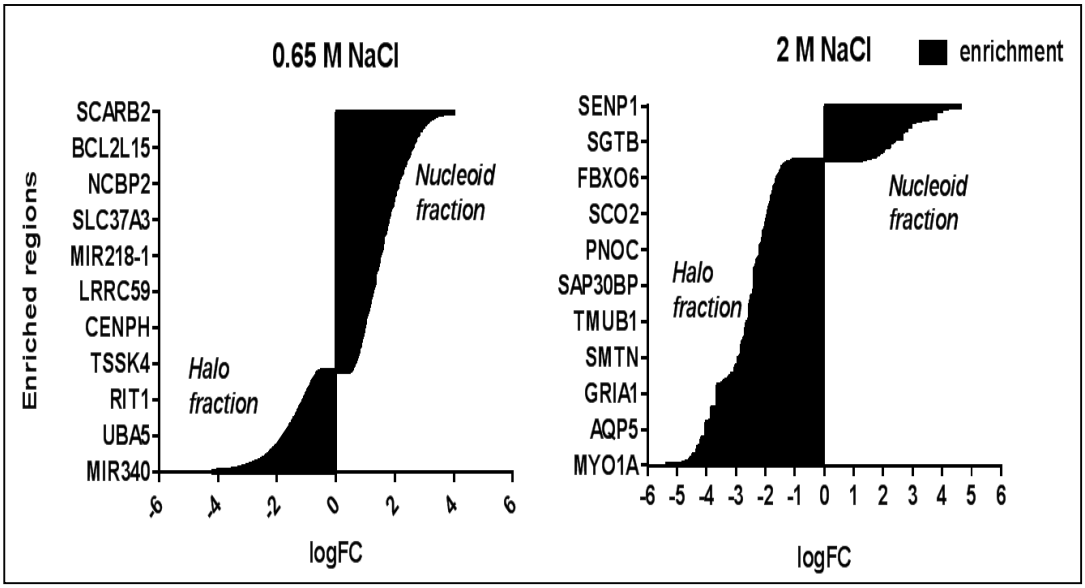

Figure 72: Clustered bars showed some examples of the significant enrichment of 5'UTR regions in halo and nucleoid fractions that generated by salt extractions on bovine sperm. This distribution pattern showed that different strength of salt concentration may extract different regions of sperm DNA.

Human	Halo	Nucleoid	Total	Percentage Halo vs Nucleoid
Low salt	**1488**	**854**	**2342**	**64% vs 36%**
High salt	**2789**	**655**	**3444**	**81% vs 19%**
Halosperm	**2509**	**806**	**3315**	**76% vs 24%**

Bovine	Halo	Nucleoid	Total	Percentage Halo vs Nucleoid
Low salt	**1281**	**3503**	**4784**	**26% vs 74%**
High salt	**653**	**115**	**768**	**85% vs 15%**

Table 6: Two tables showed the number and percentage of genes that enriched (2-fold change and above) in either halo or nucleoid fraction in salt extractions and Halosperm assay in human and bovine sperm.

5.3.3 Gene ontology of enriched regions in halos

Comparative analysis of the biological process and molecular function of the enriched sequences in halo and nucleoid fractions was undertaken through the Panther (http://www.pantherdb.org) gene ontology database. To determine statistical significant gene ontology of both DNA-fractions, a cut-off for log2 fold change was applied. In human, the most abundant biological process of the genic sequences within low salt halo-enriched features were those involved in developmental activity, including reproduction (fold enrichment, 2.27), morphogenesis (fold enrichment, 2.13) and positive regulation (fold enrichment, 1.87) (Appendix 3). Similarly, the most biological features that were enriched in halos generated by high salt extraction and Halosperm assay were developmental process involved in tube morphogenesis (fold enrichment, 2.54), embryonic organ formation (fold enrichment, 2.28), embryonic morphogenesis (fold enrichment, 2.16) (Appendix 3). In contrast, there were no enrichments for gene ontology derived from nucleoids generated by 0.65 M NaCl, 2.0 M NaCl and Halosperm buffer extraction.

In bovine, the most abundant biological process of the genic sequences within low salt halo-enriched features were those involved in cofactor metabolic process (fold enrichment, 2.64), positive regulation (fold enrichment, 1.59) and cellular process (fold enrichment, 1.38) (Appendix 3). Whereas, the most abundant biological process within low salt nucleoid-enriched features were negative regulation of cellular protein localisation (fold enrichment, 3.45), protein transport (fold enrichment, 1.96) and gene expression (fold enrichment, 1.49) (Appendix 3). As for human sperm, there were insufficient enrichments of gene ontological analysis in both halos and nucleoids extracted by high salt.

5.3.3.1 Enriched developmental gene sequences

5.3.3.1.1 Human sperm

A total number of 59 transcription factors including homeobox and zinc finger gene sequences were enriched in 0.65 M NaCl halos, while there were 36 transcription factors enriched in nucleoid fractions. Ninety-eight different developmental gene sequences including *HOXC6* (3.276 fold), *HOXC13* (3.230 fold), *PHOX2B* (3.031 fold), *LHX5* (2.260 fold) and *PAX6* (1.868 fold) were significantly enriched in the halo fraction compared to 22 genes in the nucleoid fraction.

By extracting with 2.0 M NaCl, a total of 96 transcription factors were enriched in halo fraction, while, there were only 19 transcription factors including *FOXB1*, *ZNF639* and *CT47A1* enriched in nucleoid fractions. A total number of 130 sequences of developmental genes including *OTX1* (16.84 fold), *FGF21* (4.557 fold) and *FOXA3* (23.60 fold) were highly enriched in halo fractions compared to only 12 genes enriched in nucleoid fractions.

Similarly, by using Halosperm, the number of enriched transcription factors that were found in halo fractions was higher (105 transcription factors) compared to 22 transcription factors enriched in nucleoid fractions. Additionally, 151 sequences of developmental genes including *HOXC4* (4.153 fold), *ISL2* (2.770 fold), *HOXC5* (2.246 fold) and *LHX1* (2.427 fold) were identified enriched in halo fractions compared to 23 genes enriched in nucleoid fractions.

All halo fractions produced by salt extraction or the Halosperm buffer were enriched at exonic regions of the developmental genes including *HOX* clusters (Figure 73).

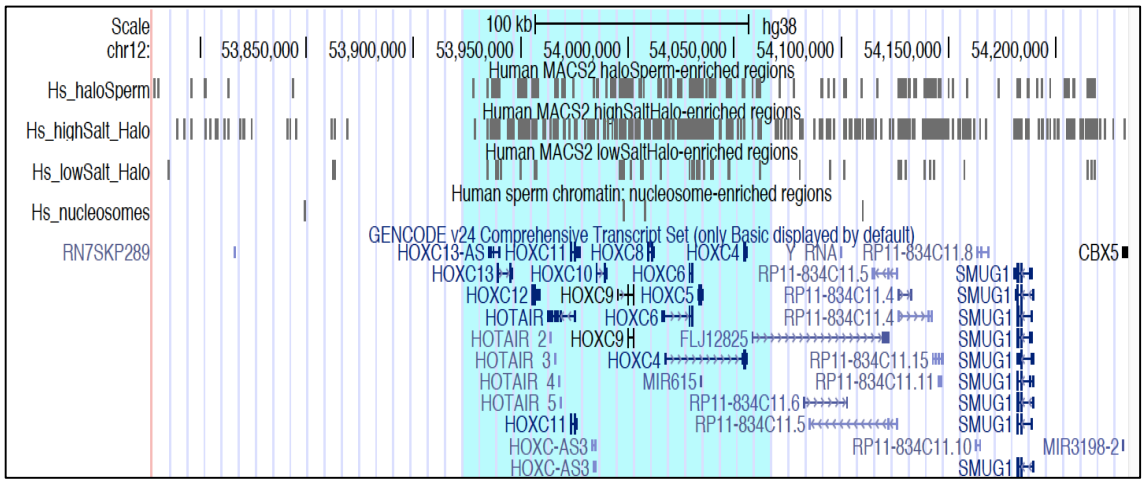

Figure 73: A screen capture shows developmental genes (for example *HOXC*) that enriched in halo fractions (highlighted) that produced by Halosperm assay, 2.0 M salt and 0.65 M salt extraction of human sperm.

5.3.3.1.2 Bovine sperm

A total number of 66 transcription factors including homeobox and zinc finger transcription factors were enriched in halos generated following extraction with 0.65 M NaCl, while, there were 196 transcription factors enriched in nucleoid fractions. In addition, 122 different sequences of developmental gene including *HOXB7* (7.388 fold), *HOXA2* (2.036 fold), *DBX1* (2.069 fold), *FGF2* (2.236 fold) and *PAX3* (13.488 fold) were found enriched in halo fractions compared to 372 genes including *HOXA3* (1.598 fold), *PHOX2A* (1.684 fold), *HOXD10* (2.772 fold),

HOXC11 (2.975 fold) and *HOXA10* (3.850 fold) that were enriched in nucleoid fractions.

However, by using 2.0 M NaCl, only 21 transcription factors such as *ZNF691*, *GTF2F1* and *ATF4* were enriched in halo fractions compared to only 7 transcription factors were enriched in nucleoid fractions. A total number of 39 developmental gene sequences including *Lhx3* (16.119 fold), *SPRY2* (6.921 fold), *PAX3* (3.976 fold) and *STAT5A* (4.873 fold) were highly enriched in 2.0 M NaCl halo fractions compared to only 12 genes enriched in nucleoid fractions.

5.3.4 Summary on the enriched regions in halo and nucleoid fractions

The digested halo and nucleoid (residual) fractions were subjected to deep sequencing, which generates data that is far more extensive and comprehensive than can be achieved with microarrays. In sperm, previous evidence suggested that the closer developmental genes are to the nuclear periphery, the more they may be at risk of attack by external agents such as oxidative radicals (Arpanahi et al., 2009). In addition, recent findings suggested that chromatin domains most at risk for oxidative DNA damage, may be associated with the nuclear matrix and nucleosome-rich regions, are respectively located at the basal domains and at the periphery of the mouse sperm nucleus (Noblanc et al., 2013).

Earlier experiments in the current study, for example in chapter 5 (page 123), investigated the correlation of halo size and DNA fragmentation and showed that the greater the exposure to oxidation, the smaller the halo size. Also, in chapter 2 (page 38), immunofluorescence results indicated that histones were located at the periphery of the nucleus. Other research on mice has linked nuclear chromatin structure and DNA sequence with the male pronucleus formation and the first round of DNA replication after fertilisation (Shaman et al., 2007a). A major

consideration of the work carried out for this dissertation is that DNA-fragments isolated from low salt halos of sperm nuclei are enriched for genes involved in early developmental processes in the zygote. Hence, sequencing halo-DNA should provide evidence for the development relevance of this assumption. For example, analysis of CpG islands (Meyer et al., 2013) showed that the halo-enriched CpGs produced by low salt solution were enriched at the developmental genes such as *HOX* gene (Figure 74).

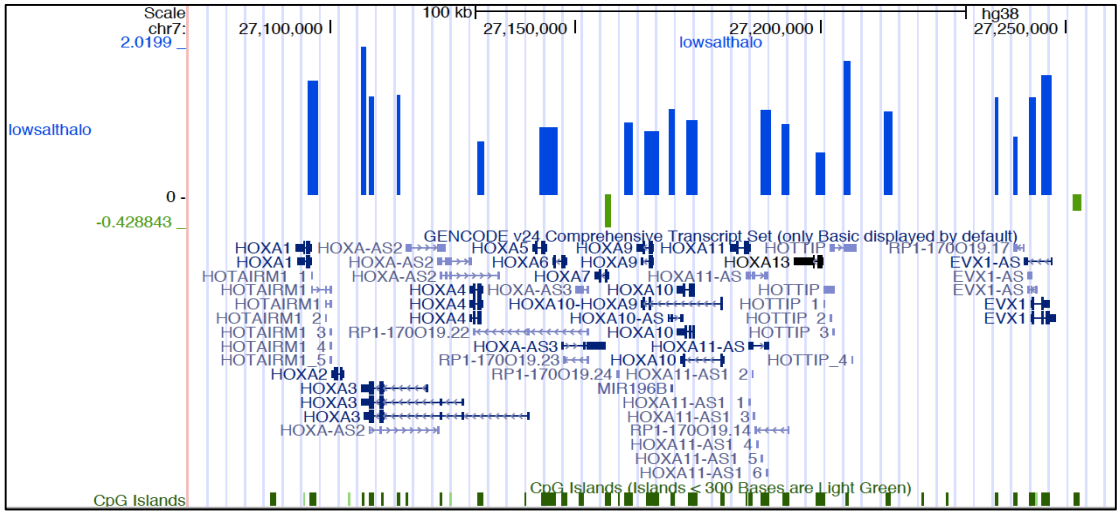

Figure 74: A screen capture showed the significant halo-associated CpG islands (blue bars), which were highly enriched at the *HOX* clusters compared to nucleoid-associated (green bars).

In addition, the analysis of the highly halo-enriched 5'UTR regions, which also retrieved from the UCSC browser showed that 5'UTR regions were located in the 5'-upstream region of the developmental genes such as *HOX* clusters and *LHX5* (Figure 75). Similarly, the nucleoid-enriched 5'UTR regions were located in the 5'-upstream regions of the developmental genes such as *DUSP1* (Figure 76).

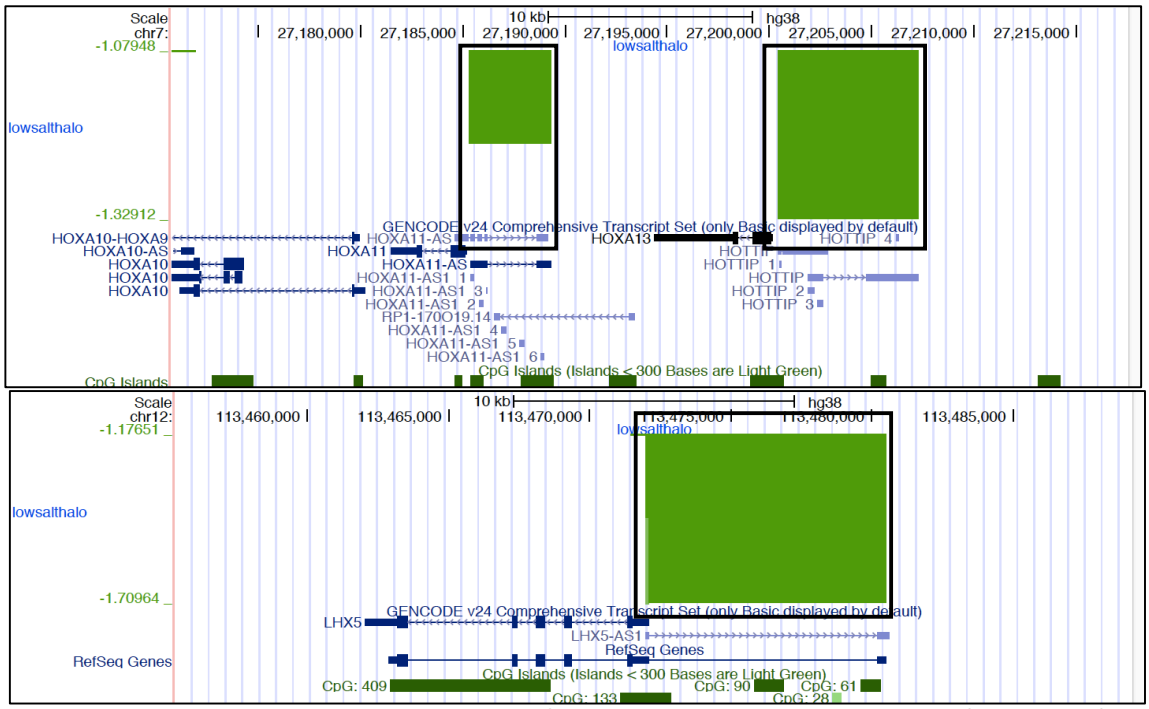

Figure 75: A screen capture showed the significant halo-enriched 5'UTR regions (green bars), which were located upstream of the *HOX* clusters **(A)**, and *LHX5* in halo fractions **(B)** (highlighted in black boxes).

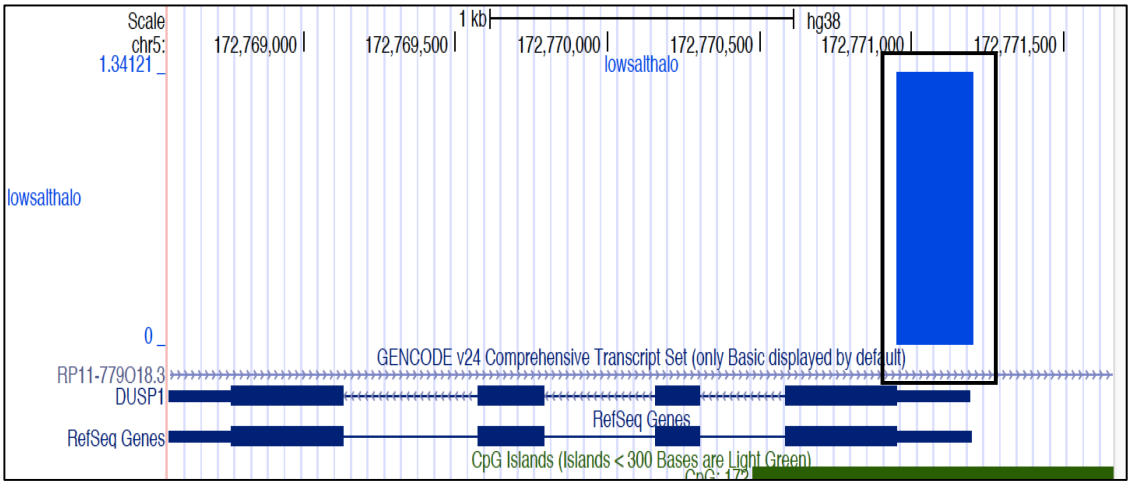

Figure 76: A screen capture showed the significant nucleoid-enriched 5'UTR regions (blue bar), which were located upstream of the *DUSP1* gene (highlighted in a black box).

5.3.4.1 Human sperm

A Venn diagram was generated to allow a visual comparison between the sequences enriched in sperm halos and nucleoids generated following salt extraction. In human sperm, hundreds of regions were enriched in halo fractions,

however, a total of 316 genes were common to all three types of halos (Figure 77).

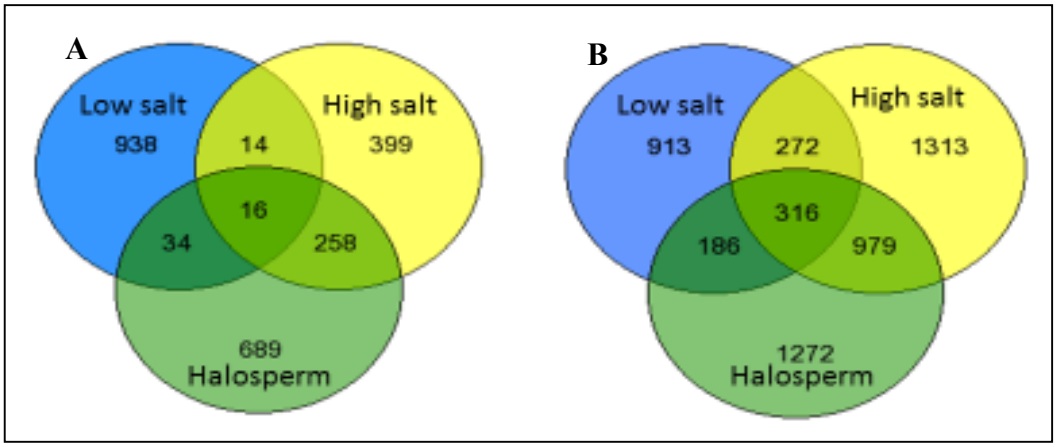

Figure 77: Venn diagrams of numebrs of UTRs in enriched regions (common and different) to 5UTRs in each DNA fraction of human sperm in different experiments (salt-extraction and Halosperm assay), nucloids (A) and halos (B).

Twenty-four genes were present among these shared regions that were identified as developmental genes, including *HOXC13, FGF3*, transcription factor *AP-2-E and LHX5* (RNA binding protein). As indicated by Edge R analysis of human fractions, a number of sequences of developmental genes and transcription factors were significantly over-represented in all three types of halo fractions such as *HOXC13, HOXB13, CRIP1, DUSP5, CDX2 and LHX5*.

In contrast, although thousands of regions were significantly enriched in nucleoid fractions, only 16 of them were common to all extraction methods (Figure 75). These common regions were mainly related to metabolic proteins (metalloprotease nucleic acid binding transcription factor) and as shown in Table 7, few sequences of developmental genes such as *KSR2, DUSP1, CDKL2* and *ROCK1* were overrepresented in nucleoid fractions.

DNA fractions	0.65 M of NaCl	2 M of NaCl	Halosperm
Halo	*LHX5*	*LHX5*	*LHX5*
	HOXC13	*HOXC13*	*HOXC13*
	FAT1		
	ZIC1		
		CDC42BPB	*CDC42BPB*
		CRIP1	*CRIP1*
		DUSP2	*DUSP2*
		DUSP5	*DUSP5*
		CDX2	
		LHX1	*LHX1*
			LRP6
			RGS19
Nucleoid	*KSR2*		
	DUSP1		
	NANOS2		
		CDKL2	*CDKL2*
			ROCK1

Table 7: Number of developmental genes that were significantly overrepresented (2-fold change) in either halo or nucleoid fractions of human sperm.

5.3.4.2 Bovine sperm

As shown in Figure 76, a total of 1428 regions were enriched in halos generated by 0.65 M of NaCl, whereas, the number of significantly enriched regions was reduced by half in halos generated by extraction with 2.0 M of NaCl. A total of 286 of the enriched genes were overlapped between both salt extracted halos (Figure 78). Among these overlapped regions, there were 26 genes that were identified as developmental genes such as *PAX3*, *Lhx3*, *GATA3* and *TGFB1*.

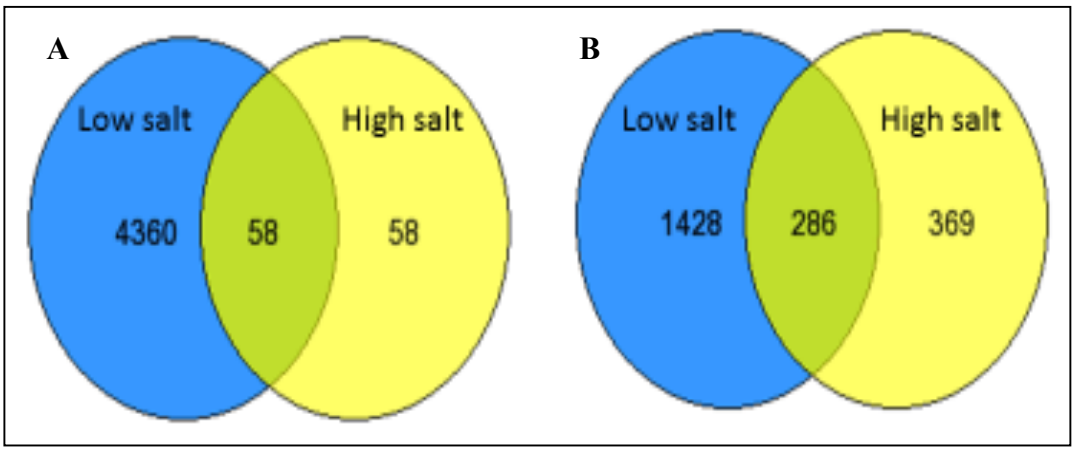

Figure 78: Venn diagrams of numebrs of the enriched regions (common and different) to 5UTRs in each DNA fraction of salt-extracted bovine sperm, nucloids (A) and halos (B).

As indicated by Edge R analysis of bovine fractions, sequences from developmental genes (for example *MEF2D* and *TESK1*) were significantly enriched in DNA isolated from both salt extracted halos and in general, the low salt halo was more strongly enriched for developmental gene sequences (Table 8).

Only 58 gene sequences were shared between high and low salt extracted nucleoids (Figure 78). Most of these common regions represent regulators for molecular functions including developmental processes (*HOXC11, LMO1* and *GLI1*, for example). Indeed, sequences from 17 developmental genes were significantly enriched in nucleoid fractions of 0.65 M NaCl extracted nuclei compared to only one enriched gene sequence in nucleoid fraction of 2.0 M NaCl extracted nuclei (Table 8).

DNA fractions	0.65 M NaCl	2 M NaCl
Halo		*GSK3A*
	MEF2D	*MEF2D*
	CDKL1	
	Lhx3	*Lhx3*
	DLX3	
	TESK1	*TESK1*
	VGLL2	
	CDK2	
	MEF2A	
		Lhx3
Nucleoid	*RGS19*	
	LEF1	
	RALB	
	DPPA3	
	DLX2	
	CDK6	
	LMO1	
	CRIP1	
	GLI1	
	DUSP2	
	DLX5	
	RALA	*RALA*
	HOXD10	
	DUSP6	
	LMO2	
	HOXC11	
	LMO3	

Table 8: Number of embryonic developmental genes that were significantly overrepresented in either halo or nucleoid fractions of bovine sperm.

5.3.5 The overlap between sperm halo fractions and nucleosome distribution

In this current study, the NGS data indicated that halo fractions were enriched with DNA sequences for developmental genes, CpG islands and transcription factors. Previous studies on human sperm suggested that embryonic developmental genes including transcription factors are packaged by retained nucleosomes with modified histones (Arpanahi et al., 2009; Brykczynska et al., 2010). To test this hypothesis, an available recently published NGS data of modified nucleosomes of human and bovine sperm (Samans et al., 2014) was

used to display the overlap (if any) of nucleosome distribution and enrichment regions with halo fractions.

In human sperm, the distribution analyses of DNA sequences from retained nucleosomes revealed clear overlap with developmental gene sequences from the *HOX* clusters (*HOXD*, *HOXB, HOXC* and *HOXA*), *GSK3A* and *LRP6* enriched in halo fractions (Figure 79-82).

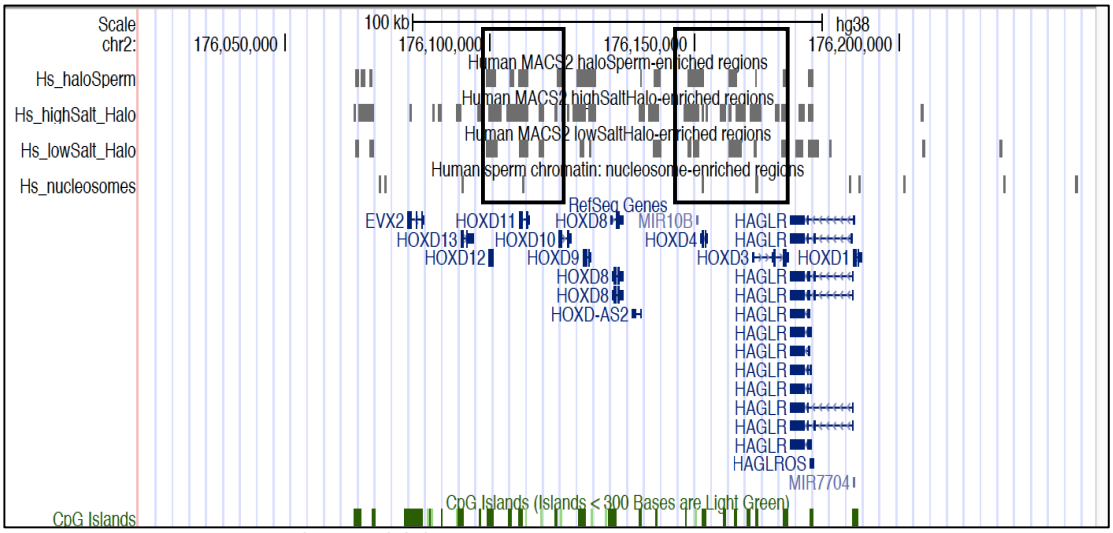

Figure 79: A screenshot from UCSC captured image showed the overlapping peaks between halo fractions and retained nucleosomes in *HOXD* genes of human sperm (highlighted black boxes).

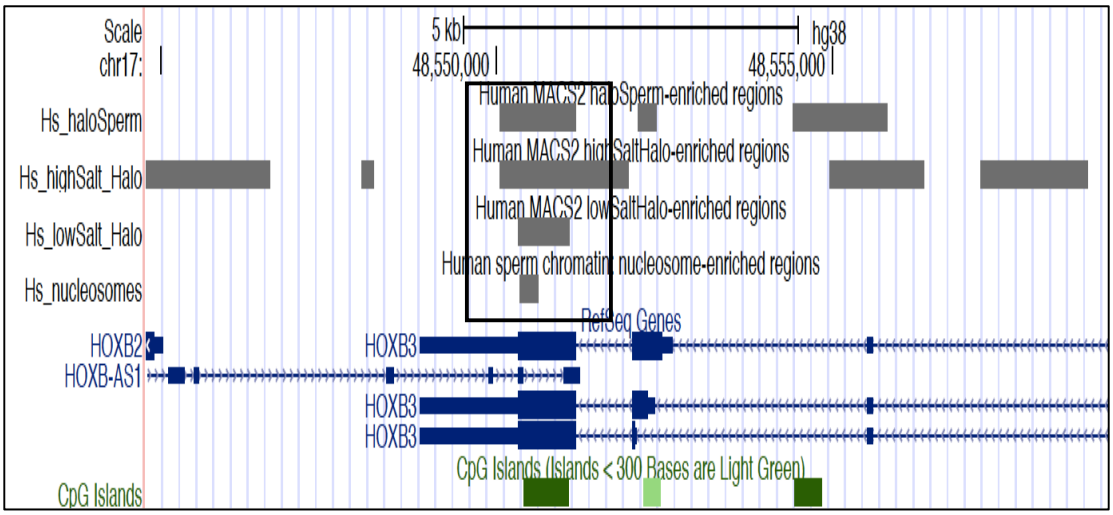

Figure 80: A screenshot from UCSC captured image showed the overlapping peaks between halo fractions and retained nucleosomes in *HOXB* genes of human sperm (highlighted black boxes).

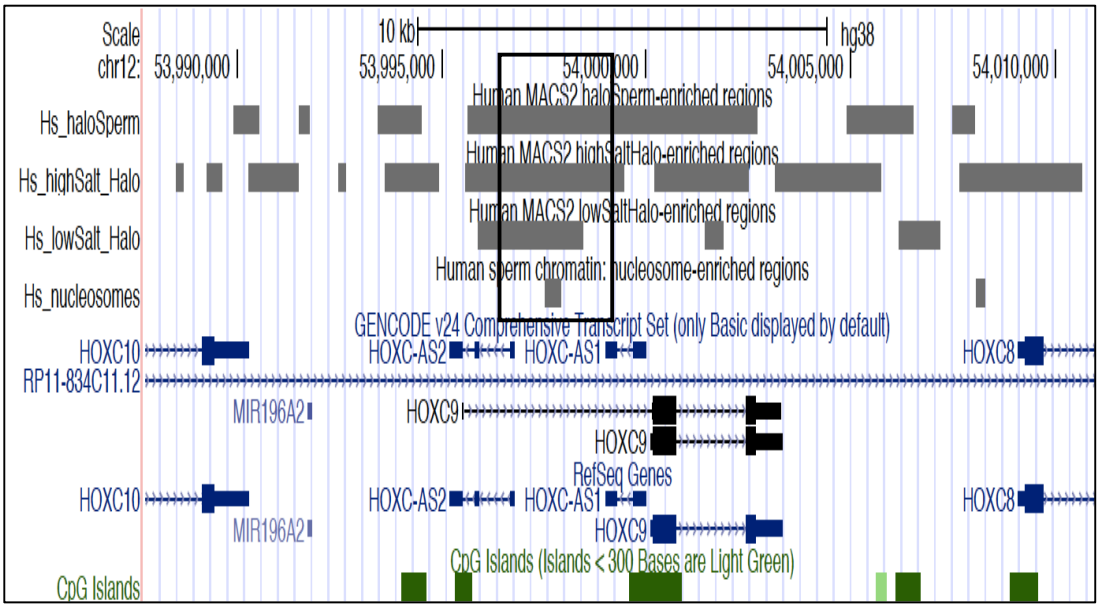

Figure 81: A screenshot from UCSC captured image showed the overlapping peaks between halo fractions and retained nucleosomes in *HOXC* genes of human sperm (highlighted black boxes).

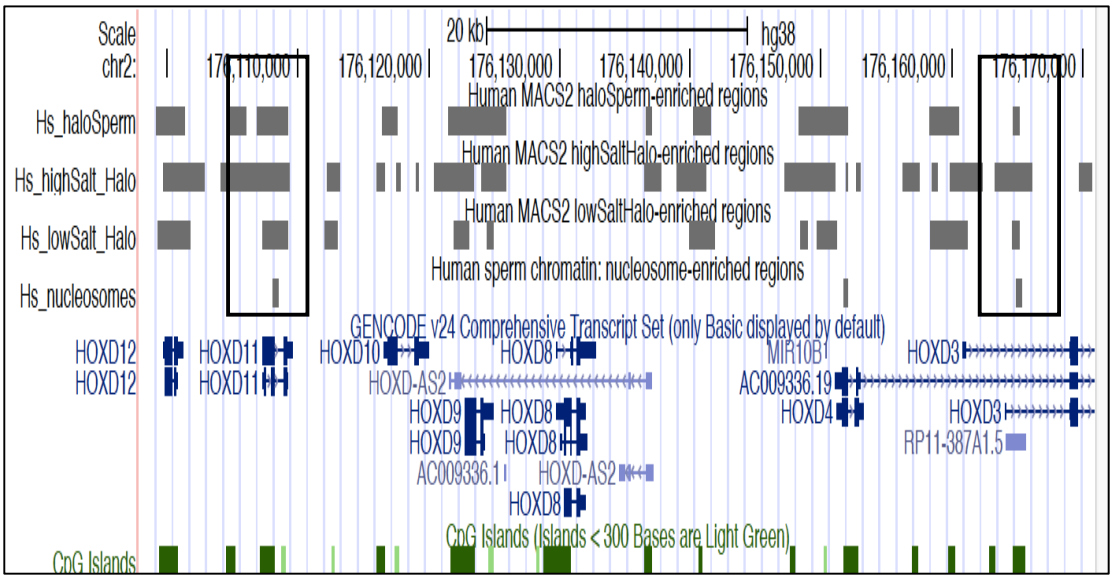

Figure 82: A screenshot from UCSC captured image showed the overlapping peaks between halo fractions and retained nucleosomes in *HOXA* genes of human sperm (highlighted black boxes).

Similar overlapping patterns of nucleosome distribution with nucleoid-enriched gene sequences were detected for *KSR2*, *CDKL2* and *LHX4* (Figure 83-84).

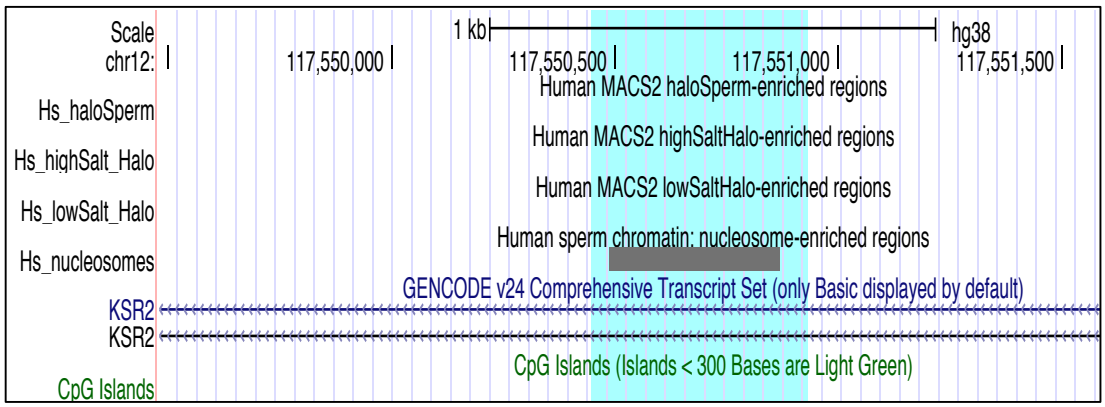

Figure 83: A screenshot from UCSC captured image showed the overlapping peaks between nucleoid fractions (depleted peaks, as MACS2 showed only regions that enriched in halo fractions) and retained nucleosomes in *KSR2* gene of human sperm (highlighted).

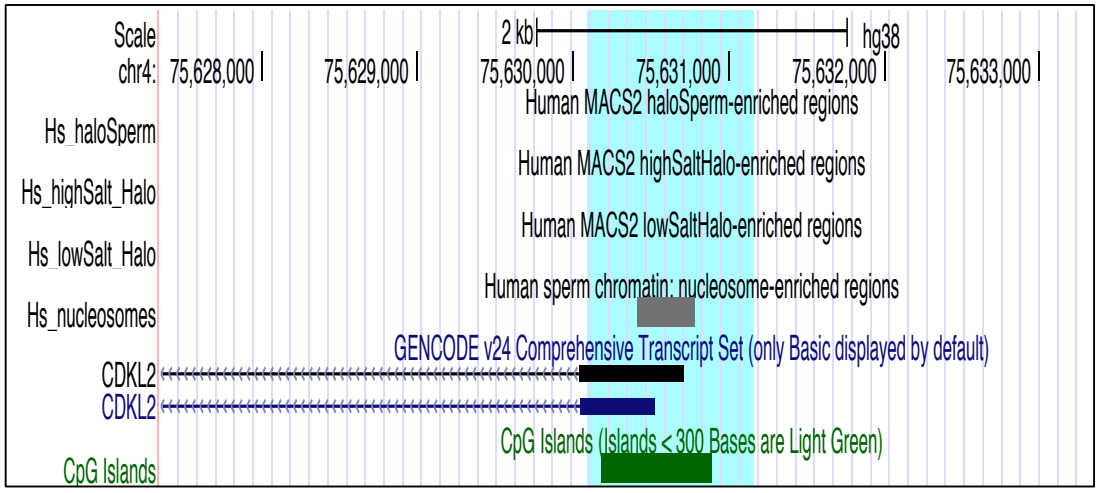

Figure 84: A screenshot from UCSC captured image showed the overlapping peaks between nucleoid fractions (depleted peaks, as MACS2 showed only regions that enriched in halo fractions) and retained nucleosomes in *CDKL2* gene of human sperm (highlighted).

Halo gene sequences from bovine sperm had a less distinctive overlap with retained nucleosomes with fewer developmental genes. For example, *LRFN5, EDNRB* and *ADAM10* were enriched in low salt halos, however, there was no clear overlap with nucleosomal sequences associated with *HOX* clusters. Similarly, in the nucleoid fractions, the distribution analyses of retained nucleosomes were found to be overlapped with some highly enriched developmental genes such as *LEF1, ZMAT3, FSHR* and *CDH18* (Figure 85-86).

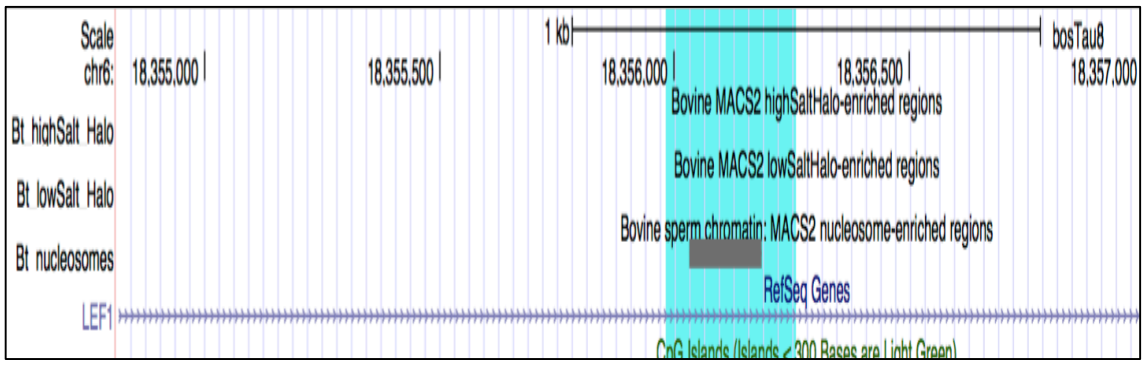

Figure 85: A screenshot from UCSC captured image showed the overlapping peaks between nucleoid fractions (depleted peaks, as MACS2 showed only regions that enriched in halo fractions) and retained nucleosomes in *LEF1* gene of bovine sperm (highlighted).

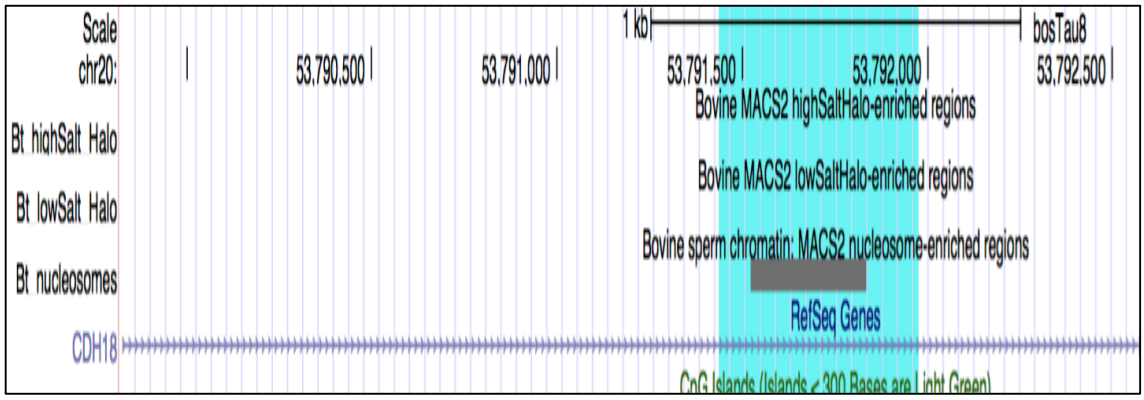

Figure 86: A screenshot from UCSC captured image showed the overlapping peaks between nucleoid fractions (depleted peaks, as MACS2 showed only regions that enriched in halo fractions) and retained nucleosomes in *CDH18* gene of bovine sperm (highlighted).

5.3.6 Validation of NGS data by qPCR

Six low-salt enriched intervals (three from halo and three from nucleoid fractions), were validated by qPCR. Validation was applied to halo- and nucleoid-DNA from both 0.65 M and 2.0 M NaCl experiments. The calculated fold enrichment of these six intervals were clearly correlated with the peak values obtained from NGS data (Table 9). As a complementary test, the densitometric quantitation of DNA in the qPCR products resolved by gel electrophoresis was measured using Image J (Figure 87) and shown to closely correspond with qPCR result (Figure 89).

Intervals	fraction enrichment from NGS data	fold enrichment form qPCR	fraction enrichment from qPCR data	Intervals	fraction of enrichment from NGS data	fold enrichment from qPCR	fraction enrichment from qPCR data
0.65 M NaCl				**2.0 M NaCl**			
MAP4	Nucleoid	1.83	Nucleoid	**MAP4**	Halo	1.26	Halo
CYTH3	Halo	4.93	Halo	**CYTH3**	Halo	2.71	Halo
SLC7A14	Nucleoid	1.28	Nucleoid	**SLC7A14**	Halo	1.29	Halo
CAPS2	Halo	7.84	Halo	**CAPS2**	Halo	4.10	Halo
DHX30	Nucleoid	1.03	Nucleoid	**DHX30**	Halo	2.11	Halo
MOB3B	Halo	12.92	Halo	**MOB3B**	Halo	4.44	Halo

Table 9: Fold enrichment of each interval in both 0.65 M and 2.0 M NaCl experiments.

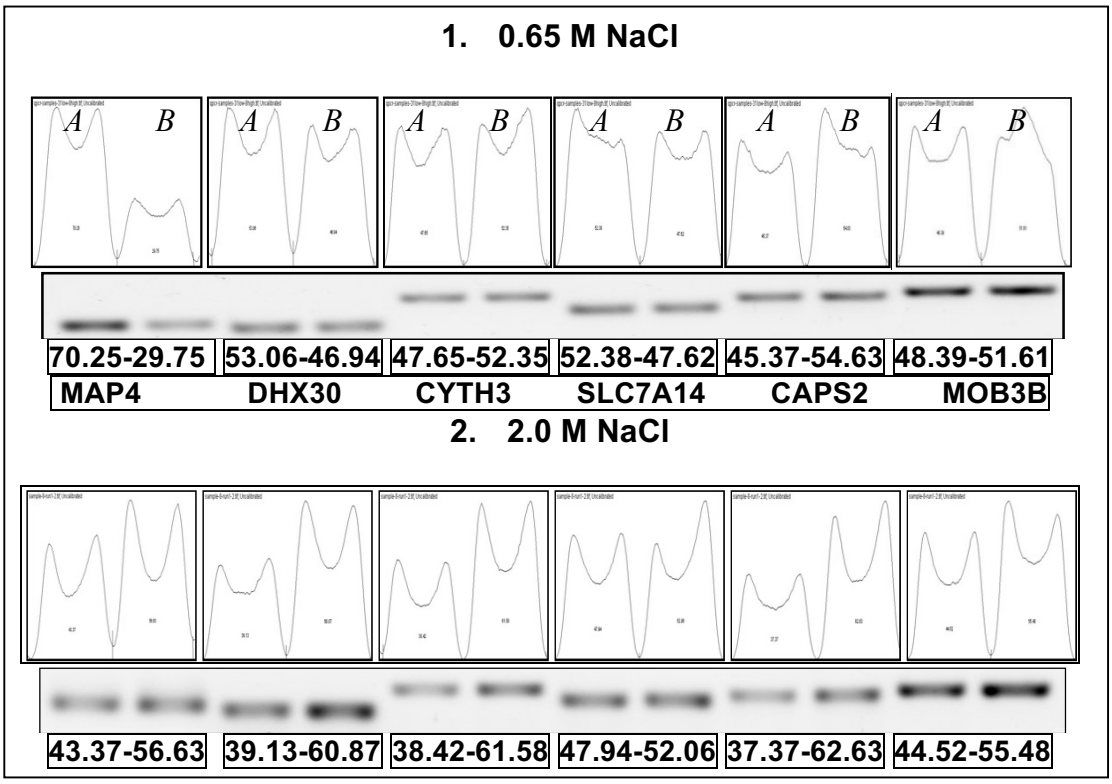

Figure 87: Analysis of DNA band intensity of gel electrophoresis for the qPCR products for both 0.65 M and 2 M NaCl samples. (A) nucleoid-DNA, (B) halo-DNA. Image J measured the area under the scan curve and calculated the percentage of each peak of nucleoid compared to the related peak of halo.

5.4 Discussion

5.4.1 Sperm DNA repeats analysis

Repetitive DNA sequence (the fraction of the genome comprising repeats) seem to be crucial for particular genome functions such as genome replication, developmental process and the three-dimensional (3D) chromosome folding (Shapiro and Sternberg, 2005; Foster et al., 2005). In addition, a large proportion of repetitive DNA is present as multiple patterns of repeating nucleotides or isochores (Treangen and Salzberg, 2012) in somatic cell nuclei. In the current study, examination of repetitive DNA sequences was undertaken to help understand the output of the sequencing data in relation to the halo and nucleoid origins. Results from low salt extraction suggests that telomeres and centromeres for most chromosomes were enriched in nucleoid fractions, which indicates that the arrangement of chromosomes in the sperm nucleus is not random. A previous study reported that telomeric DNA is histone-bound and located close to the nuclear periphery (Zalenskaya et al., 2000). Moreover, the majority of repetitive reads in halo fractions mapped to regions rich in satellite, retroviral and LTR, whereas the majority of reads in nucleoid fractions were mapped to Long (LINE) and Short (SINE) Interspersed Nuclear Elements.

These findings also correspond with previous studies reporting a non-random organisation of chromosomes in the nuclei of human sperm (Mudrak et al., 2005; Zalensky et al., 1995; Zalenskaya and Zalensky, 2004). In addition, the results suggest that almost the entire X and Y chromosomes as well as much of chromosomes 22, 19, 17 and 20, are more resistant to salt extraction because they have higher levels of repeating elements (respectively, 41.9%, 55%, 45.5%, 42%) than other chromosomes (Deloukas et al., 2001; Zody et al., 2006;

Grimwood et al., 2004; Dunham et al., 1999) and are likely to be heterochromatic. Chromosome 18, for example, was described previously as not enriched in repetitive sequences (Nusbaum et al., 2005), however, it was found enriched in the halo fractions generated during the course of this study. Chromosomes might be organised according to their size as suggested by Sun and Yokota (1999), where the physically smaller chromosomes are located closer to the centre of the nucleus. Other hypotheses suggest that chromosome distribution correlates more with gene density than with chromosome size. The X chromosome is relatively large and previous studies suggested that it is positioned at the anterior region of sperm nuclei (Zalenskaya and Zalensky, 2004; Luetjens et al., 1999; Hazzouri et al., 2000b). If positioning is related to gene density, another study, which sequenced the entire human X chromosome indicating that chromosome X is relatively gene-poor is relevant (Ross et al., 2005). The X chromosome may be 'unexpectedly' enriched in the nucleoid fraction because it has one of the lowest gene densities among chromosomes. Perhaps gene density alongside chromosome dimensions may be fundamental factors regulating chromosome location in the nucleus of human sperm (Manvelyan et al., 2008).

CpGs are not uniformly distributed in the entire genome and are also found to be strongly associated with genic regions (Stanley et al., 2006). Therefore, the analysis of the enrichment of CpG profiles in both DNA fractions produced by low salt extraction was used to explore the association between gene density and salt accessibility following halo formation. The result showed that the distribution patterns of CpGs and DNA repetitive sequences were similar, possibly due to the high representation of HERV elements in both low and high salt halo fractions. In the current study, NGS data suggested that the reported distribution and

enrichment of repetitive DNA, particularly CpGs, may be influenced by respective gene densities in halo- and nucleoid-DNA, which may have an influence on the original positioning of the chromosomes in sperm nuclei (Mahy et al., 2002). Therefore, localisation of the chromosomes in sperm nuclei may consequently make them differentially accessible to salt extraction (Arpanahi et al., 2009). This suggestion might correspond with a previous suggestion that soluble chromatin (salt extraction and endonuclease digestion) is located close to the peripheral part of the sperm nucleus (Arpanahi et al., 2009; Saida et al., 2011). In this context, relatively (salt) accessible is halo and relatively inaccessible is nucleoid.

5.4.2 GAT analysis

Based on the correspondence between repeat content and the strength of the salt extraction buffers used to generate halos, the sequencing data suggested that other regions in human sperm chromatin may not be randomly packaged. To test this possibility, the GAT tool was used to examine the association of specific genomic features including promoters, 5'-UTRs and CpG islands with halo and nucleoid fractions. Promoter, 5'-UTRs and CpG island rich sequences occurred more frequently in halo fractions generated by low salt extraction of human sperm, than would be expected by chance. This finding was replicated, though less sharply, in halo fractions produced by high salt extraction of both human and bovine sperm, suggesting that the distribution of halo-enriched sequences was non-random.

In contrast, intronic and intergenic regions were not enriched in halo fractions. Differences, however, between low and high salt extraction buffers were noted. In bovine sperm, for example, 3'-UTRs were not associated with halo fractions generated by low salt extraction, but were more associated with equivalent halo

fractions generated by extraction with 2.0 M NaCl. These findings support the argument that functional regions (CpGs, 5'-UTR, codon and promoter) are preferentially packaged by histones (Rathke et al., 2014; Gardiner-Garden et al., 1998; Gatewood et al., 1987) and may subsequently be more likely to encounter ooplasmic factors after fertilisation that together, may regulate early embryonic development. The enrichment of 5'-UTR and promoter regions in halo fractions also supports the suggestion that chromatin is not randomly packaged in the sperm nucleus (Wykes and Krawetz, 2003).

Results from 3'-UTR and intergenic regions distribution may be explained if it assumed that the sperm halo is composed of relaxed DNA loop domains attached to the sperm nuclear matrix (Ward et al., 1989). For example, 5'-UTRs of some genes with long coding sequences may locate to the halo fraction, while their 3'-UTRs remain in the nucleoid fraction, as their promoter and 5'-UTRs were accessible to salt extraction leaving the naked 5' DNA exposed to restriction digestion. Whereas, in genes with short coding sequences, both UTRs may be extracted together into halo fractions. This assumption may be varied depend on the length of DNA in a halo loop and their fragments size after digestion of the halo by restriction enzymes (EcoR1 and BamH1).

5.4.3 The enrichment of developmental genes

HOX genes play an important role in the regulation of embryo development (Min et al., 2016; Mallo and Alonso, 2013) and recent evidence in mouse suggests that both chromatin structure and imprinting modifications are essential for *Hox* gene expression (Noordermeer et al., 2011). At 0.65 M of NaCl, the ionic strength of the extraction buffer is ideal for destabilising nucleohistones from the chromatin-protamine complex in sperm nuclei (Wykes and Krawetz, 2003;

Arpanahi et al., 2009). In this current study, NGS data from both halo and nucleoid fractions were used to gain insights into the partitioning behaviour of developmental genes. In human, the results showed that some developmental genes, such as *HOX* genes were enriched in halo fractions, which is consistent with findings of previous studies using ChIP-CHIP and ChIP-seq (Arpanahi et al., 2009; Hammoud et al., 2009). No *HOX* genes were located in nucleoid fractions generated by 0.65 M or 2.0 M of NaCl. As promotor sequences were enriched in the soluble fractions, these findings suggest that halo-DNA is enriched with developmentally important genes that may regulate embryonic development (Arpanahi et al., 2009; Johnson et al., 2011; Castillo et al., 2014a). In the bovine, more developmental genes such as *HOXA2*, *HOXB7* and *FGF2* were enriched in halo fractions obtained by 0.65 M of NaCl compared with 2.0 M of NaCl extraction. These differing partitioning profiles suggest that developmental genes in sperm chromatin have different levels of accessibility to salt extraction buffers. Moreover, many transcription factors such as *STAT5B*, *EVX1/2, PITX1*, *LHX5, HOXC13* and *SOX9* were found enriched in halo fractions and may be contributing actively to early gene transcription post-fertilisation. These findings correspond with a previous study that showed *LHX5*, for example, is found in regions that significantly enriched in rRNA sequences, which play a role in zygote development (Johnson et al., 2016). However, a higher number of transcription factors were enriched in halo fractions obtained by nuclear extraction with 2.0 M of NaCl and Halosperm buffer compared to 0.65 M, which may indicate that high salt concentrations access and extract additional nuclear layers of sperm chromatin. In addition, results of NGS showed a similar pattern of gene enrichment in both DNA fractions of 2.0 M of NaCl and Halosperm assay and the

buffer solution used in the Halosperm assay contains 2.0 M NaCl (Fernandez et al., 2003).

In bovine, many transcription factors such as *STAT5A*, *LHX3*, *SPRY2* and *PITX2* were enriched in halo fractions produced by nuclear extraction with 0.65 M NaCl. However, unlike human, compared to 0.65 M of NaCl, the total number of transcription factors enriched in halo fractions obtained by nuclear extraction with 2.0 M of NaCl was lower which indicates that some of the gene regulatory sequences might be more accessible to 0.65 M of NaCl treatment compared to 2.0 M NaCl.

5.4.4 The overlap distribution of retained nucleosome

Although previous studies suggested that gene promoters, *HOX* clusters, and developmental transcription factors are probably packaged by nucleosomes in sperm chromatin (Hammoud et al., 2009), the distribution of these retained nucleosomes in relation to sperm halo formation is still a matter of debate. To investigate the overlap between the enrichment revealed by NGS in halo and nucleoid fractions and the distribution of nucleosomes, available online data of nucleosome positioning in human and bovine sperm were analysed in parallel with the respective MACS2 enrichment output files for each fraction. The results revealed a clear overlap between the distribution of nucleosomes and the halo enrichment of developmental genes including transcription factors in human and bovine sperm. In addition, a clear overlap between nucleosome retention and several genomic regions such as CpG islands and simple repeats was also revealed. These overlaps suggest that developmental regulatory genes may be poised for transcriptional activation following fertilisation (Hammoud et al., 2009; Li et al., 2013; Castillo et al., 2014a). Interestingly, nucleosome distribution was

enriched at *HOX* clusters in human sperm, which corresponds with previous studies (Hammoud et al., 2009).

Chapter 6: General Discussion

The main experimental aims of this study were to

- Examine the relationship between halo formation and the histone compartment of sperm chromatin.
- Probe chromatin structure and organisation within the nucleus of the mature sperm in the context of sperm DNA fragmentation.
- Link the importance of DNA fragmentation to halo formation by DNA sequencing.

To these ends, localisation of protamines and histones in intact and halo-forming nuclei in mature sperm were considered in Chapter 2 using immunocytochemical microscopy, FISH and western blotting. In Chapters 3 and 4, DNA damage and its association with chromatin structure in mature sperm was investigated using different assays including AO and the comet assays, AB and SCD (Halosperm) assay. Alongside the DNA fragmentation assays that quantify DNA damage in different ways, the various qualitative outcomes from the immunocytochemical and related surveys of sperm chromatin must be taken into consideration when interpreting the DNA sequencing outcomes covered in Chapter 5.

6.1 Localisation of protamines and histones in the mature sperm nucleus in relation to DNA fragmentation

Correct sperm function may depend on molecular and architectural features of the chromatin that could render it susceptible to damage or disruption. Considering that 5-15% of the DNA in the human sperm nucleus remains bound to nucleosomes (Zalensky et al., 2002; Hammoud et al., 2009; Ioannou et al.,

2016), the appropriate localisation of histone-rich and protamine-rich domains within sperm chromatin may be an important factor in determining sperm quality. Previous studies revealed that nucleosomes may contribute significantly to the organisation of sperm chromatin as well as gene expression in early embryo development (Vieweg et al., 2015; Johnson et al., 2011). Moreover, modified histones in sperm may carry important epigenetic signals for regulating early embryonic development in human and other species (Wykes and Krawetz, 2003; Hammoud et al., 2009). In this study, the analysis of peroxide -induced DNA damage in the nuclei of spermatozoa harvested from the two DDGC subpopulations showed significant differences, where sperm populations from interface fractions were more susceptible to DNA damage as shown by acridine orange staining. Furthermore, higher numbers of sperm with weakly condensed chromatin were found in the interface layers following staining with AB, suggesting that incomplete chromatin compaction was at least in part, responsible for the increased sensitivity to oxidative DNA damage. These results complement findings that incomplete condensation (protamination insufficiency) of sperm nuclear chromatin is associated with DNA damage (Aitken and De Iuliis, 2007), which in turn, could increase the risk of pregnancy failure (Miller et al., 2010; Coughlan et al., 2015; Robinson and Klein, 2012).

Immunocytochemistry (Chapter 2) showed that histones were located towards the posterior region of the intact nucleus of human and bovine sperm and this positioning corresponded with earlier reports on human sperm (Yan Li, 2008; Van Roijen et al., 1998). Correspondingly, assessing sperm DNA fragmentation using acridine orange showed that DNA damage first appeared in the posterior region of the sperm nucleus, co-localising with the main positioning of histones and

moved progressively forward towards the anterior end as exposure to peroxide was continued until DNA fragmentation covered the entire nucleus. Complementing these findings, following exposure to peroxide for increasing periods of time, 8'd-OHG was always first detected at the posterior end of the sperm nucleus and signals progressively appeared further forward as exposure time to the oxidant was increased. The distribution of protamines was found to be scattered relatively uniformly throughout the nuclei of human sperm, which is also consistent with previous studies (Yan Li, 2008). Similarly, in bovine, the distribution of protamines was also dispersed throughout the nucleus. The slightly higher concentration of protamines seen at the sub-acrosomal region of the nucleus may be an indication of an abnormal sperm head (Dogan et al., 2015).

These results suggest that sperm nucleosomes are particularly prevalent towards the rear of the sperm nucleus, which corresponding with previous findings that showed somatic histones localised within the postacrosomal sheath of the mature bovine sperm (Tovich et al., 2004). However, the distribution pattern of histones in the intact sperm nucleus was subsequently transformed after halo formation as shown by a ring-shape structure at the nuclear periphery. This change may result as a consequence of mild chromatin disruption due to the salt extraction of nucleosomes while retaining the integrity of the nuclear matrix (Ward et al., 1999a). This apparent retention of the nuclear matrix in salt-extracted sperm suggests that the matrix is inaccessible to salt extraction. A previous mouse study indicated that a stable nuclear matrix may be necessary for normal fertilisation and embryo development (Ward et al., 1999b). Hence, sperm chromatin structure may not be a random and functionally disorganised, and that abnormal chromatin packaging may be associated with compromised embryo development and even

pregnancy loss (Noblanc et al., 2014). Additionally, histone-bound regions in mature sperm may be cooperatively accessible and transitionally targeted by maternal factors immediately following fertilisation (Miller et al., 2010).

6.2 Halo formation and DNA fragmentation

Having established a relationship between the localisation of sperm nucleosomes and susceptibility to DNA damage/fragmentation, work moved on to look at how this relationship might be connected with halo formation, which is used both directly and indirectly as an indicator of DNA fragmentation. Acridine orange epifluorescence, which was used to monitor DNA fragmentation in response to oxidative exposure, distinguishes between single-stranded (red) and double-stranded (green) DNAs that arise through both single and double-stranded DNA breaks although it cannot measure these breaks directly (McFeters et al., 1991). The comet assay uses a form of diffusion halo where halo DNA, fragmented by oxidative or other damaging agent is drawn towards the anode in an electric field (Fang et al., 2015) and where the level of DNA fragmentation is related to the distance of tail migration and the intensity of tail vs head fluorescence (Cortés-Gutiérrez et al., 2015). In this study, although the same samples were not used for both assays, results from both acridine orange and comet assays for oxidative damage to sperm DNA were generally concordant. These results suggest that the diffusion halo and AO staining of fixed DNA gives complementary results, but neither is particularly amenable to exploring the relationship between sperm DNA fragmentation and the differential packaging of sperm chromatin.

Dispersion halos are more amenable to exploring this relationship because they can be generated while more easily retaining the nucleoprotein context from which they arose (Fernández et al., 2011). The commercially available

Halosperm assay uses a dispersion halo, the area of which is inversely proportional to the extent of DNA fragmentation (Fernández et al., 2005). As a clinically developed product, Halosperm is a useful 'bridge' between basic research questions into sperm differential DNA packaging and clinically significant sperm DNA damage; however, the lysis and extraction buffers used by this assay are relatively harsh, losing most of the nucleoprotein positional information we sought to preserve. By generating dispersion halos using gentler nucleoprotein extraction conditions, however, this positional information is more likely to be retained sufficiently for immunocytochemical and FISH based investigations.

Hence, in addition to Halosperm halos, dispersion halos were generated using two different salt-containing buffers. The weaker of the two (containing 0.65 M NaCl) has long been used in gene expression footprinting analysis and was previously applied to human sperm to look at differential DNA packaging, focusing on the cells' nucleosomal compartment (Gardiner-Garden et al., 1998; Arpanahi et al., 2009; Castillo et al., 2015).

A higher strength buffer (2.0 M NaCl) was also used as it is intermediate between the lower strength and the harsher Halosperm buffer, which includes an acid denaturation step and detergent in the lysis buffer (Fernández et al., 2005).

Taken together, this study has helped to inform consideration of the likely differential susceptibility of the sperm histone compartment to DNA damage in relation to clinical impact as supported by three observations. Firstly, as indicated above and in Chapter 4, dispersion halo size is directly related to the extent of DNA fragmentation. Secondly, the results of western blotting (Chapter 2) showed that only histones were present in the recovered salt extracts obtained during the

sperm processing leading to halo formation with no evidence for the presence of protamines in these extracts. Thirdly, immunocytochemical and DNA fragmentation evidence from human and bovine sperm (Chapter 2 and 3) indicates that DNA damage originates in the histone compartment of the intact sperm nucleus, which is likely to be less compact than the protamine compartment and so less well protected from iatrogenic damage.

In this regard, the evidence from this study suggests that the (low salt) sperm halo is quite likely to be derived from DNA that was mostly based on nucleosomal packaging (Miller, 2015). This conclusion is supported by the likelihood that nucleosomal chromatin is in a more open and more euchromatic configuration than protamine based chromatin and so more accessible to low salt destablisation. The more open the chromatin, the more susceptible it is to DNA damage, particularly if it is localised to the periphery of the nucleus as suggested by FISH analysis (Chapter 2). However, even nucleosomal chromatin located at deeper levels in the nucleus is likely to be more susceptible.

The DNA sequencing data acquired during the course of this study (Chapter 5) provided evidence for a significant enrichment of developmentally important gene sequences in halo-DNA compared with the residual nucleoid DNA. Enrichment was particularly high in low salt halos and less so in high salt and Halosperm generated halos. This makes sense in relation to the known differential packaging of sperm DNA (Arpanahi et al., 2009; Hammoud et al., 2009) and the preferential extraction of nucleosomes by low salt, is enriched with developmental gene sequences that may play an important role in early embryo development. As the level of DNA damage has a direct influence on halo size, it is reasonable to

hypothesise that developmentally significant genes destined for delivery by the sperm to the oocyte may be at higher risk of deleterious iatrogenic damage.

6.3 Dispersion halos provide readouts for prior chromatin packaging

Halo-formation is dependent on the relative extraction efficiencies of the reagents used to generate them. In this study, salt-extraction used two different strengths of NaCl containing buffers, with progressively greater potential to extract DNA binding and other basic proteins by weakening electrostatic interactions that contribute to chromatin formation (Balhorn, 1982). A relatively mild buffer containing 0.65 M NaCl was used to differentially extract histones from sperm nuclei while leaving protamine-based chromatin essentially intact (Gardiner-Garden et al., 1998; Arpanahi et al., 2009). A stronger buffer containing 2.0 M NaCl should be sufficient to extract all proteins from somatic cell and most proteins from sperm nuclei (Guillou et al., 2010).

The commercial Halosperm assay is used to measure DNA fragmentation by halo size and is based on an extraction buffer containing 2 M NaCl and 0.4 M Tris, with 1% SDS that will remove all proteins from sperm nuclei (Fernandez et al., 2003). Sequencing data supported the differential extraction of sperm proteins, because the greatest differences in sequence composition was observed between the halo and nucleoid DNAs generated by low salt compared with the higher salt extraction buffers. In the former, fewer regions of DNA are left exposed to endonuclease digestion and these regions were likely to be nucleosome based. Moreover, because of the differential packaging of sperm chromatin into histone and protamine bound compartments (Miller et al., 2005), accessibility to salt extraction (and endonuclease digestion) is unlikely to be uniform across the genome (Arpanahi et al., 2009) and by the same logic, sperm chromatin

susceptibility to DNA fragmentation is also unlikely to be the same across the genome (Nakato and Shirahige, 2016),

Summarising, using different salt concentrations allowed us to explore the sperm chromatin landscape by accessing the most accessible chromatin through extraction in weaker salt solutions, which destabilises nucleosome but not protamine-bound DNA (Arpanahi et al., 2009; Castillo et al., 2015). Higher salt concentrations will extract more tightly bound proteins and so potentially permit access to deeper or more condensed layers or regions of the sperm nucleus (Kim et al., 1996; Linnemann and Krawetz, 2009). Different sizes of chromatin dispersion halos were observed following treatment of sperm nuclei with different salt concentrations (2.0 M and 0.65 M of NaCl) and Halosperm assay (see Chapter 2, section 2.2.9).

Low salt extraction (0.65 M NaCl) generated small dispersion halos compared with sperm extracted with higher salt buffers. The DNA sequencing data (see Chapter 5, section 5.4) and the data from previous studies suggests that the DNA released from low salt halos is enriched in protein-coding and gene-rich DNA sequences compared with the corresponding nucleoid or insoluble chromatin (Miller, 2015).

These results support the conclusion that low salt extracts the most accessible and/or most loosely or relatively weakly compacted regions that are probably nucleosomal in origin and may be located in close proximity to the nuclear periphery. Whereas higher salt concentrations extract sufficient levels of proteins to permit endonuclease access to a more extensive range of DNA sequences packaged in regions enriched in more compact, heterochromatic nucleoprotamine rich regions. In terms of differential DNA content, low and high

salt concentrations would be expected to access different genic sequences (Henikoff et al., 2009), and as the salt concentration rises, the wide differences observed between halo and nucleoid content is narrowed. It follows that sequencing the DNA in these differentially salt accessible chromatin compartments may help to identify those sequences that are most susceptible to DNA damage. Integrating these data should permit a clearer understanding of the relationship between DNA fragmentation, halo formation and the DNA sequences subject to damage.

6.4 Next-Generation Sequencing data analysis of the halo-enriched regions in relation to retained histones compartment

Salt extraction of sperm nuclei has been successfully used to separate histone- from protamine-bound chromatin in the sperm nucleus (Wykes and Krawetz, 2003; Kramer and Krawetz, 1996; Gardiner-Garden et al., 1998; Arpanahi et al., 2009). In this study, results of western blotting suggested that only histones were present in salt extracts and although histones were also detected in nucleoid fractions. Although unidentified higher molecular mass signals in both halo and nucleoid fractions were detected, which may be due to cross-reactivity between anti-PRM1 and histones, PRM1 was not detected in these extracts. Protamines may not have been detectable in the higher salt extracts because despite being destabilised and so permitting wider access to the endonucleases used to digest out the now more accessible DNA, protamines were still sufficiently associated with the nuclear matrix to resist separation from the bulk sperm chromatin and so remained in the nucleoid. Detecting histones in the salt soluble fractions of human sperm corresponds with previous studies showing that modified histones such as H2A.Z and H3.3 are enriched in these fractions (Chen et al., 2013; Weber et al.,

2010). These and related studies suggest that nucleosome-enriched sequences correspond with low salt halo-DNA that was originally associated with the histone compartment of sperm chromatin and may reflect a chromatin that is poised for transcription or some other interaction with maternal factors after fertilisation (Arpanahi et al., 2009; Castillo et al., 2014b).

In this regard, NGS data analysis showed that halo DNA contained many developmental gene sequences and their promoter sequences alongside transcription factor sequences. GAT analysis, for example, revealed that particularly important regions such as CpGs, 5'-UTR, exons and promoter regions were more enriched in halo fraction of human and bovine sperm, whereas, intronic and intragenic regions were correspondingly depleted. Sequences representing the *HOX* gene clusters as well as many transcription factors and zinc fingers were found to be among those enriched in halo fractions of human sperm (Hammoud et al., 2009; Castillo et al., 2014a).

Comparing the study's NGS data with available online data (Samans et al., 2014), which has been re-analysed with regard to nucleosome enrichment in human and bovine sperm, added support to the suggestion that halo-DNA arises from a chromatin compartment that was most likely packaged by nucleosomes (Arpanahi et al., 2009; Erkek et al., 2013). The analysis of the enrichment of the nucleosome retention at the highly-enriched embryo developmental regions in the halo fraction, alongside the presence of histones in both halo and nucleoid fractions, indicate that even residual histones were differentially accessible to salt extraction (dependent on salt strength). There is a possibility that histone-bound DNA enriched in the nucleoid fraction may be associated with the nuclear matrix (Noblanc et al., 2014), as the association or connecting points between halo DNA

and the nuclear matrix are conserved (Ward et al., 1989). Thus, these findings suggest that halo DNA reflects a compartment that may be important for early developmental processes after fertilisation.

6.5 The concept of the nuclear matrix in relation to the current study's findings

Although several studies have suggested a fundamental role of the nuclear matrix in DNA replication and gene expression (Hancock, 2000; Albrethsen et al., 2009), the concept of the nuclear matrix itself is still controversial. Other studies have focused on different aspects of the nuclear matrix, such as protein composition (Mika and Rost, 2005), visualising the nuclear matrix (Barboro et al., 2003) and characterising the DNA attached to the nuclear scaffold (Boulikas, 1993). These reports and other studies suggest that the three-dimensional architecture of the nucleus should be explored in order to provide further evidence for the concept of the nuclear matrix and its association with chromatin (Razin et al., 2014b). DNA that is closely associated with the nuclear matrix is inaccessible to even high-salt extraction (Cook et al., 1976; Linnemann and Krawetz, 2009; Wilson and Coverley, 2013). Dispersion halo formation is very likely to be dependent on the nuclear matrix because a matrix attachment site or region is required to secure the bases of the loops in situ. Without an intact matrix, or under conditions where the DNA is fragmented and the packaging compression forces are reduced or lost, the chromatin will be unable to disperse out from the nucleus and so be unable to form a dispersion halo. Indeed, failure to form a halo as a measure of DNA fragmentation requires an intact scaffold (Tandara et al., 2014).

6.6 Conclusion

In this study, salt extraction methods allowed us to partition sperm chromatin into two DNA fractions; salt-soluble (halo) and salt-insoluble (nucleoid). Both compartments were investigated by several complementary techniques, including high-throughput DNA sequencing. Interestingly, FISH used the extracted and labelled nucleoid DNA on sperm nuclei labelled DNA in a ring-like structure at the periphery of the nucleus but within the nuclear boundary (unlike the halo-FISH, which labelled DNA extending beyond the boundary). In addition, western blot analysis showed that histones were present in both the halo and nucleoid fractions; however, PRM was detected only in the nucleoid fraction. Blotting suggested that halo DNA was associated mainly or exclusively with nucleosomes, while a proportion of nucleoid DNA retain nucleosomes, probably to link adjacent protamine toroids and attach them to the nuclear matrix (Brewer et al., 1999). Also, while it was present in the nucleoid fraction, the absence of PRM in the halo fraction suggests that the sperm nuclear matrix is associated with salt-inaccessible chromatin that is strongly attached to protamines, and that the histones contained within it are equally inaccessible (Miller et al., 2010).

Experiments on induced DNA damage using external oxidative agents, and the location of retained histones in the nucleus of mature human and bovine spermatozoa, support the suggestion that there is a link between the localisation of nuclear histones and the positioning of the first signs of DNA damage, as determined by acridine orange staining and the immunocytochemical detection of sperm histones in the mature sperm nucleus. The analysis by halo-FISH, and the histone compartment in halo nuclei, support the connection between the sperm nuclear matrix and its association with retained histones. In addition, the

enrichment of halo DNA with sequences for important developmental genes, promotors and transcription factors suggest that the genes concerned might play a role in early embryo development and could be transcriptionally activated post-fertilisation.

6.7 Future work

Although the current study aimed to investigate sperm chromatin architecture of human and bovine sperm in relation to DNA damage and differential histone/protamine-based DNA packaging, there are many further investigations that could be carried out to support the results of the current findings:

- NGS data analysis displayed massive DNA sequence information for human and bovine sperm, which can be further analysed using different analysis tools and platforms in order to target genomic sequences that essential for fertilisation as well as investigate their susceptibility to damage by a low level of sperm DNA fragmentation.

- NGS results showed that the enriched regions in halo fraction may play an important role in early developmental processes after fertilisation, therefore, performing a deep RNA sequencing (RNA-Seq) of extracted RNAs from zygotes may identify genes that actively expressed following fertilisation, which consequently would confirm the outcomes of the current study.

- Significant susceptibility to DNA damage by an external oxidative agent is positively correlated with increased exposure to the agent. Sequencing of the fragmented DNA would confirm its linkage with the composition of the halo DNA.

- NGS results showed that the number of reads for enriched regions in either halo or nucleoid fractions differed among all extraction experiments. The GAT results showed that specific genomic regions such as 5'-UTR, CpGs and promotors were

significantly enriched in halos compared to nucleoid fraction but that the level of enrichment was reduced as higher salt concentrations were used. NGS could, therefore, be used to better determine the location of such regions using HI-C (mathematical modelling) (Van Berkum et al., 2010). The aims would be the development of a three-dimensional structure of the different chromatin compartments in sperm nuclei that could transform our understanding of male infertility, which consequently increase the future commercial or clinical value for such application.

- Finally, the NGS findings support the conclusion that chromatin is not randomly distributed in the sperm nucleus. Although there are major differences between somatic cells and sperm in terms of chromosome organisation due to the absence of a DNA-protamine complex, sequencing halo and nucleoid fractions of somatic cells could help consolidate the existing evidence for the nuclear matrix and the importance of its organisation framework in all cell types.

References

Adenot, P.G., Mercier, Y., Renard, J.-P. and Thompson, E.M. 1997. Differential H4 acetylation of paternal and maternal chromatin precedes DNA replication and differential transcriptional activity in pronuclei of 1-cell mouse embryos. *Development.* **124**(22), pp.4615-4625.

Agarwal, A. and Allamaneni, S. 2004. The effect of sperm DNA damage on assisted reproduction outcomes. *Minerva Ginecol.* **56**(3), pp.235-245.

Agarwal, A. and Said, T. 2004. *Sperm chromatin assessment.* [Online].

Agarwal, A. and Said, T.M. 2003. Role of sperm chromatin abnormalities and DNA damage in male infertility. *Hum Reprod Update.* **9**(4), pp.331-345.

Agarwal, A. and Said, T.M. 2005. Oxidative stress, DNA damage and apoptosis in male infertility: a clinical approach. *BJU International.* **95**(4), pp.503-507.

Agarwal, A., Saleh, R.A. and Bedaiwy, M.A. 2003. Role of reactive oxygen species in the pathophysiology of human reproduction. *Fertility and Sterility.* **79**(4), pp.829-843.

Agarwal, A., Virk, G., Ong, C. and du Plessis, S.S. 2014. Effect of oxidative stress on male reproduction. *The World Journal of Men's Health.* **32**(1), pp.1-17.

Ahmadi, A. and Ng, S.-C. 1999. Developmental capacity of damaged spermatozoa. *Human Reproduction.* **14**(9), pp.2279-2285.

Aitken, R., Bronson, R., Smith, T. and De Iuliis, G. 2013. The source and significance of DNA damage in human spermatozoa; a commentary on diagnostic strategies and straw man fallacies. *Molecular Human Reproduction.* pgat025.

Aitken, R.J. and De Iuliis, G.N. 2007. Origins and consequences of DNA damage in male germ cells. *Reproductive Biomedicine Online.* **14**(6), pp.727-733.

Albrethsen, J., Knol, J.C. and Jimenez, C.R. 2009. Unravelling the nuclear matrix proteome. *Journal of Proteomics.* **72**(1), pp.71-81.

Andersen, A.N., Goossens, V., Ferraretti, A., Bhattacharya, S., Felberbaum, R., De Mouzon, J. and Nygren, K. 2008. Assisted reproductive technology in Europe, 2004: results generated from European registers by ESHRE. *Human Reproduction.* **23**(4), pp.756-771.

Andrabi, S. 2007. Mammalian sperm chromatin structure and assessment of DNA fragmentation. *Journal of Assisted Reproduction and Genetics.* **24**(12), pp.561-569.

Anifandis, G., Bounartzi, T., Messini, C., Dafopoulos, K., Markandona, R., Sotiriou, S., Tzavella, A. and Messinis, I. 2015. Sperm DNA fragmentation measured by Halosperm does not impact on embryo quality and ongoing pregnancy rates in IVF/ICSI treatments. *Andrologia.* **47**(3), pp.295-302.

Aoki, F., Worrad, D.M. and Schultz, R.M. 1997. Regulation of transcriptional activity during the first and second cell cycles in the preimplantation mouse embryo. *Developmental Biology.* **181**(2), pp.296-307.

Aoki, V.W., Moskovtsev, S.I., Willis, J., Liu, L., Mullen, J.B.M. and Carrell, D.T. 2005. DNA Integrity Is Compromised in Protamine-Deficient Human Sperm. *Journal of Andrology.* **26**(6), pp.741-748.

Aranda-Anzaldo, A., Dent, M.A. and Martínez-Gómez, A. 2014. The higher-order structure in the cells nucleus as the structural basis of the post-mitotic state. *Progress in Biophysics and Molecular Biology.* **114**(3), pp.137-145.

Arpanahi, Brinkworth, M., Iles, D., Krawetz, S.A., Paradowska, A., Platts, A.E., Saida, M., Steger, K., Tedder, P. and Miller, D. 2009. Endonuclease-sensitive regions of human spermatozoal chromatin are highly enriched in promoter and CTCF binding sequences. *Genome Res.* **19**(8), pp.1338-1349.

Auger, J., Mesbah, M., Huber, C. and Dadoune, J. 1990. Aniline blue staining as a marker of sperm chromatin defects associated with different semen characteristics discriminates between proven fertile and suspected infertile men. *International Journal of Andrology.* **13**(6), pp.452-462.

Avendaño, C., Franchi, A., Duran, H. and Oehninger, S. 2010. DNA fragmentation of normal spermatozoa negatively impacts embryo quality and intracytoplasmic sperm injection outcome. *Fertility and Sterility.* **94**(2), pp.549-557.

Ayala, A., Muñoz, M.F. and Argüelles, S. 2014. Lipid peroxidation: production, metabolism, and signaling mechanisms of malondialdehyde and 4-hydroxy-2-nonenal. *Oxidative Medicine and Cellular Longevity.* **2014**.

Balhorn, R. 1982. A model for the structure of chromatin in mammalian sperm. *The Journal of Cell Biology.* **93**(2), pp.298-305.

Balhorn, R. 2007. The protamine family of sperm nuclear proteins. *Genome Biol.* **8**(9), p227.

Balhorn, R., Gledhill, B. and Wyrobek, A. 1977. Mouse sperm chromatin proteins: quantitative isolation and partial characterization. *Biochemistry.* **16**(18), pp.4074-4080.

Balhorn, R., Reed, S. and Tanphaichitr, N. 1988. Aberrant protamine 1/protamine 2 ratios in sperm of infertile human males. *Experientia.* **44**(1), pp.52-55.

Barboro, P., D'Arrigo, C., Mormino, M., Coradeghini, R., Parodi, S., Patrone, E. and Balbi, C. 2003. An intranuclear frame for chromatin compartmentalization and higher-order folding. *Journal of Cellular Biochemistry.* **88**(1), pp.113-120.

Barone, J.G., De Lara, J., Cummings, K.B. and Ward, W.S. 1994. DNA organization in human spermatozoa. *Journal of Andrology.* **15**, pp.139-139.

Barratt, C.L., Aitken, R.J., Björndahl, L., Carrell, D.T., de Boer, P., Kvist, U., Lewis, S.E., Perreault, S.D., Perry, M.J. and Ramos, L. 2010. Sperm DNA: organization, protection and vulnerability: from basic science to clinical applications—a position report. *Human Reproduction.* **25**(4), pp.824-838.

Barroso, G., Valdespin, C., Vega, E., Kershenovich, R., Avila, R., Avendano, C., & Oehninger, S. JAGER and WIJCHMAN, J. 2009. Developmental sperm contributions: fertilization and beyond. *Fertil Steril.* **92**(3), pp. 835-848.

Bashiri, A., Harlev, A. and Agarwal, A. 2016. *Recurrent Pregnancy Loss: Evidence-Based Evaluation, Diagnosis and Treatment.* Springer.

Benson, L.J., Gu, Y., Yakovleva, T., Tong, K., Barrows, C., Strack, C.L., Cook, R.G., Mizzen, C.A. and Annunziato, A.T. 2006. Modifications of H3 and H4 during chromatin replication, nucleosome assembly, and histone exchange. *J Biol Chem.* **281**(14), pp.9287-9296.

Berezney, R. and Coffey, D.S. 1974. Identification of a nuclear protein matrix. *Biochemical and Bbiophysical Rresearch Communications.* **60**(4), pp.1410-1417.

Bernardi, G. 2015. Chromosome architecture and genome organization. *PloS one.* **10**(11), pe0143739.

Biegeleisen, K. 2006. The probable structure of the protamine-DNA complex. *J Theor Biol.* **241**(3), pp.533-540.

Boerke, A., Dieleman, S.J. and Gadella, B.M. 2007. A possible role for sperm RNA in early embryo development. *Theriogenology.* **68 Suppl 1**, pp.S147-155.

Bönisch, C. and Hake, S.B. 2012. Histone H2A variants in nucleosomes and chromatin: more or less stable? *Nucleic Acids Research.* **40**(21), pp.10719-10741.

Borini, A., Tarozzi, N., Bizzaro, D., Bonu, M.A., Fava, L., Flamigni, C. and Coticchio, G. 2006. Sperm DNA fragmentation: paternal effect on early post-implantation embryo development in ART. *Hum Reprod.* **21**(11), pp.2876-2881.

Boulikas, T. 1993. Nature of DNA sequences at the attachment regions of genes to the nuclear matrix. *Journal of Cellular Biochemistry.* **52**(1), pp.14-22.

Braun, R.E. 2001. Packaging paternal chromosomes with protamine. *Nat Genet.* **28**(1), pp.10-12.

Brewer, L.R., Corzett, M. and Balhorn, R. 1999. Protamine-induced condensation and decondensation of the same DNA molecule. *Science.* **286**(5437), pp.120-123.

Brunelle, J.L. and Green, R. 2014. Coomassie blue staining. *Methods in Enzymology.* **541**, p161.

Brykczynska, U., Hisano, M., Erkek, S., Ramos, L., Oakeley, E.J., Roloff, T.C., Beisel, C., Schübeler, D., Stadler, M.B. and Peters, A.H. 2010. Repressive and active histone methylation mark distinct promoters in human and mouse spermatozoa. *Nature Structural & Molecular Biology.* **17**(6), pp.679-687.

Carrell, D.T., Emery, B.R. and Hammoud, S. 2007. Altered protamine expression and diminished spermatogenesis: what is the link? *Human Reproduction Update.* **13**(3), pp.313-327.

Carrell, D.T. and Hammoud, S.S. 2010. The human sperm epigenome and its potential role in embryonic development. *Molecular Human Reproduction.* **16**(1), pp.37-47.

Carrell, D.T., Liu, L., Peterson, C. M., Jones, K. P., Hatasaka, H. H., Erickson, L. & Campbell, B. 2003. Sperm DNA fragmentation is increased in couples with unexplained recurrent pregnancy loss. *Archives of Andrology* **49**(1), pp.49–55.

Castellani, R.J., Nunomura, A., Rolston, R.K., Moreira, P.I., Takeda, A., Perry, G. and Smith, M.A. 2008. Sublethal RNA oxidation as a mechanism for neurodegenerative disease. *International Journal of Molecular Sciences.* **9**(5), pp.789-806.

Castillo, J., Amaral, A., Azpiazu, R., Vavouri, T., Estanyol, J.M., Ballescà, J.L. and Oliva, R. 2014a. Genomic and proteomic dissection and characterization of the human sperm chromatin. *Molecular Human Reproduction.* **20**(11), pp.1041-1053.

Castillo, J., Amaral, A. and Oliva, R. 2014b. Sperm nuclear proteome and its epigenetic potential. *Andrology.* **2**(3), pp.326-338.

Castillo, J., Estanyol, J.M., Ballescà, J.L. and Oliva, R. 2015. Human sperm chromatin epigenetic potential: genomics, proteomics, and male infertility. *Asian Journal of Andrology.* **17**(4), p601.

Castillo, J., Simon, L., Mateo, S., Lewis, S. and Oliva, R. 2011. Protamine/DNA ratios and DNA damage in native and density gradient centrifuged sperm from infertile patients. *Journal of Andrology.* **32**(3), pp.324-332.

Chauviere, M., Martinage, A., Debarle, M., Sautiere, P. and Chevaillier, P. 1992. Molecular characterization of six intermediate proteins in the processing of mouse protamine P2 precursor. *European Journal of Biochemistry.* **204**(2), pp.759-765.

Chen, P., Zhao, J., Wang, Y., Wang, M., Long, H., Liang, D., Huang, L., Wen, Z., Li, W. and Li, X. 2013. H3. 3 actively marks enhancers and primes gene transcription via opening higher-ordered chromatin. *Genes & Development.* **27**(19), pp.2109-2124.

Cho, C., Jung-Ha, H., Willis, W.D., Goulding, E.H., Stein, P., Xu, Z., Schultz, R.M., Hecht, N.B. and Eddy, E.M. 2003. Protamine 2 deficiency leads to sperm DNA damage and embryo death in mice. *Biology of Reproduction.* **69**(1), pp.211-217.

Cho, C., Willis, W.D., Goulding, E.H., Jung-Ha, H., Choi, Y.C., Hecht, N.B. and Eddy, E.M. 2001. Haploinsufficiency of protamine-1 or -2 causes infertility in mice. *Nat Genet.* **28**(1), pp.82-86.

Chohan, K., Griffin, J. and Carrell, D.T. 2004. Evaluation of chromatin integrity in human sperm using acridine orange staining with different fixatives and after cryopreservation. *Andrologia.* **36**(5), pp.321-326.

Chohan, K.R., Griffin, J.T., Lafromboise, M., De Jonge, C.J. and Carrell, D.T. 2006. Comparison of chromatin assays for DNA fragmentation evaluation in human sperm. *J Androl.* **27**(1), pp.53-59.

Ciejek, E.M., Tsai, M.-J. and O'Malley, B.W. 1983. Actively transcribed genes are associated with the nuclear matrix.

Cissen, M., van Wely, M., Scholten, I., Mansell, S., de Bruin, J.P., Mol, B.W., Braat, D., Repping, S. and Hamer, G. 2016. Measuring Sperm DNA Fragmentation and Clinical Outcomes of Medically Assisted Reproduction: A Systematic Review and Meta-Analysis. *PloS one.* **11**(11), pe0165125.

Clermont, Y. 1972. Kinetics of spermatogenesis in mammals: seminiferous epithelium cycle and spermatogonial renewal. *Physiol Rev.* **52**(1), pp.198-236.

Chohan, K.R., Griffin, J.T., Lafromboise, M., De Jonge, C.J. and Carrell, D.T. 2006. Comparison of chromatin assays for DNA fragmentation evaluation in human sperm. *J Androl.* **27**(1), pp.53-59.

Colleu, D., Lescoat, D. and Gouranton, J. 1996. Nuclear maturity of human spermatozoa selected by swim-up or by Percoll gradient centrifugation procedures. *Fertility and Sterility.* **65**(1), pp.160-164.

Collins, A.R., Oscoz, A.A., Brunborg, G., Gaivao, I., Giovannelli, L., Kruszewski, M., Smith, C.C. and Stetina, R. 2008. The comet assay: topical issues. *Mutagenesis.* **23**(3), pp.143-151.

Cook, P., Brazell, I. and Jost, E. 1976. Characterization of nuclear structures containing superhelical DNA. *Journal of Cell Science.* **22**(2), pp.303-324.

Cook, P.R. and Brazell, I. 1980. Mapping sequences in loops of nuclear DNA by their progressive detachment from the nuclear cage. *Nucleic Acids Research.* **8**(13), pp.2895-2906.

Cooper, T.G., Noonan, E., Von Eckardstein, S., Auger, J., Baker, H.G., Behre, H.M., Haugen, T.B., Kruger, T., Wang, C. and Mbizvo, M.T. 2010. World Health Organization reference values for human semen characteristics. *Human Reproduction Update.* **16**(3), pp.231-245.

Cortés-Gutiérrez, E.I., Dávila-Rodríguez, M.I., Fernández, J.L., López-Fernández, C., Aragón-Tovar, A.R., Urbina-Bernal, L.C. and Gosálvez, J. 2016. DNA damage in spermatozoa from infertile men with varicocele evaluated by sperm chromatin dispersion and DBD-FISH. *Archives of Gynecology and Obstetrics.* **293**(1), pp.189-196.

Cortés-Gutiérrez, E.I., López-Fernández, C., Fernández, J.L., Dávila-Rodríguez, M.I., Johnston, S.D. and Gosálvez, J. 2015. Interpreting

sperm DNA damage in a diverse range of mammalian sperm by means of the two-tailed comet assay. *30 years of the Comet Assay: an overview with some new insights.* p123.

Costantini, M., Clay, O., Auletta, F. and Bernardi, G. 2006. An isochore map of human chromosomes. *Genome Research.* **16**(4), pp.536-541.

Coughlan, C., Clarke, H., Cutting, R., Saxton, J., Waite, S., Ledger, W., Li, T. and Pacey, A.A. 2015. Sperm DNA fragmentation, recurrent implantation failure and recurrent miscarriage. *Asian Journal of Andrology.* **17**(4), p681.

Cozzi, P., Milanesi, L. and Bernardi, G. 2015. Segmenting the human genome into isochores. *Evolutionary Bioinformatics Online.* **11**, p253.

Dadoune, J.-P. 1995. The nuclear status of human sperm cells. *Micron.* **26**(4), pp.323-345.

Dadoune, J., Mayaux, M. and Guihard-Moscato, M. 1988. Correlation between defects in chromatin condensation of human spermatozoa stained by aniline blue and semen characteristics. *Andrologia.* **20**(3), pp.211-217.

Dadoune, J.P., Siffroi, J.P. and Alfonsi, M.F. 2004. Transcription in haploid male germ cells. *Int Rev Cytol.* **237**, pp.1-56.

De Iuliis, G.N., Thomson, L.K., Mitchell, L.A., Finnie, J.M., Koppers, A.J., Hedges, A., Nixon, B. and Aitken, R.J. 2009. DNA Damage in Human Spermatozoa Is Highly Correlated with the Efficiency of Chromatin Remodeling and the Formation of 8-Hydroxy-2′-Deoxyguanosine, a Marker of Oxidative Stress 1. *Biology of Reproduction.* **81**(3), pp.517-524.

De Kretser, D., Loveland, K., Meinhardt, A., Simorangkir, D. and Wreford, N. 1998. Spermatogenesis. *Human Reproduction.* **13**(suppl 1), pp.1-8.

Del Mazo, J. 2013. *Reproductive toxicology: in vitro germ cell developmental toxicology, from science to social and industrial demand.* Springer Science & Business Media.

Delgado, N.M., Reyes, R., Huacuja, L., Merchant, H. and Rosado, A. 1982. Heparin binding sites in the human spermatozoa membrane. *Arch Androl.* **8**(2), pp.87-95.

Deloukas, P., Matthews, L., Ashurst, J., Burton, J., Gilbert, J., Jones, M., Stavrides, G., Almeida, J., Babbage, A. and Bagguley, C. 2001. The DNA sequence and comparative analysis of human chromosome 20. *Nature.* **414**(6866), pp.865-871.

Denny Sakkas, E.M., Giancarlo Manicardi, Davide Bizzaro, Patrizia G. Bianchi and Umberto Bianchi. 1999. Origin of DNA damage in ejaculated human spermatozoa. *Reproduction* **4**, pp.31–37.

Dogan, S., Vargovic, P., Oliveira, R., Belser, L.E., Kaya, A., Moura, A., Sutovsky, P., Parrish, J., Topper, E. and Memili, E. 2015. Sperm protamine-status correlates to the fertility of breeding bulls. *Biology of Reproduction.* pbiolreprod. 114.124255.

Donnelly, E.T., McClure, N. and Lewis, S.E. 1999. The effect of ascorbate and α-tocopherol supplementation in vitro on DNA integrity and hydrogen peroxide-induced DNA damage in human spermatozoa. *Mutagenesis.* **14**(5), pp.505-512.

Douglas K. Palmer, K.O.D., Robert L. Margolis 1990. The centromere specific histone CENP-A is selectively retained in discrete foci in mammalian sperm nuclei. *Chromosoma.* **100** (1), pp.32-36.

Dunham, I., Hunt, A., Collins, J., Bruskiewich, R., Beare, D., Clamp, M., Smink, L., Ainscough, R., Almeida, J. and Babbage, A. 1999. The DNA sequence of human chromosome 22. *Nature.* **402**(6761), pp.489-495.

Dym, M. 1994. Spermatogonial stem cells of the testis. *Proceedings of the National Academy of Sciences of the United States of America.* **91**(24), p11287.

Enciso, M., Lopez-Fernandez, C., Fernandez, J.L., Garcia, P., Gosalbez, A. and Gosalvez, J. 2006a. A new method to analyze boar sperm DNA fragmentation under bright-field or fluorescence microscopy. *Theriogenology.* **65**(2), pp.308-316.

Enciso, M., Muriel, L., Fernández, J.L., Goyanes, V., Segrelles, E., Marcos, M., Montejo, J.M., Ardoy, M., Pacheco, A. and Gosálvez, J. 2006b. Infertile men with varicocele show a high relative proportion of sperm cells with intense nuclear damage level, evidenced by the sperm chromatin dispersion test. *Journal of Andrology.* **27**(1), pp.106-111.

Erenpreiss, J., Bars, J., Lipatnikova, V., Erenpreisa, J. and Zalkalns, J. 2001. Comparative study of cytochemical tests for sperm chromatin integrity. *Journal of Andrology.* **22**(1), pp.45-53.

Erkek, S., Hisano, M., Liang, C.-Y., Gill, M., Murr, R., Dieker, J., Schübeler, D., van der Vlag, J., Stadler, M.B. and Peters, A.H. 2013. Molecular determinants of nucleosome retention at CpG-rich sequences in mouse spermatozoa. *Nature Structural & Molecular Biology.* **20**(7), pp.868-875.

Evenson, D., Darzynkiewicz, Z., Jost, L., Janca, F. and Ballachey, B. 1986. Changes in accessibility of DNA to various fluorochromes during spermatogenesis. *Cytometry.* **7**(1), pp.45-53.

Evenson, D., Darzynkiewicz, Z. and Melamed, M. 1980. Relation of mammalian sperm chromatin heterogeneity to fertility. *Science.* **210**(4474), pp.1131-1133.

Evenson, D.P., Larson, K.L. and Jost, L.K. 2002. Sperm chromatin structure assay: its clinical use for detecting sperm DNA fragmentation in male infertility and comparisons with other techniques. *J Androl.* **23**(1), pp.25-43.

Evenson, D.P. and Wixon, R. 2006. Clinical aspects of sperm DNA fragmentation detection and male infertility. *Theriogenology.* **65**(5), pp.979-991.

Fang, L., Neutzner, A., Turtschi, S., Flammer, J. and Mozaffarieh, M. 2015. Comet Assay as an Indirect Measure of Systemic Oxidative Stress. *Journal of Visualized Experiments: JoVE.* (99).

Feng, J., Liu, T. and Zhang, Y. 2011. Using MACS to identify peaks from ChIP-Seq data. *Current Protocols in Bioinformatics.* pp.2.14. 11-12.14. 14.

Fernández, J.L., Cajigal, D., López-Fernández, C. and Gosálvez, J. 2011. Assessing sperm DNA fragmentation with the sperm chromatin dispersion test. *DNA Damage Detection In Situ, Ex Vivo, and In Vivo: Methods and Protocols.* pp.291-301.

Fernandez, J.L., Muriel, L., Goyanes, V., Segrelles, E., Gosalvez, J., Enciso, M., LaFromboise, M. and De Jonge, C. 2005a. Simple determination of human sperm DNA fragmentation with an improved sperm chromatin dispersion test. *Fertil Steril.* **84**(4), pp.833-842.

Fernández, J.L., Muriel, L., Goyanes, V., Segrelles, E., Gosálvez, J., Enciso, M., LaFromboise, M. and De Jonge, C. 2005b. Halosperm® is an easy, available, and cost-effective alternative for determining sperm DNA fragmentation. *Fertility and Sterility.* **84**(4), p860.

Fernandez, J.L., Muriel, L., Rivero, M.T., Goyanes, V., Vazquez, R. and Alvarez, J.G. 2003. The sperm chromatin dispersion test: a simple method for the determination of sperm DNA fragmentation. *Journal of Andrology.* **24**(1), pp.59-66.

Filomeni, G., De Zio, D. and Cecconi, F. 2015. Oxidative stress and autophagy: the clash between damage and metabolic needs. *Cell Death & Differentiation.* **22**(3), pp.377-388.

Foster, H.A., Abeydeera, L.R., Griffin, D.K. and Bridger, J.M. 2005. Non-random chromosome positioning in mammalian sperm nuclei, with migration of the sex chromosomes during late spermatogenesis. *Journal of Cell Science.* **118**(9), pp.1811-1820.

Fraga, C., Motchnik, P., Wyrobek, A., Rempel, D. and Ames, B. 1996. Smoking and low antioxidant levels increase oxidative damage to sperm DNA. *Mutation Research/Fundamental and Molecular Mechanisms of Mutagenesis.* **351**(2), pp.199-203.

Francis, S., Yelumalai, S., Jones, C. and Coward, K. 2014. Aberrant protamine content in sperm and consequential implications for infertility treatment. *Human Fertility.* **17**(2), pp.80-89.

Fujita, P.A., Rhead, B., Zweig, A.S., Hinrichs, A.S., Karolchik, D., Cline, M.S., Goldman, M., Barber, G.P., Clawson, H. and Coelho, A. 2010. The UCSC genome browser database: update 2011. *Nucleic Acids Research.* pgkq963.

Füllgrabe, J., Kavanagh, E. and Joseph, B. 2011. Histone onco-modifications. *Oncogene.* **30**(31), pp.3391-3403.

Galaz-Leiva, S., Perez-Rodriguez, G., Blazquez-Castro, A. and Stockert, J. 2012a. A simplified chromatin dispersion (nuclear halo) assay for

detecting DNA breakage induced by ionizing radiation and chemical agents. *Biotechnic & Histochemistry.* **87**(3), pp.208-217.

Galaz-Leiva, S., Perez-Rodriguez, G., Blazquez-Castro, A. and Stockert, J.C. 2012b. A simplified chromatin dispersion (nuclear halo) assay for detecting DNA breakage induced by ionizing radiation and chemical agents. *Biotech Histochem.* **87**(3), pp.208-217.

Gardiner-Garden, M., Ballesteros, M., Gordon, M. and Tam, P.P. 1998. Histone- and protamine-DNA association: conservation of different patterns within the β-globin domain in human sperm. *Molecular and Cellular Biology.* **18**(6), pp.3350-3356.

Gatewood, J., Cook, G., Balhorn, R., Bradbury, E. and Schmid, C. 1987. Sequence-specific packaging of DNA in human sperm chromatin. *Science.* **236**(4804), pp.962-964.

Gaucher, J., Reynoird, N., Montellier, E., Boussouar, F., Rousseaux, S. and Khochbin, S. 2010. From meiosis to postmeiotic events: the secrets of histone disappearance. *FEBS J.* **277**(3), pp.599-604.

Gilbert, N., Gilchrist, S. and Bickmore, W.A. 2004. Chromatin organization in the mammalian nucleus. *International Review of Cytology.* **242**, pp.283-336.

Gilbert, S.F. 2000. Spermatogenesis.

Golan, R., Shochat, L., Weissenberg, R., Soffer, Y., Marcus, Z., Oschry, Y. and Lewin, L.M. 1997. Evaluation of chromatin condensation in human spermatozoa: a flow cytometric assay using acridine orange staining. *Mol Hum Reprod.* **3**(1), pp.47-54.

Gosálvez, J., Cortés-Gutiérrez, E.I., Nuñez, R., Fernández, J.L., Caballero, P., López-Fernández, C. and Holt, W.V. 2009. A dynamic assessment of sperm DNA fragmentation versus sperm viability in proven fertile human donors. *Fertility and Sterility.* **92**(6), pp.1915-1919.

Govin, J., Caron, C., Lestrat, C., Rousseaux, S. and Khochbin, S. 2004. The role of histones in chromatin remodelling during mammalian spermiogenesis. *European Journal of Biochemistry.* **271**(17), pp.3459-3469.

Govin, J., Dorsey, J., Gaucher, J., Rousseaux, S., Khochbin, S. and Berger, S.L. 2010. Systematic screen reveals new functional dynamics of histones H3 and H4 during gametogenesis. *Genes Dev.* **24**(16), pp.1772-1786.

Govin, J., Escoffier, E., Rousseaux, S., Kuhn, L., Ferro, M., Thévenon, J., Catena, R., Davidson, I., Garin, J. and Khochbin, S. 2007. Pericentric heterochromatin reprogramming by new histone variants during mouse spermiogenesis. *The Journal of Cell Biology.* **176**(3), pp.283-294.

Grimes, S.R., Jr. and Henderson, N. 1983. Acetylation of histones during spermatogenesis in the rat. *Arch Biochem Biophys.* **221**(1), pp.108-116.

Grimwood, J., Gordon, L.A., Olsen, A., Terry, A., Schmutz, J., Lamerdin, J., Hellsten, U., Goodstein, D., Couronne, O. and Tran-Gyamfi, M. 2004.

The DNA sequence and biology of human chromosome 19. *Nature.* **428**(6982), pp.529-535.

Griswold, M.D. 1998. The central role of Sertoli cells in spermatogenesis.

Grudzinskas, J.G. and Yovich, J.L. 1995. *Gametes-the spermatozoon.* Cambridge University Press.

Guillou, E., Ibarra, A., Coulon, V., Casado-Vela, J., Rico, D., Casal, I., Schwob, E., Losada, A. and Méndez, J. 2010. Cohesin organizes chromatin loops at DNA replication factories. *Genes & Development.* **24**(24), pp.2812-2822.

Guraya, S.S. 2012. *Biology of spermatogenesis and spermatozoa in mammals.* Springer Science & Business Media.

Gusse, M., Sautiere, P., Belaiche, D., Martinage, A., Roux, C., Dadoune, J.P. and Chevaillier, P. 1986. Purification and characterization of nuclear basic proteins of human sperm. *Biochim Biophys Acta.* **884**(1), pp.124-134.

Guz, J., Gackowski, D., Foksinski, M., Rozalski, R., Zarakowska, E., Siomek, A., Szpila, A., Kotzbach, M., Kotzbach, R. and Olinski, R. 2013. Comparison of oxidative stress/DNA damage in semen and blood of fertile and infertile men. *PLoS One.* **8**(7), pe68490.

Hammoud, S.S., Nix, D.A., Hammoud, A.O., Gibson, M., Cairns, B.R. and Carrell, D.T. 2011. Genome-wide analysis identifies changes in histone retention and epigenetic modifications at developmental and imprinted gene loci in the sperm of infertile men. *Human Reproduction.* **26**(9), pp.2558-2569.

Hammoud, S.S., Nix, D.A., Zhang, H., Purwar, J., Carrell, D.T. and Cairns, B.R. 2009. Distinctive chromatin in human sperm packages genes for embryo development. *Nature.* **460**(7254), pp.473-478.

Hancock, R. 2000. A new look at the nuclear matrix. *Chromosoma.* **109**(4), pp.219-225.

Hazzouri, M., Pivot-Pajot, C., Faure, A.-K., Usson, Y., Pelletier, R., Sèle, B., Khochbin, S. and Rousseaux, S. 2000a. Regulated hyperacetylation of core histones during mouse spermatogenesis: involvement of histone-deacetylases. *European Journal of Cell Biology.* **79**(12), pp.950-960.

Hazzouri, M., Rousseaux, S., Mongelard, F., Usson, Y., Pelletier, R., Faure, A., Vourc'h, C. and Sele, B. 2000b. Genome organization in the human sperm nucleus studied by FISH and confocal microscopy. *Molecular Reproduction and Development.* **55**(3), pp.307-315.

Hecht, N., Cavalcanti, M.C., Nayudu, P., Behr, R., Reichenbach, M., Weidner, W. and Steger, K. 2011. Protamine-1 represents a sperm specific gene transcript: a study in Callithrix jacchus and Bos taurus. *Andrologia.* **43**(3), pp.167-173.

Heger, A., Webber, C., Goodson, M., Ponting, C.P. and Lunter, G. 2013. GAT: a simulation framework for testing the association of genomic intervals. *Bioinformatics.* **29**(16), pp.2046-2048.

Henkel, R.R. and Schill, W.-B. 2003. Sperm preparation for ART. *Reprod Biol Endocrinol.* **1**(1), p108.

Hancock, J. 1952. The morphology of bull spermatozoa. *Journal of Experimental Biology.* **29**(3), pp.445-453.

Hosen, M.B., Islam, M.R., Begum, F., Kabir, Y. and Howlader, M.Z.H. 2015. Oxidative stress induced sperm DNA damage, a possible reason for male infertility. *Iranian Journal of Reproductive Medicine.* **13**(9), p525.

Hosken, D.J. and Hodgson, D.J. 2014. Why do sperm carry RNA? Relatedness, conflict, and control. *Trends in Ecology & Evolution.* **29**(8), pp.451-455.

Huang, D.W., Sherman, B.T., Tan, Q., Kir, J., Liu, D., Bryant, D., Guo, Y., Stephens, R., Baseler, M.W. and Lane, H.C. 2007. DAVID Bioinformatics Resources: expanded annotation database and novel algorithms to better extract biology from large gene lists. *Nucleic Acids Research.* **35**(suppl 2), pp.W169-W175.

Hughes, C.M., Lewis, S., McKelvey-Martin, V.J. and Thompson, W. 1998. The effects of antioxidant supplementation during Percoll preparation on human sperm DNA integrity. *Human Reproduction.* **13**(5), pp.1240-1247.

Hughes, C.M., Lewis, S.E., McKelvey-Martin, V.J. and Thompson, W. 1997. Reproducibility of human sperm DNA measurements using the alkaline single cell gel electrophoresis assay. *Mutat Res.* **374**(2), pp.261-268.

Hughes, C.M., McKelvey-Martin, V.J. and Lewis, S.E. 1999. Human sperm DNA integrity assessed by the Comet and ELISA assays. *Mutagenesis.* **14**(1), pp.71-75.

Iarovaia, O.V., Bystritskiy, A., Ravcheev, D., Hancock, R. and Razin, S.V. 2004. Visualization of individual DNA loops and a map of loop domains in the human dystrophin gene. *Nucleic Acids Research.* **32**(7), pp.2079-2086.

Ioannou, D., Miller, D., Griffin, D.K. and Tempest, H.G. 2016. Impact of sperm DNA chromatin in the clinic. *Journal of Assisted Reproduction and Genetics.* **33**(2), pp.157-166.

Jackson, D. 2005. Understanding nuclear organization: when information becomes knowledge. *EMBO Reports.* **6**(3), pp.213-217.

Jackson, D.A. 2003. The principles of nuclear structure. *Chromosome Research.* **11**(5), pp.387-401.

Jenkins, T.G. and Carrell, D.T. 2012. Dynamic alterations in the paternal epigenetic landscape following fertilization. *Frontiers in Genetics.* **3**.

Johnson, G.D., Jodar, M., Pique-Regi, R. and Krawetz, S.A. 2016. Nuclease Footprints in Sperm Project Past and Future Chromatin Regulatory Events. *Scientific Reports.* **6**.

Johnson, G.D., Lalancette, C., Linnemann, A.K., Leduc, F., Boissonneault, G. and Krawetz, S.A. 2011. The sperm nucleus: chromatin, RNA, and the nuclear matrix. *Reproduction.* **141**(1), pp.21-36.

Kalandadze, A., Bushara, S., Vassetzky, Y. and Razin, S. 1990. Characterization of DNA pattern in the site of permanent attachment to

the nuclear matrix located in the vicinity of replication origin. *Biochemical and Biophysical Research Communications.* **168**(1), pp.9-15.

Kasai, H. 1997. Analysis of a form of oxidative DNA damage, 8-hydroxy-2′-deoxyguanosine, as a marker of cellular oxidative stress during carcinogenesis. *Mutation Research/Reviews in Mutation Research.* **387**(3), pp.147-163.

Kasai, H., Hayami, H., Yamaizumi, Z., Saito, H. and Nishimura, S. 1984. Detection and identification of mutagens and carcinogens as their adducts with guanosine derivatives. *Nucleic Acids Research.* **12**(4), pp.2127-2136.

Katz, D.F. 1983. The evolution of mammalian sperm motility in the male and female reproductive tracts. *The Sperm Cell.* Springer, pp.340-344.

Keel, B.A. 2010. Reproductive Endocrinology and Infertility: Integrating Modern Clinical and Laboratory Practice. *Reproductive Laboratory Regulations, Certifications and Reporting Systems.*

Kim, M.K., Lesoon-Wood, L.A., Weintraub, B.D. and Chung, J.H. 1996. A soluble transcription factor, Oct-1, is also found in the insoluble nuclear matrix and possesses silencing activity in its alanine-rich domain. *Molecular and Cellular Biology.* **16**(8), pp.4366-4377.

Kimmins, S. and Sassone-Corsi, P. 2005. Chromatin remodelling and epigenetic features of germ cells. *Nature.* **434**(7033), pp.583-589.

Kong, A., Frigge, M.L., Masson, G., Besenbacher, S., Sulem, P., Magnusson, G., Gudjonsson, S.A., Sigurdsson, A., Jonasdottir, A. and Jonasdottir, A. 2012. Rate of de novo mutations and the importance of father/'s age to disease risk. *Nature.* **488**(7412), pp.471-475.

Kono, T., Obata, Y., Wu, Q., Niwa, K., Ono, Y., Yamamoto, Y., Park, E.S., Seo, J.-S. and Ogawa, H. 2004. Birth of parthenogenetic mice that can develop to adulthood. *Nature.* **428**(6985), pp.860-864.

Kramer, J.A. and Krawetz, S.A. 1996. Nuclear matrix interactions within the sperm genome. *Journal of Biological Chemistry.* **271**(20), pp.11619-11622.

Kumar, N. and Singh, A.K. 2015. Trends of male factor infertility, an important cause of infertility: A review of literature. *Journal of Human Reproductive Sciences.* **8**(4), p191.

Laemmli, U.K. 1970. Cleavage of structural proteins during the assembly of the head of bacteriophage T4. *Nature.* **227**, pp.680-685.

Lander, E.S., Linton, L.M., Birren, B., Nusbaum, C., Zody, M.C., Baldwin, J., Devon, K., Dewar, K., Doyle, M. and FitzHugh, W. 2001. Initial sequencing and analysis of the human genome. *Nature.* **409**(6822), pp.860-921.

Lewis, J.D., Saperas, N., Song, Y., Zamora, M.J., Chiva, M. and Ausió, J. 2004. Histone H1 and the origin of protamines. *Proceedings of the National Academy of Sciences.* **101**(12), pp.4148-4152.

Lewis, S.E. 2013. The place of sperm DNA fragmentation testing in current day fertility management. *Middle East Fertility Society Journal.* **18**(2), pp.78-82.

Lewis, S.E. and Agbaje, I.M. 2008. Using the alkaline comet assay in prognostic tests for male infertility and assisted reproductive technology outcomes. *Mutagenesis.* **23**(3), pp.163-170.

Li, L., Lu, X. and Dean, J. 2013. The maternal to zygotic transition in mammals. *Molecular Aspects of Medicine.* **34**(5), pp.919-938.

Li, Y., Lalancette, C., Miller, D. and Krawetz, S.A. 2008a. Characterization of nucleohistone and nucleoprotamine components in the mature human sperm nucleus. *Asian J Androl.* **10**(4), pp.535-541.

Li, Y., Lalancette, C., Miller, D. and Krawetz, S.A. 2008b. Characterization of nucleohistone and nucleoprotamine components in the mature human sperm nucleus. *Asian Journal of Andrology.* **10**(4).

Liao, Y., Smyth, G.K. and Shi, W. 2013. The Subread aligner: fast, accurate and scalable read mapping by seed-and-vote. *Nucleic Acids Research.* **41**(10), pp.e108-e108.

Liao, Y., Smyth, G.K. and Shi, W. 2014. featureCounts: an efficient general purpose program for assigning sequence reads to genomic features. *Bioinformatics.* **30**(7), pp.923-930.

Lin, D. 2005. An efficient Monte Carlo approach to assessing statistical significance in genomic studies. *Bioinformatics.* **21**(6), pp.781-787.

Lin, Y., Mahan, K., Lathrop, W.F., Myles, D.G. and Primakoff, P. 1994. A hyaluronidase activity of the sperm plasma membrane protein PH-20 enables sperm to penetrate the cumulus cell layer surrounding the egg. *The Journal of Cell Biology.* **125**(5), pp.1157-1163.

Linnemann, A.K. and Krawetz, S.A. 2009. Maintenance of a functional higher order chromatin structure: the role of the nuclear matrix in normal and disease states. *Gene Therapy & Molecular Biology.* **13**(1), p231.

Liu, D.Y. and Baker, H.G. 1992. Sperm nuclear chromatin normality: relationship with sperm morphology, sperm-zona pellucida binding, and fertilization rates in vitro. *Fertility and Sterility.* **58**(6), pp.1178-1184.

Liu, L., Aston, K.I. and Carrell, D.T. 2013. Protamine extraction and analysis of human sperm protamine 1/protamine 2 ratio using Acid gel electrophoresis. *Spermatogenesis: Methods and Protocols.* pp.445-450.

Lo Monte, G., Murisier, F., Piva, I., Germond, M. and Marci, R. 2013. Focus on intracytoplasmic morphologically selected sperm injection (IMSI): a mini-review. *Asian J Androl.* **15**(5), pp.608-615.

Loutradi, K.E., Tarlatzis, B.C., Goulis, D.G., Zepiridis, L., Pagou, T., Chatziioannou, E., Grimbizis, G.F., Papadimas, I. and Bontis, I. 2006. The effects of sperm quality on embryo development after intracytoplasmic sperm injection. *Journal of Assisted Reproduction and Genetics.* **23**(2), pp.69-74.

Luetjens, C.M., Payne, C. and Schatten, G. 1999. Non-random chromosome positioning in human sperm and sex chromosome anomalies following intracytoplasmic sperm injection. *The Lancet.* **353**(9160), p1240.

Luger, K. 2003. Structure and dynamic behavior of nucleosomes. *Current Opinion in Genetics & Development.* **13**(2), pp.127-135.

Luger, K., Mäder, A.W., Richmond, R.K., Sargent, D.F. and Richmond, T.J. 1997. Crystal structure of the nucleosome core particle at 2.8 Å resolution. *Nature.* **389**(6648), pp.251-260.

Lusser, A. 2002. Acetylated, methylated, remodeled: chromatin states for gene regulation. *Current Opinion in Plant Biology.* **5**(5), pp.437-443.

Mahy, N.L., Perry, P.E. and Bickmore, W.A. 2002. Gene density and transcription influence the localization of chromatin outside of chromosome territories detectable by FISH. *The Journal of Cell Biology.* **159**(5), pp.753-763.

Malik, A., Haron, A.W., Yusoff, R., Bukar, M., Kasim, A. and Sabri, M. 2011. Verification of X-and Y-spermatozoa separation by nested polymerase chain reaction (PCR), motility and membrane integrity in bovine. *African Journal of Biotechnology.* **10**(85), p19796.

Mallo, M. and Alonso, C.R. 2013. The regulation of Hox gene expression during animal development. *Development.* **140**(19), pp.3951-3963.

Manvelyan, M., Hunstig, F., Bhatt, S., Mrasek, K., Pellestor, F., Weise, A., Simonyan, I., Aroutiounian, R. and Liehr, T. 2008. Chromosome distribution in human sperm–a 3D multicolor banding-study. *Molecular Cytogenetics.* **1**(1), p1.

Mao, C., Brown, C.R., Falkovskaia, E., Dong, S., Hrabeta-Robinson, E., Wenger, L. and Boeger, H. 2010. Quantitative analysis of the transcription control mechanism. *Molecular Systems Biology.* **6**(1), p431.

Mardis, E.R. 2008. Next-generation DNA sequencing methods. *Annu. Rev. Genomics Hum. Genet.* **9**, pp.387-402.

McCall, M.R. and Frei, B. 1999. Can antioxidant vitamins materially reduce oxidative damage in humans? *Free Radical Biology and Medicine.* **26**(7), pp.1034-1053.

McEvoy, A., Roberts, P., Yap, K. and Matson, P. 2014. Development of a simplified method of human semen storage for the testing of sperm DNA fragmentation using the Halosperm G2 test kit. *Fertility and Sterility.* **102**(4), pp.981-988.

McFeters, G., Singh, A., Byun, S., Callis, P. and Williams, S. 1991. Acridine orange staining reaction as an index of physiological activity in Escherichia coli. *Journal of Microbiological Methods.* **13**(2), pp.87-97.

McLay, D.W. and Clarke, H.J. 2003. Remodelling the paternal chromatin at fertilization in mammals. *Reproduction.* **125**(5), pp.625-633.

Meistrich, M.L., Brock, W.A., Grimes, S.R. . 1978. Nuclear protein transition during spermatogenesis. *Fed. Proc.* **37**, pp.2522–2525.

Meyer, L.R., Zweig, A.S., Hinrichs, A.S., Karolchik, D., Kuhn, R.M., Wong, M., Sloan, C.A., Rosenbloom, K.R., Roe, G. and Rhead, B. 2013. The UCSC Genome Browser database: extensions and updates 2013. *Nucleic Acids Research.* **41**(D1), pp.D64-D69.

Mika, S. and Rost, B. 2005. NMPdb: database of nuclear matrix proteins. *Nucleic Acids Research.* **33**(suppl 1), pp.D160-D163.

Miller, D. 2014. Sperm RNA as a mediator of genomic plasticity. *Advances in Biology.* **2014**.

Miller, D. 2015. Confrontation, Consolidation, and Recognition: The Oocyte's Perspective on the Incoming Sperm. *Cold Spring Harbor Perspectives in Medicine.* **5**(8), pa023408.

Miller, D., Brinkworth, M. and Iles, D. 2010. Paternal DNA packaging in spermatozoa: more than the sum of its parts? DNA, histones, protamines and epigenetics. *Reproduction.* **139**(2), pp.287-301.

Miller, D., Ostermeier, G.C. and Krawetz, S.A. 2005. The controversy, potential and roles of spermatozoal RNA. *Trends Mol Med.* **11**(4), pp.156-163.

Min, H., Kong, K.A., Lee, J.Y., Hong, C.P., Seo, S.H., Roh, T.Y., Bae, S.S. and Kim, M.H. 2016. CTCF-mediated Chromatin Loop for the Posterior Hoxc Gene Expression in MEF Cells. *IUBMB Life.* **68**(6), pp.436-444.

Mohammed, E.-E.M., Mosad, E., Zahran, A.M., Hameed, D.A., Taha, E.A. and Mohamed, M.A. 2015. Acridine Orange and Flow Cytometry: Which Is Better to Measure the Effect of Varicocele on Sperm DNA Integrity? *Advances in Urology.* **2015**.

Mohar, I., Szczygiel, M.A., Yanagimachi, R. and Ward, W.S. 2002. Sperm nuclear halos can transform into normal chromosomes after injection into oocytes. *Molecular Reproduction and Development.* **62**(3), pp.416-420.

Morris, I., Ilott, S., Dixon, L. and Brison, D. 2002. The spectrum of DNA damage in human sperm assessed by single cell gel electrophoresis (Comet assay) and its relationship to fertilization and embryo development. *Human Reproduction.* **17**(4), pp.990-998.

Morrissey, J.H. 1981. Silver stain for proteins in polyacrylamide gels: a modified procedure with enhanced uniform sensitivity. *Analytical Biochemistry.* **117**(2), pp.307-310.

Motoishi, M., Goto, K., Tomita, K., OOKUTSU, S. and NAKANISHI, Y. 1996. Decondensation of Bull and Human Sperm Nuclei by Dithiothreitol and/or Heparin. *Journal of Reproduction and Development.* **42**(1), pp.7-13.

Mounkes, L. and Stewart, C.L. 2004. Structural organization and functions of the nucleus in development, aging, and disease. *Current Topics in Developmental Biology.* **61**, pp.191-228.

Mudrak, O., Tomilin, N. and Zalensky, A. 2005. Chromosome architecture in the decondensing human sperm nucleus. *Journal of Cell Science.* **118**(19), pp.4541-4550.

Mudrak, O.S., Nazarov, I.B., Jones, E.L. and Zalensky, A.O. 2012. Positioning of chromosomes in human spermatozoa is determined by ordered centromere arrangement. *PLoS One.* **7**(12), pe52944.

Muriel, L., Meseguer, M., Fernández, J.L., Alvarez, J., Remohí, J., Pellicer, A. and Garrido, N. 2006. Value of the sperm chromatin dispersion test in predicting pregnancy outcome in intrauterine insemination: a blind prospective study. *Human Reproduction.* **21**(3), pp.738-744.

Nadel, B., de Lara, J., Finkernagel, S.W. and Ward, W.S. 1995. Cell-specific organization of the 5S ribosomal RNA gene cluster DNA loop domains in spermatozoa and somatic cells. *Biology of Reproduction.* **53**(5), pp.1222-1228.

Nakai, M., Kashiwazaki, N., Takizawa, A., Maedomari, N., Ozawa, M., Noguchi, J., Kaneko, H., Shino, M. and Kikuchi, K. 2006. Morphologic changes in boar sperm nuclei with reduced disulfide bonds in electrostimulated porcine oocytes. *Reproduction.* **131**(3), pp.603-611.

Nakato, R. and Shirahige, K. 2016. Recent advances in ChIP-seq analysis: from quality management to whole-genome annotation. *Briefings in Bioinformatics.* pbbw023.

Nandi, N., Sen, A., Banerjee, R., Kumar, S., Kumar, V., Ghosh, A.N. and Das, P. 2010. Hydrogen peroxide induces apoptosis-like death in Entamoeba histolytica trophozoites. *Microbiology.* **156**(7), pp.1926-1941.

Noblanc, A., Damon-Soubeyrand, C., Karrich, B., Henry-Berger, J., Cadet, R., Saez, F., Guiton, R., Janny, L., Pons-Rejraji, H. and Alvarez, J.G. 2013. DNA oxidative damage in mammalian spermatozoa: where and why is the male nucleus affected? *Free Radical Biology and Medicine.* **65**, pp.719-723.

Noblanc, A., Kocer, A. and Drevet, J.R. 2014. Recent knowledge concerning mammalian sperm chromatin organization and its potential weaknesses when facing oxidative challenge. *Basic and Clinical Andrology.* **24**(1), p1.

Noordermeer, D., Leleu, M., Splinter, E., Rougemont, J., De Laat, W. and Duboule, D. 2011. The dynamic architecture of Hox gene clusters. *Science.* **334**(6053), pp.222-225.

Nusbaum, C., Zody, M.C., Borowsky, M.L., Kamal, M., Kodira, C.D., Taylor, T.D., Whittaker, C.A., Chang, J.L., Cuomo, C.A. and Dewar, K. 2005. DNA sequence and analysis of human chromosome 18. *Nature.* **437**(7058), pp.551-555.

Oko, R., Jando, V., Wagner, C., Kistler, W. and Hermo, L. 1996. Chromatin reorganization in rat spermatids during the disappearance of testis-specific histone, H1t, and the appearance of transition proteins TP1 and TP2. *Biology of Reproduction.* **54**(5), pp.1141-1157.

Oliva, R. 2006. Protamines and male infertility. *Human Reproduction Update.* **12**(4), pp.417-435.

Oliva, R. and Ballescà, J.L. 2012. Altered histone retention and epigenetic modifications in the sperm of infertile men. *Asian J Androl.* **14**(2), pp.239-240.

Oliva, R. and Castillo, J. 2011. Proteomics and the genetics of sperm chromatin condensation. *Asian J Androl.* **13**(1), pp.24-30.

Oliva, R., Martinez-Heredia, J., de Mateo, S., Gazquez, C., Oriola, J., Estanyol, J., Guimerà, M., Balasch, J. and Ballesca, J. 2006. Proteomics of human spermatozoa, protamine content and assisted reproduction outcome. *Society of Reproduction and Fertility Supplement.* **65**, pp.527-530.

Olivares, C., Vera, M.L. and Ruíz-Lara, S. 1993. Coexistence of two chromatin structures in sperm nuclei of the bivalve molluscProtothaca thaca. *Molecular and Cellular Biochemistry.* **125**(1), pp.87-95.

Olive, P.L. and Banath, J.P. 2006. The comet assay: a method to measure DNA damage in individual cells. *Nat Protoc.* **1**(1), pp.23-29.

Ostermeier, G.C., Goodrich, R.J., Moldenhauer, J.S., Diamond, M.P. and Krawetz, S.A. 2005. A suite of novel human spermatozoal RNAs. *J Androl.* **26**(1), pp.70-74.

Ostermeier, G.C., Liu, Z., Martins, R.P., Bharadwaj, R.R., Ellis, J., Draghici, S. and Krawetz, S.A. 2003. Nuclear matrix association of the human β-globin locus utilizing a novel approach to quantitative real-time PCR. *Nucleic Acids Research.* **31**(12), pp.3257-3266.

Palmer, D.K., O'Day, K. and Margolis, R.L. 1990. The centromere specific histone CENP-A is selectively retained in discrete foci in mammalian sperm nuclei. *Chromosoma.* **100**(1), pp.32-36.

Parrish, J., Krogenaes, A. and Susko-Parrish, J. 1995. Effect of bovine sperm separation by either swim-up or Percoll method on success of in vitro fertilization and early embryonic development. *Theriogenology.* **44**(6), pp.859-869.

Pasqualotto, F.F., Sharma, R.K., Nelson, D.R., Thomas, A.J. and Agarwal, A. 2000. Relationship between oxidative stress, semen characteristics, and clinical diagnosis in men undergoing infertility investigation. *Fertility and Sterility.* **73**(3), pp.459-464.

Pérez-Cerezales, S., Miranda, A. and Gutiérrez-Adán, A. 2012. Comparison of four methods to evaluate sperm DNA integrity between mouse caput and cauda epididymidis. *Asian Journal of Andrology.* **14**(2), p335.

Perreault, S.D., Barbee, R.R. and Slott, V.L. 1988. Importance of glutathione in the acquisition and maintenance of sperm nuclear decondensing activity in maturing hamster oocytes. *Developmental Biology.* **125**(1), pp.181-186.

Pittoggi, C., Renzi, L., Zaccagnini, G., Cimini, D., Degrassi, F., Giordano, R., Magnano, A.R., Lorenzini, R., Lavia, P. and Spadafora, C. 1999. A fraction of mouse sperm chromatin is organized in nucleosomal hypersensitive domains enriched in retroposon DNA. *J Cell Sci.* **112 (Pt 20)**, pp.3537-3548.

Poccia, D. 1986. Remodeling of nucleoproteins during gametogenesis, fertilization, and early development. *Int Rev Cytol.* **105**, pp.1-65.

Pogany, G.C., Corzett, M., Weston, S. and Balhorn, R. 1981. DNA and protein content of mouse sperm. Implications regarding sperm chromatin structure. *Exp Cell Res.* **136**(1), pp.127-136.

Quinlan, A.R. and Hall, I.M. 2010. BEDTools: a flexible suite of utilities for comparing genomic features. *Bioinformatics.* **26**(6), pp.841-842.

Racki, W.J. and Richter, J.D. 2006. CPEB controls oocyte growth and follicle development in the mouse. *Development.* **133**(22), pp.4527-4537.

Rajender, S., Avery, K. and Agarwal, A. 2011. Epigenetics, spermatogenesis and male infertility. *Mutation Research/Reviews in Mutation Research.* **727**(3), pp.62-71.

Rao, S.R., Trivedi, S., Emmanuel, D., Merita, K. and Hynniewta, M. 2010. DNA repetitive sequences-types, distribution and function: A review. *J Cell and Mol Biol.* **7**(2), pp.1-11.

Rathke, C., Baarends, W.M., Awe, S. and Renkawitz-Pohl, R. 2014. Chromatin dynamics during spermiogenesis. *Biochimica et Biophysica Acta (BBA)-Gene Regulatory Mechanisms.* **1839**(3), pp.155-168.

Rato, L., Alves, M.G., Socorro, S., Duarte, A.I., Cavaco, J.E. and Oliveira, P.F. 2012. Metabolic regulation is important for spermatogenesis. *Nature Reviews Urology.* **9**(6), pp.330-338.

Razin, S., Borunova, V., Iarovaia, O. and Vassetzky, Y. 2014a. Nuclear matrix and structural and functional compartmentalization of the eucaryotic cell nucleus. *Biochemistry (Moscow).* **79**(7), pp.608-618.

Razin, S., Iarovaia, O. and Vassetzky, Y. 2014b. A requiem to the nuclear matrix: from a controversial concept to 3D organization of the nucleus. *Chromosoma.* **123**(3), pp.217-224.

Razin, S., RZESZOWSKAWOLNY, J., Moreau, J. and Scherrer, K. 1985. Localization of sites of DNA attachment to the nuclear matrix in the domain of the chicken alpha-globin genes in functionally active and functionally inactive nuclei. *Molecular Biology.* **19**(2), pp.376-384.

Razin, S.V., Gavrilov, A.A., Ioudinkova, E.S. and Iarovaia, O.V. 2013. Communication of genome regulatory elements in a folded chromosome. *FEBS Letters.* **587**(13), pp.1840-1847.

Razin, S.V., Iarovaia, O.V., Sjakste, N., Sjakste, T., Bagdoniene, L., Rynditch, A.V., Eivazova, E.R., Lipinski, M. and Vassetzky, Y.S. 2007. Chromatin domains and regulation of transcription. *Journal of Molecular Biology.* **369**(3), pp.597-607.

Robinson, D.P. and Klein, S.L. 2012. Pregnancy and pregnancy-associated hormones alter immune responses and disease pathogenesis. *Hormones and Behavior.* **62**(3), pp.263-271.

Robinson, L., Gallos, I.D., Conner, S.J., Rajkhowa, M., Miller, D., Lewis, S., Kirkman-Brown, J. and Coomarasamy, A. 2012. The effect of sperm

DNA fragmentation on miscarriage rates: a systematic review and meta-analysis. *Human Reproduction.* pdes261.

Robinson, M.D., McCarthy, D.J. and Smyth, G.K. 2010. edgeR: a Bioconductor package for differential expression analysis of digital gene expression data. *Bioinformatics.* **26**(1), pp.139-140.

Roca, J. and Mezquita, C. 1989. DNA topoisomerase II activity in nonreplicating, transcriptionally inactive, chicken late spermatids. *The EMBO Journal.* **8**(6), p1855.

Rodman, T.C., Pruslin, F.H., Hoffmann, H.P. and Allfrey, V.G. 1981. Turnover of basic chromosomal proteins in fertilized eggs: a cytoimmunochemical study of events in vivo. *The Journal of Cell Biology.* **90**(2), pp.351-361.

Ramos, L., Van Der Heijden, G., Derijck, A., Berden, J., Kremer, J., Van Der Vlag, J. and De Boer, P. 2008. Incomplete nuclear transformation of human spermatozoa in oligo-astheno-teratospermia: characterization by indirect immunofluorescence of chromatin and thiol status. *Human Reproduction.* **23**(2), pp.259-270.

Ross, M.T., Grafham, D.V., Coffey, A.J., Scherer, S., McLay, K., Muzny, D., Platzer, M., Howell, G.R., Burrows, C. and Bird, C.P. 2005. The DNA sequence of the human X chromosome. *Nature.* **434**(7031), pp.325-337.

Rybar, R., Faldikova, L., Faldyna, M., Machatkova, M. and Rubes, J. 2004. Bull and boar sperm DNA integrity evaluated by sperm chromatin structure assay in the Czech Republic. *Vet. Med.* **49**(1), pp.1–8.

Saida, M., Iles, D., Elnefati, A., Brinkworth, M. and Miller, D. 2011. Key gene regulatory sequences with distinctive ontological signatures associate with differentially endonuclease accessible mouse sperm chromatin. *Reproduction.* pp.REP-10-0536.

Sakkas, D. and Alvarez, J.G. 2010. Sperm DNA fragmentation: mechanisms of origin, impact on reproductive outcome, and analysis. *Fertility and Sterility.* **93**(4), pp.1027-1036.

Sakkas, D., Mariethoz, E., Manicardi, G., Bizzaro, D., Bianchi, P.G. and Bianchi, U. 1999. Origin of DNA damage in ejaculated human spermatozoa. *Rev Reprod.* **4**(1), pp.31-37.

Saleh, R.A., Agarwal, A., Nada, E.A., El-Tonsy, M.H., Sharma, R.K., Meyer, A., Nelson, D.R. and Thomas, A.J. 2003. Negative effects of increased sperm DNA damage in relation to seminal oxidative stress in men with idiopathic and male factor infertility. *Fertility and Sterility.* **79**, pp.1597-1605.

Samans, B., Yang, Y., Krebs, S., Sarode, G.V., Blum, H., Reichenbach, M., Wolf, E., Steger, K., Dansranjavin, T. and Schagdarsurengin, U. 2014. Uniformity of nucleosome preservation pattern in mammalian sperm and its connection to repetitive DNA elements. *Developmental Cell.* **30**(1), pp.23-35.

Sánchez-Vázquez, M.L., Flores-Alonso, J.C., Merchant-Larios, H. and Reyes, R. 2008. Presence and release of bovine sperm histone H1 during

chromatin decondensation by heparin-glutathione. *Systems Biology in Reproductive Medicine.* **54**(6), pp.221-230.

Sanocka, D. and Kurpisz, M. 2004. Reactive oxygen species and sperm cells. *Reproductive Biology and Endocrinology.* **2**(1), p1.

Santos, F., Hendrich, B., Reik, W. and Dean, W. 2002. Dynamic reprogramming of DNA methylation in the early mouse embryo. *Developmental Biology.* **241**(1), pp.172-182.

Sati, L. and Huszar, G. 2013. Methodology of aniline blue staining of chromatin and the assessment of the associated nuclear and cytoplasmic attributes in human sperm. *Spermatogenesis: Methods and Protocols.* pp.425-436.

Sarrate, Z. and Anton, E. 2009. Fluorescence in situ hybridization (FISH) protocol in human sperm. *Journal of visualized experiments: JoVE.* (31).

Sassone-Corsi, P. 2002. Unique chromatin remodeling and transcriptional regulation in spermatogenesis. *Science.* **296**(5576), pp.2176-2178.

Schulte, R.T., Ohl, D.A., Sigman, M. and Smith, G.D. 2010. Sperm DNA damage in male infertility: etiologies, assays, and outcomes. *Journal of Assisted Reproduction and Genetics.* **27**(1), pp.3-12.

Schwartz, S., Meshorer, E. and Ast, G. 2009. Chromatin organization marks exon-intron structure. *Nature Structural & Molecular Biology.* **16**(9), pp.990-995.

Seisenberger, S., Peat, J.R., Hore, T.A., Santos, F., Dean, W. and Reik, W. 2013. Reprogramming DNA methylation in the mammalian life cycle: building and breaking epigenetic barriers. *Phil. Trans. R. Soc. B.* **368**(1609), p20110330.

Sellami, A., Chakroun, N., Ben Zarrouk, S., Sellami, H., Kebaili, S., Rebai, T. and Keskes, L. 2013. Assessment of chromatin maturity in human spermatozoa: useful aniline blue assay for routine diagnosis of male infertility. *Advances in Urology.* **2013**.

Sestili, P. 2009. The fast-halo assay for the assessment of DNA damage at the single-cell level. *DNA Replication.* Springer, pp.517-533.

Sestili, P., Martinelli, C. and Stocchi, V. 2006. The fast halo assay: an improved method to quantify genomic DNA strand breakage at the single-cell level. *Mutation Research/Genetic Toxicology and Environmental Mutagenesis.* **607**(2), pp.205-214.

Schulte, R.T., Ohl, D.A., Sigman, M. and Smith, G.D. 2010. Sperm DNA damage in male infertility: etiologies, assays, and outcomes. *Journal of Assisted Reproduction and Genetics.* **27**(1), pp.3-12.

Shafik, A., Shafik, A., Sibai, O.E. and Shafik, I. 2006. Sperm DNA fragmentation. *Systems Biology in Reproductive Medicine.* **52**(3), pp.197-208.

Shaman, J.A., Prisztoka, R. and Ward, W.S. 2006. Topoisomerase IIB and an extracellular nuclease interact to digest sperm DNA in an apoptotic-like manner. *Biology of Reproduction.* **75**(5), pp.741-748.

Shaman, J.A., Yamauchi, Y. and Steven Ward, W. 2007a. Function of the sperm nuclear matrix. *Systems Biology in Reproductive Medicine.* **53**(3), pp.135-140.

Shaman, J.A., Yamauchi, Y. and Steven Ward, W. 2007b. The sperm nuclear matrix is required for paternal DNA replication. *Journal of Cellular Biochemistry.* **102**(3), pp.680-688.

Shamsi, M.B., Imam, S.N. and Dada, R. 2011. Sperm DNA integrity assays: diagnostic and prognostic challenges and implications in management of infertility. *Journal of Assisted Reproduction and Genetics.* **28**(11), pp.1073-1085.

Shapiro, J.A. and Sternberg, R. 2005. Why repetitive DNA is essential to genome function. *Biological Reviews.* **80**(2), pp.227-250.

Sharma, A. 2016. Investigation on the Effects of Exogenous H 2 O 2 on Sperm Motility, LPO, Catalase and SOD Levels in Seminal Plasma. *Health Science Journal.*

Sharma, R.K. and Agarwal, A. 1996. Role of reactive oxygen species in male infertility. *Urology.* **48**(6), pp.835-850.

Sharpe R. M. 1994. Regulation of spermatogenesis. In The physiology of reproduction (eds Knobil E., Neill J. D., editors), pp. 1363–1434. New York, NY: Raven Press.

Sharpe, R.M., McKinnell, C., Kivlin, C. and Fisher, J.S. 2003. Proliferation and functional maturation of Sertoli cells, and their relevance to disorders of testis function in adulthood. *Reproduction.* **125**(6), pp.769-784.

Shen, H.-M., Chia, S.-E., Ni, Z.-Y., New, A.-L., Lee, B.-L. and Ong, C.-N. 1997. Detection of oxidative DNA damage in human sperm and the association with cigarette smoking. *Reproductive Toxicology.* **11**(5), pp.675-680.

Shi, W. and Liao, Y. 2013. *Subread/Rsubread Users Guide*.

Simon, L. and Carrell, D.T. 2013. Sperm DNA damage measured by comet assay. *Spermatogenesis: Methods and Protocols.* pp.137-146.

Simon, L., Castillo, J., Oliva, R. and Lewis, S.E. 2011a. Relationships between human sperm protamines, DNA damage and assisted reproduction outcomes. *Reprod Biomed Online.* **23**(6), pp.724-734.

Simon, L., Lutton, D., McManus, J. and Lewis, S.E. 2011b. Sperm DNA damage measured by the alkaline Comet assay as an independent predictor of male infertility and in vitro fertilization success. *Fertility and Sterility.* **95**(2), pp.652-657.

Simon, L., Murphy, K., Shamsi, M., Liu, L., Emery, B., Aston, K., Hotaling, J. and Carrell, D. 2014. Paternal influence of sperm DNA integrity on early embryonic development. *Human Reproduction.* pdeu228.

Simon, L., Zini, A., Dyachenko, A., Ciampi, A. and Carrell, D.T. 2017. A systematic review and meta-analysis to determine the effect of sperm DNA damage on in vitro fertilization and intracytoplasmic sperm injection outcome. *Asian Journal of Andrology.* **19**(1), p80.

Singh, N.P., Danner, D.B., Tice, R.R., McCoy, M.T., Collins, G.D. and Schneider, E.L. 1989. Abundant alkali-sensitive sites in DNA of human and mouse sperm. *Experimental Cell Research.* **184**(2), pp.461-470.

Singh, N.P., McCoy, M.T., Tice, R.R. and Schneider, E.L. 1988. A simple technique for quantitation of low levels of DNA damage in individual cells. *Exp Cell Res.* **175**(1), pp.184-191.

Smith, T.B., Dun, M.D., Smith, N.D., Curry, B.J., Connaughton, H.S. and Aitken, R.J. 2013. The presence of a truncated base excision repair pathway in human spermatozoa that is mediated by OGG1. *J Cell Sci.* **126**(6), pp.1488-1497.

Sotolongo, B., Huang, T.T., Isenberger, E. and Ward, W.S. 2005. An Endogenous Nuclease in Hamster, Mouse, and Human Spermatozoa Cleaves DNA into Loop-Sized Fragments. *Journal of Andrology.* **26**(2), pp.272-280.

Sotolongo, B. and Ward, W.S. 2000. DNA loop domain organization: The three-dimensional genomic code. *Journal of Cellular Biochemistry.* **79**(S35), pp.23-26.

Spano, M., Bonde, J.P., Hjollund, H.I., Kolstad, H.A., Cordelli, E. and Leter, G. 2000. Sperm chromatin damage impairs human fertility. The Danish First Pregnancy Planner Study Team. *Fertil Steril.* **73**(1), pp.43-50.

Speit, G., Vasquez, M. and Hartmann, A. 2009. The comet assay as an indicator test for germ cell genotoxicity. *Mutat Res.* **681**(1), pp.3-12.

Spinaci, M., Seren, E. and Mattioli, M. 2004. Maternal chromatin remodeling during maturation and after fertilization in mouse oocytes. *Molecular Reproduction and Development.* **69**(2), pp.215-221.

Stanley, S.M., Bailey, T.L. and Mattick, J.S. 2006. GONOME: measuring correlations between GO terms and genomic positions. *BMC Bioinformatics.* **7**(1), p1.

Stein, A. and Page, D. 1980. Core histone associations in solutions of high salt. *J. Biol. C? t. em. 225, 3629.* **3637**.

Stein, G.S. and Stein, J.L. 1989. *Histones and other basic nuclear proteins.* CRC Press.

Stuppia, L., Franzago, M., Ballerini, P., Gatta, V. and Antonucci, I. 2015. Epigenetics and male reproduction: the consequences of paternal lifestyle on fertility, embryo development, and children lifetime health. *Clinical Epigenetics.* **7**(1), p1.

Sun, H.B. and Yokota, H. 1999. Correlated positioning of homologous chromosomes in daughter fibroblast cells. *Chromosome Research.* **7**(8), pp.603-610.

Talwar, L.C.P. and Sindhu, S.G. 2012. *Step by Step: Protocols in Clinical Embryology and ART.* JP Medical Ltd.

Tandara, M., Bajić, A., Tandara, L., Bilić-Zulle, L., Šunj, M., Kozina, V., Goluža, T. and Jukić, M. 2014. Sperm DNA integrity testing: big halo is a good

predictor of embryo quality and pregnancy after conventional IVF. *Andrology.* **2**(5), pp.678-686.

Tanphaichitr, N., Sobhon, P., Taluppeth, N. and Chalermisarachai, P. 1978. Basic nuclear proteins in testicular cells and ejaculated spermatozoa in man. *Exp Cell Res.* **117**(2), pp.347-356.

Team, R.C. 2013. R: A language and environment for statistical computing.

Tempel, S. 2012. Using and understanding RepeatMasker. *Mobile Genetic Elements: Protocols and Genomic Applications.* pp.29-51.

Teperek, M. and Miyamoto, K. 2013. Nuclear reprogramming of sperm and somatic nuclei in eggs and oocytes. *Reproductive Medicine and Biology.* **12**(4), pp.133-149.

Thomas, P.D., Kejariwal, A., Campbell, M.J., Mi, H., Diemer, K., Guo, N., Ladunga, I., Ulitsky-Lazareva, B., Muruganujan, A. and Rabkin, S. 2003. PANTHER: a browsable database of gene products organized by biological function, using curated protein family and subfamily classification. *Nucleic Acids Research.* **31**(1), pp.334-341.

Tomsu, M., Sharma, V. and Miller, D. 2002. Embryo quality and IVF treatment outcomes may correlate with different sperm comet assay parameters. *Human Reproduction.* **17**(7), pp.1856-1862.

Torregrosa, N., Domínguez-Fandos, D., Camejo, M.I., Shirley, C.R., Meistrich, M.L., Ballescà, J.L. and Oliva, R. 2006. Protamine 2 precursors, protamine 1/protamine 2 ratio, DNA integrity and other sperm parameters in infertile patients. *Human Reproduction.* **21**(8), pp.2084-2089.

Toshimori, K. 2009. *Dynamics of the mammalian sperm head: modifications and maturation events from spermatogenesis to egg activation.* Springer Science & Business Media.

Tovich, P.R. and Oko, R.J. 2003. Somatic histones are components of the perinuclear theca in bovine spermatozoa. *Journal of Biological Chemistry.* **278**(34), pp.32431-32438.

Treangen, T.J. and Salzberg, S.L. 2012. Repetitive DNA and next-generation sequencing: computational challenges and solutions. *Nature Reviews Genetics.* **13**(1), pp.36-46.

Trounson, A.O. and Gosden, R.G. 2003. *Biology and pathology of the oocyte: its role in fertility and reproductive medicine.* Cambridge University Press.

Valavanidis, A., Vlachogianni, T. and Fiotakis, C. 2009. 8-hydroxy-2′-deoxyguanosine (8-OHdG): a critical biomarker of oxidative stress and carcinogenesis. *Journal of Environmental Science and Health Part C.* **27**(2), pp.120-139.

Valcarce, D., Cartón-García, F., Riesco, M., Herraez, M. and Robles, V. 2013. Analysis of DNA damage after human sperm cryopreservation in genes crucial for fertilization and early embryo development. *Andrology.* **1**(5), pp.723-730.

Vanderwall, D.K. 2008. Counting spermatozoa with a hemacytometer. *Journal of Equine Veterinary Science.* **28**(4), pp.244-246.

Van der Heijden, G., Derijck, A., Ramos, L., Giele, M., Van Der Vlag, J. and De Boer, P. 2006. Transmission of modified nucleosomes from the mouse male germline to the zygote and subsequent remodeling of paternal chromatin. *Developmental Biology.* **298**(2), pp.458-469.

Van Der Velden, A.W. and Thomas, A.A. 1999. The role of the 5′ untranslated region of an mRNA in translation regulation during development. *The International Journal of Biochemistry & Cell Biology.* **31**(1), pp.87-106.

Van Roijen, H., Ooms, M.P., Spaargaren, M.C., Baarends, W.M., Weber, R., Grootegoed, J.A. and Vreeburg, J. 1998. Immunoexpression of testis-specific histone 2B in human spermatozoa and testis tissue. *Human Reproduction.* **13**(6), pp.1559-1566.

Vavouri, T. and Lehner, B. 2011. Chromatin organization in sperm may be the major functional consequence of base composition variation in the human genome. *PLoS Genet.* **7**(4), pe1002036.

Vieweg, M., Dvorakova-Hortova, K., Dudkova, B., Waliszewski, P., Otte, M., Oels, B., Hajimohammad, A., Turley, H., Schorsch, M. and Schuppe, H.-C. 2015. Methylation analysis of histone H4K12ac-associated promoters in sperm of healthy donors and subfertile patients. *Clinical Epigenetics.* **7**(1), p1.

Villani, P., Eleuteri, P., Grollino, M.G., Rescia, M., Altavista, P., Spano, M., Pacchierotti, F. and Cordelli, E. 2010. Sperm DNA fragmentation induced by DNAse I and hydrogen peroxide: an in vitro comparative study among different mammalian species. *Reproduction.* **140**(3), pp.445-452.

Vogelstein, B., Pardoll, D.M. and Coffey, D.S. 1980. Supercoiled loops and eucaryotic DNA replication. *Cell.* **22**(1), pp.79-85.

Ward, M.A. and Ward, W.S. 2004. A model for the function of sperm DNA degradation. *Reproduction, Fertility and Development.* **16**(5), pp.547-554.

Ward, W.S. 2010. Function of sperm chromatin structural elements in fertilization and development. *Molecular Human Reproduction.* **16**(1), pp.30-36.

Ward, W.S. 2013. Isolation of sperm nuclei and nuclear matrices from the mouse, and other rodents. *Spermatogenesis: Methods and Protocols.* pp.437-444.

Ward, W.S. and Coffey, D.S. 1990. Specific organization of genes in relation to the sperm nuclear matrix. *Biochemical and Biophysical Research Communications.* **173**(1), pp.20-25.

Ward, W.S., Kimura, Y. and Yanagimachi, R. 1999a. An intact sperm nuclear matrix may be necessary for the mouse paternal genome to participate in embryonic development. *Biology of Reproduction.* **60**(3), pp.702-706.

Ward, W.S., Kishikawa, H., Akutsu, H., Yanagimachi, H. and Yanagimachi, R. 1999b. Further evidence that sperm nuclear proteins are necessary for embryogenesis. *Zygote.* **8**(01), pp.51-56.

Ward, W.S., Partin, A.W. and Coffey, D.S. 1989. DNA loop domains in mammalian spermatozoa. *Chromosoma.* **98**(3), pp.153-159.

Weber, C.M., Henikoff, J.G. and Henikoff, S. 2010. H2A. Z nucleosomes enriched over active genes are homotypic. *Nature Structural & Molecular Biology.* **17**(12), pp.1500-1507.

Weber, M., Davies, J.J., Wittig, D., Oakeley, E.J., Haase, M., Lam, W.L. and Schuebeler, D. 2005. Chromosome-wide and promoter-specific analyses identify sites of differential DNA methylation in normal and transformed human cells. *Nature Genetics.* **37**(8), pp.853-862.

White-Cooper, H. and Bausek, N. 2010. Evolution and spermatogenesis. *Philosophical Transactions of the Royal Society of London B: Biological Sciences.* **365**(1546), pp.1465-1480.

Wiland, E., Fraczek, M., Olszewska, M. and Kurpisz, M. 2016. Topology of chromosome centromeres in human sperm nuclei with high levels of DNA damage. *Scientific Reports.* **6**.

Wilson, R.H. and Coverley, D. 2013. Relationship between DNA replication and the nuclear matrix. *Genes to Cells.* **18**(1), pp.17-31.

Wlodkowic, D., Telford, W., Skommer, J. and Darzynkiewicz, Z. 2011. Apoptosis and beyond: cytometry in studies of programmed cell death. *Methods in Cell Biology.* **103**, p55.

Wu, F., Caron, C., De Robertis, C., Khochbin, S. and Rousseaux, S. 2008. Testis-specific histone variants H2AL1/2 rapidly disappear from paternal heterochromatin after fertilization. *Journal of Reproduction and Development.* **54**(6), pp.413-417.

Wykes, S.M. and Krawetz, S.A. 2003. The structural organization of sperm chromatin. *Journal of Biological Chemistry.* **278**(32), pp.29471-29477.

Yagci, A., Murk, W., Stronk, J. and Huszar, G. 2010. Spermatozoa bound to solid state hyaluronic acid show chromatin structure with high DNA chain integrity: an acridine orange fluorescence study. *Journal of Andrology.* **31**(6), pp.566-572.

Yan Li, C.L., David Miller, Stephen A. Krawetz. 2008. Characterization of nucleohistone and nucleoprotamine components in the mature human sperm nucleus. *Asian J Androl* **10**(4), pp.535–541.

Yu, Y.E., Zhang, Y., Unni, E., Shirley, C.R., Deng, J.M., Russell, L.D., Weil, M.M., Behringer, R.R. and Meistrich, M.L. 2000. Abnormal spermatogenesis and reduced fertility in transition nuclear protein 1-deficient mice. *Proceedings of the National Academy of Sciences.* **97**(9), pp.4683-4688.

Zalenskaya, I.A., Bradbury, E.M. and Zalensky, A.O. 2000. Chromatin structure of telomere domain in human sperm. *Biochemical and Biophysical Research Communications.* **279**(1), pp.213-218.

Zalenskaya, I.A. and Zalensky, A.O. 2004. Non-random positioning of chromosomes in human sperm nuclei. *Chromosome Research.* **12**(2), pp.163-173.

Zalensky, A., Allen, M., Kobayashi, A., Zalenskaya, I., Balhorn, R. and Bradbury, E. 1995. Well-defined genome architecture in the human sperm nucleus. *Chromosoma.* **103**(9), pp.577-590.

Zalensky, A. and Zalenskaya, I. 2007. Organization of chromosomes in spermatozoa: an additional layer of epigenetic information? *Biochemical Society Transactions.* **35**(3), pp.609-611.

Zalensky, A.O., Breneman, J.W., Zalenskaya, I.A., Brinkley, B. and Bradbury, E.M. 1993. Organization of centromeres in the decondensed nuclei of mature human sperm. *Chromosoma.* **102**(8), pp.509-518.

Zalensky, A.O., Siino, J.S., Gineitis, A.A., Zalenskaya, I.A., Tomilin, N.V., Yau, P. and Bradbury, E.M. 2002. Human testis/sperm-specific histone H2B (hTSH2B) molecular cloning and characterization. *Journal of Biological Chemistry.* **277**(45), pp.43474-43480.

Zhang, Y., Liu, T., Meyer, C.A., Eeckhoute, J., Johnson, D.S., Bernstein, B.E., Nusbaum, C., Myers, R.M., Brown, M. and Li, W. 2008. Model-based analysis of ChIP-Seq (MACS). *Genome biology.* **9**(9), p1.

Zini, A., Meriano, J., Kader, K., Jarvi, K., Laskin, C.A. and Cadesky, K. 2005. Potential adverse effect of sperm DNA damage on embryo quality after ICSI. *Human Reproduction.* **20**(12), pp.3476-3480.

Zini, A. and Sigman, M. 2009. Are tests of sperm DNA damage clinically useful? Pros and cons. *Journal of Andrology.* **30**(3), pp.219-229.

Zlatanova, J. and Leuba, S.H. 2004. *Chromatin structure and dynamics: state-of-the-art.* Gulf Professional Publishing.

Zody, M.C., Garber, M., Adams, D.J., Sharpe, T., Harrow, J., Lupski, J.R., Nicholson, C., Searle, S.M., Wilming, L. and Young, S.K. 2006. DNA sequence of human chromosome 17 and analysis of rearrangement in the human lineage. *Nature.* **440**(7087), pp.1045-1049.

Appendix

1 Bioinformatics codes

1.1 MACS2 analyses (Bam files)

1.1.1 Human samples

1.1.1.2 Low salt samples

macs2 callpeak -t
D30_Halo_Low_Salt_Human_GCCAAT_L001_R1_001_val_1.fq.hg38.subread.bam
D31_Halo_Low_Salt_Human_TGACCA_L001_R1_001_val_1.fq.hg38.subread.bam
D32_Halo_Low_Salt_Human_CGATGT_L001_R1_001_val_1.fq.hg38.subread.bam

macs2 callpeak -c
D30_Pellet_Low_Salt_Human_ACAGTG_L001_R1_001_val_1.fq.hg38.subread.bam
D31_Pellet_Low_Salt_Human_TTAGGC_L001_R1_001_val_1.fq.hg38.subread.bam
D32_Pellet_Low_Salt_Human_ATCACG_L001_R1_001_val_1.fq.hg38.subread.bam
-n Hs_low_salt -f BAMPE --outdir /path/to/Hs_macs2_output -g hs --broad --bdg --
keep-dup 1

1.1.1.3 High salt samples

macs2 callpeak -t
Halo_DNA_4_Human_TAGCTT_L003_R1_001_val_1.fq.hg38.subread.bam
Halo_DNA_7_Human_CAGATC_L001_R1_001_val_1.fq.hg38.subread.bam
Halo_DNA_8_Human_AGTTCC_L003_R1_001_val_1.fq.hg38.subread.bam
Halo_DNA_9_Human_CCGTCC_L003_R1_001_val_1.fq.hg38.subread.bam \
macs2 callpeak -c
Pelleted_DNA_4_Human_GATCAG_L003_R1_001_val_1.fq.hg38.subread.bam
Pelleted_DNA_7_Human_GGCTAC_L003_R1_001_val_1.fq.hg38.subread.bam
Pelleted_DNA_8_Human_AGTCAA_L003_R1_001_val_1.fq.hg38.subread.bam
Pelleted_DNA_9_Human_ATGTCA_L003_R1_001_val_1.fq.hg38.subread.bam \
-n Hs_high_salt –f BAMPE –outdir /path/to/Hs_macs2_output –g hs –broad –bdg –
keep-dup 1

1.1.1.3 High salt samples

macs2 callpeak -t
D287_Halo_Halosperm_Human_GCCAAT_L001_R1_001_val_1.fq.hg38.subread.ba
m
D468_Halo_Halosperm_Human_TGACCA_L001_R1_001_val_1.fq.hg38.subread.ba
m
D476_Halo_Halosperm_Human_CGATGT_L001_R1_001_val_1.fq.hg38.subread.ba
m

macs2 callpeak -c
D287_Pellet_Halosperm_Human_ACAGTG_L001_R1_001_val_1.fq.hg38.subread.b
am
D468_Pellet_Halosperm_Human_TTAGGC_L001_R1_001_val_1.fq.hg38.subread.b
am
D476_Pellet_Halosperm_Human_ATCACG_L001_R1_001_val_1.fq.hg38.subread.b
am
-n Hs_Halosperm-f BAMPE --outdir /path/to/Hs_macs2_output -g hs --broad --bdg --
keep-dup 1

1.2 Bovine samples

1.2.1 High salt samples

macs2 callpeak -t
Halo_DNA_2_Bovine_CGATGT_L003_R1_001_val_1.fq.bosTau8.subread.bam
Halo_DNA_5_Bovine_TGACCA_L003_R1_001_val_1.fq.bosTau8.subread.bam
Halo_DNA_6_Bovine_GCCAAT_L003_R1_001_val_1.fq.bosTau8.subread.bam
HALO_DNA_7_Bovine_ACTTGA_L003_R1_001_val_1.fq.bosTau8.subread.bam \
macs2 callpeak -c
Pelleted_DNA_2_Bovine_ATCACG_L003_R1_001_val_1.fq.bosTau8.subread.bam
Pelleted_DNA_5_Bovine_TTAGGC_L003_R1_001_val_1.fq.bosTau8.subread.bam
Pelleted_DNA_6_Bovine_ACAGTG_L003_R1_001_val_1.fq.bosTau8.subread.bam
Pelleted_DNA_7_Bovine_CAGATC_L003_R1_001_val_1.fq.bosTau8.subread.bam \
-n Bovine_high_salt –f BAMPE –outdir /path/to/Bt_macs2_output –g hs –broad –bdg –keep-dup 1

1.2.2 low salt samples

macs2 callpeak -t
Boss_halo_Low_salt_Bovine_mpsclnu.bam
Class_halo_Low_salt_Bovine_mpsclnu.bam
M41b_halo_Low_salt_Bovine_mpsclnu.bam
Max_halo_Low_salt_Bovine_mpsclnu.bam

macs2 callpeak -c
Boss_pellet_Low_salt_Bovine_mpsclnu.bam
Class_pellet_Low_salt_Bovine_mpsclnu.bam
M40_pellet_Low_salt_Bovine_mpsclnu.bam
Max_pellet_Low_salt_Bovine_mpsclnu.bam
-n Bt_lowSalt_05May16 -f BAMPE –outdir /home /omics /Documents /analyses/Adel_DNA-seq/bovine_bam_04May16/MACS2_outputs --broad –bdg

1.3 Output files (tracking links)

1.3.1 Human

1.3.1.1 High salt samples (bigwig_URLs)

track type=bigWig name=D7_Human_highSalt_halo description=D7_Human_highSalt_halo visibility=2 color=0,102,153 autoScale=on graphType=bar windowingFunction=maximum smoothingWindow=off maxHeightPixels=30 bigDataUrl=https://s3-eu-west-1.amazonaws.com/omicsltd.millerstudents/Adel/D7_Human_highSalt_halo.bw

track type=bigWig name=D7_Human_highSalt_pellet description=D7_Human_highSalt_pellet visibility=2 color=102,102,153 autoScale=on graphType=bar windowingFunction=maximum smoothingWindow=off maxHeightPixels=30 bigDataUrl=https://s3-eu-west-1.amazonaws.com/omicsltd.millerstudents/Adel/D7_Human_highSalt_pellet.bw

track type=bigWig name=D8_Human_highSalt_halo description=D8_Human_highSalt_halo visibility=2 color=0,102,153 autoScale=on graphType=bar windowingFunction=maximum smoothingWindow=off maxHeightPixels=30 bigDataUrl=https://s3-eu-west-1.amazonaws.com/omicsltd.millerstudents/Adel/D8_Human_highSalt_halo.bw

track type=bigWig name=D8_Human_highSalt_pellet
description=D8_Human_highSalt_pellet visibility=2 color=102,102,153 autoScale=on
graphType=bar windowingFunction=maximum smoothingWindow=off
maxHeightPixels=30 bigDataUrl=https://s3-eu-west-
1.amazonaws.com/omicsltd.millerstudents/Adel/D8_Human_highSalt_pellet.bw

track type=bigWig name=D9_Human_highSalt_halo
description=D9_Human_highSalt_halo visibility=2 color=0,102,153 autoScale=on
graphType=bar windowingFunction=maximum smoothingWindow=off
maxHeightPixels=30 bigDataUrl=https://s3-eu-west-
1.amazonaws.com/omicsltd.millerstudents/Adel/D9_Human_highSalt_halo.bw

track type=bigWig name=D9_Human_highSalt_pellet
description=D9_Human_highSalt_pellet visibility=2 color=102,102,153 autoScale=on
graphType=bar windowingFunction=maximum smoothingWindow=off
maxHeightPixels=30 bigDataUrl=https://s3-eu-west-
1.amazonaws.com/omicsltd.millerstudents/Adel/D9_Human_highSalt_pellet.bw

track type=bigWig name=D4_Human_highSalt_halo
description=D4_Human_highSalt_halo visibility=2 color=0,102,153 autoScale=on
graphType=bar windowingFunction=maximum smoothingWindow=off
maxHeightPixels=30 bigDataUrl=https://s3-eu-west-
1.amazonaws.com/omicsltd.millerstudents/Adel/D4_Human_highSalt_halo.bw

track type=bigWig name=D4_Human_highSalt_pellet
description=D4_Human_highSalt_pellet visibility=2 color=102,102,153 autoScale=on
graphType=bar windowingFunction=maximum smoothingWindow=off
maxHeightPixels=30 bigDataUrl=https://s3-eu-west-
1.amazonaws.com/omicsltd.millerstudents/Adel/D4_Human_highSalt_pellet.bw

1.3.1.2 Low salt samples (bigwig_URLs),
track type=bigWig name=D32_Human_lowSalt_halo
description=D32_Human_lowSalt_halo visibility=2 color=0,102,153 autoScale=on
graphType=bar windowingFunction=maximum smoothingWindow=off
maxHeightPixels=30 bigDataUrl=https://s3-eu-west-
1.amazonaws.com/omicsltd.millerstudents/Adel/D32_Human_lowSalt_halo.bw

track type=bigWig name=D32_Human_lowSalt_pellet
description=D32_Human_lowSalt_pellet visibility=2 color=102,102,153 autoScale=on
graphType=bar windowingFunction=maximum smoothingWindow=off
maxHeightPixels=30 bigDataUrl=https://s3-eu-west-
1.amazonaws.com/omicsltd.millerstudents/Adel/D32_Human_lowSalt_pellet.bw

track type=bigWig name=D30_Human_lowSalt_halo
description=D30_Human_lowSalt_halo visibility=2 color=0,102,153 autoScale=on
graphType=bar windowingFunction=maximum smoothingWindow=off
maxHeightPixels=30 bigDataUrl=https://s3-eu-west-
1.amazonaws.com/omicsltd.millerstudents/Adel/D30_Human_lowSalt_halo.bw

track type=bigWig name=D30_Human_lowSalt_pellet
description=D30_Human_lowSalt_pellet visibility=2 color=102,102,153 autoScale=on
graphType=bar windowingFunction=maximum smoothingWindow=off
maxHeightPixels=30 bigDataUrl=https://s3-eu-west-
1.amazonaws.com/omicsltd.millerstudents/Adel/D30_Human_lowSalt_pellet.bw

track type=bigWig name=D31_Human_lowSalt_halo description=D31_Human_lowSalt_halo visibility=2 color=0,102,153 autoScale=on graphType=bar windowingFunction=maximum smoothingWindow=off maxHeightPixels=30 bigDataUrl=https://s3-eu-west-1.amazonaws.com/omicsltd.millerstudents/Adel/D31_Human_lowSalt_halo.bw

track type=bigWig name=D31_Human_lowSalt_pellet description=D31_Human_lowSalt_pellet visibility=2 color=102,102,153 autoScale=on graphType=bar windowingFunction=maximum smoothingWindow=off maxHeightPixels=30 bigDataUrl=https://s3-eu-west-1.amazonaws.com/omicsltd.millerstudents/Adel/D31_Human_lowSalt_pellet.bw

1.3.1.2 Halosperm samples (bigwig_URLs),

track type=bigWig name=D287_Human_haloSperm_halo description=D287_Human_haloSperm_halo visibility=2 color=0,102,153 autoScale=on graphType=bar windowingFunction=maximum smoothingWindow=off maxHeightPixels=30 bigDataUrl=https://s3-eu-west-1.amazonaws.com/omicsltd.millerstudents/Adel/D287_Human_haloSperm_halo.bw

track type=bigWig name=D287_Human_haloSperm_pellet description=D287_Human_haloSperm_pellet visibility=2 color=102,102,153 autoScale=on graphType=bar windowingFunction=maximum smoothingWindow=off maxHeightPixels=30 bigDataUrl=https://s3-eu-west-1.amazonaws.com/omicsltd.millerstudents/Adel/D287_Human_haloSperm_pellet.bw

track type=bigWig name=D468_Human_haloSperm_halo description=D287_Human_haloSperm_halo visibility=2 color=0,102,153 autoScale=on graphType=bar windowingFunction=maximum smoothingWindow=off maxHeightPixels=30 bigDataUrl=https://s3-eu-west-1.amazonaws.com/omicsltd.millerstudents/Adel/D287_Human_haloSperm_halo.bw

track type=bigWig name=D468_Human_haloSperm_pellet description=D287_Human_haloSperm_pellet visibility=2 color=102,102,153 autoScale=on graphType=bar windowingFunction=maximum smoothingWindow=off maxHeightPixels=30 bigDataUrl=https://s3-eu-west-1.amazonaws.com/omicsltd.millerstudents/Adel/D287_Human_haloSperm_pellet.bw

track type=bigWig name=D476_Human_haloSperm_halo description=D287_Human_haloSperm_halo visibility=2 color=0,102,153 autoScale=on graphType=bar windowingFunction=maximum smoothingWindow=off maxHeightPixels=30 bigDataUrl=https://s3-eu-west-1.amazonaws.com/omicsltd.millerstudents/Adel/D287_Human_haloSperm_halo.bw

track type=bigWig name=D476_Human_haloSperm_pellet description=D287_Human_haloSperm_pellet visibility=2 color=102,102,153 autoScale=on graphType=bar windowingFunction=maximum smoothingWindow=off maxHeightPixels=30 bigDataUrl=https://s3-eu-west-1.amazonaws.com/omicsltd.millerstudents/Adel/D287_Human_haloSperm_pellet.bw

1.3.2 bovine

1.3.2.1 High salt samples (bigwig_URLs),

track type=bigWig name=D2_Bovine_highSalt_halo description=D2_Bovine_highSalt_halo visibility=2 color=0,102,153 autoScale=on graphType=bar windowingFunction=maximum smoothingWindow=off maxHeightPixels=30 bigDataUrl=https://s3-eu-west-1.amazonaws.com/omicsltd.millerstudents/Adel/D2_Bovine_highSalt_halo.bw

track type=bigWig name=D2_Bovine_highSalt_pellet description=D2_Bovine_highSalt_pellet visibility=2 color=102,102,153 autoScale=on graphType=bar windowingFunction=maximum smoothingWindow=off maxHeightPixels=30 bigDataUrl=https://s3-eu-west-1.amazonaws.com/omicsltd.millerstudents/Adel/D2_Bovine_highSalt_pellet.bw

track type=bigWig name=D6_Bovine_highSalt_halo description=D6_Bovine_highSalt_halo visibility=2 color=0,102,153 autoScale=on graphType=bar windowingFunction=maximum smoothingWindow=off maxHeightPixels=30 bigDataUrl=https://s3-eu-west-1.amazonaws.com/omicsltd.millerstudents/Adel/D6_Bovine_highSalt_halo.bw

track type=bigWig name=D6_Bovine_highSalt_pellet description=D6_Bovine_highSalt_pellet visibility=2 color=102,102,153 autoScale=on graphType=bar windowingFunction=maximum smoothingWindow=off maxHeightPixels=30 bigDataUrl=https://s3-eu-west-1.amazonaws.com/omicsltd.millerstudents/Adel/D6_Bovine_highSalt_pellet.bw

track type=bigWig name=D5_Bovine_highSalt_halo description=D5_Bovine_highSalt_halo visibility=2 color=0,102,153 autoScale=on graphType=bar windowingFunction=maximum smoothingWindow=off maxHeightPixels=30 bigDataUrl=https://s3-eu-west-1.amazonaws.com/omicsltd.millerstudents/Adel/D5_Bovine_highSalt_halo.bw

track type=bigWig name=D5_Bovine_highSalt_pellet description=D5_Bovine_highSalt_pellet visibility=2 color=102,102,153 autoScale=on graphType=bar windowingFunction=maximum smoothingWindow=off maxHeightPixels=30 bigDataUrl=https://s3-eu-west-1.amazonaws.com/omicsltd.millerstudents/Adel/D5_Bovine_highSalt_pellet.bw

track type=bigWig name=D7_Bovine_highSalt_halo description=D7_Bovine_highSalt_halo visibility=2 color=0,102,153 autoScale=on graphType=bar windowingFunction=maximum smoothingWindow=off maxHeightPixels=30 bigDataUrl=https://s3-eu-west-1.amazonaws.com/omicsltd.millerstudents/Adel/D7_Bovine_highSalt_halo.bw

track type=bigWig name=D7_Bovine_highSalt_pellet description=D7_Bovine_highSalt_pellet visibility=2 color=102,102,153 autoScale=on graphType=bar windowingFunction=maximum smoothingWindow=off maxHeightPixels=30 bigDataUrl=https://s3-eu-west-1.amazonaws.com/omicsltd.millerstudents/Adel/D7_Bovine_highSalt_pellet.bw

1.3.2.2 Low salt samples (bigwig_URLs),

track type=bigWig name=M40_Bovine_lowSalt_pellet description=M40_Bovine_lowSalt_pellet visibility=2 color=102,102,153 autoScale=on

graphType=bar windowingFunction=maximum smoothingWindow=off maxHeightPixels=30 bigDataUrl=https://s3-eu-west-1.amazonaws.com/omicsltd.millerstudents/Adel/M40_Bovine_lowSalt_pellet.bw

track type=bigWig name=M41b_Bovine_lowSalt_halo description=M41b_Bovine_lowSalt_halo visibility=2 color=0,102,153 autoScale=on graphType=bar windowingFunction=maximum smoothingWindow=off maxHeightPixels=30 bigDataUrl=https://s3-eu-west-1.amazonaws.com/omicsltd.millerstudents/Adel/M41b_Bovine_lowSalt_halo.bw

track type=bigWig name=Max_Bovine_lowSalt_halo description=Max_Bovine_lowSalt_halo visibility=2 color=0,102,153 autoScale=on graphType=bar windowingFunction=maximum smoothingWindow=off maxHeightPixels=30 bigDataUrl=https://s3-eu-west-1.amazonaws.com/omicsltd.millerstudents/Adel/Max_Bovine_lowSalt_halo.bw

track type=bigWig name=Max_Bovine_lowSalt_pellet description=Max_Bovine_lowSalt_pellet visibility=2 color=102,102,153 autoScale=on graphType=bar windowingFunction=maximum smoothingWindow=off maxHeightPixels=30 bigDataUrl=https://s3-eu-west-1.amazonaws.com/omicsltd.millerstudents/Adel/Max_Bovine_lowSalt_pellet.bw

track type=bigWig name=Class_Bovine_lowSalt_halo description=Class_Bovine_lowSalt_halo visibility=2 color=0,102,153 autoScale=on graphType=bar windowingFunction=maximum smoothingWindow=off maxHeightPixels=30 bigDataUrl=https://s3-eu-west-1.amazonaws.com/omicsltd.millerstudents/Adel/Class_Bovine_lowSalt_halo.bw

track type=bigWig name=Boss_Bovine_lowSalt_halo description=Boss_Bovine_lowSalt_halo visibility=2 color=0,102,153 autoScale=on graphType=bar windowingFunction=maximum smoothingWindow=off maxHeightPixels=30 bigDataUrl=https://s3-eu-west-1.amazonaws.com/omicsltd.millerstudents/Adel/Boss_Bovine_lowSalt_halo.bw

track type=bigWig name=Boss_Bovine_lowSalt_pellet description=Boss_Bovine_lowSalt_pellet visibility=2 color=102,102,153 autoScale=on graphType=bar windowingFunction=maximum smoothingWindow=off maxHeightPixels=30 bigDataUrl=https://s3-eu-west-1.amazonaws.com/omicsltd.millerstudents/Adel/Boss_Bovine_lowSalt_pellet.bw

1.3.3 Saman's nucleosomal data

1.3.3.1 Human

https://s3-eu-west-1.amazonaws.com/omicsltd.millerstudents/Adel/Hs_nucleosomes_13May16_peaks.ed.broadPeak

track type=bigWig name=Hs_nucleosomes.bw description=Hs_nucleosomes_pileup visibility=2 color=0,102,153 autoScale=on graphType=bar windowingFunction=maximum smoothingWindow=off maxHeightPixels=30 bigDataUrl=https://s3-eu-west-1.amazonaws.com/omicsltd.millerstudents/Adel/Hs_nucleosomes_noControl_13May16_treat_pileup.bw

1.3.3.2 Bovine

https://s3-eu-west-1.amazonaws.com/omicsltd.millerstudents/Adel/Bt_nucleosomes_14May16_peaks.ed.broadPeak

1.4 QC and *fastq* processing

The command line ($ fastqc *fq.gz)
And later, trim_galore using the following options;
$ trim_galore --fastqc --paired --dont_gzip

1.5 Alignments

> readfile1 <- list.files (path='/full/path/to/validated_reads', pattern='*val_1.fq', full.names=TRUE)
> readfile2 <- list.files (path='/full/path/to/validated_reads', pattern='*val_2.fq', full.names=TRUE)
> setwd ('/full/path/to/genome/index')
> align ('<name of the genome index inserted here>_index', readfile1, readfile2, input_format="FASTQ",output_file=paste(readfile1,"bam",sep="."), nthreads=8, unique=FALSE, nBestLocations=1, minFragLength=30, maxFragLength=1000)

1.6 GAT commands

1.6.1 Gene features

$ gat-run.py \
--segment-file=Hs_high_salt_peaks.broadPeak \
--workspace-file=hg38_gapped_genome.bed \
--annotation-file=hg38_annotations_18Dec15.bed \
--isochore-bed-file=hg38.isochores.tab \
--ignore-segment-tracks \
--num-samples=10000 \
--log=highSalt_vs_hg38genes_10e4_gat_08Jan16.log >
highSalt_vs_hg38genes_10e4_gat_08Jan16.tsv

1.6.2 Promoters

$ gat-run.py \
--segment-file=Hs_high_salt_peaks.broadPeak \
--workspace-file=hg38_gapped_genome.bed \
--annotation-file=hg38_promoters_merged_anno \
--isochore-bed-file=hg38.isochores.tab \
--ignore-segment-tracks \
--num-samples=10000 \
--log=highSalt_vs_hg38promoters_10e4_gat_08Jan16.log >
highSalt_vs_hg38promoters_10e4_gat_08Jan16.tsv

1.6.3 Repeats

$ gat-run.py \
--segment-file=Hs_high_salt_peaks.broadPeak \
--workspace-file=hg38_gapped_genome.bed \
--annotation-file=repeatMask_anno_frequent \
--isochore-bed-file=hg38.isochores.tab \
--ignore-segment-tracks \
--num-samples=10000 \

```
--log=highSalt_vs_hg38rmsk_red_10e4_gat_08Jan16.log >
highSalt_vs_hg38rmsk_red_10e4_gat_08Jan16.tsv
```

1.6.4 Non-coding RNAs

```
$ gat-run.py \
--segment-file=Hs_high_salt_peaks.broadPeak \
--workspace-file=hg38_gapped_genome.bed \
--annotation-file=linc_anno \
--isochore-bed-file=hg38.isochores.tab \
--ignore-segment-tracks \
--num-samples=10000 \
--log=highSalt_vs_hg38linc_10e4_gat_08Jan16.log >
highSalt_vs_hg38linc_10e4_gat_08Jan16.tsv
```

1.6.5 CpG islands

```
$ gat-run.py \
--segment-file=Hs_high_salt_peaks.broadPeak \
--workspace-file=hg38_gapped_genome.bed \
--annotation-file=hg38_CpGislands_15Dec15.sorted.txt \
--isochore-bed-file=hg38.isochores.tab \
--ignore-segment-tracks \
--num-samples=10000 \
--log=highSalt_vs_hg38CpGi_10e4_gat_08Jan16.log >
highSalt_vs_hg38CpGi_10e4_gat_08Jan16.tsv
```

2 Enrichment regions in halo and nucleoid fractions (top 100)

2.1 Human samples

2.1.1 Low salt (halo-enriched)

GeneID	Chr	logFC	logCPM	PValue	FDR	symbol
NM_001168378	chr3	-5.6860	5.341707	8.08E-07	0.000824	ZIC4
NM_030935	chr7	-5.0666	5.105007	0.000165	0.020645	TSC22D4
NR_131942	chr2	-4.6596	5.344574	0.005844	0.145689	LOC102725079
NM_001244644	chr3	-4.6497	4.615399	0.000983	0.053726	CHMP2B
NM_207518	chr19	-4.5009	5.238224	0.004758	0.129632	PRKACA
NM_001110354	chr7	-4.3641	4.929097	0.016817	0.249963	ZP3
NM_001303619	chr18	-4.3038	4.7765	0.005336	0.139296	CD226
NM_006208	chr6	-4.3035	4.779699	0.005336	0.139296	ENPP1
NM_052907	chr12	-4.3034	4.820717	0.005336	0.139296	TMEM132B
NM_002312	chr13	-4.2168	5.440202	7.79E-05	0.012704	LIG4
NM_001200016	chr3	-4.1319	5.594879	7.08E-06	0.003115	NAT6
NM_012192	chr11	-4.1176	4.64456	0.016623	0.248321	TIMM10B
NR_029500	chr2	-4.1152	5.606639	2.5E-06	0.001668	MIR26B
NM_032496	chr12	-4.0837	4.876238	0.018789	0.265115	ARHGAP9
NM_001107	chr14	-4.0393	4.943147	5.54E-06	0.002631	ACYP1
NM_001005466	chr14	-4.0342	4.9081	0.026312	0.309584	OR10G2
NM_014947	chr1	-3.8772	5.103838	0.039401	0.376215	FOXJ3
NR_030279	chr1	-3.8511	4.749124	0.031195	0.336955	MIR553
NM_001172477	chr8	-3.8511	4.544381	0.031245	0.336955	RRM2B
NM_001167924	chr3	-3.8472	4.595231	0.02898	0.325424	CMSS1
NM_001286780	chr4	-3.8471	4.673999	0.02898	0.325424	ANTXR2
NM_144601	chr16	-3.8471	4.786028	0.02898	0.325424	CMTM3
NM_032870	chr6	-3.8471	4.597384	0.02898	0.325424	PNISR
NM_001136475	chr1	-3.8469	4.802575	0.02898	0.325424	VASH2
NM_000645	chr1	-3.8453	4.955205	0.046684	0.405533	AGL
NM_001306147	chr4	-3.8073	5.409549	0.000338	0.030412	SEPT11
NM_001080533	chr12	-3.7414	5.511744	0.005612	0.14305	UNC119B
NM_016218	chr5	-3.6502	5.155871	7.53E-07	0.000824	POLK
NM_001300959	chr7	-3.5971	5.592249	0.002478	0.09036	ZMIZ2
NM_001130688	chr4	-3.4688	4.761992	0.000611	0.041947	HMGB2
NR_120517	chr7	-3.4346	6.003261	3.68E-05	0.008237	LOC102723885
NM_001172	chr14	-3.3529	5.951044	8E-06	0.003182	ARG2
NM_000831	chr1	-3.3161	5.965159	1.22E-08	9.2E-05	GRIK3
NM_206937	chr13	-3.3024	5.475245	2.98E-06	0.001931	LIG4
NR_039813	chr9	-3.2689	5.291416	0.000622	0.042465	MIR4667
NR_037619	chr16	-3.2487	5.29146	0.001589	0.070477	CMTM3
NR_039648	chr3	-3.2144	5.006702	0.002831	0.098539	MIR4446
NM_198467	chr7	-3.1066	5.635989	1.99E-05	0.005532	RSBN1L
NM_004388	chr1	-3.0801	5.665993	9.36E-05	0.014048	CTBS
NM_152763	chr1	-3.0680	5.350477	0.006032	0.147302	AKNAD1
NM_024960	chr20	-3.0678	5.473611	0.0006	0.04163	PANK2
NR_045682	chr2	-3.0678	5.142217	0.006032	0.147302	MYO3B
NM_001289608	chr11	-3.0655	4.792794	0.009345	0.186953	SYTL2
NM_025029	chr2	-3.0541	6.318879	1.56E-07	0.000322	MZT2B
NM_017849	chr2	-3.0006	5.143597	0.001874	0.076808	TMEM127
NM_153366	chr9	-2.9878	6.180547	0.000951	0.053358	SVEP1
NM_001086	chr3	-2.9545	4.679853	0.03998	0.376392	AADAC
NM_001145541	chr11	-2.9476	5.906197	5.57E-06	0.002631	TCP11L1
NM_020395	chr4	-2.9441	4.958148	0.000822	0.050083	INTS12

NM_001244815	chr3	-2.9404	5.311381	0.001332	0.063804	FOXP1
NM_001001701	chr4	-2.9319	6.104243	2.48E-06	0.001668	C4orf3
NM_001164440	chr5	-2.9239	5.988831	0.000236	0.024763	ANKRD33B
NR_039773	chr5	-2.9100	4.776388	0.030519	0.332972	MIR3977
NM_001258357	chr2	-2.9068	5.028643	0.013839	0.226086	HPCAL1
NM_001166386	chrX	-2.9053	4.932071	0.012746	0.218901	MAGEA12
NM_001199839	chr14	-2.9052	4.835239	0.012746	0.218901	BCL2L2
NM_001134285	chr1	-2.9010	4.821969	0.020923	0.27825	ESRRG
NM_176877	chr1	-2.8789	6.025016	8.78E-07	0.000826	PATJ
NM_000989	chr8	-2.8561	6.082723	3.38E-06	0.00207	RPL30
NM_001001330	chr10	-2.8504	5.973926	0.001033	0.05559	REEP3
NM_003683	chr21	-2.8475	5.641318	0.001669	0.071909	RRP1
NM_019051	chr9	-2.8330	5.432395	0.000691	0.045118	MRPL50
NM_003302	chr7	-2.8307	5.832424	3.18E-05	0.007494	TRIP6
NM_016255	chr6	-2.8287	5.896108	0.000209	0.023563	FAM8A1
NM_199051	chr1	-2.8013	5.426914	0.000257	0.025528	BRINP3
NM_001289145	chr20	-2.7631	5.334729	0.012657	0.218613	FAM110A
NM_003013	chr4	-2.7550	6.265404	1.48E-05	0.004789	SFRP2
NM_145280	chr2	-2.7537	5.406015	0.007728	0.171861	METTL21A
NM_015188	chr10	-2.7516	5.698448	0.000111	0.015479	TBC1D12
NM_001291976	chr4	-2.7493	5.369593	0.005783	0.145452	SPARCL1
NM_001271457	chr11	-2.7479	5.458626	6.5E-05	0.011505	COLCA2
NM_018076	chr10	-2.7451	5.196556	0.008925	0.183023	ARMC4
NM_000921	chr12	-2.7407	6.116746	4.03E-06	0.002229	PDE3A
NM_001039582	chrX	-2.7396	5.616863	3.04E-05	0.007402	PNCK
NM_177404	chrX	-2.7343	5.058659	0.004038	0.117917	MAGEB1
NM_022073	chr14	-2.7329	6.334383	1.17E-05	0.004139	EGLN3
NM_001308294	chr16	-2.7324	5.168787	0.002588	0.092635	SH2B1
NM_001102612	chr15	-2.7316	5.011096	0.003745	0.113906	PGPEP1L
NM_001142557	chr5	-2.7313	4.646359	0.030895	0.335696	HMMR
NM_152402	chr4	-2.7313	6.269349	0.000185	0.021518	TRAM1L1
NR_030753	chr12	-2.7235	5.658582	0.001497	0.068244	MIR615
NR_125430	chr8	-2.7218	4.925065	0.026653	0.311175	LOC101929066
NM_014181	chr2	-2.7145	6.589021	3.97E-06	0.002229	LGALSL
NM_013435	chr18	-2.7113	6.372631	3.8E-07	0.000573	RAX
NM_001007563	chr9	-2.7095	5.837264	1.27E-07	0.000321	IGFBPL1
NM_006670	chr6	-2.7082	6.665384	3.15E-08	0.000179	TPBG
NM_017658	chr14	-2.6712	5.946476	6.82E-07	0.000824	KLHL28
NR_120472	chr12	-2.6657	5.484063	0.000625	0.04251	LOC101928471
NR_122079	chr4	-2.6603	5.907939	9.11E-07	0.000826	LOC439933
NR_120547	chr11	-2.6504	5.01875	0.01004	0.192808	WT1-AS
NM_001101341	chr14	-2.6442	7.058957	8.2E-07	0.000824	SFTA3
NM_003248	chr5	-2.6424	6.215118	2.73E-05	0.007108	THBS4
NM_017567	chr2	-2.6398	6.4765	8.98E-06	0.003508	NAGK
NM_005190	chr6	-2.6296	5.679415	2.93E-05	0.007294	CCNC
NM_033427	chr7	-2.6189	6.440959	4.91E-08	0.000215	CTTNBP2
NR_125937	chr4	-2.6108	5.239436	0.005214	0.137377	LOC102724776
NM_001297704	chr1	-2.6106	5.171448	0.005214	0.137377	ADGRL2
NM_170606	chr7	-2.5944	6.219439	2.34E-06	0.001668	KMT2C
NM_024829	chr12	-2.5929	5.569814	0.001832	0.075527	PLBD1
NM_018275	chr7	-2.5910	5.712773	0.001843	0.07579	C7orf43

2.1.2 Low salt (nucleoid-enriched)

GeneID	Chr	logFC	logCPM	PValue	FDR	symbol
NM_033142	chr19	6.0862	5.662486	7.56E-05	0.012556	CGB7
NM_001318151	chr22	5.2808	5.501844	4.92E-05	0.00979	MRPL40
NM_005061	chr16	5.2051	5.324402	8.6E-05	0.013257	RPL3L
NM_001282131	chr17	4.9682	5.442089	0.002474	0.09036	SSH2
NM_013347	chrX	4.9497	5.146912	0.000458	0.036494	RPA4
NM_001242894	chr6	4.9492	5.214904	0.000482	0.036731	ZKSCAN3
NM_001142674	chr11	4.9461	5.353929	0.001856	0.076188	CHID1
NR_110931	chr16	4.8535	5.156348	0.0008	0.049425	LOC101927817
NM_005516	chr6	4.8502	5.31058	0.001147	0.058956	HLA-E
NR_039697	chr9	4.7397	5.361446	0.015247	0.236327	MIR4479
NM_024733	chr19	4.6531	5.368865	0.009146	0.184629	ZNF665
NR_004390	chr11	4.6451	4.973157	0.009576	0.188859	SNORA57
NM_001042367	chr15	4.6395	4.847019	0.002444	0.089469	REC114
NM_001199954	chr17	4.6395	5.190451	0.002444	0.089469	ACTG1
NM_033176	chr20	4.6394	5.046314	0.002444	0.089469	NKX2-4
NM_001018138	chr17	4.6393	4.868385	0.002444	0.089469	NME2
NM_007219	chr20	4.6393	4.91769	0.002444	0.089469	RNF24
NM_001319138	chr20	4.6381	5.310398	0.003084	0.103373	GDF5
NM_001169	chr16	4.6352	5.079184	0.003648	0.112174	AQP8
NM_001001410	chr16	4.5192	5.132669	0.004271	0.121439	TSR3
NM_001135676	chr8	4.5191	4.980865	0.004271	0.121439	SMIM19
NM_016148	chr19	4.5191	5.085487	0.004271	0.121439	SHANK1
NR_031573	chr19	4.5191	5.002152	0.004271	0.121439	MIR1283-1
NM_019844	chr12	4.5162	4.88825	0.006714	0.158	SLCO1B3
NM_001204159	chr19	4.5025	5.120104	0.011958	0.212363	SPHK2
NM_006978	chrX	4.3886	4.83109	0.00777	0.171879	RNF113A
NM_001320792	chr19	4.3880	4.954837	0.007465	0.168328	ZNF544
NM_004278	chr17	4.3879	4.892711	0.007465	0.168328	PIGL
NM_203347	chr9	4.3879	5.005519	0.007465	0.168328	LCN15
NM_002427	chr11	4.3878	4.839682	0.007465	0.168328	MMP13
NM_024653	chr7	4.3878	4.952905	0.007465	0.168328	PRKRIP1
NM_005337	chr12	4.3871	5.013973	0.008875	0.182823	NCKAP1L
NM_001164425	chr19	4.3868	4.925795	0.025283	0.301472	MBD3L3
NM_001004699	chr19	4.3737	5.015562	0.021819	0.285009	OR2Z1
NM_018159	chrX	4.3703	5.04334	0.017718	0.256384	NUDT11
NM_001281444	chr20	4.2517	5.186008	0.027797	0.318949	PKIG
NR_029840	chr11	4.2493	4.860234	0.015593	0.239077	MIR34C
NM_001012978	chrX	4.2461	4.825037	0.017836	0.257275	BEX5
NM_001168531	chrX	4.2441	4.925116	0.013416	0.22231	ASB9
NR_030203	chr19	4.2436	4.953315	0.01305	0.220642	MIR521-2
NM_003992	chr15	4.2435	4.920185	0.01305	0.220642	CLK3
NM_001083601	chr16	4.2435	5.178831	0.01305	0.220642	NAA60
NM_031440	chr3	4.2371	5.045423	0.018172	0.260625	RTP3
NM_024877	chr19	4.2302	4.98531	0.021192	0.278881	CNTD2
NM_001286429	chr15	4.0907	5.060243	0.030286	0.331961	THSD4
NM_002034	chr19	4.0832	5.142963	0.022815	0.289152	FUT5
NM_001288762	chr19	4.0831	4.592816	0.022815	0.289152	ZNF180
NM_001243764	chr1	4.0831	4.849201	0.022815	0.289152	RABGAP1L
NM_001013848	chr10	4.0831	5.023811	0.022815	0.289152	EXOC6
NM_021052	chr6	4.0831	4.739297	0.022815	0.289152	HIST1H2AE
NM_172251	chr19	4.0831	5.059468	0.022815	0.289152	MRPL54
NM_033185	chr17	4.0830	4.714812	0.022815	0.289152	KRTAP3-3

NM_001282145	chrX	4.0823	4.956917	0.034121	0.351298	NLGN4X
NM_001039709	chr20	4.0823	4.930686	0.038171	0.372037	CBFA2T2
NM_001005752	chr1	4.0817	4.918114	0.045058	0.398536	GJB3
NM_015884	chrX	4.0804	4.920045	0.02467	0.299166	MBTPS2
NR_111989	chr17	4.0795	5.135462	0.036446	0.36383	PGS1
NM_173598	chr12	4.0788	4.751867	0.041774	0.383957	KSR2
NM_019016	chr17	4.0770	4.763981	0.031041	0.336704	KRT24
NM_000894	chr19	4.0759	4.925357	0.040296	0.37765	LHB
NM_001289114	chr17	4.0718	4.978483	0.036499	0.364046	SHBG
NM_139158	chr2	4.0702	4.968141	0.039484	0.376215	CDK15
NR_039911	chr20	3.9101	4.880404	0.049014	0.415612	MIR4755
NR_039609	chr5	3.9070	5.04448	0.043837	0.393073	MIR378E
NR_031568	chr19	3.9048	5.04467	0.047669	0.410022	MIR1323
NM_020742	chrX	3.9032	4.93311	0.045448	0.399905	NLGN4X
NM_030763	chrX	3.9027	4.895809	0.039892	0.376215	HMGN5
NR_002604	chr17	3.9026	4.957308	0.040325	0.377762	SNORD10
NM_001167749	chr1	3.9026	4.744227	0.039892	0.376215	ADCY10
NM_001171137	chr9	3.9026	5.051597	0.039892	0.376215	STRBP
NM_001199281	chr22	3.9026	4.913755	0.039892	0.376215	CABIN1
NR_026886	chr11	3.9026	4.944023	0.039892	0.376215	LRTOMT
NM_001163558	chr6	3.9026	4.718912	0.039892	0.376215	PRL
NM_001318152	chr22	3.9026	5.048735	0.039892	0.376215	MRPL40
NM_021014	chrX	3.9026	4.937228	0.039892	0.376215	SSX3
NM_001288826	chr5	3.9025	4.810001	0.039892	0.376215	GDF9
NM_001190242	chr3	3.9025	4.700734	0.039892	0.376215	IFT80
NM_002195	chr9	3.9025	4.824817	0.039892	0.376215	INSL4
NM_032464	chr7	3.9025	4.648329	0.039892	0.376215	LAT2
NM_001320876	chr15	3.9025	4.84668	0.039892	0.376215	DPP8
NM_001080140	chrX	3.9025	4.906325	0.039892	0.376215	CT47A7
NM_005212	chr4	3.9021	4.74663	0.045715	0.40091	CSN3
NR_030370	chr19	3.9019	4.916294	0.049177	0.416128	MIR640
NM_006912	chr1	3.8988	4.858988	0.048171	0.412391	RIT1
NM_020191	chr3	3.8981	4.984255	0.043975	0.39367	MRPS22
NM_016641	chr16	3.6814	5.504061	0.00018	0.021359	GDE1
NM_152221	chr22	3.5815	5.454389	0.004198	0.120681	CSNK1E
NM_144570	chr16	3.4807	5.347213	0.003003	0.101868	HN1L
NM_000526	chr17	3.4751	5.277509	0.002807	0.097849	KRT14
NM_001172663	chr16	3.4712	5.468637	0.001067	0.056472	RAB40C
NM_004558	chr19	3.4390	6.117242	0.000134	0.017985	NRTN
NM_024855	chr20	3.4021	5.370664	0.000449	0.036341	ACTR5
NM_000120	chr1	3.4020	5.217563	0.000449	0.036341	EPHX1
NM_002794	chr1	3.3224	5.382503	0.001157	0.059195	PSMB2
NM_138393	chr19	3.2616	5.509092	0.011197	0.204243	REEP6
NR_023360	chr8	3.2459	5.197101	0.001241	0.061236	CHRAC1
NM_001193465	chr17	3.1631	5.567573	0.003421	0.108733	KANSL1
NM_017729	chr19	3.1611	5.437513	0.002056	0.080987	EPS8L1
NM_001286836	chr9	3.1609	5.012474	0.002056	0.080987	CBWD5
NM_024698	chr11	3.1446	5.685345	0.00112	0.057961	SLC25A22

2.1.3 High salt (halo-enriched)

GeneID	Chr	logFC	logCPM	PValue	FDR	symbol
NM_173587	chr11	-6.0098	6.588942	3.25E-05	0.003951	RCOR2
NM_022467	chr19	-5.9121	6.89639	7.74E-06	0.001583	CHST8
NM_005632	chr16	-5.8049	6.600528	5.18E-06	0.001263	CAPN15
NM_001319108	chr22	-5.7534	6.370243	8.13E-06	0.001608	OSM
NM_007046	chr2	-5.6907	6.629908	3.44E-05	0.0041	EMILIN1
NM_173804	chr19	-5.6700	6.548929	1.3E-05	0.002168	TMEM86B
NM_014181	chr2	-5.6553	6.589021	9.14E-05	0.007845	LGALSL
NM_022835	chr19	-5.6422	6.459767	3.46E-05	0.004109	PLEKHG2
NM_001017963	chr14	-5.6285	6.557519	5.96E-05	0.006113	HSP90AA1
NM_001161498	chr14	-5.6237	6.455784	3.91E-05	0.004494	PLEKHD1
NM_198573	chr9	-5.6230	6.950914	2.27E-05	0.00322	ENHO
NM_003580	chr8	-5.6226	6.643424	0.000216	0.013482	NSMAF
NM_199242	chr17	-5.5791	6.466323	4.69E-05	0.005169	UNC13D
NM_001278639	chr22	-5.5732	6.269347	0.000133	0.009946	RANBP1
NM_003195	chr20	-5.5633	6.660265	0.000108	0.008745	TCEA2
NM_020247	chr1	-5.5530	6.640355	0.000282	0.015995	ADCK3
NM_001318506	chr16	-5.4996	6.437421	0.000213	0.01339	CES4A
NM_018725	chr3	-5.4941	6.089068	0.00019	0.012578	IL17RB
NM_002567	chr12	-5.4814	6.281525	0.000396	0.019573	PEBP1
NM_207370	chr1	-5.4733	6.293759	0.00025	0.014766	GPR153
NM_001195072	chr22	-5.4683	6.405689	5.27E-05	0.005629	TMEM184B
NM_001278641	chr22	-5.4406	6.272633	8.48E-05	0.007503	RANBP1
NM_145798	chr17	-5.4010	6.279061	0.000491	0.021546	OSBPL7
NM_001080453	chr7	-5.3952	6.425422	0.000179	0.012163	INTS1
NM_000428	chr14	-5.3882	6.473622	0.000222	0.013778	LTBP2
NM_002773	chr16	-5.3715	6.017166	5.71E-05	0.005961	PRSS8
NM_001081563	chr19	-5.2902	6.212366	0.000394	0.019529	DMPK
NM_013348	chr19	-5.2901	6.164757	0.000271	0.015645	KCNJ14
NM_033309	chr16	-5.2852	6.694872	0.000852	0.029577	B3GNT9
NM_001702	chr8	-5.2837	6.163261	9.41E-05	0.00796	ADGRB1
NM_033425	chr11	-5.2805	6.291548	0.000123	0.009515	DIXDC1
NM_004998	chr15	-5.2798	6.338205	0.000313	0.017025	MYO1E
NM_001267560	chr19	-5.2748	6.057897	0.000152	0.010974	TJP3
NM_015492	chr15	-5.2692	6.548035	0.000678	0.025847	C15orf39
NM_198722	chr3	-5.2604	6.278157	0.001069	0.033698	AMIGO3
NM_001270945	chr1	-5.2472	6.333351	0.000215	0.013473	LOC643355
NM_016239	chr17	-5.2410	6.48936	0.000467	0.020922	MYO15A
NM_001065	chr12	-5.2286	5.995971	0.000444	0.020624	TNFRSF1A
NM_001290190	chr19	-5.2210	5.877207	0.000888	0.030309	MYADM
NM_207413	chr8	-5.2198	6.399822	0.000212	0.013355	FAM150A
NM_013401	chr11	-5.1856	6.220696	0.000523	0.022374	RAB3IL1
NM_001113496	chr17	-5.1840	6.203313	0.000226	0.01393	SEPT9
NM_138401	chr19	-5.1834	6.007561	0.000507	0.021981	MVB12A
NM_003459	chr2	-5.1814	6.197848	0.001126	0.03458	SLC30A3
NM_003437	chr19	-5.1808	6.006304	0.000473	0.021021	ZNF136
NM_145807	chr19	-5.1801	6.021303	0.000951	0.031501	NTN5
NM_001243646	chr16	-5.1783	5.931612	0.001191	0.035753	CD2BP2
NM_145214	chr1	-5.1779	6.126593	0.000424	0.020128	TRIM11
NM_025268	chr14	-5.1712	6.248898	0.000713	0.026438	TMEM121
NM_153254	chr1	-5.1704	6.206335	0.000955	0.031501	TTLL10
NM_032488	chr19	-5.1570	5.86915	0.000954	0.031501	CNFN
NM_006477	chr22	-5.1567	6.541378	0.000539	0.022675	RASL10A

NM_015175	chr3	-5.1544	6.030653	0.000268	0.015554	NBEAL2
NM_178812	chr8	-5.1296	6.435138	0.000188	0.012555	MTDH
NM_018009	chr12	-5.1250	5.998018	0.000365	0.018828	TAPBPL
NM_000199	chr17	-5.0985	6.00301	0.000182	0.01231	SGSH
NM_001129	chr7	-5.0931	6.085851	0.001139	0.03475	AEBP1
NM_201379	chr8	-5.0807	6.224882	0.000392	0.019511	PLEC
NM_005481	chr19	-5.0804	6.112121	0.00038	0.019176	MED16
NM_005462	chrX	-5.0762	6.051548	0.000276	0.015797	MAGEC1
NM_001145722	chr19	-5.0680	6.02821	0.00044	0.020578	HOMER3
NM_015164	chr1	-5.0538	6.176831	0.000617	0.02452	PLEKHM2
NM_001311	chr14	-5.0537	6.271323	0.000256	0.015012	CRIP1
NM_001162407	chr2	-5.0455	6.459078	0.000224	0.013872	CLK1
NM_003012	chr8	-5.0373	6.335904	0.000803	0.028301	SFRP1
NM_018509	chr17	-5.0186	6.070205	0.00064	0.025011	LRRC59
NM_020378	chr19	-5.0026	6.152421	0.000897	0.030483	NAT14
NR_106801	chr11	-5.0006	5.544991	0.000404	0.019627	MIR6743
NM_015871	chr1	-4.9982	5.976424	0.000682	0.02594	ZNF593
NM_013239	chrX	-4.9975	6.096122	0.000761	0.027425	PPP2R3B
NM_001113494	chr17	-4.9869	6.008625	0.000463	0.020914	SEPT9
NM_001113493	chr17	-4.9704	6.150139	0.001136	0.034733	SEPT9
NM_020962	chr15	-4.9702	5.806009	0.000667	0.025529	IGDCC4
NM_177402	chr1	-4.9688	6.010784	0.000905	0.030693	SYT2
NM_005248	chr1	-4.9671	5.974923	0.001204	0.03601	FGR
NM_012448	chr17	-4.9663	6.15696	0.000634	0.024887	STAT5B
NM_001199862	chr1	-4.9662	5.937249	0.000361	0.018695	KCNAB2
NM_001204192	chr1	-4.9650	6.064486	0.000555	0.023034	TP73
NR_126041	chr19	-4.9645	5.753002	0.002196	0.052714	LOC101930071
NM_001303627	chr12	-4.9582	5.721454	0.000105	0.008654	MLEC
NM_001276480	chr19	-4.9553	6.096363	0.002003	0.049727	LONP1
NM_012324	chr22	-4.9549	5.833778	0.000645	0.02508	MAPK8IP2
NM_001193621	chr19	-4.9548	5.815019	0.000926	0.031178	PINLYP
NM_001014440	chr22	-4.9423	5.975122	0.002217	0.052942	ODF3B
NM_002953	chr1	-4.9395	6.242916	0.000283	0.016055	RPS6KA1
NM_000383	chr21	-4.9392	6.083346	0.001099	0.034213	AIRE
NM_001304460	chr12	-4.9374	5.907122	0.000544	0.022727	ANKRD33
NM_013262	chr6	-4.9365	6.095789	0.001205	0.03601	MYLIP
NR_024483	chr22	-4.9295	5.724138	0.000454	0.020793	CECR5-AS1
NM_001018000	chr1	-4.9240	6.197387	0.001403	0.040029	KAZN
NM_014722	chr6	-4.9108	6.23693	0.000522	0.022374	FAM65B
NM_032756	chr1	-4.9095	6.354197	0.000912	0.030788	HPDL
NM_000201	chr19	-4.8971	6.094255	0.001812	0.046989	ICAM1
NM_019037	chr8	-4.8941	5.705209	0.001849	0.047712	EXOSC4
NM_015253	chr17	-4.8941	6.324374	0.001054	0.033319	WSCD1
NR_029965	chr14	-4.8813	5.904708	0.001684	0.045221	MIR431
NM_005091	chr19	-4.8810	6.104612	0.001786	0.046677	PGLYRP1
NM_182539	chr6	-4.8780	6.349825	0.002282	0.054015	TCTE1
NR_109831	chr3	-4.8711	5.956516	0.000742	0.026992	RASSF1-AS1
NM_001145855	chr4	-4.8701	5.819142	0.000571	0.023224	SH3BP2

2.1.4 High salt (nucleoid-enriched)

GeneID	Chr	logFC	logCPM	PValue	FDR	symbol
NM_001256787	chr12	4.8842	5.280102	0.003402	0.06939	PLEKHA5
NM_001199756	chr1	4.8438	4.86594	0.004532	0.081575	PPP2R5A
NM_001308088	chr5	4.7819	5.416835	0.001966	0.04944	PRR16
NM_000128	chr4	4.6193	5.157043	0.005549	0.091385	F11
NM_006393	chr10	4.6190	5.135676	0.001966	0.04944	NEBL
NM_130846	chr12	4.6061	5.162774	0.009172	0.123427	PTPRR
NM_001080551	chr9	4.5193	4.856712	0.015515	0.168071	C9orf84
NR_033427	chr3	4.4343	4.691216	0.007844	0.111862	ARL13B
NM_001083589	chr8	4.4243	5.187328	0.00888	0.121302	E2F5
NM_000842	chr11	4.3824	5.311954	0.018778	0.185257	GRM5
NM_024969	chr2	4.3499	5.000919	0.019714	0.191288	CSRNP3
NR_002717	chr13	4.2574	6.541228	4.15E-08	4.48E-05	ATXN8OS
NR_036066	chr1	4.2548	4.933643	0.011127	0.139001	MIR3120
NR_125719	chr7	4.2460	4.73877	0.025707	0.219789	POT1-AS1
NM_001010874	chr4	4.2233	4.876954	0.015672	0.168071	TECRL
NM_001258282	chr9	4.2229	5.356104	0.015672	0.168071	LINGO2
NM_001160154	chr2	4.2129	4.636489	0.01905	0.187192	MGAT4A
NM_000867	chr2	4.2124	4.780207	0.017029	0.17645	HTR2B
NM_002009	chr15	4.1685	5.27653	7.8E-06	0.001583	FGF7
NM_004061	chr5	4.1100	5.931102	3.58E-05	0.004165	CDH12
NR_039610	chr6	4.0936	4.895415	0.04401	0.289062	MIR548H5
NM_001290768	chr4	4.0705	5.372864	1.56E-05	0.002398	TBCK
NM_000700	chr9	4.0197	4.918367	0.041095	0.279857	ANXA1
NM_177988	chr3	4.0002	5.39518	0.036354	0.264684	MRPL47
NR_046186	chr4	3.9945	5.715373	0.002256	0.053617	PDLIM5
NM_001042521	chr2	3.9908	5.316572	0.038155	0.271981	C2orf88
NM_001077197	chr2	3.9817	5.279285	0.033975	0.255953	PDE11A
NM_016519	chr4	3.9756	4.736718	0.031317	0.244043	AMBN
NM_030966	chr17	3.9756	4.971823	0.031317	0.244043	KRTAP1-3
NM_015011	chr13	3.9754	5.139787	0.031317	0.244043	MYO16
NM_199421	chr14	3.9754	4.759291	0.031317	0.244043	SOCS4
NM_001178129	chr7	3.9753	4.991587	0.031317	0.244043	SEMA3E
NM_139240	chr1	3.9753	4.868863	0.031317	0.244043	C1orf105
NM_001308112	chr14	3.9752	4.934103	0.031317	0.244043	KLHL28
NM_004951	chr13	3.9752	4.865283	0.031317	0.244043	GPR183
NM_001164436	chr3	3.9748	4.71038	0.032222	0.248502	TMEM212
NR_046342	chr15	3.9717	4.660497	0.038906	0.272205	USP3
NM_145764	chr12	3.9669	4.927237	0.03357	0.25451	MGST1
NM_001317222	chr5	3.9619	6.557895	6.33E-08	6.08E-05	CDH10
NR_107029	chr20	3.9563	4.869069	0.038278	0.272205	MIR8062
NM_000699	chr1	3.9558	4.846718	0.049616	0.311626	AMY2A
NM_001300767	chr4	3.9426	5.093415	0.045768	0.296027	PRIMPOL
NR_047025	chr13	3.8446	5.843	0.000215	0.013473	LINC00440
NM_201550	chr12	3.8439	5.517071	0.000192	0.012626	LRRC10
NM_022375	chr1	3.7487	5.174211	0.001859	0.047822	OCLM
NR_109941	chr5	3.7318	5.284383	0.000247	0.014607	MEF2C-AS1
NM_001018077	chr5	3.6324	5.401941	0.001474	0.041279	NR3C1
NR_024016	chr3	3.6217	5.252024	0.000713	0.026438	PQLC2L
NR_045563	chr2	3.5988	5.280986	0.000493	0.021563	GULP1
NR_110286	chr2	3.5826	5.292727	0.017267	0.1781	LOC101927926
NR_131919	chr13	3.5471	5.519383	0.00015	0.010901	LOC105370306
NM_001302350	chr7	3.5374	5.252975	0.018411	0.183772	UMAD1

NR_132411	chr3	3.5348	5.520178	0.011931	0.144975	LOC728290
NR_109989	chr3	3.5230	5.905101	9.27E-05	0.007895	LOC100507661
NR_034138	chr4	3.5150	5.791879	0.00238	0.055342	EPHA5-AS1
NR_047699	chr13	3.3527	5.851205	4.7E-05	0.005169	LINC00348
NR_110079	chr7	3.3455	6.484833	9.13E-07	0.000383	LOC101927378
NM_001282787	chr9	3.3218	5.607047	0.00836	0.116371	NFIB
NR_038896	chr21	3.3073	5.269658	0.006658	0.102154	DSCAM-AS1
NR_046449	chr12	3.3051	5.432581	0.004976	0.085689	LOC374443
NM_032041	chr8	3.2936	5.492517	0.005345	0.089257	NCALD
NM_001013399	chr6	3.2925	5.151937	0.005753	0.093788	CCNC
NM_001203246	chr5	3.2889	5.425039	0.003926	0.075467	GPBP1
NM_001159596	chr13	3.2888	4.820177	0.001966	0.04944	BIVM
NM_178563	chr7	3.2877	5.804071	6.86E-05	0.006575	AGBL3
NM_022569	chr4	3.2775	5.647043	0.004868	0.084703	NDST4
NM_005664	chr15	3.2766	5.48251	0.005616	0.09216	MKRN3
NR_046871	chr13	3.1981	6.164509	2.3E-05	0.003223	LINC00333
NR_134282	chr5	3.1732	5.499144	0.004221	0.078798	LOC101927059
NR_134640	chr4	3.1530	6.68461	2.55E-06	0.00078	LOC729307
NM_001304446	chr2	3.1301	5.28343	0.010651	0.135445	LCLAT1
NR_110041	chr14	3.1195	5.905131	2.15E-05	0.003103	MIR4307HG
NR_024596	chr11	3.1144	4.856764	0.0407	0.278135	C11orf73
NM_019600	chr15	3.1118	5.344088	0.004194	0.078742	FAM214A
NM_000806	chr5	3.1076	4.956362	0.008114	0.114133	GABRA1
NM_052831	chr6	3.1049	5.330374	0.007844	0.111862	SLC18B1
NR_132371	chr13	3.1028	5.14522	0.007994	0.113072	LINC00430
NM_005447	chr12	3.1014	5.275873	0.029847	0.242076	RASSF9
NM_001290224	chr21	3.0905	5.237738	0.044771	0.292221	TPTE
NR_134287	chr5	3.0876	5.365601	0.00976	0.128046	LOC646241
NM_001300784	chr12	3.0791	5.076966	0.047015	0.301728	ERP27
NM_001297550	chr4	3.0642	5.19187	0.037493	0.269469	APELA
NM_001261448	chr4	3.0402	5.055623	0.022536	0.204274	GPM6A
NM_001286139	chr11	3.0386	5.659527	0.00372	0.07336	SLC36A4
NR_002574	chr13	3.0311	4.871185	0.022322	0.203636	SNORD102
NR_105024	chr5	3.0152	5.699194	0.007192	0.108007	LOC731157
NR_033922	chr1	3.0095	6.529361	8.7E-05	0.007568	LOC440704
NR_033921	chr18	2.9868	6.586714	0.000636	0.024887	LOC643542
NM_001286624	chr21	2.9452	5.602552	0.000959	0.031501	MAP3K7CL
NR_024476	chr7	2.9329	5.706365	5.12E-05	0.005528	PAXIP1-AS2
NR_002769	chr2	2.9161	6.157719	6.03E-05	0.006159	PCGEM1
NM_145020	chr18	2.9111	5.388616	0.004529	0.081575	CFAP53
NM_005570	chr18	2.9092	5.249838	0.031825	0.246641	LMAN1
NM_001271650	chr3	2.8936	5.052875	0.015672	0.168071	AZI2
NM_020345	chr3	2.8934	5.140967	0.015672	0.168071	NKIRAS1
NM_015669	chr5	2.8933	5.075822	0.015672	0.168071	PCDHB5
NM_004664	chr12	2.8932	5.309581	0.015672	0.168071	LIN7A
NM_177553	chr11	2.8932	5.324967	0.015672	0.168071	GAS2
NR_037605	chr1	2.8847	5.563538	0.017622	0.180119	GAS5-AS1
NM_001001888	chrX	2.8806	5.121168	0.033597	0.254543	VCX3B

2.1.5 Halosperm (halo-enriched)

GeneID	Chr	logFC	logCPM	PValue	FDR	symbol
NM_012405	chr1	-6.3192	5.61196	2.69E-07	0.000609	ICMT
NM_025015	chr10	-6.3080	5.78093	1.58E-05	0.005191	HSPA12A
NR_132983	chr16	-6.2832	5.93502	6.17E-09	4.66E-05	MIR193BHG
NM_001451	chr16	-5.8868	5.49939	1.48E-05	0.005191	FOXF1
NM_001176	chr16	-5.6021	5.53668	0.003566	0.077422	ARHGDIG
NM_004699	chrX	-5.5730	5.17089	0.001786	0.054387	FAM50A
NM_004807	chr2	-5.5115	5.42660	0.000907	0.03943	HS6ST1
NM_001042403	chr12	-5.4665	5.29020	0.000108	0.013705	USP44
NM_018275	chr7	-5.4131	5.71277	0.000807	0.037958	C7orf43
NR_029692	chr15	-5.3498	5.32986	2.82E-05	0.00637	MIR9-3
NM_001304	chr17	-5.3434	5.36275	6.43E-05	0.010192	CPD
NM_032595	chr17	-5.3300	5.10772	0.000131	0.015063	PPP1R9B
NM_017550	chr19	-5.3117	5.58284	0.00076	0.03718	MIER2
NM_001243752	chr7	-5.2622	5.30664	0.002382	0.061824	C7orf49
NM_001199784	chr20	-5.2017	5.04432	0.000528	0.030837	SDCBP2
NM_001127621	chr1	-5.1990	5.32257	0.000226	0.020054	GALE
NM_014555	chr11	-5.1720	5.26361	0.00088	0.039081	TRPM5
NR_031694	chr22	-4.9772	5.05642	0.004688	0.08973	MIR1281
NM_001005374	chr9	-4.9689	5.07170	0.000458	0.029392	LRSAM1
NM_001128826	chr9	-4.9686	5.04820	0.000458	0.029392	NCS1
NM_024578	chr19	-4.9680	5.06684	0.001011	0.041508	OCEL1
NM_172388	chr18	-4.9264	5.25673	0.007098	0.112317	NFATC1
NM_002854	chr22	-4.8879	5.01961	0.005716	0.100464	PVALB
NM_001319838	chr1	-4.8799	5.30992	0.001224	0.046057	ARHGEF10L
NM_003200	chr19	-4.8781	4.96481	0.0008	0.037868	TCF3
NM_001033576	chr17	-4.7979	5.12788	0.006195	0.104448	UNC45B
NM_032753	chr19	-4.7823	4.94887	0.001399	0.048975	RAX2
NR_030160	chr14	-4.7823	5.10463	0.001399	0.048975	MIR485
NM_032737	chr19	-4.7734	5.05853	0.001632	0.05245	LMNB2
NM_005558	chr1	-4.6914	6.34457	6.95E-06	0.003353	LAD1
NM_001202859	chr1	-4.6800	5.06044	0.001399	0.048975	SHC1
NM_004344	chrX	-4.6796	5.03672	0.002444	0.062719	CETN2
NM_006993	chr10	-4.6795	5.10557	0.002444	0.062719	NPM3
NM_001168243	chr4	-4.6498	4.96471	0.004628	0.089446	C4orf48
NM_001290331	chr19	-4.6089	5.00035	0.011335	0.141552	DENND1C
NM_032430	chr19	-4.5678	5.73019	1.17E-07	0.000345	BRSK1
NM_018216	chr1	-4.5297	4.80311	0.022914	0.203421	PANK4
NM_001204824	chr8	-4.4589	4.87557	0.00961	0.129601	KCNQ3
NM_019554	chr1	-4.4497	5.09032	0.011883	0.146185	S100A4
NM_001009877	chr5	-4.4488	5.12902	0.007465	0.114769	BRD9
NM_006737	chr19	-4.4486	4.75658	0.007465	0.114769	KIR3DL2
NM_152236	chr22	-4.4485	4.75428	0.007465	0.114769	GAS2L1
NM_001145124	chr9	-4.4405	4.79005	0.012034	0.14717	SPATA31C1
NR_037463	chr6	-4.4043	4.86337	0.030976	0.234292	MIR3692
NR_029850	chrX	-4.3316	4.66972	0.009875	0.132151	MIR362
NR_036478	chr12	-4.3178	4.86598	0.01305	0.154182	TMEM198B
NM_007022	chr3	-4.3178	4.65773	0.01305	0.154182	CYB561D2
NM_003604	chrX	-4.3150	5.01279	0.015216	0.165752	IRS4
NM_001939	chrX	-4.2660	4.74469	0.039233	0.267445	DRP2
NM_001131025	chr12	-4.2550	5.18204	0.023474	0.205704	PEX5
NM_020888	chr1	-4.2056	5.47565	0.000134	0.015063	KIAA1522
NM_001320732	chr2	-4.2022	5.04359	0.019867	0.18924	CAPG

NM_001282562	chr1	-4.1908	4.74850	0.017164	0.175257	EYA3
NM_020693	chr11	-4.1740	4.93307	0.01305	0.154182	DSCAML1
NM_021126	chr22	-4.1739	5.01664	0.022815	0.203421	MPST
NM_003992	chr15	-4.1738	4.92019	0.022815	0.203421	CLK3
NM_014235	chrX	-4.1736	4.80217	0.022815	0.203421	UBL4A
NM_001271959	chr1	-4.1704	4.90243	0.026097	0.216541	SLC39A1
NM_001142298	chr5	-4.0913	5.64868	5.65E-05	0.009548	SQSTM1
NM_004952	chr1	-4.0565	5.81206	0.000722	0.036729	EFNA3
NM_138391	chr1	-4.0556	5.65032	3.88E-05	0.007939	TMEM183A
NM_001174102	chr5	-4.0268	4.89061	0.030418	0.231537	PRR7
NM_001318802	chr16	-4.0224	5.06208	0.031792	0.237689	COX4I1
NR_037449	chr17	-4.0142	4.81653	0.022815	0.203421	MIR3678
NM_001014764	chr17	-4.0142	5.07779	0.022815	0.203421	EMC6
NM_001127501	chr1	-4.0141	4.82993	0.022815	0.203421	ALPL
NR_000020	chr19	-4.0140	4.71001	0.039892	0.267847	SNORD33
NM_001002916	chrX	-4.0138	4.66048	0.039892	0.267847	H2BFWT
NM_001294347	chr1	-3.9891	5.42590	1.49E-06	0.001686	COL8A2
NM_001257390	chr12	-3.9545	5.55191	8.77E-05	0.012417	CD63
NM_001243784	chr11	-3.9378	5.57072	6.36E-06	0.003183	PDE2A
NM_178013	chr14	-3.8687	5.97825	1.51E-05	0.005191	PRIMA1
NM_014786	chr11	-3.8368	5.57399	8.36E-05	0.012073	ARHGEF17
NM_001282306	chr2	-3.8340	4.77887	0.039892	0.267847	STK25
NR_120455	chr12	-3.8340	4.68670	0.039892	0.267847	LOC101927905
NM_001169111	chr22	-3.8333	4.68811	0.040687	0.270129	SCO2
NM_018269	chr2	-3.7838	5.76595	0.001135	0.044252	ADI1
NM_001290330	chr16	-3.7026	5.96010	1.41E-07	0.000355	LOC100129697
NM_014947	chr1	-3.6977	5.10384	0.00074	0.036779	FOXJ3
NM_001163257	chrX	-3.6947	5.38912	3.42E-05	0.007245	PLXNB3
NM_000147	chr1	-3.6396	5.49040	3.42E-05	0.007245	FUCA1
NM_147127	chr4	-3.6308	5.49299	0.004047	0.083208	EVC2
NM_144772	chr1	-3.6210	5.27800	0.000302	0.023026	NAXE
NM_001780	chr12	-3.6097	5.67287	0.00084	0.038394	CD63
NM_144617	chr19	-3.6090	5.46416	0.002406	0.062179	HSPB6
NM_145245	chr19	-3.5958	6.22672	0.00027	0.02199	EVI5L
NM_012387	chr1	-3.5820	5.31233	5.74E-05	0.009562	PADI4
NM_032283	chr1	-3.5479	5.37435	0.009519	0.128702	ZDHHC18
NM_016364	chr10	-3.5164	5.52948	0.000279	0.022183	DUSP13
NR_134570	chr7	-3.5140	5.47070	0.000239	0.020715	GS1-124K5.4
NM_001271830	chr19	-3.5045	5.30889	0.000827	0.038083	PCP2
NM_033482	chr6	-3.5037	5.46998	0.000482	0.029752	POM121L2
NM_018663	chr12	-3.4968	5.33823	0.001722	0.053424	PXMP2
NM_014587	chr16	-3.4837	5.89084	1.75E-05	0.005191	SOX8
NM_006339	chr19	-3.4834	6.13042	8.48E-07	0.001161	HMG20B
NM_001080452	chr19	-3.4783	5.27928	0.002335	0.06138	GPR108
NM_001001794	chr22	-3.4675	5.64518	0.000592	0.032674	DENND6B
NM_001316324	chr19	-3.4597	5.37429	0.000161	0.0164	POLR2E
NM_003294	chr16	-3.4592	5.35501	0.000161	0.0164	TPSAB1
NM_014442	chr19	-3.4585	5.24550	0.000431	0.028514	SIGLEC8

2.1.6 Halosperm (nucleoid-enriched)

GeneID	Chr	logFC	logCPM	PValue	FDR	symbol
NR_030294	chr3	5.0307	4.87914	7.79E-05	0.011433	MIR551B
NM_001320708	chr1	4.9529	4.86189	0.00107	0.042828	PKN2
NM_001136043	chr15	4.7509	5.27455	0.001858	0.055254	VWA9
NR_073058	chr7	4.5759	4.69982	0.002965	0.070289	C7orf55
NM_001278389	chr12	4.4438	4.79322	0.005166	0.095331	SLC38A1
NM_025047	chr3	4.4092	4.86700	0.002517	0.063793	ARL14
NM_001128598	chr21	4.4036	4.69461	0.005336	0.097037	KRTAP25-1
NM_001281533	chr18	4.4035	4.90562	0.005336	0.097037	EPB41L3
NM_001197219	chr5	4.1958	5.03408	0.012952	0.153348	PDE4D
NM_001282278	chr5	4.1925	4.67793	0.012433	0.149948	MATR3
NR_003200	chr14	4.1925	4.62695	0.012433	0.149948	SNORD114-8
NR_107003	chr4	4.1925	4.53859	0.012433	0.149948	MIR7849
NM_013380	chr19	4.1923	4.65067	0.012433	0.149948	ZNF112
NM_003033	chr8	4.1922	4.90223	0.012433	0.149948	ST3GAL1
NM_016260	chr2	4.1808	4.61903	0.049006	0.297291	IKZF2
NM_005246	chr5	4.1618	4.87151	0.022107	0.200538	FER
NM_022154	chr4	4.1612	5.25088	0.022413	0.20195	SLC39A8
NR_049811	chr19	4.1420	4.66799	0.024871	0.211957	MIR5088
NR_104034	chr1	4.0339	4.62761	0.040399	0.269146	GNRHR2
NM_001205315	chr7	4.0174	4.71041	0.030448	0.231537	STEAP4
NM_130782	chr1	4.0101	4.68873	0.022193	0.200921	RGS18
NM_001206729	chr1	3.9722	4.54185	0.048108	0.294484	AKT3
NM_000856	chr4	3.9652	5.01887	0.035392	0.25213	GUCY1A3
NM_001242917	chr15	3.9452	4.51403	0.02898	0.226246	ZFAND6
NM_001134664	chr1	3.9452	4.57444	0.02898	0.226246	SAMD13
NM_001168300	chrX	3.9452	4.56464	0.02898	0.226246	KLHL13
NM_000780	chr8	3.9451	4.62083	0.02898	0.226246	CYP7A1
NM_007124	chr6	3.9450	4.67229	0.02898	0.226246	UTRN
NM_001127443	chr7	3.9449	4.53820	0.02898	0.226246	CD36
NM_001197098	chr9	3.9114	4.62246	0.042892	0.277402	PRSS3
NM_015312	chr4	3.7077	4.49054	0.046957	0.290057	KIAA1109
NM_206923	chrX	3.5408	5.39847	3.93E-05	0.007939	YY2
NR_046999	chr13	3.4496	5.80708	4.26E-07	0.00079	LINC00366
NM_033050	chr3	3.2948	4.86099	0.011686	0.144635	SUCNR1
NM_000842	chr11	3.2277	5.31195	0.001167	0.044688	GRM5
NR_039848	chr12	3.2174	4.74556	0.006032	0.103144	MIR4699
NM_183044	chr13	3.2068	5.19155	0.000144	0.015807	RNF6
NM_001201574	chr14	3.2067	5.14136	0.000144	0.015807	NUBPL
NR_125908	chr4	3.1384	5.70068	4.44E-05	0.008304	LOC101928942
NM_001306207	chr18	3.1024	5.18896	0.000726	0.036744	TCF4
NM_001101337	chr3	3.0612	4.92931	0.011135	0.139711	C3orf79
NM_020346	chr11	3.0608	5.62311	0.0002	0.018709	SLC17A6
NR_029514	chr21	3.0597	4.74979	0.006721	0.109097	MIR99A
NM_001040432	chr3	3.0543	5.06472	0.012746	0.151914	ZCWPW2
NM_018073	chr11	3.0543	4.81477	0.012746	0.151914	TRIM68
NM_001199053	chr16	3.0058	5.10246	0.022497	0.202247	LOC81691
NM_001134470	chr3	3.0052	5.17876	0.000129	0.015062	C3orf58
NM_001289074	chr10	2.9390	4.68241	0.041384	0.271978	HELLS
NM_001278355	chr12	2.9222	4.75097	0.042782	0.277392	FRS2
NM_002173	chr9	2.9107	4.74870	0.024991	0.212591	IFNA16
NM_006685	chr4	2.9094	5.00103	0.028366	0.224289	SMR3B
NM_001278580	chr2	2.8768	4.95204	0.029871	0.22946	ACVR2A

NM_001162497	chr13	2.8724	4.89583	0.01346	0.156087	LPAR6
NM_152774	chr7	2.8704	4.85925	0.026653	0.217438	TMEM196
NR_027132	chr15	2.8703	4.62429	0.026653	0.217438	LINC00924
NM_007288	chr3	2.8703	4.90316	0.026653	0.217438	MME
NR_047532	chr9	2.8703	4.67764	0.026653	0.217438	CDKN2B-AS1
NM_033122	chr4	2.8701	4.93091	0.026653	0.217438	CABS1
NM_015983	chr7	2.8693	4.98560	0.026884	0.219063	UBE2D4
NM_001308116	chr3	2.8572	4.99680	0.04311	0.278088	PHC3
NM_001198806	chr9	2.8571	4.76741	0.030082	0.230651	MSANTD3
NM_013444	chrX	2.7910	5.16695	0.001829	0.054901	UBQLN2
NM_153838	chr6	2.7729	5.52559	1.63E-05	0.005191	ADGRF4
NM_003194	chr6	2.7726	5.02523	0.003792	0.080012	TBP
NM_001168499	chr18	2.7712	4.99111	0.002588	0.064551	CNDP2
NM_015669	chr5	2.7711	5.07582	0.000611	0.033434	PCDHB5
NM_023920	chr12	2.7707	5.05704	0.005214	0.095974	TAS2R13
NM_001042550	chr9	2.7707	4.93585	0.001319	0.048104	SMC2
NM_080874	chr4	2.7707	5.12012	0.005214	0.095974	ASB5
NM_000689	chr9	2.7672	5.28294	0.00922	0.126544	ALDH1A1
NM_001114175	chr4	2.7439	5.49626	3.79E-06	0.002385	GABRA2
NM_001290258	chr7	2.7372	5.29348	0.000516	0.030446	ASB15
NM_006820	chr1	2.7060	4.91384	0.041532	0.272169	IFI44L
NM_001177591	chr8	2.7057	4.70050	0.042991	0.277617	PPP2R2A
NM_001143837	chr11	2.6968	5.62570	0.000414	0.027891	NOX4
NM_001115131	chr5	2.6935	4.84021	0.041125	0.271071	C6
NR_029678	chr12	2.6774	4.75753	0.043241	0.278613	MIR135A2
NM_001144971	chr18	2.6610	4.83966	0.027215	0.22041	NEDD4L
NM_005135	chr15	2.6459	5.10518	0.006911	0.110726	SLC12A6
NM_000786	chr7	2.6344	5.25844	0.012656	0.151742	CYP51A1
NR_111952	chr1	2.6281	5.11173	0.002114	0.058594	LINC00869
NM_173611	chr15	2.5822	5.07164	0.044621	0.282285	FAM98B
NR_000039	chr5	2.5813	5.32325	0.000642	0.034209	RAB9BP1
NM_004932	chr5	2.5654	5.81774	2.34E-05	0.005895	CDH6
NM_173487	chr4	2.5279	5.39587	0.002259	0.059881	C4orf33
NM_052831	chr6	2.5243	5.33037	0.002114	0.058594	SLC18B1
NM_001278515	chr18	2.5237	5.20413	0.004097	0.083716	GTSCR1
NR_126011	chr21	2.5058	5.53580	0.000432	0.028514	LOC284825
NM_006770	chr2	2.4914	4.96308	0.010389	0.134465	MARCO
NM_006911	chr9	2.4911	5.15652	0.020439	0.191546	RLN1
NM_001321047	chr2	2.4911	5.12561	0.020439	0.191546	PMS1
NM_001080140	chrX	2.4910	4.90632	0.020439	0.191546	CT47A7
NM_001319194	chr10	2.4908	5.15932	0.020439	0.191546	EXOC6
NM_182505	chr9	2.4754	5.59974	0.001214	0.045922	C9orf85
NM_001287258	chr8	2.4744	5.43545	0.02152	0.197488	XKR9
NM_001256865	chr1	2.4681	5.28033	0.019487	0.187087	DNAJC6
NM_144651	chr8	2.4600	5.15146	0.049373	0.298171	PXDNL
NM_005687	chr2	2.4411	5.29087	0.012288	0.149631	FARSB
NM_001873	chr4	2.4229	5.84574	0.00082	0.038026	CPE
NM_199328	chr21	2.4114	5.15296	0.007849	0.117566	CLDN8

2.2 Bovine samples

2.2.1 Low salt (halo-enriched)

GeneID	Chr	logFC	logCPM	PValue	FDR	symbol
NR_031208	chr7	-4.1580	7.27860	0.001481	0.02511	MIR340
NM_001083763	chr11	-4.1121	7.22191	2.05E-06	0.000389	NPAS2
NM_001040529	chr26	-4.1077	8.81065	1.42E-06	0.000288	ZWINT
NR_031373	chr8	-3.9963	8.43827	1.71E-09	2.92E-06	MIR124A-1
NM_177502	chr26	-3.8575	9.58997	1.21E-10	5.18E-07	GOT1
NM_001034371	chr29	-3.7977	9.01734	1.42E-09	2.92E-06	FOXRED1
NM_001105499	chr14	-3.7734	8.25306	1.22E-05	0.001298	CSMD3
NM_001035281	chr8	-3.7550	9.32278	5.6E-06	0.000735	PTGR1
NM_001206818	chr2	-3.7536	10.07681	4.18E-12	3.56E-08	PAX3
NM_001167660	chr13	-3.7361	7.01160	8.14E-05	0.004286	20ALPHA-HSD
NM_177521	chr25	-3.7348	7.02536	6.36E-05	0.003691	SULT1A1
NM_001075279	chrX	-3.7347	7.01562	6.36E-05	0.003691	RRAGB
NM_001037448	chr11	-3.7265	7.78151	6.32E-06	0.000793	C1D
NM_182788	chr4	-3.7224	9.30546	9.08E-06	0.001047	TFPI2
NR_031020	chr6	-3.7082	7.73956	0.000117	0.005377	MIR302C
NM_001025341	chr11	-3.6605	7.96828	4.34E-05	0.00295	RPL31
NM_001113227	chr4	-3.6073	8.41821	2.22E-06	0.000403	ELMO1
NM_001037473	chr29	-3.5724	8.82077	2.4E-07	8.63E-05	AAMDC
NM_001098934	chr11	-3.5489	8.14744	1.49E-06	0.000295	DCTN1
NM_175811	chr10	-3.5362	9.13790	5.81E-06	0.000752	ALDH6A1
NM_001099069	chr27	-3.5308	9.00019	5.31E-08	3.02E-05	TTI2
NM_001076133	chr22	-3.5271	9.15729	2.73E-06	0.000466	PDE12
NM_001102529	chr5	-3.5083	9.61634	2.31E-09	3.28E-06	SCYL2
NM_001046209	chr25	-3.4940	8.81953	3.87E-05	0.002731	RAB26
NM_001034547	chr10	-3.4932	9.47202	6.29E-10	1.79E-06	EMC4
NM_001192559	chr26	-3.4678	8.87518	1E-07	4.76E-05	POLL
NM_001034736	chr7	-3.4635	7.84108	2.45E-06	0.000436	SPATA9
NM_001034594	chr9	-3.4303	9.91164	2.33E-05	0.002005	ZUFSP
NM_001192346	chr25	-3.4295	8.55027	2.76E-07	9.41E-05	WBSCR16
NM_001038053	chr25	-3.4117	8.21780	8.55E-06	0.001027	EIF2AK1
NM_001035013	chr12	-3.4026	9.31759	7.95E-07	0.000188	MTRF1
NM_001034747	chr14	-3.3942	8.90148	7.85E-09	6.7E-06	ENY2
NM_001304966	chr6	-3.3829	9.64545	2.03E-08	1.33E-05	PGM2
NM_001034549	chr8	-3.3749	9.15473	2.11E-07	8.57E-05	SLC25A37
NR_031021	chr6	-3.3674	6.83429	0.000998	0.020018	MIR302B
NM_001076210	chr9	-3.3669	8.42130	0.000133	0.006003	COQ3
NM_001193141	chr5	-3.3576	8.53721	1.69E-05	0.001616	HDAC7
NM_001103103	chr1	-3.3341	8.73716	0.000336	0.010908	SELT
NM_001192027	chr8	-3.3330	8.30123	1.21E-05	0.001298	ZNF484
NM_001038562	chr1	-3.3299	7.18531	0.001635	0.026274	FXR1
NR_031000	chr5	-3.3250	8.45644	4.53E-06	0.000655	MIR2426
NM_001102374	chr6	-3.2899	8.47592	1.49E-05	0.001499	LOC536190
NR_031319	chr6	-3.2873	7.46593	0.000176	0.007059	MIR367
NM_001076988	chr4	-3.2736	9.79426	3.09E-07	0.000102	TMEM60
NM_001076880	chr14	-3.2679	8.71224	1.2E-07	5.41E-05	NUDCD1
NM_001245936	chr8	-3.2646	8.28060	0.000121	0.00554	IFN-TAU
NR_031365	chr21	-3.2408	8.08427	9.41E-06	0.001057	MIR127
NM_001077069	chr11	-3.2402	7.14573	0.005755	0.050304	TMEM247
NM_001075987	chr10	-3.2356	9.48055	1.63E-07	6.94E-05	TMOD3
NM_001075420	chr1	-3.2331	9.34621	4.46E-09	4.76E-06	NMD3
NM_001103266	chr3	-3.2329	8.68142	0.000922	0.019325	RPAP2

NM_001077842	chr21	-3.2163	9.92435	4.07E-05	0.002799	COCH
NM_001205873	chr3	-3.2086	9.47757	3.96E-07	0.000113	VSIG8
NM_001205552	chr26	-3.2085	9.45346	6.12E-07	0.000154	SLC25A28
NR_031067	chr21	-3.1947	7.66936	0.000397	0.012266	MIR432
NM_001075247	chr19	-3.1885	9.21117	1.16E-06	0.000241	WDR45B
NM_001075322	chr7	-3.1816	9.54449	9.41E-09	7.3E-06	CYP4F2
NM_001098948	chr21	-3.1798	9.05241	5.08E-06	0.00071	SNRPA1
NM_001038117	chr1	-3.1791	7.63710	0.004997	0.046755	SPICE1
NM_001110443	chr19	-3.1743	8.09042	6.34E-05	0.003691	ZNF286A
NM_001038099	chr18	-3.1707	9.52488	3.92E-09	4.76E-06	CENPN
NM_001075407	chr5	-3.1583	7.64305	0.001082	0.020744	SPX
NM_001015564	chr23	-3.1575	8.38228	0.00019	0.007416	WDR46
NR_107809	chr3	-3.1415	7.97040	0.00042	0.012588	MIR2284Z-4
NM_001205277	chr19	-3.1314	8.32064	9.28E-07	0.000208	ARRB2
NM_001206171	chr13	-3.1287	9.33413	1.04E-06	0.000225	MKKS
NM_001076919	chr23	-3.1087	9.14748	8.36E-08	4.33E-05	PPP1R18
NM_001083452	chr2	-3.1051	7.99773	2.46E-05	0.002042	MDH1B
NM_001206131	chr3	-3.0931	7.35091	5.13E-05	0.003242	INSL5
NM_001075444	chr29	-3.0925	10.08597	1.86E-08	1.32E-05	STX5
NM_001076157	chr29	-3.0917	8.55020	4.45E-07	0.000122	ACTN3
NM_001081577	chr11	-3.0880	9.81429	6.15E-09	5.83E-06	SLC1A4
NM_001014845	chr4	-3.0866	9.35037	2.43E-07	8.63E-05	NPY
NM_174323	chr8	-3.0776	10.52875	1.78E-05	0.001643	GNA14
NM_001104992	chr3	-3.0742	8.88327	0.000192	0.007476	TCEANC2
NM_001031754	chr10	-3.0578	8.83609	5.65E-07	0.000146	LRRC57
NM_001205673	chr7	-3.0563	8.71243	3.43E-07	0.000102	TMEM161B
NM_001192560	chr5	-3.0497	7.75605	0.000532	0.014203	GRAP2
NM_001192726	chr9	-3.0349	8.76382	1.59E-05	0.001539	EPHA7
NM_174239	chr8	-3.0302	7.05818	0.007707	0.058667	ALDH1A1
NM_001034753	chr8	-3.0213	9.98029	1.05E-06	0.000225	CARD19
NM_001099719	chr6	-3.0195	8.38168	0.00074	0.017006	STX18
NM_001076416	chr11	-3.0014	8.78122	0.000178	0.007062	EXOC6B
NM_001001439	chr18	-2.9969	9.35626	5.43E-06	0.000735	COX4I1
NM_001046017	chr11	-2.9946	9.20471	5.57E-06	0.000735	SF3B6
NM_001078033	chr19	-2.9945	7.73663	2.73E-05	0.002137	KLHL10
NM_001080730	chr1	-2.9939	8.52422	2.52E-05	0.002042	MRPL39
NM_001034474	chr19	-2.9924	7.33375	0.002532	0.032529	TAX1BP3
NM_001038154	chr25	-2.9920	8.57795	3.1E-05	0.002297	MGC134577
NM_001079648	chr18	-2.9841	8.06846	3.06E-05	0.002297	C18H16orf78
NM_001100292	chr11	-2.9721	8.50022	0.001034	0.020144	POLR1B
NM_001101127	chr10	-2.9697	8.66025	8.35E-05	0.004346	GALNT16
NM_001037610	chr4	-2.9663	8.07299	8.29E-05	0.004338	GGCT
NM_001083484	chr11	-2.9583	7.52500	4.59E-05	0.003032	SMYD1
NM_001075140	chr18	-2.9500	8.76753	7.79E-05	0.004178	MT2A
NM_001076490	chr13	-2.9450	7.49400	0.001242	0.022459	WFDC2
NM_001244199	chr19	-2.9388	9.05643	0.000108	0.005101	LOC508666
NM_001034731	chr13	-2.9381	8.74519	2.99E-05	0.002279	SNRPB
NM_001078124	chr6	-2.9363	9.63458	1.8E-05	0.001643	RHOH
NR_030805	chr23	-2.9246	8.06748	0.001627	0.026274	MIR2325B

2.2.2 Low salt (nucleoid-enriched)

GeneID	Chr	logFC	logCPM	PValue	FDR	symbol
NM_001075511	chr27	4.0805	7.68527	7.45E-05	0.004046	AGA
NM_001102153	chr6	4.0011	7.63458	7.9E-06	0.000963	SCARB2
NM_001272010	chr19	3.9803	7.63465	8.86E-05	0.004524	GPRC5C
NM_001098107	chr7	3.9641	7.61126	2.63E-05	0.002079	ZBED8
NM_001192146	chr14	3.9443	7.59685	6.94E-05	0.003895	MSC
NM_001191145	chr4	3.8842	7.56256	3.46E-05	0.00248	TWIST1
NM_001109790	chr2	3.8709	7.55083	6.06E-05	0.003606	FAM168B
NM_001192114	chr22	3.8690	7.54842	3.15E-05	0.00232	GATA2
NM_001081728	chr16	3.8242	7.53444	5.52E-05	0.003383	PPP2R5A
NM_001192340	chr17	3.7816	7.49470	0.000326	0.010737	GNB1L
NM_001076974	chr8	3.7803	7.50847	9.72E-05	0.004764	FBXW2
NM_001205722	chr18	3.7802	7.50745	4.89E-05	0.003138	KIAA0895L
NM_001102348	chr3	3.7347	7.48091	6.77E-05	0.003838	ARL4C
NM_001037319	chr3	3.7304	7.46459	0.000176	0.007059	SLC16A1
NM_001191305	chr5	3.7269	7.46132	0.000292	0.00985	ITGA7
NM_001075742	chr9	3.7097	7.45521	0.000257	0.008971	TBP
NM_001034585	chr10	3.6894	7.45722	4.77E-05	0.003104	ACTC1
NM_001075314	chr7	3.6851	7.43873	0.000101	0.004917	RNF126
NM_001034598	chr3	3.6798	7.44334	9.3E-05	0.004665	NFYC
NM_001046194	chr8	3.6347	7.41113	4.93E-05	0.003138	CDCA2
NM_001205434	chr7	3.6150	7.39500	0.000223	0.008182	PURA
NM_001130752	chr10	3.6084	7.41427	0.001016	0.020018	MAP2K1
NM_001105627	chr19	3.6054	7.38686	0.000336	0.010908	MPRIP
NM_001102218	chr15	3.6008	7.39616	0.000256	0.008971	NRIP3
NM_001046418	chr2	3.6002	7.38952	0.000708	0.016487	ARMC9
NM_001103086	chr16	3.5833	7.36839	0.001178	0.021751	CAPN2
NM_001046012	chr15	3.5724	7.37744	0.000161	0.006778	DCUN1D5
NM_001083679	chr3	3.5600	7.37297	0.000365	0.011538	SMG5
NM_001076442	chr18	3.5317	7.35027	0.000645	0.015656	LYPD4
NM_001075189	chr24	3.5314	7.36796	0.00023	0.008271	USP14
NM_001206476	chr8	3.5296	7.36579	0.00021	0.007907	PSIP1
NM_001206735	chr11	3.5253	7.35791	0.001184	0.021786	IL1R1
NM_181005	chr21	3.5239	7.34987	0.000158	0.006719	CHGA
NM_174663	chr19	3.4977	7.33001	0.00124	0.022459	PAFAH1B1
NM_176657	chr18	3.4794	7.33704	0.000446	0.012999	FCGRT
NM_001013603	chr19	3.4777	7.31841	0.000292	0.00985	IFT20
NM_001193087	chr3	3.4712	7.32944	0.001425	0.024269	INTS3
NM_001205412	chr3	3.4688	7.31278	0.000482	0.013623	GPR88
NM_001102508	chr15	3.4622	7.31039	0.00033	0.010792	MAPK8IP1
NM_001076470	chr26	3.4604	7.30126	0.000425	0.012636	SLC35G1
NM_001076072	chr1	3.4559	7.30371	0.000435	0.012793	NCK1
NM_001098922	chr19	3.4520	7.31246	0.000215	0.008055	CD7
NM_001192215	chr3	3.4388	7.30697	0.001252	0.022574	S100A5
NM_001076946	chr18	3.4270	7.30918	0.003875	0.040723	CCDC155
NM_001075679	chr10	3.4225	7.30460	0.000995	0.020018	RMDN3
NM_173950	chr10	3.4214	7.29935	0.00253	0.032529	PGF
NM_001076101	chr2	3.4108	7.29668	0.003345	0.038454	TMEFF2
NM_175830	chr1	3.4101	7.30161	0.000256	0.008971	NDUFV3
NM_173942	chr25	3.4087	7.28948	0.000422	0.012588	CPSF4
NM_001075858	chr5	3.4085	7.28724	0.000422	0.012588	AMN1
NM_205802	chr14	3.4073	7.28328	0.000467	0.013334	LAPTM4B
NM_001076183	chr11	3.4038	7.28602	0.000812	0.017648	CNRIP1

NM_001205958	chr19	3.3824	7.27835	0.002428	0.031819	NEUROD2
NM_001076869	chr17	3.3663	7.78248	7.95E-05	0.004236	RNF10
NM_001079779	chr25	3.3623	7.25372	0.000585	0.014841	KDELR2
NM_001205671	chr4	3.3612	7.76548	6.99E-05	0.003895	ZNF800
NM_001075656	chr7	3.3480	7.25241	0.000561	0.014588	JUNB
NM_001075182	chr16	3.3470	7.25695	0.000422	0.012588	CPTP
NM_001192271	chr2	3.3466	7.24718	0.000491	0.013731	ATP13A2
NM_001206039	chr18	3.3439	7.23636	0.000875	0.018532	CNOT1
NM_001076083	chr5	3.3432	7.24318	0.000546	0.014315	PMM1
NM_001015630	chr13	3.3406	7.23641	0.001222	0.022236	GSS
NM_001040511	chr10	3.3234	7.24820	0.004521	0.044369	SQRDL
NM_001099066	chr3	3.3227	7.22756	0.000619	0.015351	LOC534742
NM_001077942	chr13	3.3211	7.22584	0.000601	0.015162	DLGAP4
NM_001078091	chr14	3.3134	7.25567	0.002715	0.033868	FAM135B
NM_001075302	chr12	3.3035	7.21992	0.002032	0.029575	HSPH1
NM_001102163	chr20	3.2880	7.22484	0.007673	0.058667	SLC38A9
NM_001103328	chr13	3.2838	7.70064	0.000127	0.005741	SNX21
NM_001206077	chr26	3.2828	7.21575	0.00106	0.020506	SLK
NM_001034482	chr25	3.2817	7.22263	0.00076	0.017053	CDIPT
NM_001076882	chr15	3.2816	7.23006	0.00076	0.017053	ZNF215
NM_001046485	chr16	3.2816	7.21857	0.00076	0.017053	TARDBP
NM_001192360	chr18	3.2816	7.21857	0.00076	0.017053	ZNF599
NM_001099028	chr23	3.2811	7.20943	0.00076	0.017053	RNF144B
NM_001046086	chr11	3.2809	7.20786	0.00076	0.017053	WDR54
NR_132744	chr11	3.2808	7.20534	0.00076	0.017053	LOC100335806
NM_001205372	chr5	3.2794	7.21938	0.001068	0.020562	RBFOX2
NM_001024523	chr4	3.2789	7.20566	0.001688	0.02681	GNG11
NM_001109766	chr14	3.2778	7.72617	0.000175	0.007059	SHARPIN
NM_001045868	chr21	3.2772	7.20355	0.001078	0.020703	NFKBIA
NM_001206598	chr15	3.2760	7.20482	0.001579	0.025861	SLC43A1
NM_001205540	chr12	3.2699	7.20254	0.000961	0.019754	KBTBD6
NM_001206173	chr16	3.2676	7.69226	4.88E-05	0.003138	MIIP
NM_001038038	chr3	3.2670	7.21864	0.005085	0.047155	ATP6V0B
NM_001103230	chr16	3.2669	7.19892	0.000766	0.017082	VWA1
NM_001103245	chr16	3.2649	7.20161	0.001284	0.023011	EFHD2
NM_001193243	chr23	3.2511	7.19334	0.003043	0.036565	ADGRF5
NM_001101916	chr18	3.2489	7.70785	0.000182	0.007198	MGC139164
NM_001099157	chr4	3.2387	7.20059	0.000674	0.015835	BET1
NM_001075226	chr17	3.2380	7.67650	7.27E-05	0.003999	RILPL1
NM_001192130	chr19	3.2304	7.67867	0.000116	0.005366	RPTOR
NM_001076818	chr19	3.2287	7.20087	0.003691	0.039612	KAT7
NM_001206537	chr12	3.2237	7.19772	0.001867	0.028081	COG3
NM_001191288	chr10	3.2209	7.67586	0.000105	0.004998	REC8
NM_001075395	chr18	3.2205	7.18039	0.000875	0.018532	PIH1D1
NM_001077871	chr21	3.2201	7.21306	0.003669	0.039465	SLC25A29
NM_001075296	chr11	3.2197	7.17986	0.00087	0.018532	LRSAM1
NM_001099211	chr7	3.2192	7.18525	0.017394	0.093916	SF3A2
NM_001102257	chr5	3.2134	7.18711	0.001361	0.023715	NOP2

2.2.3 High salt (halo-enriched)

GeneID	Chr	logFC	logCPM	PValue	FDR	symbol
NM_174395	chr5	-5.3441	8.58871	3.21E-06	0.009991	MYO1A
NM_001098881	chr3	-5.0455	8.42532	5.33E-05	0.05819	ARHGEF2
NM_001102237	chr29	-4.8679	8.33548	0.000222	0.133243	TMEM132A
NM_001192829	chr1	-4.7802	8.29500	0.000321	0.146723	EPHB1
NM_001046188	chr19	-4.6798	8.24654	0.001773	0.245201	EIF4A3
NM_001103293	chr23	-4.6765	8.24500	0.000494	0.157044	MED20
NR_030883	chr2	-4.6764	8.24460	0.000494	0.157044	MIR26B
NM_001083664	chr17	-4.6718	8.24142	0.000677	0.181773	TMEM119
NM_001075415	chr19	-4.5661	8.19573	0.00215	0.257912	SLC25A39
NM_001077858	chr3	-4.5658	8.19767	0.000494	0.157044	CTPS1
NM_174385	chr10	-4.5656	8.19280	0.000986	0.223078	LTBP2
NM_001083793	chr5	-4.5505	8.19189	0.003591	0.306543	SMAGP
NM_001075460	chr5	-4.5177	8.18657	0.006666	0.338735	HDAC10
NM_001080329	chr20	-4.5006	8.18486	0.010594	0.386484	PLPP1
NM_176672	chr7	-4.4517	8.14711	0.001529	0.245201	NDUFA13
NM_001105438	chr2	-4.4502	8.14475	0.003994	0.306581	KIAA2012
NM_001101074	chr11	-4.4456	8.14219	0.001968	0.245201	NAIF1
NM_001193186	chr13	-4.4456	8.14191	0.001968	0.245201	COX4I2
NM_001075373	chrX	-4.4456	8.14150	0.001968	0.245201	LOC508820
NM_001101893	chr18	-4.4455	8.13977	0.001968	0.245201	ZNF423
NM_001076977	chr18	-4.4453	8.14342	0.002584	0.285171	HCST
NM_001191241	chr17	-4.4199	8.13776	0.006059	0.338735	HRK
NM_001081627	chr19	-4.4141	8.13659	0.006312	0.338735	KCNAB3
NR_031285	chr19	-4.3228	8.09164	0.006184	0.338735	MIR2346
NM_001079643	chr7	-4.3223	8.09304	0.003285	0.306035	NMRK2
NM_180998	chr22	-4.3148	8.09123	0.001968	0.245201	LTF
NM_174531	chr25	-4.3148	8.08929	0.001968	0.245201	CYP3A5
NM_001192271	chr2	-4.3147	8.08767	0.00393	0.306543	ATP13A2
NM_001037456	chr25	-4.3147	8.08761	0.00393	0.306543	SLX1A
NM_001105452	chr2	-4.3147	8.08754	0.00393	0.306543	PADI2
NM_001102313	chr18	-4.3131	8.08586	0.004177	0.312303	HRC
NM_001192150	chrX	-4.3061	8.08545	0.00548	0.338735	FMR1
NR_031155	chr29	-4.3018	8.08744	0.012933	0.406204	MIR483
NM_001035109	chr16	-4.2980	8.08522	0.007867	0.338735	DFFB
NM_205796	chr3	-4.2980	8.08522	0.00787	0.338735	APOA1BP
NM_001191440	chr18	-4.2920	8.08376	0.008128	0.342538	AP2A1
NM_001017954	chr25	-4.2815	8.08382	0.013723	0.420663	ATP6V0C
NM_001105646	chr2	-4.2785	8.08335	0.013926	0.425553	ALDH4A1
NM_001076323	chr17	-4.2629	8.08160	0.018074	0.473831	DERL3
NM_001040469	chr7	-4.2438	8.07986	0.025693	0.53593	C3
NM_001077943	chr5	-4.1792	8.03618	0.007873	0.338735	ESYT1
NM_174641	chr17	-4.1709	8.03547	0.00393	0.306543	GUCY1B3
NM_001098923	chr28	-4.1708	8.03335	0.00393	0.306543	C28H10orf35
NM_001046073	chr14	-4.1708	8.03300	0.00393	0.306543	TBC1D31
NR_107797	chr15	-4.1708	8.03300	0.00393	0.306543	MIR6528
NM_001082471	chr26	-4.1708	8.03293	0.00393	0.306543	BAG3
NM_001038115	chr16	-4.1707	8.03117	0.00393	0.306543	ACTRT2
NM_001102354	chr4	-4.1707	8.03117	0.00393	0.306543	XRCC2
NM_001101237	chr10	-4.1707	8.03094	0.007849	0.338735	GMFB
NM_205817	chr5	-4.1707	8.03088	0.007849	0.338735	NDUFA9
NM_001192950	chr11	-4.1677	8.03287	0.00667	0.338735	FOSL2
NM_001075634	chr29	-4.1663	8.03242	0.006785	0.338735	TCIRG1

NM_001099146	chr7	-4.1647	8.03283	0.013241	0.408499	ATG4D
NM_001083374	chr29	-4.1595	8.02905	0.010766	0.389884	SLC22A18
NM_001076182	chr19	-4.1543	8.03065	0.018027	0.473831	FN3K
NM_001024543	chr11	-4.1494	8.02876	0.01489	0.432581	DOK1
NM_001101125	chr5	-4.1380	8.02728	0.017727	0.468537	ENO2
NM_001101040	chr22	-4.1278	8.02693	0.023973	0.524576	GNAI2
NM_001034495	chr11	-4.0282	7.97891	0.018296	0.475316	RPL35
NM_001083753	chr7	-4.0146	7.97767	0.009989	0.372923	SH3RF2
NM_001101067	chr1	-4.0143	7.97755	0.009901	0.372181	UBA5
NM_001038569	chr7	-4.0109	7.97647	0.007849	0.338735	ACTL9
NM_001099386	chr10	-4.0109	7.97647	0.007849	0.338735	PSMB11
NM_001078139	chr7	-4.0108	7.97433	0.007849	0.338735	RPL36
NM_001206692	chr7	-4.0108	7.97433	0.007849	0.338735	QTRT1
NM_001102308	chr3	-4.0108	7.97427	0.007849	0.338735	LRRFIP1
NM_001035352	chr3	-4.0108	7.97404	0.007849	0.338735	PRUNE
NM_001038139	chr9	-4.0108	7.97404	0.007849	0.338735	ORC3
NM_001040486	chr22	-4.0108	7.97404	0.007849	0.338735	SLC38A3
NM_001193028	chr19	-4.0108	7.97404	0.007849	0.338735	PLCD3
NR_031305	chr29	-4.0108	7.97404	0.007849	0.338735	MIR2406
NM_001034036	chr5	-4.0108	7.97397	0.007849	0.338735	PPARA
NM_001034331	chr25	-4.0108	7.97397	0.007849	0.338735	AZGP1
NM_001038147	chr1	-4.0108	7.97248	0.007849	0.338735	CCDC50
NM_001103338	chr11	-4.0108	7.97248	0.007849	0.338735	ACTR1B
NM_001008669	chr18	-4.0107	7.97219	0.007849	0.338735	PSENEN
NM_001038620	chr11	-4.0107	7.97219	0.007849	0.338735	LHX3
NM_001191160	chr5	-4.0107	7.97219	0.007849	0.338735	AQP5
NM_001192403	chr8	-4.0107	7.97219	0.007849	0.338735	PLPPR1
NM_001102025	chr18	-4.0107	7.97213	0.007849	0.338735	TMEM150B
NM_175782	chr5	-4.0107	7.97213	0.007849	0.338735	LGALS1
NM_001038140	chr27	-4.0103	7.97553	0.014195	0.431009	MYOM2
NM_001101238	chr22	-4.0094	7.97439	0.009023	0.359657	GPR62
NM_001035301	chr27	-4.0093	7.97420	0.008998	0.359657	PDGFRL
NM_001099001	chr13	-4.0087	7.97368	0.009009	0.359657	NFS1
NR_031354	chr21	-4.0030	7.97410	0.017444	0.462351	MIR487A
NM_001075587	chr11	-4.0029	7.97254	0.011087	0.389884	CRAT
NM_001076858	chr29	-3.9953	7.97225	0.026875	0.545397	PKP3
NM_001046360	chr2	-3.9902	7.97034	0.024277	0.524631	TCEA3
NM_001075351	chr1	-3.9811	7.97041	0.032286	0.547524	MFSD1
NM_175772	chr25	-3.9811	7.97041	0.032312	0.547524	ELN
NM_001083672	chr11	-3.9804	7.97028	0.032265	0.547524	COQ4
NR_030810	chr7	-3.9787	7.97005	0.032651	0.547524	MIR1434
NM_001034342	chr5	-3.8920	8.74059	4.17E-06	0.009991	ATF4
NM_001167904	chr15	-3.8512	7.91870	0.029346	0.547524	POLD3
NM_001192725	chr29	-3.8310	7.91713	0.015679	0.432581	KCNK7
NM_001101285	chr2	-3.8310	7.91706	0.015679	0.432581	CXCR2
NM_001083415	chr3	-3.8310	7.91677	0.015679	0.432581	STXBP3
NM_001031759	chr29	-3.8310	7.91490	0.015679	0.432581	HEPACAM
NM_001105407	chr20	-3.8309	7.91467	0.015679	0.432581	SUB1

2.2.4 High salt (nucleoid-enriched)

GeneID	Chr	logFC	logCPM	PValue	FDR	symbol
NM_001206876	chr5	4.6063	8.15953	0.001	0.223078	SENP1
NM_001102140	chr16	4.4747	8.10437	0.001968	0.245201	BRINP3
NM_001077444	chr6	4.1689	7.98731	0.007849	0.338735	PDLIM5
NM_001034636	chr7	4.1682	7.98728	0.021839	0.511183	PAIP2
NM_001113221	chr11	3.9892	7.92553	0.029235	0.547524	RTN4
NM_001278621	chr4	3.9877	7.92530	0.017071	0.454998	CD36
NM_001077002	chr1	3.9877	7.92541	0.015679	0.432581	GPR171
NM_001098078	chr3	3.9871	7.92516	0.029065	0.547524	RIT1
NR_030907	chr11	3.9867	7.92508	0.028989	0.547524	MIR181A-2
NM_001191525	chr6	3.7808	7.86055	0.037822	0.547524	AFF1
NM_001077122	chr1	3.7808	7.86055	0.037816	0.547524	MGC133804
NM_174756	chr12	3.7806	7.86047	0.037731	0.547524	DNAJC3
NM_001046353	chr18	3.7804	7.86047	0.031328	0.547524	SULT2A1
NM_174278	chr6	3.7804	7.86041	0.031328	0.547524	CNGA1
NM_001046493	chr14	3.7804	7.86039	0.031328	0.547524	TCEB1
NM_001080272	chr20	3.7804	7.86039	0.031328	0.547524	OSMR
NM_001038056	chr27	3.7804	7.86036	0.031328	0.547524	TM2D2
NM_001166609	chr2	3.7804	7.86036	0.031328	0.547524	HSPD1
NM_001076805	chr23	3.7804	7.86033	0.031328	0.547524	FARS2
NM_001103312	chr10	3.7804	7.86025	0.031328	0.547524	OTP
NM_001099133	chr10	3.7804	7.86025	0.031328	0.547524	LACTB
NM_001102087	chr25	3.7804	7.86025	0.031328	0.547524	SEPT14
NM_174504	chr1	3.7802	7.86033	0.037614	0.547524	ATP6V1A
NM_001013001	chr4	3.7801	7.86030	0.037736	0.547524	WNT2
NM_183362	chr7	3.7799	7.86022	0.037587	0.547524	RETN
NM_001101043	chrX	3.7798	7.86017	0.03744	0.547524	FIGF
NM_001017943	chr5	3.5059	8.40699	0.000659	0.181773	B4GALNT1
NM_001101907	chr12	3.4098	8.36041	0.000801	0.197032	ZMYM2
NM_001080346	chrX	3.2763	10.41184	1.47E-19	1.41E-15	MGC148328
NM_001075227	chr4	3.0752	8.21165	0.006396	0.338735	KLHDC10
NM_001105443	chr4	3.0751	8.21198	0.006396	0.338735	ZNRF2
NM_001076110	chr7	3.0751	8.21190	0.006396	0.338735	C7H5orf24
NM_001034644	chr4	3.0750	8.21192	0.006742	0.338735	RALA
NM_001110087	chr9	3.0749	8.21171	0.006783	0.338735	AKIRIN2
NM_001077042	chr9	2.9436	8.15678	0.01179	0.389884	MPC1
NM_001046522	chr19	2.9436	8.15841	0.01179	0.389884	TMEM100
NM_001046607	chr15	2.9436	8.15870	0.01179	0.389884	BDNF
NM_001105495	chr11	2.9422	8.15834	0.018504	0.476107	FAM228B
NM_174841	chr22	2.9419	8.15855	0.025822	0.536279	ITPR1
NM_001098984	chr15	2.9418	8.15874	0.016756	0.449809	PGM2L1
NM_001102304	chr2	2.9415	8.15857	0.016547	0.447234	STPG1
NM_001099023	chr1	2.9411	8.15871	0.018573	0.476107	ZNF639
NM_001206766	chr1	2.8046	8.10162	0.033113	0.547524	TOPBP1
NM_001075971	chr11	2.8035	8.10128	0.033303	0.547524	STAMBP
NM_001143741	chr13	2.7988	8.10339	0.021587	0.511183	ATP5E
NM_001206077	chr26	2.7987	8.10371	0.021587	0.511183	SLK
NM_001206133	chr28	2.7987	8.10360	0.021587	0.511183	ARID4B
NM_001206586	chr10	2.7983	8.10325	0.025086	0.530486	SYNE2
NM_001075426	chr16	2.7981	8.10352	0.033891	0.547524	ANGPTL1
NM_001038075	chr4	2.7978	8.10344	0.033826	0.547524	BCAP29
NM_001040586	chr22	2.7967	8.10307	0.033027	0.547524	SEC61G
NM_001040575	chr3	2.7964	8.10376	0.033608	0.547524	SVBP

NM_001191137	chr1	2.6822	8.40575	0.005051	0.338735	CGGBP1
NM_001025325	chr6	2.6406	8.04436	0.045949	0.600115	PLAC8
NM_001191138	chr17	2.6378	8.04594	0.039203	0.547524	ELF2
NM_001033627	chr19	2.6378	8.04592	0.039203	0.547524	BECN1
NM_001038129	chr11	2.6378	8.04589	0.039203	0.547524	CDKL4
NM_001191532	chr8	2.6378	8.04600	0.039203	0.547524	DOCK8
NM_001034230	chr2	2.6378	8.04643	0.039203	0.547524	SPC25
NM_001191501	chr3	2.6378	8.04638	0.039203	0.547524	INADL
NM_001015658	chr3	2.6378	8.04629	0.039203	0.547524	VPS72
NM_001102190	chr14	2.6378	8.04627	0.039203	0.547524	RIMS2
NM_001079793	chr11	2.6377	8.04616	0.039203	0.547524	YPEL5
NM_001100384	chr16	2.6374	8.04614	0.043987	0.589677	DESI2
NM_001101149	chr1	2.6374	8.04613	0.046471	0.600115	PLOD2
NM_001099181	chr24	2.6373	8.04597	0.043756	0.588008	CDH19
NM_174595	chr3	2.6372	8.04591	0.043731	0.588008	S100A4
NM_001035384	chr2	2.6371	8.04597	0.046377	0.600115	EPB41L5
NM_001102020	chr11	2.6363	8.04627	0.046408	0.600115	CLIP4
NM_001078003	chr7	2.6360	8.04610	0.046263	0.600115	LIX1
NM_001205743	chr3	2.3904	8.53499	0.002909	0.296328	VANGL1
NM_001110095	chr14	2.3553	8.26036	0.031159	0.547524	ZHX1
NM_001099013	chr3	2.3518	8.26030	0.030722	0.547524	WDR63
NM_001206200	chr7	2.3516	8.25981	0.023643	0.524455	ZFYVE16
NM_001076473	chr3	2.3452	8.26199	0.035102	0.547524	PLPP3
NM_001008413	chr4	2.2996	8.49395	0.004999	0.338735	SPAM1
NM_001102321	chr19	2.2845	8.49470	0.046454	0.600115	ULK2
NM_001192791	chr20	2.2176	8.21067	0.038762	0.547524	SGTB
NM_001077994	chr28	2.2176	8.21060	0.038762	0.547524	FAM149B1
NM_173948	chr7	2.2176	8.21093	0.038762	0.547524	PAM
NM_001024549	chr5	2.2176	8.21099	0.038762	0.547524	RASSF8
NM_001037622	chr5	2.2176	8.21085	0.038762	0.547524	MRPL42
NM_001192040	chr1	2.2166	8.21136	0.04241	0.57475	CDV3
NM_001078105	chr1	2.2165	8.21109	0.042056	0.573294	CYYR1
NM_001076437	chr6	2.2165	8.21101	0.041913	0.572869	CCSER1
NM_001076188	chr16	2.2032	8.45029	0.008208	0.342538	B3GALT2
NM_001102215	chr3	2.1955	8.45050	0.022007	0.511183	ZZZ3
NM_001206072	chr9	2.1929	8.44971	0.048529	0.619917	MYO6
NM_001101304	chr3	2.0343	8.57522	0.049502	0.619917	FMO5
NM_001104991	chr10	2.0273	8.57697	0.013108	0.407041	PNMA1
NM_001192706	chr28	1.9896	8.35728	0.025997	0.537587	OGDHL
NM_001102239	chr10	1.9893	8.35655	0.022891	0.514386	RNF111
NM_001144105	chr6	1.9886	8.35904	0.022437	0.511183	NEUROG2
NM_001102107	chr2	1.9879	8.35893	0.023927	0.524576	CALCRL
NM_001101263	chr16	1.9867	8.35932	0.026129	0.538354	FAM72A
NM_001191213	chr8	1.9839	8.35870	0.044646	0.592497	NOL8
NM_001079797	chr21	1.9352	8.53540	0.023667	0.524455	SNRPN
NM_001192584	chr7	1.8685	8.31053	0.035378	0.547524	FGFR4
NM_001046399	chr15	1.8683	8.31082	0.03601	0.547524	CWC15
NM_001199064	chr10	1.8668	8.31051	0.04058	0.560238	KATNBL1

3 Gene ontology

3.1 Human

3.1.1 low salt halos

GO biological process complete	Homo sapiens	fold Enrichment	P-value
developmental process involved in reproduction (GO:0003006)	635	2.27	1.83E-02
animal organ morphogenesis (GO:0009887)	879	2.13	3.50E-03
anatomical structure formation involved in morphogenesis (GO:0048646)	824	2.1	1.51E-02
anatomical structure morphogenesis (GO:0009653)	1956	1.88	4.95E-06
positive regulation of developmental process (GO:0051094)	1210	1.87	1.49E-02
negative regulation of transcription, DNA-templated (GO:0045892)	1096	1.87	4.95E-02
tissue development (GO:0009888)	1541	1.8	4.61E-03
negative regulation of gene expression (GO:0010629)	1447	1.74	4.77E-02
regulation of multicellular organismal development (GO:2000026)	1743	1.69	1.99E-02
animal organ development (GO:0048513)	2888	1.63	7.50E-05
cellular response to organic substance (GO:0071310)	1954	1.62	4.53E-02
regulation of developmental process (GO:0050793)	2296	1.61	7.25E-03
positive regulation of cellular process (GO:0048522)	4736	1.52	6.35E-07
positive regulation of cellular metabolic process (GO:0031325)	2848	1.52	1.74E-02
positive regulation of metabolic process (GO:0009893)	3037	1.49	1.96E-02
system development (GO:0048731)	4042	1.47	7.51E-04
positive regulation of biological process (GO:0048518)	5267	1.45	5.53E-06
anatomical structure development (GO:0048856)	4986	1.44	5.34E-05
multicellular organism development (GO:0007275)	4640	1.43	4.51E-04
developmental process (GO:0032502)	5333	1.41	1.35E-04
single-organism developmental process (GO:0044767)	5239	1.41	2.35E-04
single-multicellular organism process (GO:0044707)	5417	1.4	1.83E-04
biological_process (GO:0008150)	17072	1.09	3.09E-02

3.1.2 High salt halos

GO biological process complete	Homo sapiens	fold Enrichmer	P-value
epithelial tube morphogenesis (GO:0060562)	301	2.54	5.54E-03
tube morphogenesis (GO:0035239)	339	2.38	1.26E-02
tube development (GO:0035295)	575	2.29	2.75E-05
embryonic organ development (GO:0048568)	420	2.28	4.70E-03
response to peptide hormone (GO:0043434)	398	2.24	1.61E-02
response to peptide (GO:1901652)	440	2.22	6.80E-03
morphogenesis of an epithelium (GO:0002009)	422	2.22	1.26E-02
embryonic morphogenesis (GO:0048598)	561	2.16	8.45E-04
response to hormone (GO:0009725)	841	1.97	1.72E-04
embryo development (GO:0009790)	934	1.91	1.82E-04
cellular response to endogenous stimulus (GO:0071495)	1050	1.9	3.11E-05
response to organonitrogen compound (GO:0010243)	821	1.84	9.40E-03
animal organ morphogenesis (GO:0009887)	879	1.81	7.60E-03
cellular response to oxygen-containing compound (GO:1901701)	872	1.8	1.09E-02
response to endogenous stimulus (GO:0009719)	1469	1.79	2.87E-06
response to organic cyclic compound (GO:0014070)	951	1.77	1.05E-02
response to lipid (GO:0033993)	909	1.75	2.50E-02
response to oxygen-containing compound (GO:1901700)	1492	1.74	2.57E-05
epithelium development (GO:0060429)	924	1.72	4.40E-02
negative regulation of multicellular organismal process (GO:0051241)	1025	1.68	4.85E-02
tissue development (GO:0009888)	1541	1.6	4.57E-03
regulation of cell differentiation (GO:0045595)	1569	1.54	2.98E-02
anatomical structure morphogenesis (GO:0009653)	1956	1.54	1.66E-03
regulation of multicellular organismal development (GO:2000026)	1743	1.54	1.11E-02
cellular response to organic substance (GO:0071310)	1954	1.51	6.93E-03
regulation of developmental process (GO:0050793)	2296	1.51	7.29E-04
nervous system development (GO:0007399)	2207	1.5	1.90E-03
animal organ development (GO:0048513)	2888	1.46	2.83E-04
regulation of multicellular organismal process (GO:0051239)	2690	1.42	6.86E-03
response to organic substance (GO:0010033)	2669	1.42	9.88E-03
system development (GO:0048731)	4042	1.41	9.72E-06
single-multicellular organism process (GO:0044707)	5417	1.37	3.03E-07
multicellular organism development (GO:0007275)	4640	1.36	2.03E-05
regulation of biological quality (GO:0065008)	3571	1.36	5.45E-03
anatomical structure development (GO:0048856)	4986	1.34	3.15E-05
negative regulation of cellular process (GO:0048523)	4281	1.33	2.87E-03
negative regulation of biological process (GO:0048519)	4622	1.32	1.21E-03
developmental process (GO:0032502)	5333	1.32	6.89E-05
single-organism developmental process (GO:0044767)	5239	1.32	1.10E-04
positive regulation of cellular process (GO:0048522)	4736	1.3	3.58E-03
multicellular organismal process (GO:0032501)	6482	1.26	4.89E-04
positive regulation of biological process (GO:0048518)	5267	1.25	4.14E-02
regulation of cellular process (GO:0050794)	10467	1.15	7.44E-03
regulation of biological process (GO:0050789)	10998	1.14	2.38E-02
biological regulation (GO:0065007)	11627	1.13	1.78E-02
Unclassified (UNCLASSIFIED)	3900	0.74	0.00E+00
sensory perception of chemical stimulus (GO:0007606)	529	0.24	4.57E-02

3.1.3 Halosperm halos

GO biological process complete	Homo sapiens	fold Enrichmen	P-value
sensory organ morphogenesis (GO:0090596)	249	2.49	1.72E-02
embryonic morphogenesis (GO:0048598)	561	2.15	1.06E-04
pattern specification process (GO:0007389)	413	2.08	3.13E-02
sensory organ development (GO:0007423)	519	1.97	1.86E-02
animal organ morphogenesis (GO:0009887)	879	1.95	1.01E-05
embryo development (GO:0009790)	934	1.76	2.35E-03
regulation of anatomical structure morphogenesis (GO:0022603)	975	1.72	4.18E-03
response to endogenous stimulus (GO:0009719)	1469	1.64	1.97E-04
negative regulation of multicellular organismal process (GO:0051241)	1025	1.64	3.16E-02
cellular response to endogenous stimulus (GO:0071495)	1050	1.62	4.70E-02
positive regulation of developmental process (GO:0051094)	1210	1.62	9.67E-03
anatomical structure morphogenesis (GO:0009653)	1956	1.58	2.55E-05
tissue development (GO:0009888)	1541	1.58	1.63E-03
regulation of cell proliferation (GO:0042127)	1575	1.54	5.21E-03
neurogenesis (GO:0022008)	1500	1.53	1.37E-02
regulation of cell differentiation (GO:0045595)	1569	1.51	1.83E-02
regulation of multicellular organismal development (GO:2000026)	1743	1.5	9.14E-03
regulation of developmental process (GO:0050793)	2296	1.5	1.53E-04
nervous system development (GO:0007399)	2207	1.49	4.31E-04
regulation of multicellular organismal process (GO:0051239)	2690	1.45	1.24E-04
cell differentiation (GO:0030154)	3291	1.38	4.56E-04
animal organ development (GO:0048513)	2888	1.38	4.70E-03
cellular developmental process (GO:0048869)	3371	1.37	6.79E-04
single-multicellular organism process (GO:0044707)	5417	1.35	7.15E-08
multicellular organism development (GO:0007275)	4640	1.34	1.17E-05
system development (GO:0048731)	4042	1.34	2.38E-04
single-organism developmental process (GO:0044767)	5239	1.31	1.19E-05
developmental process (GO:0032502)	5333	1.31	1.02E-05
anatomical structure development (GO:0048856)	4986	1.31	5.33E-05
positive regulation of cellular process (GO:0048522)	4736	1.3	5.04E-04
negative regulation of cellular process (GO:0048523)	4281	1.3	3.82E-03
negative regulation of biological process (GO:0048519)	4622	1.27	1.22E-02
positive regulation of biological process (GO:0048518)	5267	1.24	1.74E-02
multicellular organismal process (GO:0032501)	6482	1.22	4.48E-03
single-organism process (GO:0044699)	12544	1.12	3.58E-03
cellular process (GO:0009987)	14596	1.1	7.29E-04
biological_process (GO:0008150)	17072	1.07	2.81E-04
Unclassified (UNCLASSIFIED)	3900	0.68	0.00E+00
detection of stimulus involved in sensory perception (GO:0050906)	527	0.24	8.56E-03

3.2 Bovine

3.2.1 Low salt halos

GO biological process complete	Bos taurus - RE	fold Enrichmen	P-value
cofactor metabolic process (GO:0051186)	249	2.64	1.29E-02
positive regulation of biosynthetic process (GO:0009891)	1424	1.59	1.28E-02
heterocycle metabolic process (GO:0046483)	2792	1.5	3.12E-05
cellular aromatic compound metabolic process (GO:0006725)	2825	1.49	2.88E-05
nucleobase-containing compound metabolic process (GO:0006	2684	1.48	1.35E-04
organic cyclic compound metabolic process (GO:1901360)	2956	1.47	5.38E-05
cellular biosynthetic process (GO:0044249)	2711	1.38	3.46E-02
cellular nitrogen compound metabolic process (GO:0034641)	3351	1.38	2.40E-03
nitrogen compound metabolic process (GO:0006807)	3644	1.37	1.37E-03
positive regulation of biological process (GO:0048518)	4157	1.34	9.46E-04
positive regulation of cellular process (GO:0048522)	3778	1.32	2.14E-02
cellular metabolic process (GO:0044237)	6394	1.23	5.65E-03
Unclassified (UNCLASSIFIED)	4075	0.8	0.00E+00
system process (GO:0003008)	1891	0.49	1.80E-04
G-protein coupled receptor signaling pathway (GO:0007186)	1601	0.48	9.12E-04
neurological system process (GO:0050877)	1523	0.26	1.84E-10

3.2.2 Low salt nucleoids

GO biological process complete	Bos taurus - RE	fold Enrichmen	P-value
negative regulation of cellular protein localization (GO:1903828	111	3.45	1.98E-02
protein transport (GO:0015031)	801	1.96	7.75E-05
establishment of protein localization (GO:0045184)	910	1.87	1.42E-04
organic substance transport (GO:0071702)	1385	1.69	1.15E-04
protein localization (GO:0008104)	1295	1.66	1.18E-03
macromolecule localization (GO:0033036)	1563	1.62	3.14E-04
organonitrogen compound metabolic process (GO:1901564)	1469	1.57	7.24E-03
cellular localization (GO:0051641)	1484	1.54	1.94E-02
gene expression (GO:0010467)	2252	1.49	4.78E-04
cellular nitrogen compound biosynthetic process (GO:0044271)	1942	1.47	1.10E-02
cellular biosynthetic process (GO:0044249)	2711	1.47	5.26E-05
RNA metabolic process (GO:0016070)	1838	1.47	2.21E-02
organic substance biosynthetic process (GO:1901576)	2778	1.44	3.46E-04
macromolecule biosynthetic process (GO:0009059)	2058	1.43	2.84E-02
cellular macromolecule biosynthetic process (GO:0034645)	2034	1.43	3.56E-02
biosynthetic process (GO:0009058)	2855	1.42	4.63E-04
nitrogen compound metabolic process (GO:0006807)	3644	1.42	6.20E-06
single-organism metabolic process (GO:0044710)	2634	1.38	1.78E-02
cellular nitrogen compound metabolic process (GO:0034641)	3351	1.38	6.14E-04
cellular metabolic process (GO:0044237)	6394	1.37	9.35E-12
nucleobase-containing compound metabolic process (GO:0006	2684	1.36	3.87E-02
heterocycle metabolic process (GO:0046483)	2792	1.35	4.52E-02
cellular protein metabolic process (GO:0044267)	2894	1.35	3.14E-02
cellular macromolecule metabolic process (GO:0044260)	4866	1.33	1.66E-05
metabolic process (GO:0008152)	7430	1.32	1.72E-11
primary metabolic process (GO:0044238)	6583	1.31	2.48E-08
organic substance metabolic process (GO:0071704)	6954	1.3	1.95E-08
macromolecule metabolic process (GO:0043170)	5511	1.27	6.29E-04
regulation of metabolic process (GO:0019222)	4900	1.24	4.63E-02
cellular process (GO:0009987)	12534	1.11	1.41E-02
Unclassified (UNCLASSIFIED)	4075	0.77	0.00E+00
system process (GO:0003008)	1891	0.54	7.96E-04
neurological system process (GO:0050877)	1523	0.43	1.75E-05
G-protein coupled receptor signaling pathway (GO:0007186)	1601	0.34	2.41E-09
sensory perception (GO:0007600)	1280	0.24	1.85E-10

4 Semen parameters

4.1 Donor semen samples

Donor No.	Sperm count/mL	Motility %	Semen volume (mL)	Age
D113	96×10^6	37.36	2.0	20
D108	170×10^6	59	1.2	20
D104	63×10^6	85	3.0	24
D101	90×10^6	65	3.0	21
D100	85×10^6	55	2.5	19
D94	65.5×10^6	46	1.0	20
D43	56×10^6	67.5	4.0	21
D32	128×10^6	80.6	4.5	19
D65	75×10^6	85	2.5	26
D70	233×10^6	92	1.5	28
D25	149×10^6	47	3.0	22
D7	110×10^6	73	2.5	21
D8	101×10^6	55	4.0	20
D9	82×10^6	79	4.5	28
D4	55×10^6	15	1.0	20
D30	122×10^6	70	2.0	22
D31	200×10^6	90	1.5	36
D28	93×10^6	55	6.0	24
D19	64×10^6	89	3.5	24
D66	50×10^6	54.1	3.3	21

4.2 Seacroft semen samples

Seacroft's patients No.	Sperm count/mL	Motility %	Semen volume (mL)	Age
D287	57×10^6	53	2.8	38
D315	103×10^6	59	3.95	33
D452	96.2×10^6	67	1.3	45
D244	70×10^6	67	8.1	31
D343	94×10^6	76	1.1	39
D347	90×10^6	42	2.5	31
D356	58×10^6	53	2.0	38
D377	60×10^6	56	0.5	22
D394	40×10^6	62	1.0	38
D397	83×10^6	68	4.0	43
D456	115×10^6	72	8.0	32
D476	54×10^6	59	1.8	39
D480	102×10^6	50	0.7	29
D468	57×10^6	36	3.75	43
D487	132×10^6	72	1.0	36
D489	316×10^6	61	0.5	33

D520	44 x 10^6	40	4.2	39
D458	117 x 10^6	39	0.8	26
D439	122 x 10^6	69	1.0	37
D466	77 x 10^6	52	2.5	34
D455	73 x 10^6	51	2.0	26

4.3 Bovine semen samples

Bulls name	Bulls no.	Sperm count/mL	Motility %	Semen volume (straw)
Freddy	113115	93.75 x 10^6	57	250 µL
Javelin	4884	91 x 10^6	73	250 µL
Zelgadis	115331	34.75 x 10^6	45	250 µL
Classic	116218	27.5 x 10^6	64	250 µL
Bossman	113114	72.75 x 10^6	37	250 µL
Forbidden	486	171 x 10^6	86	250 µL
Zeber	115324	40.5 x 10^6	42	250 µL